https://doi.org/10.5194/essd-2026-895
Preprint. Discussion started: 10 November 2026
© Author(s) 2026. CC BY 4.0 License.



Open Access Earth System Science Data Discussions

Global Carbon Budget 2026

Pierre Friedlingstein[1,2], Michael O'Sullivan[1], Robbie M. Andrew[3], Judith Hauck[4,5], Matthew W. Jones[6,7], Peter Landschützer[8], Corinne Le Quéré[6], Hongmei Li[9,10], Ingrid T. Luijkx[11], Are Olsen[12,13], Glen P. Peters[3], Wouter Peters[11,14], Julia Pongratz[15], Clemens Schwingshackl[15], Stephen Sitch[1], Josep G. Canadell[16], Philippe Ciais[17], Kjetil Aas[3], Simone R. Alin[18], Vivek Arora[19], Nicholas R. Bates[20,21], Kimberly Bedard[22], David Martin Belda[23], Nicolas Bellouin[24], Alice Benoit-Cattin[25], Carla F. Berghoff[26], Sarah Berthet[27], Laurent Bopp[2], Ida Bagus Mandhara Brasika[1,28], Eleanor Burke[29], Leon Casse[30,31], Matthew A. Chamberlain[32], Frédéric Chevallier[17], Louise P. Chini[33], Margot Cronin[34], Susan E. Curless[35,18], Tim DeVries[36], Tobias Ehmen[12,13], Matthew P. Enright[20], Kazutaka Enyo[37], Michael Erb[38,39], Wiley Evans[22], Amanda R Fay[40], Ben Felzer[41], Daniel J. Ford[1], Adrianna Foster[42], Filippa Fransner[12,13], Agneta Fransson[43], Andrew Friedman[44], Thomas Gasser[45], Marion Gehlen[17], Thanos Gkritzalis[8], Giacomo Grassi[46], Luke Gregor[47,48], Nicolas Gruber[47], Özgür Gürses[4], Wensu Hao[49], Kirsty Harrington[50], Jens Heinke[51], George C. Hurtt[33], Tatiana Ilyina[9], Akihiko Ito[52], Andrew R. Jacobson[53,54], Atul K. Jain[55], Rajesh Janardanan[56], Tereza Jarníková[6], Annika Jersild[57], Fei Jiang[58], Zhe Jin[59], Linus Kamb[35,18], Etsushi Kato[60], Ralph F. Keeling[61], Kees Klein Goldewijk[62], Jürgen Knauer[63], Jan Ivar Korsbakken[3], Taro Kunimitsu[3], Xin Lan[53,54], Vladimir Lapin[64], Siv K. Lauvset[65,13], Simone Le Chevère[4], Woo-Sung Lee[66], Enhui Liao[67], Junjie Liu[68,69], Zhu Liu[70], Sebastiaan Luyssaert[71], Lei Ma[33], Suman Maity[56], Gregg Marland[38,39], Patrick C. McGuire[72], Nicolas Metzl[73], Juliette Mignot[73], Natalie M. Monacci[74], Eric J. Morgan[61], Jens D. Müller[75,76,77], David R. Munro[53,54], Miaki Muramatsu[37], Shin-Ichiro Nakaoka[56], Craig Neill[32], Tobias Nützel[15], Léa Olivier[4,15], Timothy Osborn[78], Xosé A. Padín[79], Paul I Palmer[80,81], Sudhanshu Pandey[68], Denis Pierrot[82], Ben Poulter[83], Zhangcai Qin[84], Yumou Qiu[85], Gregor Rehder[86], Laure Resplandy[87], Christian Rödenbeck[88], Alizée Roobaert[8], Thais M. Rosan[1], Simone Rossi[46], Jörg Schwinger[13,65], Gereon Seeberg[15], Roland Séférian[27], Elisabeth H. Shadwick[32,89], Ingunn Skjelvan[65,13], Karolina Slominska-Durdasiak[88], T. Luke Smallman[80,81], Mohanan G. Sreeush[4], Qing Sun[90,76,77], Adrienne J. Sutton[18], Colm Sweeney[54], Shintaro Takao[56], Hiroaki Tatebe[91,92], Jens Terhaar[76,77], Hanqin Tian[49], Bronte Tilbrook[32,89], Takahiro Toyoda[93], Joaquin A. Triñanes[94], Francesco Tubiello[30], Guido R. van der Werf[11], Auke M. van der Woude[11], Sebastiaan J. van de Velde[95,96], Anthony P. Walker[97], Rik Wanninkhof[82], Xiaojuan Yang[97], Wenping Yuan[59], Xu Yue[98], Jiye Zeng[56], Ning Zheng[33], and Bo Zheng[99]

[1]Faculty of Environment, Science and Economy, University of Exeter, Exeter, EX4 4QF, UK
[2]Laboratoire de Météorologie Dynamique, Institut Pierre-Simon Laplace, CNRS, École Normale Supérieure, Université PSL, Sorbonne Université, École Polytechnique, Paris, France
[3]CICERO Center for International Climate Research, Oslo 0855, Norway

https://doi.org/10.5194/essd-2026-895
Preprint. Discussion started: 10 November 2026
© Author(s) 2026. CC BY 4.0 License.



Open Access Earth System Science Data Discussions

[4]Alfred-Wegener-Institut, Helmholtz-Zentrum für Polar- und Meeresforschung, Am Handelshafen 12, 27570 Bremerhaven, Germany

[5]FB02 Biology/Chemistry Bremen, Universität Bremen, Bremen, Germany

[6]Tyndall Centre for Climate Change Research, School of Environmental Sciences, University of East Anglia, Norwich Research Park, Norwich NR4 7TJ, UK

[7]School of Geography, Earth and Environmental Sciences, University of Birmingham, Edgbaston, Birmingham, B15 2TT, UK

[8]Flanders Marine Institute (VLIZ), Jacobsenstraat 1, 8400, Ostend, Belgium

[9]Max Planck Institute for Marine Microbiology, Celsiusstraße 1, 28359 Bremen, Germany

[10]Helmholtz-Zentrum Hereon, Max-Planck-Straße 1, 21502 Geesthacht, Germany

[11]Environmental Sciences Group, Wageningen University, P.O. Box 47, 6700AA, Wageningen, the Netherlands

[12]Geophysical Institute, University of Bergen, Allégaten 70, 5007 Bergen, Norway

[13]Bjerknes Centre for Climate Research, Bergen, Norway

[14]Centre for Isotope Research, University of Groningen, Groningen, the Netherlands

[15]Ludwig-Maximilians-Universität München, Luisenstr. 37, 80333 München, Germany

[16]CSIRO Environment, Canberra, ACT 2101, Australia

[17]Laboratoire des Sciences du Climat et de l'Environnement (LSCE), CEA, CNRS, UVSQ, Université Paris-Saclay, 91191 Gif-sur-Yvette, France

[18]National Oceanic and Atmospheric Administration, Pacific Marine Environmental Laboratory (NOAA/PMEL), 7600 Sand Point Way NE, Seattle, WA 98115, USA

[19]Climate Research Division, Environment and Climate Change Canada, Victoria, BC, Canada

[20]ASU-BIOS, 17 Biological Lane, Ferry Reach, St. Georges, GE01, Bermuda

[21]School of Ocean Futures (SOF), Arizona State University (ASU), Tempe, Arizona, USA

[22]Hakai Institute, 1713 Hyacinthe Bay Rd, Heriot Bay, BC, V0P 1H0, Canada

[23]Karlsruhe Institute of Technology, Institute of Meteorology and Climate Research/Atmospheric Environmental Research, 82467 Garmisch-Partenkirchen, Germany

[24]Department of Meteorology, University of Reading, Reading, RG6 6BB, UK

[25]Marine and Freshwater Research Institute, Hafnarfjörður, Iceland

[26]Instituto Nacional de Investigación y Desarrollo Pesquero (INIDEP), Paseo Victoria Ocampo No 1, B7602HSA, Mar del Plata, Argentina

[27]Centre National de Recherches Météorologiques, Université de Toulouse, Météo-France, CNRS, UMR 3589, Toulouse, France

[28]Faculty of Marine Science and Fisheries, Udayana University, Denpasar, Bali, 80361, Indonesia

https://doi.org/10.5194/essd-2026-895
Preprint. Discussion started: 10 November 2026
© Author(s) 2026. CC BY 4.0 License.



Open Access Earth System Science Data Discussions

[29]Met Office Hadley Centre, FitzRoy Road, Exeter, EX1 3PB, UK
[30]Statistics Division, Food and Agriculture Organization of the United Nations, Via Terme di Caracalla, Rome 00153, Italy
[31]Environmental Engineering, School of Civil Engineering, The University of Sydney, Sydney, NSW, Australia
[32]CSIRO Environment, Castray Esplanade, Hobart, Tasmania 7004, Australia
[33]Department of Geographical Sciences, University of Maryland, College Park, MD 20742, USA
[34]Marine Institute, Rinville, Oranmore, Co Galway H91 R673, Ireland
[35]Cooperative Institute for Climate, Ocean and Ecosystem Studies, University of Washington, 3737 Brooklyn Ave NE, Seattle, WA 98105, USA
[36]Department of Geography, University of California, Santa Barbara, CA 93106, USA
[37]Japan Meteorological Agency, 3-6-9 Toranomon, Minato City, Tokyo, 105-8431, Japan
[38]Research Institute for Environment, Energy, and Economics, Appalachian State University, Boone, North Carolina, USA
[39]Department of Geological and Environmental Sciences, Appalachian State University, Boone, North Carolina, USA
[40]Lamont-Doherty Earth Observatory, Columbia University, New York, NY, USA
[41]Department of Earth and Environmental Sciences, Lehigh University, Bethlehem, PA 18015, USA
[42]Climate and Global Dynamics Laboratory, National Center for Atmospheric Research, Boulder, CO 80305, USA
[43]Norwegian Polar Institute, 9296 Tromsø, Norway
[44]National Centre for Atmospheric Science (NCAS), Climatic Research Unit, University of East Anglia, Norwich, NR4 7TJ, UK
[45]International Institute for Applied Systems Analysis (IIASA), Schlossplatz 1, 2361 Laxenburg, Austria
[46]European Commission, Joint Research Centre (JRC), Ispra, Italy
[47]Environmental Physics Group, Institute of Biogeochemistry and Pollutant Dynamics and Center for Climate Systems Modeling (C2SM), ETH Zürich, Zurich, Switzerland
[48]Swiss Data Science Center, 8050 Zurich, Switzerland
[49]Schiller Institute of Integrated Science and Society, Department of Earth and Environmental Sciences, Boston College, Chestnut Hill, MA 02467, USA
[50]Smith School for Enterprise and the Environment, University of Oxford, Oxford, UK
[51]Potsdam Institute for Climate Impact Research (PIK), member of the Leibniz Association, P.O. Box 60 12 03, 14412 Potsdam, Germany
[52]Graduate School of Agricultural and Life Sciences, University of Tokyo, Tokyo, Japan

https://doi.org/10.5194/essd-2026-895
Preprint. Discussion started: 10 November 2026
© Author(s) 2026. CC BY 4.0 License.



Open Access Earth System Science Data Discussions

[53]Cooperative Institute for Research in Environmental Sciences (CIRES), University of Colorado Boulder, Boulder, CO 80305, USA

[54]National Oceanic and Atmospheric Administration Global Monitoring Laboratory (NOAA/GML), 325 Broadway R/GML, Boulder, CO 80305, USA

[55]Department of Climate, Meteorology and Atmospheric Sciences, University of Illinois, Urbana, IL 61801, USA

[56]Earth System Division, National Institute for Environmental Studies (NIES), 16-2 Onogawa, Tsukuba Ibaraki, 305-8506, Japan

[57]Earth System Science Interdisciplinary Center, University of Maryland, College Park, MD 20740, USA

[58]Jiangsu Provincial Key Laboratory for Advanced Remote Sensing and Geographic Information Technology, International Institute for Earth System Science, Nanjing University, Nanjing, 210023, China

[59]Institute of Carbon Neutrality, Sino-French Institute for Earth System Science, College of Urban and Environmental Sciences, Peking University, Beijing, China

[60]Institute of Applied Energy (IAE), Minato-ku, Tokyo 105-0003, Japan

[61]University of California, San Diego, Scripps Institution of Oceanography, La Jolla, CA 92093-0244, USA

[62]Utrecht University, Faculty of Geosciences, Department IMEW, Copernicus Institute of Sustainable Development, Heidelberglaan 2, P.O. Box 80115, 3508 TC, Utrecht, the Netherlands

[63]School of Life Sciences, Faculty of Science, University of Technology Sydney, Ultimo, NSW 2007, Australia

[64]Barcelona Supercomputing Center, Barcelona, Spain

[65]NORCE Research, Jahnebakken 5, 5007 Bergen, Norway

[66]Climate Modelling Research Division, Environment and Climate Change Canada, Victoria, BC, Canada

[67]State Key Laboratory of Submarine Geoscience, School of Oceanography, Shanghai Jiao Tong University, Shanghai 200240, China

[68]Jet Propulsion Laboratory, California Institute of Technology, Pasadena, CA, USA

[69]Division of Geological and Planetary Sciences, California Institute of Technology, Pasadena, CA, USA

[70]Department of Earth System Science, Tsinghua University, Beijing, China

[71]A-LIFE, Vrije Universiteit Amsterdam, Amsterdam, the Netherlands

[72]Department of Meteorology and National Centre for Atmospheric Science, University of Reading, Reading, UK

https://doi.org/10.5194/essd-2026-895
Preprint. Discussion started: 10 November 2026
© Author(s) 2026. CC BY 4.0 License.



Open Access Earth System Science Data Discussions

[73]LOCEAN Laboratory (Sorbonne Université, CNRS, IRD, MNHN), 4 Place Jussieu, 75005 Paris, France
[74]College of Fisheries and Ocean Sciences, University of Alaska Fairbanks, Fairbanks, Alaska 99775-7220, USA
[75]Carbon to Sea Initiative, Washington D.C., USA
[76]Climate and Environmental Physics, Physics Institute, University of Bern, Bern, Switzerland
[77]Oeschger Centre for Climate Change Research, University of Bern, Bern, Switzerland
[78]Climatic Research Unit, School of Environmental Sciences, University of East Anglia, Norwich Research Park, Norwich, NR4 7TJ, UK
[79]Instituto de Investigacións Mariñas (IIM-CSIC), Eduardo Cabello 6, 36208 Vigo, Spain
[80]National Centre for Earth Observation, University of Edinburgh, Edinburgh, EH9 3FE, UK
[81]School of Geosciences, University of Edinburgh, Edinburgh, EH9 3FE, UK
[82]National Oceanic and Atmospheric Administration, Atlantic Oceanographic and Meteorological Laboratory (NOAA/AOML), 4301 Rickenbacker Causeway, Miami, FL 33149, USA
[83]Spark Climate Solutions, Covina, CA, USA
[84]School of Atmospheric Sciences, Sun Yat-sen University, Zhuhai 519000, China
[85]School of Mathematical Sciences and Center for Statistical Science, Peking University, Beijing, China
[86]Leibniz Institute for Baltic Sea Research Warnemünde (IOW), Seestrasse 15, 18119 Rostock, Germany
[87]Princeton University, Department of Geosciences and Princeton Environmental Institute, Princeton, NJ, USA
[88]Max Planck Institute for Biogeochemistry, P.O. Box 600164, Hans-Knöll-Str. 10, 07745 Jena, Germany
[89]Australian Antarctic Program Partnership, University of Tasmania, Hobart, Australia
[90]Wyss Academy for Nature, University of Bern, Bern, Switzerland
[91]Research Center for Environmental Modeling and Application, Japan Agency for Marine-Earth Science and Technology, Yokohama, Japan
[92]Advanced Institute for Marine Ecosystem Change, Japan Agency for Marine-Earth Science and Technology, Yokohama, Japan
[93]JMA Meteorological Research Institute, Tsukuba, Ibaraki, Japan
[94]Department of Electronics and Computer Science, Universidade de Santiago de Compostela, Santiago de Compostela, Spain
[95]Department of Marine Science, University of Otago, Ōtepoti Dunedin, 9016, Aotearoa New Zealand
[96]Earth Sciences New Zealand, Te Whanganui-a-Tara Wellington, 6021, Aotearoa New Zealand
[97]Environmental Sciences Division, Oak Ridge National Laboratory, Oak Ridge, TN 37831, USA

https://doi.org/10.5194/essd-2026-895
Preprint. Discussion started: 10 November 2026
© Author(s) 2026. CC BY 4.0 License.



Open Access Earth System Science Data Discussions

[98]School of Environmental Science and Engineering, Nanjing University of Information Science and Technology (NUIST), Nanjing, 210044, China

[99]Shenzhen Key Laboratory of Ecological Remediation and Carbon Sequestration, Institute of Environment and Ecology, Tsinghua Shenzhen International Graduate School, Tsinghua University, Shenzhen, China

Correspondence to: Pierre Friedlingstein (p.friedlingstein@exeter.ac.uk)

Abstract

Accurate assessment of anthropogenic carbon dioxide (CO_2) emissions and their partitioning among the atmosphere, ocean, and terrestrial biosphere in a changing climate is critical to better understand the global carbon cycle, supporting the development of climate policies, and project future climate change. Here we describe and synthesise datasets and methodologies to quantify the five major components of the global carbon budget and their uncertainties. Fossil CO_2 emissions (E_{FOS}) are based on energy and cement production data. Emissions from land-use change (E_{LUC}) are estimated by bookkeeping models based on land-use data. The global atmospheric CO_2 growth rate (G_{ATM}) is computed from changes in concentration measured at surface stations. The global net uptake of CO_2 by the ocean (S_{OCEAN}) is estimated with global ocean biogeochemistry models and observation-based fCO_2-products. The global net uptake of CO_2 by the land (S_{LAND}) is estimated with dynamic global vegetation models. Additional lines of evidence are provided by atmospheric inversions, atmospheric oxygen measurements, ocean interior observation-based estimates, and Earth System Models. The sum of all sources and sinks results in the carbon budget imbalance (B_{IM}), a measure of imperfect data and incomplete understanding of the contemporary carbon cycle. All uncertainties are reported as ±1σ.

For the year 2025, E_{FOS} increased by 1.2% relative to 2024, with fossil emissions at 10.5 ± 0.5 GtC yr^{-1} (including the cement carbonation sink, 0.2GtC yr^{-1}), E_{LUC} was 1.2 ± 0.7 GtC yr^{-1}, for total anthropogenic CO_2 emissions of 11.7 ± 0.9 GtC yr^{-1} (42.8 ± 3.2 $GtCO_2$ yr^{-1}). Also, for 2025, G_{ATM} was 4.4 ± 0.2 GtC yr^{-1} (2.06 ± 0.1 ppm yr^{-1}), 3.6 GtC lower than the record high 2024 growth rate. S_{OCEAN} was 3.2 ± 0.7 GtC yr^{-1} and S_{LAND} was 3.6 ± 0.9 GtC yr^{-1}, with a small B_{IM} (0.5 GtC yr^{-1}). The global atmospheric CO_2 concentration averaged over 2025 reached 425.6 ± 0.1 ppm. Preliminary data for 2026 suggest a decrease in E_{FOS} relative to 2025 of 0.40% (-1.5% to +0.6%) globally, and atmospheric CO_2 concentration increasing by 2.2 ppm reaching 427.7 ppm, 54% above the pre-industrial level (around 278 ppm in 1750). Overall, the mean and trend in the components of the global carbon budget are consistently estimated over the period 1959-2025, with a small positive overall budget imbalance, (0.6 GtC yr^{-1} averaged over the period 1959-2025), although discrepancies of up to around 1 GtC yr^{-1} persist for the representation of annual to decadal variability in CO_2 fluxes. Comparison of estimates

https://doi.org/10.5194/essd-2026-895
Preprint. Discussion started: 10 November 2026
© Author(s) 2026. CC BY 4.0 License.



Open Access Earth System Science Data Discussions

from multiple approaches and observations shows: (1) a persistent large uncertainty in the estimate of land-use change emissions, (2) a low agreement between the different estimates on the magnitude of the land CO_2 flux, particularly in the northern extra-tropics, and (3) a discrepancy between the different estimates on the mean ocean sink and its trend.

This living data update documents changes in methods and datasets applied to this most-recent global carbon budget as well as evolving community understanding of the global carbon cycle. The data presented in this work are available at https://doi.org/10.18160/GCP-2026 (Friedlingstein et al., 2026b).

Executive Summary

Global fossil CO_2 emissions (including cement carbonation) are expected to decrease in 2026 by -0.4% relative to 2025 (range -1.5% to +0.6%), bringing fossil emissions to an expected 10.4 GtC yr^{-1} (38.2 $GtCO_2$ yr^{-1}) [1]. Emissions from oil and gas in 2026 are expected to be below their 2025 levels (by -1.9% and -0.3% respectively), with these decreases partly compensated by an expected growth in emissions from coal (0.6%). These preliminary estimates are based on available data for 2026. Consolidated data confirm a growth of 1.2% in 2025 relative to 2024, with fossil CO_2 emissions of 10.5 ± 0.5 GtC yr^{-1} (38.4 ± 1.8 $GtCO_2$ yr^{-1}) in 2025.

Regionally, fossil emissions are projected to decrease in 2026 in China, the USA, the European Union and Japan, and to grow in India. The decrease in fossil emissions in 2026 relative to 2025 is projected to be -0.9% (-2.6% to +0.8%) for China, -1.3% (-3.4% to +0.8%) for the United States, -1.5% (-4.0% to +0.9%) for the European Union, and -1.0% (-2.5% to +0.6%) for Japan. However, 2025 emissions for India are projected to increase by 4.4% (1.7% to 7.1%). Emissions are also projected to decrease by -1.0% for both international aviation and for international shipping, and to decrease by -0.7% (-2.9% to +1.5%) for the rest of the world in aggregate.

Fossil CO_2 emissions decreased ($p<0.05$) in 40 countries with growing GDP ($p<0.05$) during the decade 2016-2025. The list of decarbonising economies is considerably longer than in the previous decade (2006-2015; 22 countries). These 40 decarbonising economies contribute 2.8 GtC yr^{-1} (10.1 $GtCO_2$) fossil fuel CO_2 emissions over the last decade in aggregate, representing 26% of the world CO_2 fossil emissions. The global carbon intensity of energy has consistently decreased over the past decade (-0.4% yr^{-1}), indicating decarbonisation of the energy system in China (-0.8% yr^{-1}), the European Union (-1.1% yr^{-1}), and the USA (-1.1% yr^{-1}), but no decline in India; the intensity of the rest of the world in aggregate also declined (-0.3% yr^{-1}). These trends are not sufficient to offset the growth in global

[1] All growth rates use a leap year adjustment that corrects for the extra day in 2024.

https://doi.org/10.5194/essd-2026-895
Preprint. Discussion started: 10 November 2026
© Author(s) 2026. CC BY 4.0 License.



Open Access Earth System Science Data Discussions

energy demand, which is driven by growing GDP globally and a weakening decline in energy per GDP, particularly in China and the USA.

Global net CO_2 emissions from land use averaged 1.3 ± 0.7 GtC yr^{-1} (4.9 ± 2.6 $GtCO_2$ yr^{-1}) for the 2016-2025 period. Emissions from clearing of forest and other vegetation, the main driver of global gross emissions, remain high at around 2.2 GtC yr^{-1} over the 2016-2025 period, highlighting the strong potential of halting deforestation for emissions reductions. Sequestration of 1.6 GtC yr^{-1} through re-/afforestation and forest regrowth in shifting cultivation cycles offsets more than two thirds of the deforestation emissions. In addition, smaller net emissions are due to wood harvest & forest management, peat drainage and peat fire. Regionally, the highest net emitters during 2016-2025 were Brazil, Indonesia, and the Democratic Republic of the Congo, with these 3 countries contributing 0.7 GtC yr^{-1}, more than half of global land-use CO_2 emissions. Net carbon dioxide removals from re-/afforestation were highest in China, the EU27, and the USA, with combined removals of 0.2 GtC yr^{-1} during 2016-2025.

Since the late-1990s, emissions from land use show a statistically significant decrease at a rate of around 0.2 GtC per decade, with a larger drop within the most recent decade. Preliminary data for 2026 suggest emissions to be around 1.4 GtC yr^{-1} (5.1 $GtCO_2$ yr^{-1}), 0.2 GtC above the 2025 level, partly due to increased emissions from Southeast Asia in response to the emerging El Niño.

Besides conventional carbon dioxide removal (CDR) through re/afforestation and storage in long-lived harvested wood products, novel CDR occurs through a variety of methods. Vegetation-based CDR methods, primarily biochar and bioenergy with carbon capture and storage, account for removals of about 0.0006 GtC yr^{-1} in 2025. Non-vegetation-based CDR transfers carbon from the atmosphere to the geosphere and amounts to about 0.000003 GtC yr^{-1}, primarily through enhanced rock weathering and alkalinity enhancement of water bodies, with a smaller contribution from direct air carbon capture and storage. Novel CDR represents less than 30 minutes of annual fossil CO_2 emissions

Total anthropogenic emissions (fossil and land use, including the carbonation sink) were 11.7 ± 0.9 GtC yr^{-1} (42.8 ± 3.2 $GtCO_2$ yr^{-1}) in 2025, with a preliminary estimate of 11.8 GtC yr^{-1} (43.3 $GtCO_2$ yr^{-1}) for 2026. Total anthropogenic emissions have grown more slowly over the last decade (0.3% yr^{-1} over the 2016-2025 period) compared to the previous decade (1.7% yr^{-1} over 2006-2015).

The remaining carbon budget from the beginning of 2027 for a 50% likelihood to limit warming to 1.5°C is nearly exhausted (40 GtC, 150 $GtCO_2$ left, equivalent to less than 4 years at the 2026 emissions levels), consistent with the warming of the planet attributed to human activities, which reached 1.37°C in 2025. The remaining carbon budgets to limit warming to 1.7°C and 2°C above the 1850-1900 level have been reduced to 140 GtC (510 $GtCO_2$, 12 years) and 280 GtC (1035 $GtCO_2$, 24 years) respectively.

https://doi.org/10.5194/essd-2026-895
Preprint. Discussion started: 10 November 2026
© Author(s) 2026. CC BY 4.0 License.



Open Access Earth System Science Data Discussions

The concentration of CO_2 in the atmosphere is set to reach 427.7 ppm in 2026, 53% above pre-industrial levels. The atmospheric CO_2 growth rate was 5.4 ± 0.02 GtC yr^{-1} (2.5 ppm) during the decade 2016-2025 (48% of total CO_2 emissions). The preliminary 2026 growth rate estimate is 4.6 GtC (2.2 ppm).

The ocean sink, the global uptake of anthropogenic CO_2 by the ocean, has taken up 27% of the total emissions in the past decade. The ocean sink has been stagnant since 2016, largely in response to climate variability modulating the growing sink trend. The ocean CO_2 sink was 3.0 ± 0.6 GtC yr^{-1} during the decade 2016-2025, with a preliminary estimate of 3.1 GtC yr^{-1} for 2026, slightly below 2025 levels.

The land sink, which is the global net uptake of CO_2 by the land excluding land use, has taken up 22% of the total emissions in the past decade. The land sink has been relatively stagnant since 2000, largely in response to climate variability and climate change offsetting the CO_2 induced growth. The land CO_2 sink was 2.5 ± 0.8 GtC yr^{-1} during the 2016-2025 decade but was increased to 3.6 GtC ± 0.8 GtC yr^{-1} in 2025, recovering from the El Niño induced reduced sink in 2024. The preliminary estimate for the land sink in 2026 is a further increase to 4.1 GtC.

The effects of climate change and climate variability act to reduce the ocean and land CO_2 sinks by 8% and 19% respectively, on average for the 2016-2025 period. Since 1960, the effect of climate change on the ocean and land sinks has contributed 7.3 ± 4.5 ppm (7%) to the observed atmospheric CO_2 increase ([6.6%]). The land sink is negatively affected by warming with decreased tropical plant productivity and enhanced ecosystem respiration globally. The ocean sink is negatively affected by altered oceanic circulation and surface warming which decreases CO_2 solubility**.**

So far in 2026, global fire carbon emissions have been close to the 2016-2025 average. Compared with fire CO_2 emissions for January-September periods throughout 2016-2025, global emissions of 2026 were between 8% below average in GFED5.1 and 3% above average in GFAS. Large positive emissions anomalies were seen in Southeast Asia,, while negative anomalies were seen in South America and North America. Our fire emissions estimates should not be directly compared with land-use emissions or the land sink because they represent a gross carbon flux to the atmosphere and do not account for post-fire recovery. They also do not distinguish between natural, climate-driven and land-use-related fires.

https://doi.org/10.5194/essd-2026-895
Preprint. Discussion started: 10 November 2026
© Author(s) 2026. CC BY 4.0 License.



Open Access Earth System Science Data Discussions

304

305 1 Introduction

306 The concentration of carbon dioxide (CO_2) in the atmosphere has increased from approximately 278
307 parts per million (ppm) in 1750 (Gulev et al., 2021), the beginning of the Industrial Era, to 425.6 ± 0.1
308 ppm in 2025 (Lan et al., 2026; Figure 1). The atmospheric CO_2 increase above pre-industrial levels was,
309 initially, primarily caused by the release of carbon to the atmosphere from deforestation and other land-
310 use change activities (Canadell et al., 2021). While emissions from fossil fuels started before the
311 Industrial Era, they became the dominant source of anthropogenic emissions to the atmosphere from
312 around 1950 and their relative share has continued to increase until present. Anthropogenic emissions
313 occur on top of an active natural carbon cycle that circulates carbon between the reservoirs of the
314 atmosphere, ocean, and terrestrial biosphere on time scales from sub-daily to millennial, while
315 exchanges with geologic reservoirs occur on longer timescales (Archer et al., 2009).

316 The global carbon budget (GCB) presented here refers to the mean, variations, and trends in the
317 perturbation of CO_2 in the environment, referenced to the beginning of the Industrial Era (defined here
318 as 1750). This paper describes the components of the global carbon cycle over the historical period with
319 a stronger focus on the recent period (since 1959, onset of robust atmospheric CO_2 measurements), the
320 last decade (2016-2025), the last year (2025) and the current year (2026). Finally, it provides
321 cumulative emissions from fossil fuels and land-use change since the year 1750, and since the year
322 1850 (the reference year for historical simulations in IPCC).

323 We quantify the input of CO_2 to the atmosphere by emissions from human activities, the growth rate of
324 atmospheric CO_2 concentration, and the resulting changes in the storage of carbon in the land and ocean
325 reservoirs in response to increasing atmospheric CO_2 levels, climate change and variability, and other
326 anthropogenic and natural changes (Figure 2). An understanding of this perturbation budget over time
327 and the underlying variability and trends of the natural carbon cycle is necessary to understand the
328 response of natural sinks to changes in climate, CO_2 and land-use change drivers, and to quantify
329 emissions compatible with a given climate stabilisation target.

330 The components of the CO_2 budget that are reported annually in this paper include separate and
331 independent estimates for the CO_2 emissions from (1) fossil fuel combustion and oxidation from all
332 energy and industrial processes; also including cement production and carbonation (E_{FOS}; GtC yr^{-1}) and
333 (2) the emissions resulting from deliberate human activities on land, including those leading to land-use
334 change (E_{LUC}; GtC yr^{-1}); and their partitioning among (3) the growth rate of atmospheric CO_2
335 concentration (G_{ATM}; GtC yr^{-1}), and the uptake of CO_2 (the 'CO_2 sinks') in (4) the ocean (S_{OCEAN}; GtC
336 yr^{-1}) and (5) on land (S_{LAND}; GtC yr^{-1}). The CO_2 sinks as defined here conceptually include the response
337 of the land (including inland waters and estuaries) and ocean (including coastal and marginal seas) to

https://doi.org/10.5194/essd-2026-895
Preprint. Discussion started: 10 November 2026
© Author(s) 2026. CC BY 4.0 License.



elevated CO_2 and changes in climate and other environmental conditions, although in practice not all processes are fully accounted for (see Section 2.10). Note that the term sink means that the net transfer of carbon is from the atmosphere to land or the ocean, but it does not imply any permanence of that sink in the future.

Global emissions and their partitioning among the atmosphere, ocean and land are in mass balance in the real world. Due to the combination of imperfect spatial and/or temporal data coverage, errors in each estimate, and smaller terms not included in our budget estimate (discussed in Section 2.10), the GCB independent estimates (1) to (5) above do not necessarily add up to zero. We hence estimate a budget imbalance (B_{IM}), which is a measure of the mismatch between the estimated emissions and the estimated changes in the atmosphere, land, and ocean, as follows:

$$B_{IM} = E_{FOS} + E_{LUC} - (G_{ATM} + S_{OCEAN} + S_{LAND}) \quad (1)$$

G_{ATM} is usually reported in ppm yr^{-1}, which we convert to units of carbon mass per year, GtC yr^{-1}, using 1 ppm = 2.124 GtC (Ballantyne et al., 2012; Table 1). Units of gigatonnes of CO_2 (or billion tonnes of CO_2) used in policy are equal to 3.664 multiplied by the value in units of GtC.

We also assess a set of additional lines of evidence derived from global atmospheric inversion system results (Section 2.7), observed changes in oxygen concentration (Section 2.8) and Earth System Models (ESMs) simulations (Section 2.9), all these methods closing the global carbon balance (zero B_{IM}).

We further quantify E_{FOS} and E_{LUC} by country, including both territorial and consumption-based accounting for E_{FOS} (see Section 2), and discuss missing terms from sources other than the combustion of fossil fuels (see Section 2.10). We also assess carbon dioxide removal (CDR) (see Sect. 2.2 and 2.3). Land-based CDR is significant, but already accounted for in E_{LUC} in equation (1) (Sect 3.2.2). Other CDR methods, not based on vegetation, are currently several orders of magnitude smaller than the other components of the budget (Sect. 3.3), hence these are not included in equation (1), or in the global carbon budget tables or figures (except for Figure 2 where CDR is shown primarily for illustrative purpose).

The global CO_2 budget has been assessed by the Intergovernmental Panel on Climate Change (IPCC) in all assessment reports (Watson et al., 1990; Schimel et al., 1995; Prentice et al., 2001; Denman et al., 2007; Ciais et al., 2013; Canadell et al., 2021), and by others (e.g., Ballantyne et al., 2012). The Global Carbon Project (GCP, www.globalcarbonproject.org, last access: 30 October 2026) has coordinated this cooperative community effort for the annual publication of global carbon budgets for the year 2005 (Raupach et al., 2007; including fossil emissions only), year 2006 (Canadell et al., 2007), year 2007 (GCP, 2008), year 2008 (Le Quéré et al., 2009), year 2009 (Friedlingstein et al., 2010), year 2010 (Peters et al., 2012), year 2012 (Le Quéré et al., 2013; Peters et al., 2013), year 2013 (Le Quéré et al., 2014), year 2014 (Le Quéré et al., 2015a; Friedlingstein et al., 2014), year 2015 (Jackson et al., 2016;

https://doi.org/10.5194/essd-2026-895
Preprint. Discussion started: 10 November 2026
© Author(s) 2026. CC BY 4.0 License.



Le Quéré et al., 2015b), year 2016 (Le Quéré et al., 2016), year 2017 (Le Quéré et al., 2018a; Peters et al., 2017a), year 2018 (Le Quéré et al., 2018b; Jackson et al., 2018), year 2019 (Friedlingstein et al., 2019; Jackson et al., 2019; Peters et al., 2020), year 2020 (Friedlingstein et al., 2020; Le Quéré et al., 2021), year 2021 (Friedlingstein et al., 2022a; Jackson et al., 2022), year 2022 (Friedlingstein et al., 2022b), the year 2023 (Friedlingstein et al., 2023), the year 2024 (Friedlingstein et al., 2025a), and most recently the year 2025 (Friedlingstein et al., 2026a). Each of these papers updated previous estimates with the latest available information for the entire time series.

We adopt a range of ±1 standard deviation (σ) to report the uncertainties in our global estimates, representing a likelihood of 68% that the true value will be within the provided range if the errors have a gaussian distribution, and no bias is assumed. Note that when less than 10 individual data are available for an estimate (e.g., atmospheric inversions, ESMs), we provide the full range, as opposed to the standard deviation. The choice of reporting a ±1 σ reflects the difficulty of characterising the uncertainty in the CO_2 fluxes between the atmosphere and the ocean and land reservoirs individually, particularly on an annual basis, as well as the difficulty of updating the CO_2 emissions from land-use change. A likelihood of 68% provides an indication of our current capability to quantify each term and its uncertainty given the available information. The uncertainties reported here combine statistical analysis of the underlying data, assessments of uncertainties in the generation of the datasets, and expert judgement of the likelihood of results lying outside this range. The limitations of current information are discussed in the paper and have been examined in detail elsewhere (Ballantyne et al., 2015; Zscheischler et al., 2017). We also use a qualitative assessment of confidence level to characterise the annual estimates from each term based on the type, amount, quality, and consistency of the different lines of evidence as defined by the IPCC (Stocker et al., 2013).

This paper provides a detailed description of the datasets and methodology used to compute the global carbon budget estimates for the industrial period, from 1750 to 2026, and in more detail for the recent period since 1959. This paper is updated every year using the format of 'living data' to keep a record of budget versions and the changes in new data, revision of data, and changes in methodology that lead to changes in estimates of the carbon budget. All underlying data used to produce the budget and additional materials associated with the release of each new version are available via the Global Carbon Budget website (https://globalcarbonbudget.org/ , last access: 30 October 2026), with emissions also available through the Global Carbon Atlas (http://www.globalcarbonatlas.org, last access: 30 October 2026) and Our World in Data ((https://ourworldindata.org/co2-emissions, last access: 30 October 2026). See data availability section for more information. With this approach, we aim to provide the highest transparency and traceability in the reporting of CO_2, the key driver of climate change.

https://doi.org/10.5194/essd-2026-895
Preprint. Discussion started: 10 November 2026
© Author(s) 2026. CC BY 4.0 License.



2 Methods

Multiple organisations and research groups around the world generated the original measurements and data used to complete the global carbon budget. The effort presented here is thus mainly one of synthesis, where results from individual groups are collated, analysed, and evaluated for consistency. We facilitate access to original data with the understanding that primary datasets will be referenced in future work (see Table 2 for how to cite the datasets, and Section on data availability). Descriptions of the measurements, models, and methodologies follow below, with more detailed descriptions of each component provided as Supplementary Information (Supplement Tables S1 to S5). In the GCB, when possible, we account for adjustments and corrections to the components estimates. We refer to 'adjustments' when accounting for known processes not included in one estimate (e.g. river adjustment for atmospheric inversions and fCO_2-products), while we refer to 'corrections' when addressing known biases in one estimate (e.g. warm layer and cool skin effect correction for fCO_2-products).

This is the 21th version of the global carbon budget and the 15th revised version in the format of a living data update in Earth System Science Data. It builds on the latest published global carbon budget of Friedlingstein et al. (2026a). The main changes this year are: the inclusion of (1) data to year 2025 and a projection for the global carbon budget for year 2026; (2) a new methodology to estimate S_{LAND} from DGVMs, accounting for the historical changes in forest cover, and (3) an extended model evaluation to determine the scaling factor for the ocean models. Other methodological differences are summarised in Table 3 and previous changes since 2006 are provided in Table S10.

2.1 Fossil CO_2 emissions (E_{FOS})

2.1.1 Historical period 1850-2025

The estimates of global and national fossil CO_2 emissions (E_{FOS}) include the oxidation of fossil fuels through both combustion (e.g., transport, heating) and chemical oxidation (e.g., carbon anode decomposition in aluminium refining) activities, and the decomposition of carbonates in industrial processes (e.g. the production of cement). We also include CO_2 uptake from the cement carbonation process. Several emissions sources are not estimated or not fully covered: coverage of emissions from lime production are not global, and decomposition of carbonates in glass and ceramic production are included only for the "Annex 1" countries of the United Nations Framework Convention on Climate Change (UNFCCC) for lack of activity data. These omissions are considered to be minor. Short-cycle carbon emissions - for example from combustion of biomass - are not included here but are accounted for in the CO_2 emissions from land use (see Section 2.2).

Our estimates of fossil CO_2 emissions rely on data collection by many other parties. Our goal is to produce the best estimate of this flux, and we therefore use a prioritisation framework to combine data

https://doi.org/10.5194/essd-2026-895
Preprint. Discussion started: 10 November 2026
© Author(s) 2026. CC BY 4.0 License.



Open Access Earth System Science Data Discussions

from different sources that have used different methods, while being careful to avoid double counting and undercounting of emissions sources. We begin with official reporting from Annex 1 countries' official submissions to the UNFCCC, add in data for earlier years and other countries from the CDIAC-FF emissions dataset, itself derived largely from UN energy data, and extend emissions to 2025 using energy growth rates reported by the Energy Institute. We add process emissions from cement production from Andrew (2026) as well as lime-production emissions for some key countries, and then additionally replace estimates using data from what we consider to be superior sources. All data points are potentially subject to revision, not just the latest year. For full details see Andrew and Peters (2026).

Other estimates of global fossil CO_2 emissions exist, and these are compared by Andrew (2020a). The most common reason for differences in estimates of global fossil CO_2 emissions is a difference in which emissions sources are included in the datasets. Datasets such as those published by the Energy Institute, the US Energy Information Administration, and the International Energy Agency's 'CO_2 emissions from fuel combustion' are all generally limited to emissions from combustion of fossil fuels. In contrast, datasets such as PRIMAP-hist, CEDS, EDGAR, and GCP's dataset aim to include all sources of fossil CO_2 emissions. See Andrew (2020a) for detailed comparisons and discussion.

Cement products absorb CO_2 from the atmosphere over their lifetimes, a process known as 'cement carbonation'. We estimate this CO_2 sink, from 1931 onwards, as the average of three studies in the literature (Cao et al., 2020; Niu et al., 2025; Xiao et al., 2026). These three datasets differ in magnitude, with Xiao et al. (2026) having much lower values due partly to the intentional omission of mortar and end-of-life phases. The trends of the three studies are very similar, which can be explained by their strong dependence on annual cement production data. The estimates by Cao et al. (2020) have not been updated, but since carbonation is a function of both current and previous cement production, we extend these estimates to 2025 by using the growth rate derived from the smoothed cement emissions (10-year smoothing) fitted to the carbonation estimates. In the present budget, we always include the cement carbonation carbon sink in the fossil CO_2 emission component (E_{FOS}) unless explicitly stated otherwise.

We use the Kaya Identity for a simple decomposition of CO_2 emissions into key drivers (Raupach et al., 2007). While there are variants (Peters et al., 2017b), we focus here on a decomposition of CO_2 emissions into population, GDP per person, energy use per unit of GDP, and CO_2 emissions per unit of energy. Multiplying these individual components together returns the CO_2 emissions. Using the decomposition, it is possible to attribute the change in CO_2 emissions to the change in each of the drivers. This method gives a first order understanding of what causes CO_2 emissions to change each year.

https://doi.org/10.5194/essd-2026-895
Preprint. Discussion started: 10 November 2026
© Author(s) 2026. CC BY 4.0 License.



2.1.2 2026 projection

We provide a projection of global fossil CO_2 emissions in 2026 by combining separate projections for China, USA, EU, India, Japan, and for all other countries combined. The methods are different for each of these. For China we use growth rates from the 2026 edition of the National Bureau of Statistics' Statistical Communique along with cement clinker trade data and estimated changes in lime production. For the USA our projection is taken directly from the Energy Information Administration's (EIA) Short-Term Energy Outlook (EIA, 2026), combined with the year-to-date growth rate of cement clinker production. For the EU we use monthly energy data through July/August from Eurostat to derive estimates of monthly CO_2 emissions using updated methods after Andrew (2021), with extensions of natural gas using daily demand estimates derived from ENTSOG using the method of Fernández-Blanco et al., (2024) and of coal using daily power generation data from ENTSO-E. EU cement emissions are based on available production data through August from three of the largest producers, Germany, Poland, and Spain, as well as production indices for Italy and France. India's projected emissions are derived from monthly estimates through August/September using the methods of Andrew (2020b), while Japan's emissions are derived from monthly estimates through July using the methods of Kunimitsu & Andrew (2026). Emissions from international transportation (bunkers) are estimated separately for aviation and shipping. Changes in aviation emissions are derived by analysis of monthly IATA data. Shipping emissions are derived by analysis of estimates of sales of bunker fuels and estimates of emissions from OECD. Emissions for the rest of the world are derived for coal and cement using projected growth in economic production from the IMF (2026) combined with extrapolated changes in emissions intensity of economic production; for oil using a global constraint from EIA; and for natural gas using a global constraint from IEA. More details on the E_{FOS} methodology and its 2026 projection can be found in Supplement S.1.

We compare our 2026 projection with the Carbon Monitor (2026). Carbon Monitor is a dataset of daily emissions constructed using hourly to daily proxy data (e.g., electricity consumption, travel patterns, etc) instead of energy use data (Liu et al., 2020a; Liu et al., 2020b). Emissions estimates through July are combined with a projection to give a full-year 2026 estimate.

2.2 CO_2 emissions from land-use change and land management (E_{LUC})

2.2.1 Historical period 1850-2025

The net CO_2 flux from land-use change and land management (E_{LUC}, hereafter referred to as net land-use change emissions) accounts for CO_2 emissions and removals resulting from anthropogenic land-use activities. It includes fluxes from deforestation and clearing of other natural vegetation, afforestation, logging and forest degradation (including harvest activity), shifting cultivation (cycle of cutting forest for agriculture, then abandoning), regrowth of forests and other natural vegetation (following wood

https://doi.org/10.5194/essd-2026-895
Preprint. Discussion started: 10 November 2026
© Author(s) 2026. CC BY 4.0 License.



harvest or agriculture abandonment), peat burning and peat drainage, and transitions between cropland, pasture and urban areas.

Updated estimates from the three bookkeeping models BLUE (Hansis et al., 2015), LUCE (Qin et al. 2024), and OSCAR (Gasser et al., 2020) are used to quantify gross emissions, gross removals, and the resulting net E_{LUC}. Bookkeeping models track changes in vegetation and soil carbon stocks following land-use transitions and due to land management, accounting for carbon losses through decay, carbon transfer to harvested wood products, and carbon uptake through regrowth (see Supplement S.2 for a detailed methodological description). The bookkeeping models consider the effects of environmental changes, such as atmospheric CO_2 increase, on vegetation and soil carbon densities, to estimate E_{LUC} (Gasser et al., 2020; Dorgeist et al., 2024). Emissions from peat burning and peat drainage are added from external datasets (see Supplement S.2.2): peat fire emissions from the Global Fire Emission Database (GFED5.1; van der Werf et al., 2025) and peat drainage emissions averaged from estimates of the Food Agriculture Organization (Conchedda and Tubiello, 2020; FAO, 2026a) and from simulations with the DGVM ORCHIDEE-PEAT (Qiu et al., 2021) and the DGVM LPX-Bern (Lienert and Joos, 2018; Müller and Joos, 2021). GFED5 represents a major revision of GFED4, with the most substantial change being improved accounting for burned area from small fires (Chen et al., 2023). Other improvements include a revised fuel consumption scheme and the use of higher-resolution input data, collectively resulting in a 65% increase in estimated fire carbon emissions compared with GFED4, although changes in deforestation and peatland fire emissions are smaller (van der Werf et al., 2025).

Uncertainty estimates were derived from the Dynamic Global Vegetation Models (DGVMs) ensemble for the time period prior to 1960, and using for the recent decades an uncertainty range of ±0.7 GtC yr^{-1}, which is a semi-quantitative measure for annual and decadal emissions and reflects our best value judgement that there is at least 68% chance (±1σ) that the true land-use change emission lies within the given range, for the range of processes considered here.

The GCB E_{LUC} estimates follow the CO_2 flux definition of global carbon cycle models and differ from IPCC definitions of land use, land-use change and forestry (LULUCF) adopted in national greenhouse gas inventories (NGHGI) for reporting under the UNFCCC. The latter typically include terrestrial fluxes occurring on all land that countries define as managed, following the IPCC managed land proxy approach (Grassi et al., 2018). This partly includes fluxes due to environmental change (e.g., atmospheric CO_2 increase), which are part of S_{LAND} in our definition. As a result, global emission estimates are smaller for NGHGI than for the global carbon budget definition (Grassi et al., 2023). Using the NGHGI data collected and processed in the LULUCF data hub (V4.1.0, Melo et al. 2026) and estimates of natural fluxes in managed forests from DGVMs, we translate the GCB and NGHGI definitions to each other (see Supplement S.2.4), to provide a comparison of the anthropogenic carbon budget as reported in GCB to the official country reporting to the UNFCCC convention. We further compare these estimates with the net atmosphere-to-land flux from atmospheric inversion systems (see

https://doi.org/10.5194/essd-2026-895
Preprint. Discussion started: 10 November 2026
© Author(s) 2026. CC BY 4.0 License.



Section 2.7), averaged over managed land only. We also show Food and Agriculture Organization (FAO) estimates of CO_2 land fluxes, comprised of emissions from net forest conversion (proxy of deforestation) and net fluxes on forest land (Tubiello et al., 2026), and emissions from peat drainage (Conchedda and Tubiello, 2020) and peat fires (Prosperi et al., 2020). See Supplementary S.2.4 for more details.

E_{LUC} contains a range of fluxes that are related to Carbon Dioxide Removal (CDR). CDR is defined as the set of anthropogenic activities that remove CO_2 from the atmosphere, in addition to the Earth's natural processes (such as carbon uptake in response to atmospheric CO_2 increase), and store it in durable form, such as in forest biomass, soils, long-lived products, oceans or geological reservoirs. Here, we quantify vegetation-based CDR that is implicitly or explicitly captured by land-use fluxes (CDR not based on vegetation is discussed in Section 2.3). We quantify CDR through re/afforestation from the three bookkeeping estimates by separating permanent increases in forest cover, which counts as CDR, from forest regrowth in shifting cultivation cycles (not part of CDR; see Supplement S.2.2). It should be noted that the permanence of the storage under climate risks such as fire is increasingly questioned. Other CDR activities related to land use by using biomass from terrestrial plants as input but not fully accounted for in our E_{LUC} estimate include the transfer of carbon to harvested wood products (HWP), bioenergy with carbon capture and storage (BECCS), biochar soil amendment, biomass burial, bio-oil storage, and biomass sinking (when it uses land-grown biomass) (Babiker et al., 2022; Edwards et al., 2026). The different bookkeeping models all represent HWP but with varying details concerning product usage and their lifetimes. The other CDR methods using terrestrial biomass as input are currently only represented in bookkeeping and DGVM models regarding the CO_2 removal through photosynthesis, without accounting for the durable storage. HWP, BECCS, biochar soil amendment, biomass burial, bio-oil storage, and biomass sinking are typically counted as CDR once the transfer to the durable storage site occurs and not when the CO_2 is removed from the atmosphere, which complicates a direct comparison to the GCB approach to quantify annual fluxes to and from the atmosphere. We provide estimates for CDR through HWP, BECCS, biochar soil amendment, biomass burial, bio-oil storage, and biomass sinking based on independent studies in Section 3.2.2. We do not add them to our E_{LUC} estimate to avoid potential double-counting that arises from the partial consideration of these methods in the bookkeeping and DGVM models and to avoid inconsistencies from the temporal discrepancy between transfer to storage and removal from the atmosphere. More details on the E_{LUC} methodology can be found in Supplement S.2.

2.2.2 2026 Projection

We project the 2026 net land-use emissions for BLUE, OSCAR, and LUCE based on their E_{LUC} estimates for 2025 and adding the anomalies in carbon emissions from peat fires in equatorial Asia and tropical deforestation and degradation fires (2026 emissions relative to 2025 emissions) from GFED5.1

https://doi.org/10.5194/essd-2026-895
Preprint. Discussion started: 10 November 2026
© Author(s) 2026. CC BY 4.0 License.



(van der Werf et al., 2025) estimated using active fire data (MCD14ML; Giglio et al., 2016). Peat drainage is assumed to be unaltered as it has low interannual variability.

2.3 Carbon Dioxide Removal (CDR) not based on vegetation

Some CDR involves CO_2 fluxes via land use (or marine biomass), which is included in our estimate of E_{LUC} (re/afforestation) or provided separately in Section 3.2.2 (HWP, BECCS, biochar soil amendment, biomass burial, bio-oil storage, and biomass sinking). Other CDR not based on vegetation occurs through CO_2 fluxes directly from the air to the geosphere, which is reported in Section 3.3. The majority of this derives from enhanced weathering through the application of crushed rock to soils, alkalinity enhancement of water bodies, and the production of solid mineral products with CO_2 captured from the atmosphere (including biogenic CO_2 from BECCS or biochar soil amendment, if applied this way), with smaller contributions from Direct Air Carbon Capture and Storage (DACCS). Note that Friedlingstein et al. (2026a) included bio-oil storage and biomass burial and sinking within the estimates for CDR not based on vegetation, but given these methods both use biomass to capture CO_2 they have been accounted for in the E_{LUC}. For CDR not based on vegetation, we use updated 2026 data (Edwards et al., 2026), which compiles and harmonises reported CDR from a combination of existing databases, surveys, and novel research. Currently, there are no internationally agreed methods for reporting these types of CDR, implying that estimates are based on self-disclosure by projects following their own protocols or protocols produced by third party registries. As such, the fractional uncertainty on these numbers should be viewed as substantial, and numbers are liable to change in future years as protocols are harmonised and improved.

2.4 Growth rate in atmospheric CO_2 concentration (G_{ATM})

2.4.1 Historical period 1850-2025

The rate of growth of the atmospheric CO_2 concentration is provided for years 1959-2024 by the US National Oceanic and Atmospheric Administration Global Monitoring Laboratory (NOAA/GML; Lan et al., 2026), which includes recent revisions to the calibration scale of atmospheric CO_2 measurements (WMO-CO2-X2019; Hall et al., 2021). For the 1959-1979 period, the global growth rate is based on measurements of atmospheric CO_2 concentration averaged from the Mauna Loa and South Pole stations, as observed by the CO_2 Program at Scripps Institution of Oceanography (SIO, Keeling et al., 1976). For the 1980-2024 period, the global growth rate is based on the average of multiple stations selected from the marine boundary layer sites with well-mixed background air (Lan et al., 2024), after fitting a smooth curve through the data for each station as a function of time, and averaging by latitude band (Masarie and Tans, 1995). The annual growth rate is estimated by Lan et al. (2025) from atmospheric CO_2 concentration by taking the average of the most recent December-January months corrected for the average seasonal cycle and subtracting this same average one year earlier. To obtain

https://doi.org/10.5194/essd-2026-895
Preprint. Discussion started: 10 November 2026
© Author(s) 2026. CC BY 4.0 License.



Open Access Earth System Science Data Discussions

G_{ATM}, the observation-based growth rate in units of ppm yr^{-1} is converted to units of GtC yr^{-1} by multiplying by a factor of 2.124 GtC per ppm, assuming instantaneous mixing of CO_2 throughout the atmosphere (Ballantyne et al., 2012; Table 1). There is high confidence in the observations because they are based on direct measurements from stations distributed around the world (Lan et al., 2024) with all CO_2 measurements consistently measured against the same CO_2 standard scale (WMO X2019) defined by a suite of gas standards (Hall et al., 2021). However, the conversion to estimates of G_{ATM} in GtC yr^{-1} incurs large uncertainty on annual time scale as discussed next.

The uncertainty around G_{ATM} is due to three main factors. First, the network composition of the marine boundary layer sites with some sites being introduced or removed over time, gaps in sites time series, etc. This uncertainty was estimated with a bootstrap method by constructing 100 "alternative" networks (Steele et al., 1992; Masarie and Tans, 1995; Lan et al., 2026). Second, the analytical uncertainty that describes the short- and long-term uncertainties associated with the CO_2 analyzers. A Monte Carlo method was used to estimate the total analytical uncertainty by randomly selecting errors to add to each observation from a normal distribution of combined short- and long-term uncertainties. Prior to the 1980s when analyzers were less precise and CO_2 measurement scale was slightly less well defined, larger analytical errors were assigned to account for these factors. However, the network uncertainty remains the larger term of uncertainty. The first and second uncertainties are reported as 1-sigma standard deviations (i.e., 68% confidence interval), and summed in quadrature to determine the global surface growth rate uncertainty, which averaged to 0.085 ppm (Lan et al., 2024). Third, the uncertainty associated with using the average CO_2 concentration from a surface network to approximate the true atmospheric average CO_2 concentration (mass-weighted, in 3 dimensions) as needed to assess the total atmospheric CO_2 burden. In reality, CO_2 variations measured at the stations will not exactly track changes in total atmospheric burden, with offsets in magnitude and phasing due to vertical and horizontal mixing (Pandey et al., 2025). This effect must be very small on decadal and longer time scales, when the atmosphere can be considered well mixed. The long-term CO_2 increase in the stratosphere lags the increase (meaning lower concentrations) that we observe in the marine boundary layer, while the continental boundary layer (where most of the emissions take place) leads the marine boundary layer with higher concentrations. These effects nearly cancel each other on decadal time scales, when the growth rate is nearly the same everywhere (Ballantyne et al., 2012). We therefore maintain an uncertainty around the annual growth rate based on the multiple stations dataset ranges between 0.11 and 0.72 GtC yr^{-1}, with a mean of 0.61 GtC yr^{-1} for 1959-1979 and 0.17 GtC yr^{-1} for 1980-2024, when more measurement sites were available (Lan et al., 2026). We estimate the uncertainty of the decadal averaged growth rate after 1980 at 0.02 GtC yr^{-1} based on the annual growth rate uncertainty but stretched over a 10-year interval. For years prior to 1980, we estimate the decadal averaged uncertainty to be 0.07 GtC yr^{-1} based on a factor proportional to the annual uncertainty prior and after 1980 (0.02 * [0.61/0.17] GtC yr^{-1}).

https://doi.org/10.5194/essd-2026-895
Preprint. Discussion started: 10 November 2026
© Author(s) 2026. CC BY 4.0 License.



To estimate the total carbon accumulated in the atmosphere since 1750 or 1850, we use an atmospheric CO_2 concentration of 278.0 ± 3 ppm or 287.7 ± 3 ppm, respectively (Gulev et al., 2021). For the construction of the historical budget shown in Figure 3, we use the fitted estimates of CO_2 concentration from Joos and Spahni (2008) to estimate the annual atmospheric growth rate (see Supplement S.7). The uncertainty of ±3 ppm (converted to ±1σ) is taken directly from the IPCC's AR5 assessment (Ciais et al., 2013). Typical uncertainties in the growth rate in atmospheric CO_2 concentration from ice core data are equivalent to ±0.1-0.15 GtC yr^{-1} as evaluated from the Law Dome data (Etheridge et al., 1996) for individual 20-year intervals over the period from 1850 to 1960 (Bruno and Joos, 1997).

2.4.2 Satellite-based (2010-present)

Further opportunities to estimate global CO_2 growth rates are offered by space-based platforms such as GOSAT (since 2010) and OCO-2 (since 2015). Their recorded short-wave infrared spectra allow retrieval of column-averaged dry-air mole fraction of carbon dioxide (XCO_2) over cloud-free scenes over land and ocean with footprints of 80 (GOSAT) and 3 (OCO-2) km^2 respectively. The columns are not full integrals; the sensitivity to surface and lower-tropospheric CO_2 mole fractions is much higher than to upper tropospheric and stratospheric CO_2. However, for the purpose of calculating atmospheric growth rates, the sensitivity is not limiting, as the pressure-weighted sensitivity is still above 0.5 in the stratosphere (Pandey et al. 2024) and priors used in OCO-2 account for the slow stratospheric-tropospheric exchanges using the age of air (Laughner et al. 2023). Here, we use whole atmosphere growth rates using the Growth Rate from Satellite Observations (GRESO) approach (Pandey et al., 2024). We specifically note that OCO-2 and GOSAT retrievals are evaluated against surface-based remote sensing (Total Column Carbon Observing Network) data, which in turn are tied to atmospheric observations (from aircraft and using aircore) (Wunch et al., 2017). Furthermore, OCO-2 retrievals use a CO_2 mole fraction profiles prior tied to NOAA GML in-situ flask records at Mauna Loa (MLO) and American Samoa (SMO) measurement stations (Laughner et al., 2023). For details on evaluation, bias correction, and spatiotemporal coverage of the OCO-2 retrievals we refer to O'Dell et al. (2018) and Taylor et al. (2026); the GOSAT retrievals use the same ACOS version 11 algorithm.

Relative to surface observations, the GRESO product typically reflects tropical growth rate anomalies earlier and sees whole atmosphere carbon stock changes with a lower latency. The GRESO growth rates presented here use both land and ocean observations of OCO-2 and GOSAT, providing global sampling of the atmosphere. We used GRESO to present an alternative quantification of the atmospheric carbon stock changes in G_{ATM}, using the reported 1-sigma uncertainty, which is 0.08–0.13 ppm yr^{-1} for 2015–2025 and 0.13–0.14 ppm yr^{-1} for the GOSAT-only years 2010–2014. The mean difference between GRESO and surface-data derived G_{ATM} is -0.01 ± 0.19 ppm yr^{-1} over the 2010–2025 (n=16 years) period.

https://doi.org/10.5194/essd-2026-895
Preprint. Discussion started: 10 November 2026
© Author(s) 2026. CC BY 4.0 License.



2.4.3 2026 projection

We provide an assessment of G_{ATM} for 2026 as the average of two methods. First, the GCB regression method models monthly global-average atmospheric CO_2 concentrations and derives the increment and annual average from these. The model uses lagged observations of concentration (Lan et al., 2026): both a 12-month lag, and the lowest lag that will allow model prediction to produce an estimate for the following January, recalling that the G_{ATM} increment is derived from December/January pairs. The largest driver of interannual changes is the ENSO signal (Betts et al., 2016), so the monthly ENSO 3.4 index (Huang et al., 2017) is included in the model. Given the natural lag between sea-surface temperatures and effects on the biosphere, and in turn effects on globally mixed atmospheric CO_2 concentration, a lagged ENSO index is used, and we use both a 5-month and a 6-month lag. The combination of the two lagged ENSO values helps reduce possible effects of noise in a single month. To help characterise the seasonal variation, we add month as a categorical variable. Finally, we flag the period affected by the Pinatubo eruption (August 1991 - November 1993) as a categorical variable.

The second method uses the multi-model mean and uncertainty of the 2026 G_{ATM} estimated by the ESMs prediction system (see Section 2.9). We then take the average of the GCB regression and ESMs G_{ATM} estimates, with their respective uncertainty combined quadratically.

Similarly, the projection of the 2026 global average CO_2 concentration (in ppm), is calculated as the average of the estimates from the two methods. For the GCB regression method, it is the annual average of global concentration over the 12 months of 2026; for the ESMs, it is the observed global average CO_2 concentration for 2025 plus the annual increase in 2026 of the global average CO_2 concentration, which is an average of NOAA/GML measurements from January to June (Lan et al., 2026) and predictions of the ESMs multi-model mean from July to December (see Section 2.9).

2.5 Ocean CO_2 sink

2.5.1 Historical period 1850-2025

The reported estimate of the global ocean anthropogenic CO_2 sink S_{OCEAN} is derived as the average of two estimates. The first estimate is derived as the mean over an ensemble of ten global ocean biogeochemistry models (GOBMs, Table 4 and Table S2). The second estimate is obtained as the mean over an ensemble of ten surface ocean fCO_2-observation-based data-products (Table 4 and Table S3).

The GOBMs simulate both the natural and anthropogenic CO_2 cycles in the ocean. They constrain the anthropogenic air-sea CO_2 flux (the dominant component of S_{OCEAN}) by the transport of carbon into the ocean interior, which is also the controlling factor of present-day ocean carbon uptake in the real world. They cover the full globe and all seasons and were evaluated against surface ocean carbon observations, suggesting they are suitable to estimate the annual ocean carbon sink (Hauck et al., 2020). We derive

https://doi.org/10.5194/essd-2026-895
Preprint. Discussion started: 10 November 2026
© Author(s) 2026. CC BY 4.0 License.



Open Access Earth System Science Data Discussions

713 S_{OCEAN} from GOBMs by using a simulation (sim A) with historical forcing of climate and atmospheric
714 CO_2 from GCB (Section 2.4), accounting for model biases and drift from a control simulation (sim B)
715 with constant atmospheric CO_2 and normal year climate forcing. A third simulation (sim C) with
716 historical atmospheric CO_2 increase and normal year climate forcing is used to attribute the ocean sink
717 to CO_2 (sim C minus sim B) and climate (sim A minus sim C) effects. A fourth simulation (sim D;
718 historical climate forcing and constant atmospheric CO_2) is used to compare the change in
719 anthropogenic carbon inventory in the interior ocean (sim A minus sim D) to the observation-based
720 estimate of Müller et al. (2023) with the same flux components (steady state and non-steady state
721 anthropogenic carbon flux).

722 The GOBMs capability to simulate S_{OCEAN} was assessed with the International Ocean Model
723 Benchmarking (IOMB) Scheme (Fu et al., 2022) using various statistical measures of physical and
724 biogeochemical fields (text S3.3), with an evaluation of the simulated inventories of transient tracers
725 (CFC11, CFC12, SF6, Matsumoto et al., 2004, text S3.3) and an emergent constraint approach
726 accounting for biases in circulation and carbonate chemistry in models (Terhaar et al., 2022, text S3.3).
727 These evaluations target the physical-chemical processes that drive anthropogenic carbon uptake
728 (ventilation, carbonate chemistry, solubility of CO_2 in seawater). In addition, we report the interior
729 ocean accumulation of anthropogenic carbon for GOBMs and compare this to observation-based
730 estimates (text S3.6 and section 3.6.5). This process-based evaluation provides evidence in support of
731 the GOBM ensemble average capturing S_{OCEAN} and its driving processes well (ventilation, carbonate
732 system buffer capacity, Goris et al., 2018, Terhaar et al., 2021, Bourgeois et al., 2022, Terhaar et al.,
733 2022, Vaittinada Ayar et al., 2022). Therefore, the scaling factor to account for known model biases
734 that was introduced in GCB2025 is set to 1.0, i.e. the GOBM estimate is scaled by 0% this year (section
735 3.6.5). This is applied only for the final estimate of S_{OCEAN} (text S3.2)

736 The fCO_2-products are tightly linked to observations of fCO_2 (fugacity of CO_2, which equals pCO_2
737 corrected for the non-ideal behaviour of the gas; Pfeil et al., 2013), which carry imprints of temporal
738 and spatial variability, but are also sensitive to uncertainties in gas-exchange parameterizations and
739 data-sparsity (Fay et al., 2021, Gloege et al., 2021, Hauck et al., 2023a). Their asset is the assessment of
740 the mean spatial pattern of variability and its seasonality (Hauck et al., 2020, Gloege et al. 2021, Hauck
741 et al., 2023a, McKinley et al 2026). To better understand biases and trends in fCO_2-products, the fCO_2-
742 product community conducted a series of experiments (Roobaert et al 2026, in review, see section S3).
743 Additionally, we use independent measurements from the SOCAT (Surface Ocean CO_2 Atlas) flag E
744 dataset (uncertainty less than 10 µatm) (Bakker et al., 2016) and calculated fCO_2 from the Global Ocean
745 Data Analysis Project GLODAP (Lauvset et al., 2024) to further benchmark the fCO_2 products. Since
746 GCB2025, submissions that perform a temperature correction to the underlying observations are
747 included, as new evidence emerged from field and modelling studies, recommending adopting a
748 temperature correction to the fCO_2 from measurement depth to the surface skin layer where the gas

https://doi.org/10.5194/essd-2026-895
Preprint. Discussion started: 10 November 2026
© Author(s) 2026. CC BY 4.0 License.



Open Access Earth System Science Data Discussions

exchange takes place (Dong et al., 2024a, Ford et al., 2024a, Bellenger et al., 2023, Ford et al 2026a). In GCB2026, three out of ten submissions apply such a correction (UExP-FFN-U, JMA-MLR and AOML-ET). Additionally, following Friedlingstein et al (2025b), we now also add 0.18 GtC yr^{-1} (multiplied by 7/10 as three products already include a temperature correction) to the multi fCO_2-product average when calculating S_{OCEAN} to account for the warm layer and cool skin effect (See Supplement S3.1). This correction is based on a recent field study (Ford et al., 2024a) and broadly consistent in magnitude with a GOBM study (Bellenger et al. 2023).

The global fCO_2-based flux estimates were adjusted to remove the pre-industrial natural ocean source of CO_2 to the atmosphere of 0.65 ± 0.3 GtC yr^{-1}, arising from the transfer of carbon from land to ocean via rivers (Regnier et al., 2022), to satisfy our definition of S_{OCEAN} (Hauck et al., 2020). This CO_2 outgassing adjustment was distributed over the latitudinal bands using the regional distribution of Lacroix et al. (2020; North: 0.14 GtC yr^{-1}, Tropics: 0.42 GtC yr^{-1}, South: 0.09 GtC yr^{-1}). Acknowledging that this distribution is based on only one model, the advantage is that a gridded field is available, and the adjustment can be calculated for the three latitudinal bands and the RECCAP regions (REgional Carbon Cycle Assessment and Processes, RECCAP2; Ciais et al., 2022, Poulter et al., 2022, DeVries et al., 2023). A new study suggests a roughly equal share between riverine outgassing across the three regions (Planchat et al., 2025). Accordingly, the regional distribution is associated with an additional uncertainty in addition to the large uncertainty around the global estimate (Crisp et al., 2022; Gruber et al., 2023). Anthropogenic perturbations of river carbon and nutrient transport to the ocean are not represented in the process models used to quantify S_{OCEAN}.

New this year, for the regional analysis (Figures 14 and 15), we also subtract the preindustrial mean state derived from GOBMs, to only show anthropogenic perturbation (See Supplement S3.1). This is not necessary on the global scale, where the preindustrial mean state is zero.

We calculate S_{OCEAN} as the average of the GOBM ensemble mean and the fCO_2-product ensemble mean from 1990 onwards, including the corrections on the fCO_2-product ensemble mean as described above. For the 1959-1989 period, it is calculated as the GOBM ensemble mean plus half of the offset between GOBMs and fCO_2-products ensemble means over 1990-2001, also including the above corrections. In addition, two diagnostic ocean models are used to estimate S_{OCEAN} over the industrial era (1781-1958, Khatiwala et al. (2013) and DeVries (2014)).

S_{OCEAN} is also compared to the change in the total dissolved inorganic carbon inventory in the interior ocean from the observation-based estimates of Keppler et al. (2023), Müller et al. (2023) and an observationally-constrained ocean inverse model (DeVries, 2022). To facilitate the synthesis of these comparisons into a single mean bias estimate, each of the three ocean interior products was - if needed - adjusted for missing carbon flux components to match the definition of S_{OCEAN} and scaled to full decadal periods reported in Table 6 (details of these adjustments are provided in Supplement S3.6).

https://doi.org/10.5194/essd-2026-895
Preprint. Discussion started: 10 November 2026
© Author(s) 2026. CC BY 4.0 License.



We assign a temporally varying uncertainty ranging between ± 0.53 to 0.68 GtC yr^{-1} to the ocean sink based on a combination of random (ensemble standard deviation) and systematic uncertainties (GOBMs bias in anthropogenic carbon accumulation, previously reported uncertainties in fCO_2-products) that are combined as a Gaussian mixture model (see Supplement S3.5). This approach is consistent within the GCB, and is close to the independent uncertainty assessment of the fCO_2-products alone of up to 0.76 GtC yr^{-1} [range 0.60 to 0.85 Pg C yr^{-1}] (Ford et al. 2024). We assess a medium confidence level to the annual ocean CO_2 sink and its uncertainty because it is based on multiple lines of evidence, it is consistent with ocean interior carbon estimates (see Section 3.6.5), new process-based evaluation confirms the GOBMs estimate (section 3.6.5), and the interannual variability in the GOBMs and data-based estimates is largely consistent and can be explained by climate variability. We refrain from assigning a high confidence because of the large standard deviation of the fCO_2-products and the deviation between the GOBM and fCO_2-product trends between around 2002 and 2020 and the higher S_{OCEAN} estimate from O_2:N_2 (section 2.8). More details on the S_{OCEAN} methodology can be found in Supplement S.3.

2.5.2 2026 Projection

The S_{OCEAN} forecast for the year 2026 is based on (a) the historical (Lan et al., 2026) and our 2026 estimate of atmospheric CO_2 concentration, (b) the historical and our 2026 estimate of global fossil emissions, and (c) the boreal spring (March, April, May) Oceanic Niño Index (ONI) (NCEP, 2026). Using a non-linear regression approach, i.e., a feed-forward neural network, atmospheric CO_2, ONI, and the fossil emissions are used as training data to best match S_{OCEAN} from 1959 through 2025 from this year's carbon budget. Using this relationship, the 2026 S_{OCEAN} can then be estimated from the projected 2026 input data using the non-linear relationship established during the network training. To avoid overfitting, the neural network training was done using a Monte Carlo approach, with a variable number of artificial neurons (varying between 2-5) and 20% of the randomly selected training data were withheld for independent internal testing.

Based on the best output performance (tested using the 20% withheld input data), the best performing number of neurons was selected. In a second step, we trained the network 10 times using the best number of neurons identified in step 1 and different sets of randomly selected training data. The mean of the 10 trainings is considered our best forecast, whereas the standard deviation of the 10 ensembles provides a first order estimate of the forecast uncertainty. This uncertainty is then combined with the S_{OCEAN} uncertainty of the year 2025 (±0.68 GtC yr^{-1}) to estimate the overall uncertainty of the 2026 projection. As an additional line of evidence, we also assess the 2026 atmosphere-ocean carbon flux from the ESM prediction system (see Section 2.9).

https://doi.org/10.5194/essd-2026-895
Preprint. Discussion started: 10 November 2026
© Author(s) 2026. CC BY 4.0 License.



2.6 Land CO_2 sink

2.6.1 Historical Period 1850-2025

The terrestrial land sink (S_{LAND}) is thought to be due to the combined effects of rising atmospheric CO_2, increasing N inputs, and climate change, on plant growth and terrestrial carbon storage. S_{LAND} does not include land sinks directly resulting from land-use and land-use change (e.g., regrowth of vegetation) as these are part of the land-use change emissions (E_{LUC}), although system boundaries make it difficult to attribute exactly CO_2 fluxes on land between S_{LAND} and E_{LUC} (Erb et al., 2013).

S_{LAND} is derived from the multi-model mean of 23 DGVMs (Table 4 and Table S1). DGVMs simulations include all climate variability and CO_2 effects over land. In addition to the carbon cycle represented in all DGVMs, 15 models also account for the nitrogen cycle and hence can include the effect of N inputs on S_{LAND}. The DGVMs estimates of S_{LAND} do not explicitly include the export of carbon to aquatic systems or its historical perturbation, which is discussed in Supplement S.8.3. DGVMs need to meet several criteria to be included in this assessment (see Supplement S.4.2). In addition, we use the International Land Model Benchmarking system (ILAMB; Collier et al., 2018) for the DGVMs evaluation (see Supplement S.4.2), with an additional comparison of DGVMs with a data-informed, Bayesian model-data fusion framework (CARDAMOM) (Bloom and Williams, 2015; Bloom et al., 2016). The uncertainty on S_{LAND} is taken from the DGVMs standard deviation.S_{LAND} is no longer calculated based on a transient simulation with fixed pre-industrial land cover, and in GCB2025 corrected for the Replaced Sinks and Sources bias (RSS) (Gitz and Ciais, 2003; Sitch et al., 2005, Pongratz et al., 2009; Gasser et al., 2020; Obermeier et al. 2021; Dorgeist et al., 2024; Walker et al., 2025; O'Sullivan et al. 2026a). In GCB2026 it is now calculated from DGVM simulations with transient land use change, and transient compared with fixed, pre-industrial climate and atmospheric CO_2 content. A different adjustment is now required to account for the environmental effects on vegetation subsequently converted to agriculture (δL). The δL adjustment is based on bookkeeping model results and estimated at 0.20 +/- 0.07 GtC yr^{-1} for the 2016-2025 period. More details on the S_{LAND} methodology can be found in Supplement S.4.

2.6.2 2026 Projection

In previous versions of the GCB, the land sink projection was, like the ocean sink forecast, based on a non-linear regression approach with a feed-forward neural network. This approach, however, resulted in a large uncertainty and underestimated the land sink variability in the past. Since GCB2025,we update the projection and simply calculate the land sink for 2026 as the residual of the projection of the other components of the carbon cycle ($S_{LAND}=E_{FOS}+E_{LUC}-G_{ATM}-S_{OCEAN}$). Hence, by construction the 2026 B_{IM} is set to zero.

https://doi.org/10.5194/essd-2026-895
Preprint. Discussion started: 10 November 2026
© Author(s) 2026. CC BY 4.0 License.



850

851 **2.7 Atmospheric inversion estimate**

852 The world-wide network of in-situ atmospheric measurements and satellite derived atmospheric CO_2
853 column (XCO_2) observations put a strong constraint on changes in the atmospheric abundance of CO_2.
854 This allows atmospheric inversion methods to constrain the magnitude and location of the combined
855 total surface CO_2 fluxes from all sources, including fossil and land-use change emissions and land and
856 ocean CO_2 fluxes. The inversions assume E_{FOS} to be well known, and they solve for the spatial and
857 temporal distribution of land and ocean fluxes from the residual gradients of CO_2 between stations that
858 are not explained by fossil fuel emissions. By design, such systems thus close the carbon balance (B_{IM} =
859 0) and provide an additional perspective on the independent estimates of the ocean and land fluxes.

860 This year's release includes sixteen inversion systems that are described in Table S4. Each system is
861 rooted in Bayesian inversion principles but uses different methodologies. They use a variety of
862 transport models, which previous studies have identified as a major driver of differences in the
863 latitudinal distribution of inversion-based flux estimates (Gaubert et al., 2019; Schuh et al., 2019). Also
864 other choices, such as the a-priori fluxes, inversion method of the models, and observations used (see
865 references in Table S4 for details) have been identified as drivers of the inter-system flux differences
866 (van der Woude et al., 2026). Eleven inversion systems used satellite XCO2 retrievals from GOSAT
867 and/or OCO-2, scaled to the WMO 2019 calibration scale, of which five inversions this year used these
868 XCO2 datasets in addition to the in-situ observational CO2 mole fraction records.

869 The original products delivered by the inverse modellers were modified to facilitate the comparison to
870 the other elements of the global budget, specifically on two accounts: (1) global total fossil emissions
871 including cement carbonation CO_2 uptake, (2) and riverine CO_2 transport. For the regional analysis
872 (Figures 14 and 15), we also subtract the preindustrial mean state of the atmosphere-ocean CO_2 fluxes
873 derived from GOBMs, to only show anthropogenic perturbation (Supplement S3.1). We note that with
874 these adjustments the inverse results no longer represent the contemporary net atmosphere-surface
875 exchange over land/ocean areas as sensed by atmospheric observations. Instead, for land, they become
876 the net uptake of CO_2 by vegetation and soils that is not exported by fluvial systems, similar to the
877 DGVMs estimates. For oceans, they become the net uptake of anthropogenic CO_2, similar to the
878 GOBMs estimates.

879 The inversion systems prescribe global fossil emissions based on e.g., the GCP's Gridded Fossil
880 Emissions Dataset versions 2026.0 (GCP-GridFED; Jones et al., 2026), which are updates to GCP-
881 GridFEDv2021 presented by Jones et al. (2021). GCP-GridFEDv2026.0 scales gridded estimates of
882 CO_2 emissions from EDGARv4.3.2 (Janssens-Maenhout et al., 2019) within national territories to
883 match national emissions estimates provided by the GCB for the years 1959-2025, which were

https://doi.org/10.5194/essd-2026-895
Preprint. Discussion started: 10 November 2026
© Author(s) 2026. CC BY 4.0 License.



884 compiled following the methodology described in Section 2.1. Small differences between the systems
885 due to for instance regridding to the transport model resolution, or use of different fossil fuel emissions
886 than GCP-GridFEDv2026.0, are adjusted in the latitudinal partitioning we present, to ensure agreement
887 with the estimate of E_{FOS} in this budget. We also note that the ocean fluxes used as prior by 11 out of 16
888 inversions are part of the suite of the ocean process model or fCO_2-products listed in Section 2.5.
889 Although these fluxes are further adjusted by the atmospheric inversions (except for Jena CarboScope),
890 it makes the inversion estimates of the ocean fluxes not completely independent of S_{OCEAN} assessed
891 here.

892 To facilitate comparisons to the independent S_{OCEAN} and S_{LAND}, we used the same adjustments for
893 transport and outgassing of carbon transported from land to ocean, as done for the observation-based
894 estimates of S_{OCEAN} (see Supplement S.5.1).

895 The atmospheric inversions are evaluated using vertical profiles of atmospheric CO_2 concentrations
896 (Figure S14). More than 50 aircraft programs over the globe, either regular programs or repeated
897 surveys over at least 9 months (except for SH programs), have been used to assess system performance
898 (with space-time observational coverage sparse in the SH and tropics, and denser in NH mid-latitudes;
899 Table S9). The sixteen systems are compared to the independent aircraft CO_2 measurements between 2
900 and 7 km above sea level between 2001 and 2025. Results are shown in Figure S14 and discussed in
901 Supplement S.5.2.

902 We note that as of GCB2025, the ensemble of inverse models covering a full decade is deemed
903 sufficiently large to report the 1-sigma standard deviation as uncertainty, following the convention of
904 the other components in GCB. More details on the atmospheric inversion methodology can be found in
905 Supplement S.5.

906 **2.8 Atmospheric oxygen based estimate**

907 Long-term atmospheric O_2 and CO_2 observations allow estimation of the global ocean and land carbon
908 sinks, due to the coupling of O_2 and CO_2 with distinct exchange ratios for fossil fuel emissions and land
909 uptake, and uncoupled O_2 and CO_2 ocean exchange (Keeling and Manning, 2014). The global ocean
910 and net land carbon sinks were calculated following methods and constants used in Keeling and
911 Manning (2014) but modified to also include the effective O_2 source from metal refining (Battle et al.,
912 2023). For the exchange ratio of the net land sink a value of 1.05 is used, following Resplandy et al.
913 (2019). For fossil fuels, the following values are used: gas: 1.95 ± 0.04, liquid: 1.44 ± 0.03, solid: 1.17
914 ± 0.03, cement: 0 ± 0, gas flaring: 1.98 ± 0.07 (Keeling, 1988). Atmospheric O_2 is observed as $\delta(O_2/N_2)$
915 and combined with CO_2 mole fraction observations into Atmospheric Potential Oxygen (APO, Stephens
916 et al., 1998). The APO observations from 1990 to 2025 were taken from a weighted average of flask
917 records from three stations in the Scripps O_2 program network (Alert, Canada (ALT), La Jolla,

https://doi.org/10.5194/essd-2026-895
Preprint. Discussion started: 10 November 2026
© Author(s) 2026. CC BY 4.0 License.



California (LJO), and Cape Grim, Australia (CGO), weighted per Keeling and Manning (2014). Observed CO_2 was taken from the globally averaged marine surface annual mean growth rate from the NOAA/GML Global Greenhouse Gas Reference Network (Lan et al., 2026). The O_2 source from ocean warming is based on ocean heat content from updated data from NOAA/NCEI (Levitus et al., 2012). The effective O_2 source from metal refining is based on production data from Bray (2020), Flanagan (2021), and Tuck (2022). Uncertainty was determined through a Monte Carlo approach with 20,000 iterations, using uncertainties prescribed in Keeling and Manning (2014), including observational uncertainties from Keeling et al. (2007) and autoregressive errors in fossil fuel emissions (Ballantyne et al., 2015). The reported uncertainty is 1 standard deviation of the ensemble. As for the atmospheric inversions, the O_2 based estimates also closes the carbon balance ($B_{IM} = 0$) by design and provides another independent estimate of the ocean and land fluxes. Note that the O_2 method requires a correction for global air-sea O_2 flux, which has the largest uncertainty at annual time scales, but which is still non-negligible for decadal estimates (Nevison et al., 2008). The 2016-2025 decadal average net land and ocean sinks from the atmospheric O_2 based constraint are based on provisional data from the first half of 2026. These data have not yet been corrected for long-term drift in primary standards and may be revised at a future date.

2.9 Earth System Models estimate

Reconstructions and predictions from decadal prediction systems based on Earth system models (ESMs) provide a novel line of evidence in assessing the atmosphere-land and atmosphere-ocean carbon fluxes in the past decades and predicting their changes for the current year and years to come. By assimilating physical atmospheric and oceanic data products into the ESMs, the models are able to reproduce the historical variations of the atmosphere-sea CO_2 fluxes, atmosphere-land CO_2 fluxes, and atmospheric CO_2 growth rate (Li et al., 2016, 2019; Lovenduski et al., 2019a,b; Ilyina et al., 2021; Li et al., 2023; Li et al., 2026). Furthermore, the ESM-based predictions have proven their skill in predicting the air-sea CO_2 fluxes for up to 6 years, the air-land CO_2 fluxes and atmospheric CO_2 growth for 2 years (Lovenduski et al., 2019a,b; Ilyina et al., 2021; Li et al., 2023; Li et al., 2026). The reconstructions from the fully coupled model simulations ensure a closed budget within the Earth system, i.e., no budget imbalance term.

Six ESMs have performed the set of prediction simulations. The ensemble size of initialized prediction simulations is 10, and the ensemble mean for each individual model is used here. Each ESM uses a different assimilation method and combination of data products incorporated in the system, more details on the models configuration can be found in Table 4 and Supplement Table S5. Reconstructions of atmosphere-ocean CO_2 fluxes (S_{OCEAN}) and atmosphere-land CO_2 fluxes (S_{LAND}-E_{LUC}) for the time period from 1960-2025 are assessed here. Predictions of the atmosphere-ocean CO_2 flux, atmosphere-land CO_2 flux, and atmospheric CO_2 growth for 2026 are calculated based on the predictions at lead year 1. The

https://doi.org/10.5194/essd-2026-895
Preprint. Discussion started: 10 November 2026
© Author(s) 2026. CC BY 4.0 License.



predictions of atmosphere-ocean CO_2 flux and atmosphere-land CO_2 flux are bias corrected by removing the climatological mean and linear trend biases from 1981-2021 referring to GCB2022 (Friedlingstein et al., 2022), the atmospheric CO_2 growth (G_{ATM}) is then calculated as the residual of the CO_2 emissions subtracting the carbon sinks into the ocean and the land. With the ESMs simulations, we also compute the G_{ATM} in another way based on monthly atmospheric CO_2 concentrations at 1000hPa level over the oceans to be comparable to the NOAA/GML global measurements of atmospheric CO_2 concentrations (Lan et al., 2026). The bias correction is done referring to NOAA/GML monthly CO_2 concentrations in recent years from 2015-2025 regarding mean state and linear trend, a shorter period is used because a non-linear trend for the whole period is observed from both NOAA/GML measurements and model simulations. The 2026 G_{ATM} is then calculated by the increment of atmospheric CO_2 concentration in December 2026 minus that in December 2025 multiplied by 2.124 to convert the unit from ppm to GtC. The prediction of 2026 atmospheric CO_2 concentration is an average of the available NOAA/GML measurements from January to June (Lan et al., 2026) and ESMs' predictions from July to December. Note that the two methods, i.e., one based on the residual of carbon sources and sinks and another based on atmospheric concentration increment, of calculation of G_{ATM} result in different magnitudes, which suggests the consideration of variable ratio rather than a constant value in converting CO_2 concentration to mass. More details on methods of bias correction of decadal predictions can be found in Kharin et al. (2012), Boer et al. (2016) and Li et al. (2023). The ESMs are used here to support the assessment of S_{OCEAN} and net atmosphere-land CO_2 flux (S_{LAND} - E_{LUC}) over the 1960-2025 period, and to provide an estimate of the 2026 prediction of G_{ATM} and atmospheric CO_2 concentration.

2.10 Processes not fully included in the global carbon budget

The contribution of anthropogenic CO and CH_4 to the global carbon budget is not fully accounted for in Eq. (1) and is described in Supplement S.8.1. The contributions to CO_2 emissions of decomposition of carbonates not accounted for is described in Supplement S.8.2. The contribution of anthropogenic changes in river fluxes is conceptually included in Eq. (1) in S_{OCEAN} and in S_{LAND}, but it is not represented in the process models used to quantify these fluxes, hence a correction of -0.07 GtC yr^{-1} is applied a posteriori to the S_{LAND} estimate for the 2016-2025 period, as proposed in Friedlingstein et al. (2025b). This effect is discussed in Supplement S.8.3.

3 Results

For each component of the global carbon budget, we present results for three different time periods: the full historical period, from 1850 to 2025, the decades in which we have atmospheric concentration records from Mauna Loa (1959-2025) with a specific focus on last year (2025), and the projection for the current year (2026). Subsequently, we assess the estimates of the budget components of the last decades against the top-down constraints from inverse modelling of atmospheric observations and the land/ocean partitioning derived from the atmospheric O_2 measurements. Atmospheric inversions further

https://doi.org/10.5194/essd-2026-895
Preprint. Discussion started: 10 November 2026
© Author(s) 2026. CC BY 4.0 License.



allow for an assessment of the budget components with a regional breakdown of land and ocean sinks.

3.1 Fossil CO_2 Emissions

3.1.1 Historical period 1850-2025

Cumulative fossil CO_2 emissions for 1850-2025 were 510 ± 25 GtC, including the cement carbonation sink (Table 8, with all cumulative numbers rounded to the nearest 5GtC). In this period, 46% of global fossil CO_2 emissions came from coal, 35% from oil, 15% from natural gas, 3% from decomposition of carbonates for cement production, and 1% from flaring. In 1850, the UK stood for 62% of global fossil CO_2 emissions. In 1893 the combined cumulative emissions of the current members of the European Union reached and subsequently surpassed the level of the UK. Since 1917, USA cumulative emissions have been the largest. Over the entire period 1850-2025, USA cumulative emissions amounted to 120 GtC (23% of world total), the EU's to 83 GtC (16%), China's to 81 GtC (16%), and India's to 19 GtC (4%).

In addition to the estimates of fossil CO_2 emissions that we provide here (see Section 2.1), there are three global datasets with long time series that include all sources of fossil CO_2 emissions: CDIAC-FF (Erb and Marland, 2026a, 2026b), CEDS version 2024_03_18 (Hoesly et al., 2025) and PRIMAP-hist version 2.8 (Gütschow et al., 2016; Gütschow & Pflüger, 2026), although these datasets are not entirely independent from each other (Andrew, 2020a). CEDS has cumulative emissions over 1750-2023 at 500 GtC, CDIAC-FF has 489 GtC, GCP 494 GtC, PRIMAP-hist CR 498 GtC, and PRIMAP-hist TR 502 GtC. While there are some differences in coverage, in general these four datasets are in relative agreement as to total historical global emissions of fossil CO_2.

3.1.2 Recent period 1959-2025

Global fossil CO_2 emissions, E_{FOS} (including the cement carbonation sink), have increased every decade from an average of 3.0 ± 0.2 GtC yr^{-1} for the decade of the 1960s to an average of 10.0 ± 0.5 GtC yr^{-1} during 2016-2025 (Table 7, Figure 2 and Figure 4). The growth rate in these emissions decreased between the 1960s and the 1990s, from 4.4% yr^{-1} in the 1960s (1960-1969), 3.1% yr^{-1} in the 1970s (1970-1979), 1.6% yr^{-1} in the 1980s (1980-1989), to 1.0% yr^{-1} in the 1990s (1990-1999). After this period, the growth rate began increasing again in the 2000s at an average growth rate of 2.8% yr^{-1}, decreasing to 1.2% yr^{-1} in the 2010s, and 0.9% yr^{-1} for the last decade (2016-2025). China's emissions increased by 2.7% yr^{-1} on average over the last 10 years dominating the global trend, and India's emissions increased by 3.5% yr^{-1}, while emissions decreased in EU27 (-2.9% yr^{-1}), and in the USA (-0.8% yr^{-1}) (Figure 5a). Figure 6 illustrates the spatial distribution of fossil fuel emissions for the 2016-2025 period.

https://doi.org/10.5194/essd-2026-895
Preprint. Discussion started: 10 November 2026
© Author(s) 2026. CC BY 4.0 License.



E_{FOS} reported here includes the uptake of CO_2 by cement via carbonation which has increased with increasing stocks of cement products, from an average of 13 MtC yr^{-1} (0.01 GtC yr^{-1}) in the 1960s to an average of 150MtC yr^{-1} (0.15 GtC yr^{-1}) during 2016-2025 (Figure 5b).

3.1.3 Final year 2025

Global fossil CO_2 emissions were slightly higher, 1.2%, in 2025 than in 2024, with an increase of 0.1 GtC to reach 10.5 ± 0.5 GtC (including the 0.16 GtC cement carbonation sink), distributed among coal (41%), oil (33%), natural gas (21%), cement (4%), flaring (1%), and others (1%) (Figure 4). Compared to 2024, the 2025 emissions from coal, oil, and gas increased by 0.4%, 1.9%, and 1.8% respectively, while emissions from cement decreased by 0.6%. All annual growth rates presented are adjusted for the leap year, unless stated otherwise.

In 2025, the largest absolute contributions to global fossil CO_2 emissions were from China (32%), the USA (13%), India (8%), and the EU27 (6%). These four regions account for 60% of global fossil CO_2 emissions, while the rest of the world contributed 40%, including international aviation and marine bunker fuels (3% of the total). Growth rates for these countries from 2024 to 2025 were 0.4% (China), 2.8% (USA), 0.0% (EU27), and 1.2% (India), with +0.5% for the rest of the world, including international aviation and marine bunker fuels (4.7%). The per-capita fossil CO_2 emissions in 2025 were 1.3 tC $person^{-1}$ yr^{-1} for the globe, and were 4.0 (USA), 2.4 (China), 1.5 (EU27) and 0.6 (India) tC $person^{-1}$ yr^{-1} for the four highest emitters (Figure 5c).

3.1.4 Year 2026 Projection

Globally, we estimate that global fossil CO_2 emissions (including cement carbonation, -0.15 GtC) declined by 0.4% in 2026 (-1.5% to 0.6%) to 10.4 GtC (38.2 $GtCO_2$). The estimates of changes in 2026 emissions per fuel types, relative to 2025, are projected to increase by 0.6% (range -0.6% to 1.7%) for coal, to decrease by 1.9% (range -2.6% to -1.2%) for oil, to decrease by 0.3% (range -1.6% to 0.9%) for natural gas, and to decrease by 0.6% (range -2.6% to 1.5%) for cement (Figure 5b).

The uncertainty presented for projections relates only to the estimated growth rate, and excludes the uncertainty of the baseline (i.e., 2025) level.

For China, projected fossil emissions in 2026 are expected to have decreased by 0.9% (range -2.6% to 0.8%) compared with 2025 emissions, bringing 2025 emissions for China around 3.4 GtC yr^{-1} (12.3 $GtCO_2$ yr^{-1}). Our projected changes by fuel for China are 0.3% for coal, -4.6% for oil, -0.9% for natural gas, and -6.2% for cement.

For the USA, using the Energy Information Administration (EIA) emissions estimate for 2026 combined with cement clinker data from USGS, we estimate a decrease of 1.3% (range -3.4% to 0.8%)

https://doi.org/10.5194/essd-2026-895
Preprint. Discussion started: 10 November 2026
© Author(s) 2026. CC BY 4.0 License.



compared to 2025, bringing USA 2026 emissions to around 1.4 GtC yr^{-1} (5.0 $GtCO_2$ yr^{-1}). Our estimated changes by fuel are -6.7% for coal, -1.1% for oil, 0.5% for natural gas, and 6.2% for cement.

For India, our estimate for 2026 is an increase of 4.4% over 2025 (range 1.7% to 7.1%), with 2026 emissions around 0.9 GtC yr^{-1} (3.3 $GtCO_2$ yr^{-1}). Our projected changes by fuel are 5.9% for coal, -0.9% for oil, 2.2% for natural gas, and 9.0% for cement.

For the European Union, our projection for 2026 is for a decrease of 1.5% (range -4.0% to 0.9%) relative to 2025, with 2026 emissions around 0.6 GtC yr^{-1} (2.4 $GtCO_2$ yr^{-1}). Our projected changes by fuel are -2.9% for coal, -1.8% for oil, -0.1% for natural gas, and -1.8% for cement.

For Japan, we project for 2026 a decrease of 1.0% (range -2.5% to 0.6%), with 2026 emissions around 0.3 GtC yr^{-1} (1.0 $GtCO_2$ yr^{-1}). Our projected changes by fuel are 1.7% for coal, -2.2% for oil, -4.0% for natural gas, and -3.1% for cement.

International aviation and shipping are expected to decrease by 1% in 2026, reaching 0.3 GtC yr^{-1} (1.2 $GtCO_2$ yr^{-1}), with both international aviation and international shipping projected to be 1% below 2025. For the rest of the world, the expected change for 2026 is a decrease of 0.7% (range -2.9% to 1.5%) with 2026 emissions around 3.7 GtC yr^{-1} (13.6 $GtCO_2$ yr^{-1}). The fuel-specific projected 2026 growth rates for the rest of the world are: -0.2% for coal, -1.6% for oil, -0.5% for natural gas, 1.6% for cement.

Compared to the GCB estimate, Carbon Monitor estimates an decrease in global fossil CO_2 emissions of 0.5% (-3.5% to +2.6%) for 2026 , similar to the GCB projection but with larger uncertainties. Carbon Monitor projects the 2026 emissions to decline by 2.3% (-4.4% to -0.2%) for China, 1.5% (-6.9% to +3.9%) for the USA, 1.1% (-6.8% to +4.7%) for the EU27 and 3.7% (-7.5% to +0.5%) for Japan, but to increase by 5.9% (+2.4% to +9.5%) for India consistent with the GCB projection. For the rest of the world (including international aviation and shipping), the estimated change is an increase of 0.5% (-1.2% to +2.2%).

For traceability, Table S6 provides a comparison of annual projections from GCB since 2015 with the actual emissions assessed in the subsequent GCB annual report.

3.2 Emissions from Land-Use Change

3.2.1 Historical period 1850-2025

Cumulative net CO_2 emissions from land-use change and land management (E_{LUC}) for 1850-2025 are 245 ± 50 GtC (Table 8) with a large spread among individual bookkeeping estimates of 205 GtC (OSCAR), 240 GtC (LUCE) and 290 GtC (BLUE). DGVMs show a lower estimate of 180 ± 50 GtC (excluding emissions from peat drainage and largely omitting those from peat fires which together would add 35 ± 10 GtC). Vegetation biomass observations provide independent constraints on the E_{LUC}

https://doi.org/10.5194/essd-2026-895
Preprint. Discussion started: 10 November 2026
© Author(s) 2026. CC BY 4.0 License.



estimates over the 1901-2012 period (Li et al., 2017). Over that period, the GCB bookkeeping models' cumulative E_{LUC} amounts to 180 GtC [150 to 215 GtC] and the DGVM cumulative E_{LUC} to 135 ± 35 GtC, both not significantly different from the observation-based estimate of 155 ± 50 GtC (Li et al., 2017).

3.2.2 Recent period 1959-2025

Net CO_2 emissions from land-use change and land management remained relatively constant (around 1.8 GtC yr^{-1}) over the 1959-1999 period. Since then, they have shown a statistically significant decrease of about 0.2 GtC per decade ($p<0.001$), reaching 1.3 ± 0.7 GtC yr^{-1} for the 2016-2025 period (Table 7), with a spread from 1.2 to 1.5 GtC yr^{-1} across the three bookkeeping estimates (Figure 4b). The DGVM average shows relatively constant net emissions over the 1970-2010 period, and as bookkeeping models, shows decreasing emissions in the most recent decades (Table 5).

We separate E_{LUC} into five component fluxes to gain further insight into the drivers of net emissions: deforestation and clearing of other vegetation, (re-)growth of forest and other vegetation, wood harvest and other forest management, peat drainage and peat fires, and transitions between cropland, pasture, and urban areas, with CO_2 emissions to the atmosphere being positive and CO_2 removals from the atmosphere being negative (Figure 7b; Supplement S.2.2). This year's decomposition differs from GCB2025: the clearing and (re-)growth of shrub and herbaceous vegetation, included under 'other transitions' in previous GCBs, is now attributed to 'deforestation and clearing of other vegetation (total)', and '(re-)growth of forest and other vegetation (total)', respectively. We further decompose the terms 'deforestation and clearing of other vegetation (total)' and '(re-)growth of forest and other vegetation (total)' into contributions from shifting cultivation vs permanent land cover changes (Figure 7c), where the term 'permanent' is used to align with the FAO categories 'land under permanent crops' and 'permanent meadows and pastures'. Averaged over the 2016-2025 period and over the three bookkeeping estimates, total fluxes from deforestation and clearing of other vegetation amount to emissions of 2.2 [1.9 to 2.5] GtC yr^{-1} (Table 5), of which 1.0 [0.9 to 1.1] GtC yr^{-1} are from permanent deforestation, 0.2 [0.2 to 0.2] from permanent clearing of shrub and herbaceous vegetation, and the remainder (1.0 [0.8 to 1.2] GtC yr^{-1}) from deforestation and clearing of other vegetation in shifting cultivation cycles. Total fluxes from (re-)growth of forest and other vegetation amount to a removal of -1.6 [-1.8 to -1.4] GtC yr^{-1} (Table 5), of which -0.6 [-0.7 to -0.4] GtC yr^{-1} is from permanent forest (re-)growth due to re/afforestation, -0.2 [-0.2 to -0.2] from permanent (re-)growth of shrub herbaceous vegetation, and the remainder (-0.8 [-0.9 to -0.7] GtC yr^{-1}) from regrowth of forest and other vegetation in shifting cultivation cycles. Wood harvest and other forest management causes net emissions of 0.4 [0.1 to 0.7] GtC yr^{-1} (with substantial gross fluxes largely compensating each other; see Figure S2). Emissions from peat drainage and peat fires (0.2 [0.2 to 0.3] GtC yr^{-1}) and the net flux from transitions

https://doi.org/10.5194/essd-2026-895
Preprint. Discussion started: 10 November 2026
© Author(s) 2026. CC BY 4.0 License.



between cropland, pasture and urban areas (0.1 [0.0 to 0.1] GtC yr^{-1}) are of smaller magnitude globally (Table 5).

The split into component fluxes clarifies the potentials for emission reduction and carbon dioxide removal: emissions from permanent deforestation - the largest of our component fluxes - could be halted (largely) without compromising carbon uptake by forests, contributing substantially to emissions reduction. By contrast, reducing wood harvesting would have limited potential to reduce net emissions as it would be associated with less forest regrowth; removals and emissions cannot be decoupled here on long timescales. A similar conclusion applies to removals and emissions from shifting cultivation, which we have therefore separated out. Carbon Dioxide Removal (CDR) in forests could instead be increased by permanently increasing the forest cover through re/afforestation. Currently, re/afforestation creates a removal of -0.6 [-0.7 to -0.4] GtC yr^{-1} from the atmosphere averaged over 2016-2025. Net carbon dioxide removals from re-/afforestation were highest in China, the EU27, and the USA, with combined removals of 0.2 GtC yr^{-1} during 2016-2025. The global value is similar to independent estimates derived from NGHGIs for CDR in managed forests (through re/afforestation plus forest management) for 2014-2023 (-0.6 ± 0.2 GtC yr^{-1}, Smith et al., 2026). In contrast to NGHGIs, bookkeeping estimates do not consider the impacts from natural disturbances (like fires, windthrow, insect outbreaks), which may lead to an overestimation of removals from re/afforestation. Re/afforestation constitutes most of all current CDR (Smith et al., 2026). Though they cannot be compared directly to annual fluxes from the atmosphere and are thus not included in our estimate of E_{LUC}, CDR through transfers between non-atmospheric reservoirs such as in durable HWPs or woody biochar comprise much smaller amounts of carbon. 213 MtC yr^{-1} have been estimated to be transferred to HWPs, averaged over 2014-2023 (Smith et al., 2026). The net flux of HWPs, considering the re-release of CO_2 through their decay, amounts to 89 MtC yr^{-1} over that period (Smith et al., 2026). Note that some double accounting between the CDR through HWPs and the CDR through re/afforestation exists if the HWPs are derived from newly forested areas. CDR from BECCS, biomass burial, and bio-oil storage in 2025 amount to -0.14 MtC yr^{-1}, -0.01 MtC yr^{-1}, and -0.002 MtC yr^{-1} respectively. CDR activity via biochar soil amendment amounted to -0.4 MtC yr^{-1}, of which -0.3 MtC yr^{-1} was derived from woody biomass (and constitutes a transfer between non-atmospheric reservoirs). No CDR has been reported for biomass sinking. A portion of mineralisation projects use biomass-derived carbon to enhance mineralisation reactions; these projects accounted for -0.0006 MtC yr^{-1}. “Blue carbon”, i.e., coastal wetland management such as restoration of mangrove forests, saltmarshes, and seagrass meadows, though at the interface of land and ocean carbon fluxes, are counted towards the land-use sector as well. Currently, bookkeeping models do not include blue carbon; however, current CDR deployment in coastal wetlands is small globally, less than -0.003 MtC yr^{-1} (Powis et al., 2023).

The statistically significant decrease in E_{LUC} since the late-1990s, including the larger drop within the most recent decade, is due to the combination of decreasing emissions from deforestation (in particular

https://doi.org/10.5194/essd-2026-895
Preprint. Discussion started: 10 November 2026
© Author(s) 2026. CC BY 4.0 License.



permanent deforestation) and increasing removals from forest regrowth (with those from re/afforestation stagnating globally in the last decade). Net emissions in 2016-2025 are 26% lower than in the late-1990s (1995-2004) and 20% lower than in 2005-2014. The 2018 peak in E_{LUC} is predominantly driven by a large increase in temporary crop area in Colombia according to FAO data (FAO, 2026b). The processes behind gross removals, foremost forest regrowth and soil recovery, are all slow, while gross emissions include a large instantaneous component. Short-term changes in gross emissions dynamics, such as a temporary decrease in deforestation, influences E_{LUC} faster than a change in gross removals, which rather act on longer-term timescales. Component fluxes often differ more across the bookkeeping estimates than the net flux (Figure 7b), which is expected due to different process representation; in particular, the treatment of shifting cultivation, which increases both gross emissions and gross removals, differs across models, but also net and gross wood harvest fluxes show high model spread (Figure S2). By contrast, models agree relatively well for emissions from permanent deforestation.

Overall, highest net land-use emissions occur in the tropical regions of all three continents. The top three emitters over 2016-2025 are Brazil (in particular the Amazon Arc of Deforestation), Indonesia, and the Democratic Republic of the Congo, with these 3 countries contributing 0.7 GtC yr^{-1} or 54% of the global net E_{LUC} (average over 2016-2025; Figure 6b, Figure 7a). This is related to massive expansion of cropland (FAO, 2025), particularly in the last few decades in Latin America, Southeast Asia, and sub-Saharan Africa (Hong et al., 2021), to a substantial part for export of agricultural products (Pendrill et al., 2019). Emission intensity is high in many tropical countries, particularly of Southeast Asia, due to high rates of land conversion in regions of carbon-dense and often still pristine, undegraded natural forests (Hong et al., 2021). Emissions are further increased by peat fires in equatorial Asia (GFED5.1, van der Werf et al., 2025, Chen et al., 2026), contributing substantially to emissions in individual years, typically related to dry conditions during El Niño (0.2 GtC in 2015; 0.03 GtC yr^{-1} averaged over 2016-2025). Uptake due to land-use change occurs in several regions of the world (Figure 6b) particularly due to re/afforestation. Highest nature-based CDR in the last decade is seen in China, the USA, and the EU27, with combined removals of 0.2 GtC yr^{-1} during 2016-2025, partly related to expanding forest area as a consequence of the forest transition in the 19th and 20th century and subsequent regrowth of forest (Mather 2001; McGrath et al., 2015; Zhu et al., 2025). Substantial uptake through re/afforestation also exists in other regions such as Russia, Indonesia, or Brazil where, however, emissions from deforestation and other land-use changes dominate the net land-use flux. While the mentioned patterns are robust and supported by independent literature, we acknowledge that model spread is substantially larger on regional than global levels, as has been shown for bookkeeping models (Bastos et al., 2021) as well as DGVMs (Obermeier et al., 2021). Independent assessments exist for selected regions (e.g., for Europe by Petrescu et al., 2020; for Brazil by Rosan et al., 2021; for China by Zhu et al., 2025; and for 8 selected countries/regions in comparison to inventory data by Schwingshackl et al., 2022).

https://doi.org/10.5194/essd-2026-895
Preprint. Discussion started: 10 November 2026
© Author(s) 2026. CC BY 4.0 License.



The NGHGI data under the LULUCF sector (Melo et al. 2026) differ from the GCB definition of E_{LUC} (see Section 2.2.1 and Supplement S.2.4). In the NGHGI reporting, natural land fluxes (S_{LAND}) are counted towards E_{LUC} when they occur on managed land (Grassi et al., 2018). To compare the GCB results to the NGHGI approach, we perform a translation of our E_{LUC} estimates by adding S_{LAND} in managed forest from the DGVMs simulations (2.2 GtC yr^{-1} in 2016-2025) to the GCB E_{LUC} estimate from bookkeeping models (following the methodology described in Grassi et al., 2023; see Supplement S.2.4). Adding this sink changes E_{LUC} from being a source of 1.3 GtC yr^{-1} to a sink of 0.9 GtC yr^{-1}, much closer to the NGHGI estimate reporting a sink of 1.2 GtC yr^{-1} (Figure 8c, Table S11). The net flux in managed forests agrees very well, with both NGHGI and the translated GCB estimates indicating a sink of 1.2 GtC/yr for 2016-2025. However, these values mask some compensating biases in the permanent deforestation and forest components (Figure 8a,b, Table S11). Peat emissions agree well across GCB , NGHGI, and FAO estimates, whereas discrepancies between GCB and NGHGI estimates remain for fluxes due to other transitions. We further apply a mask of managed land to the net atmosphere-to-land flux estimate from atmospheric inversions to obtain inverse estimates that are comparable to the NGHGI estimates and to the translated E_{LUC} estimates from GCB (see Supplement S.2.4). The inversion-based net flux in managed land indicates a sink of 0.9 GtC yr^{-1} for 2016-2025, which is in broad agreement with the NGHGI and the translated E_{LUC} estimates (Figure 8, Table S11). Additionally, the interannual variability of the inversion estimates and the translated E_{LUC} estimates show a remarkable agreement (Pearson correlation of 0.77 in 2000-2025), which supports the suggested translation approach. Though estimates of NGHGI and atmospheric inversions and the translated GCB estimates still differ in value and need further analysis, the approach suggested by Grassi et al. (2023), which we adopt here, provides a feasible way to translate the global models' and NGHGI definitions to each other and thus link the anthropogenic carbon budget estimates of land-use CO_2 fluxes directly to the Global Stocktake, as part of the UNFCCC Paris Agreement. The translation approach has been shown to be generally applicable also at the country-level (Grassi et al., 2023; Schwingshackl et al., 2022).

We further compare GCB, NGHGI, and inversion estimates to CO_2 fluxes reported by FAO, averaged over 2016-2025 (Figure 8d). FAO estimates of net forest conversion emissions (1.0 GtC yr^{-1} in 2016–2025) agree well with GCB estimates of permanent deforestation emissions (1.0 GtC yr^{-1}) as do the respective peat emission estimates (0.2 GtC yr^{-1}). However, the FAO forest sink (1.7 GtC yr^{-1}) is weaker than the translated GCB sink (2.2 GtC yr^{-1}), despite including fluxes from both managed and unmanaged forests (Tubiello et al., 2026). This may reflect incomplete reporting of forest carbon stock changes by countries to FAO (Tubiello et al., 2026). This difference in forest sink strength is also reflected in the FAO and translated GCB net flux LULUCF estimates (removals of 0.4 GtC yr^{-1} and 0.9 GtC yr^{-1}, respectively). It should be noted that FAO does not include non-forest land-use transitions in its LULUCF estimate, which are included in the translated GCB estimate.

https://doi.org/10.5194/essd-2026-895
Preprint. Discussion started: 10 November 2026
© Author(s) 2026. CC BY 4.0 License.



3.2.3 Final year 2025

The global CO_2 emissions from land-use change are estimated as 1.2 ± 0.7 GtC in 2025, similar to the 2024 estimate. However, confidence in the annual change remains low, as the land-use transition forcing underlying the E_{LUC} estimates was informed directly by data only up to and including 2023 (2024 for Brazil, Indonesia, and China), with a trend extrapolation to 2025 (see Supplement S.2.1).

3.2.4 Year 2026 Projection

In equatorial Asia, peat fire emissions increased substantially (157 MtC through October 24, 2026, after 6 MtC in 2025; GFED5.1, van der Werf et al., 2025, Chen et al., 2026), as did deforestation and degradation fires (63 MtC in 2026; 4 MtC in 2025), associated with drier conditions linked to the El Niño conditions that started earlier this year. Emissions from deforestation and degradation fires in South America remained low (99 MtC through October 24, 2026 after 78 MtC in 2025). El Niño-related fire impacts in the Amazon are generally expected to peak in the following year, particularly during the July-October dry season in the southern Amazon (Chen et al., 2017). Pantropical 2026 fire emission estimates from deforestation and degradation through October 24 are 306 MtC, which is about 20% more than the emissions of the full year 2025 (258 MtC). Note that the absolute fire emission estimates changed compared to GCB2025 due to our update from GFED4s to GFED5.1 (see Section 2.2). Since we use fire emission estimates relative to the previous year for the projections, the absolute changes only slightly affect our E_{LUC} projection.

For 2026 we expect E_{LUC} emissions of around 1.4 GtC (5.1 $GtCO_2$), 0.2 GtC above the 2025 level (and 0.1 GtC above the 2016-2025 average). Note that the confidence in the 2026 E_{LUC} projection remains low, as it is based on deforestation, degradation and peat fire emissions, which are only a proxy for land-use change. Projections in past GCB assessments are only partially confirmed by updated E_{LUC} estimates based on bookkeeping models in the following GCB assessments (Figure S3). Although our extrapolation includes tropical deforestation and degradation fires, the degradation attributable to selective logging, edge-effects or fragmentation is not captured. Further, deforestation and fires in deforestation zones may become more disconnected, partly due to changes in legislation in some regions. For example, Van Wees et al. (2021) found that the contribution from fires to forest loss decreased in the Amazon and in Indonesia over the period of 2003-2018.

3.3 CDR not based on vegetation

Besides the CDR through land use (Sec. 3.2), the atmosphere-to-geosphere flux of carbon resulting from carbon dioxide removal (CDR) activities in 2025 that are not based on vegetation is estimated at -0.003 MtC yr^{-1}. This results primarily from -0.001 MtC yr^{-1} each of enhanced rock weathering projects and alkalinity enhancement of water bodies, and -0.0004 MtC yr^{-1} of DACCS (Smith et al., 2026). The

https://doi.org/10.5194/essd-2026-895
Preprint. Discussion started: 10 November 2026
© Author(s) 2026. CC BY 4.0 License.



atmosphere-to-geosphere component of mineralisation CDR was -0.0001 MtC yr^{-1}, representing 14% of total mineralisation CDR. The remaining -0.0006 MtC yr^{-1} was derived from mineralisation projects which used biomass derived carbon and is therefore accounted for separately under ELUC (Section 3.2) to avoid double counting. The total estimated atmosphere-to-geosphere CDR flux for 2024 has been revised, from -0.011 MtC yr^{-1} reported in Friedlingstein et al. (2026a) to -0.006 MtC yr^{-1}. This reflects that GBC2025 included bio-oil geological storage and biomass burial (-0.0048 MtC yr^{-1} combined) within the estimates for atmosphere-to-geosphere CDR. Given these methods use biomass to capture CO_2, they are now accounted for in the E_{LUC} values, provided in Section 3.2. Additionally, late reporting of project activity on registries has slightly increased the 2024 estimates for enhanced rock weathering and alkalinity enhancement, but within rounding error. The 2025 estimate of -0.003 MtC yr^{-1} therefore represents a 50% decrease from the revised 2024 estimate, driven primarily by decreases in ERW and mineralisation. However, for these methods, registry reporting can be late in reporting CDR fluxes for a given year, as it takes time to verify removals. Therefore the 2025 estimate may increase as additional project data becomes available. The flux from atmosphere-to-geosphere CDR still remains approximately one million times smaller than current fossil CO_2 emissions.

3.4 Total anthropogenic emissions

Cumulative anthropogenic CO_2 emissions (fossil, including cement carbonation, and land-use change) for 1850-2025 totalled 755 ± 55 GtC (2765 ± 205 $GtCO_2$), of which 72% (545 GtC) occurred since 1959 and 36% (275GtC) since 2000 (Table 7 and 8). Total anthropogenic emissions more than doubled since the 1960s, from 4.9 ± 0.7 GtC yr^{-1} for the decade of the 1960s to an average of 11.3 ± 0.9 GtC yr^{-1} during 2016-2025 and reaching 11.7 ± 0.9 GtC (42.8 ± 3.2 $GtCO_2$) in 2025. However, total anthropogenic CO_2 emissions have been almost stable over the last decade (0.3% yr^{-1} average growth rate over the 2016-2025 period), much lower than the 1.7% growth rate over the previous decade (2006-2015). This slower growth is due both to the reduced growth in E_{FOS} between the two decades, and to the absolute decrease in E_{LUC} over the past decade.

During the historical period 1850-2025, 68% of historical emissions were from fossil emissions and 32% from land-use change. However, fossil emissions have grown significantly since the 1960s while net land-use change emissions have not, and consequently the contributions of land-use change to total anthropogenic emissions were smaller during recent periods, 21% during the period 1959-2024 and down to 12% over the last decade (2016-2025).

For 2026 we project global total anthropogenic CO_2 emissions from fossil and land-use changes to be around 11.8 GtC (43.3 $GtCO_2$), marginally above the 2025 level.

https://doi.org/10.5194/essd-2026-895
Preprint. Discussion started: 10 November 2026
© Author(s) 2026. CC BY 4.0 License.



3.5 Atmospheric CO_2

3.5.1 Historical period 1850-2025

Atmospheric CO_2 concentration was approximately 278 parts per million (ppm) in 1750, reaching 300 ppm in the late 1900s, 350 ppm in the late 1980s, and reaching 425.6 ± 0.1 ppm in 2025 (Lan et al., 2026; Figure 1). The mass of carbon in the atmosphere increased by 52% from 590 GtC in 1750 to 904 GtC in 2025. Current CO_2 concentrations in the atmosphere are unprecedented in the last 2 million years and the current rate of atmospheric CO_2 increase is at least 10 times faster than at any other time during the last 800,000 years (Canadell et al., 2021).

3.5.2 Recent period 1959-2025

The growth rate in atmospheric CO_2 level increased from 1.7 ± 0.07 GtC yr^{-1} in the 1960s to 5.4 ± 0.02 GtC yr^{-1} during 2016-2025 with important decadal variations (Table 7, Figure 3 and Figure 4c). During the last decade (2016-2025), the growth rate in atmospheric CO_2 concentration continued to increase, albeit with large interannual variability (Figure 9). This interannual variability is highly consistent between the surface-based CO_2 growth rate and GRESO, the XCO_2-based growth rate (Pearson correlation of 0.91), but substantial differences are seen in 2019 and 2022-2024. These reflect differences in the total atmospheric carbon stock seen within the set boundaries of Jan-1 and Dec-31 used to create an annual growth rate, as discussed in Section 2.4.1. Especially with large anomalies in tropical regions and close to January 1st, the calculation becomes sensitive to when the change is detected. This affected the 2023 and 2024 growth rates most strongly as they originated from tropical regions, and late in the calendar year (see next section). Figure 9 also shows the total annual fluxes (in GtC yr^{-1}) from the inverse models, which are derived to match the observed atmospheric increase while numerically accounting for the atmospheric transport-related delay in detection. The inversely modeled values generally match the GRESO growth rate better than the surface observations-based growth rate, indicating that the latter is more strongly influenced by the delay between the fluxes occurring and the actual observation of these signals. Note that this effect is mainly important on the annual timescale, and not over longer periods.

3.5.3 Final year 2025

The growth rate in the surface based atmospheric CO_2 concentration was 4.4 ± 0.2 GtC yr^{-1} (2.06 ± 0.08 ppm yr^{-1}) in 2025 (Figure 4c; Lan et al., 2026), well below the 2024 growth rate (8.0 ± 0.2 GtC yr^{-1}, 3.8± 0.08 ppm yr^{-1}) or the 2016-2025 average (5.4 ± 0.02 GtC yr^{-1}, 2.5 ± 0.008 ppm yr^{-1}), as to be expected in a post El Niño year. Similarly, the satellite-based GRESO growth rate was 4.2±0.2 GtC yr^{-1} (1.96±0.09 ppm yr^{-1}) for 2025, also below its 2024 growth rate (7.2±0.2 GtC yr^{-1}, 3.4±0.09 ppm yr^{-1}).

https://doi.org/10.5194/essd-2026-895
Preprint. Discussion started: 10 November 2026
© Author(s) 2026. CC BY 4.0 License.



3.5.4 Year 2026 Projection

The 2026 atmospheric CO_2 concentration, averaged over the year, is projected to reach the level of 427.7 ppm, 53% over the pre-industrial level (Lan et al., 2026). We estimate the annual growth in atmospheric CO_2 (G_{ATM}) to be about 4.6 GtC (equivalent to a 2.2 ppm increase in the global mean concentration), similar to the 2025 growth rate. While 2026 is the onset of a large El Niño event, it does not yet translate into a large positive CO_2 growth rate anomaly. Historically, the full effects of strong El Niño events (see 1997/98 and 2015/16 El Niño events) is mainly visible in the following year, thus we expect to see the full El Niño effect on atmospheric CO_2 in 2027.

For traceability, Table S7 provides a comparison of annual projections of the G_{ATM}, S_{OCEAN} and S_{LAND} from GCB since 2021 with the actual estimate assessed in the subsequent GCB annual report.

3.6 Ocean Sink

3.6.1 Historical period 1850-2025

Cumulated since 1850, the ocean sink S_{OCEAN} adds up to 200 ± 55 GtC, with more than 70% of this amount (145 ± 40 GtC) being taken up by the global ocean since 1959. Over the historical period, the ocean sink increased in pace with the anthropogenic emissions exponential increase (Figure 3). Since 1850, the ocean has removed about 26% of total anthropogenic emissions (Table 8).

3.6.2 Recent period 1959-2025

S_{OCEAN} increased from 1.3 ± 0.5 GtC yr^{-1} in the 1960s to 3.0 ± 0.6 GtC yr^{-1} during 2016-2025 (Table 7), with interannual variations of the order of a few tenths of GtC yr^{-1} (Figure 4d, Figure 10b). As described in section 2.5.1, S_{OCEAN} is corrected for identified biases in the fCO_2 products estimates. Compared to the uncorrected estimate, S_{OCEAN} is increased by 0.06 GtC yr^{-1} for the 2016-2025 period.

The ocean-borne fraction ($S_{OCEAN}/(E_{FOS}+E_{LUC})$) has been remarkably constant around 27% on average over the 1959-2025 period, with variations around this mean illustrating the decadal variability of the ocean carbon sink. So far, there is no evidence of a sustained decrease in the ocean-borne fraction from 1959 to 2025 (Figure S17).

The increase of the ocean sink is primarily driven by the increased atmospheric CO_2 concentration, with the strongest CO_2 induced signal in the North Atlantic and the Southern Ocean (Figure 12a, Figure S9). The effect of climate change as quantified by the current suite of GOBMs is much weaker, reducing the ocean sink globally by 0.22 ± 0.07 GtC yr^{-1} (-7.8% relative to the simulation that only accounts for the effect of atmospheric CO_2 increase) during 2016-2025 (all models simulate a weakening of the ocean sink by climate change, range -5.2 to -11.2%). The climate change effect leading to a reduced

https://doi.org/10.5194/essd-2026-895
Preprint. Discussion started: 10 November 2026
© Author(s) 2026. CC BY 4.0 License.



ocean sink is evident in all large-scale latitudinal bands with the largest contribution from the tropics and the smallest from the north in the multi model mean (Figure 12b, Figure S9). This is the combined effect of change and variability in all atmospheric forcing fields, previously attributed to wind and temperature changes (Le Quéré et al., 2010, Bunsen et al., 2024). The effect of warming is smaller than expected from offline calculation due to stabilising feedback from limited exchange between surface and deep waters (Bunsen et al., 2024; Müller et al., 2025).

The global net air-sea CO_2 flux is a residual of large natural and anthropogenic CO_2 fluxes into and out of the ocean with distinct regional and seasonal variations (Figure S4). Natural fluxes dominate on regional scales, but largely cancel out when integrated globally (Figure S4, Gruber et al., 2009; DeVries et al., 2023). Mid-latitudes in all basins and the high-latitude North Atlantic dominate the ocean CO_2 uptake where low temperatures and high wind speeds facilitate CO_2 uptake at the surface (Figure 6c and Figure S4, Takahashi et al., 2009). In these regions, formation of mode, intermediate and deep-water masses transport anthropogenic carbon into the ocean interior, thus allowing for continued CO_2 uptake at the surface. Outgassing of natural CO_2 occurs mostly in the tropics, especially in the equatorial upwelling region, and to a lesser extent in the North Pacific and polar Southern Ocean, mirroring a well-established understanding of regional patterns of air-sea CO_2 exchange (Figure S4; e.g., Takahashi et al., 2009, Gruber et al., 2009; DeVries et al., 2023). These patterns are also noticeable in the Surface Ocean CO_2 Atlas dataset, where an ocean fCO_2 value above the atmospheric level indicates outgassing (Figure S4). This map further illustrates the data-sparsity in the Indian Ocean and the Southern Hemisphere in general.

The largest variability in the ocean sink occurs on decadal timescales (Figure 10b). The ensemble means of GOBMs and fCO_2-products show the same patterns of decadal variability, although with a larger amplitude of variability in the fCO_2-products than in the GOBMs. The ocean sink stagnated in the 1990s and strengthened between the early 2000s and the mid-2010s (Figure 10b; Le Quéré et al., 2007; Landschützer et al., 2015, 2016; DeVries et al., 2017; Hauck et al., 2020; McKinley et al., 2020, Gruber et al., 2023). Different explanations have been proposed for the decadal variability in the 1990s and 2000s, ranging from the ocean's response to changes in atmospheric wind systems (e.g., Le Quéré et al., 2007, Keppler and Landschützer, 2019), including variations in upper ocean overturning circulation (DeVries et al., 2017) to variations in atmospheric CO_2 growth rate (McKinley et al., 2020, Terhaar, 2024, Danek & Hauck, 2026) the eruption of Mount Pinatubo in the 1990s (McKinley et al., 2020, Fay et al., 2023). The main origin of the decadal variability is a matter of debate with several studies initially pointing to the Southern Ocean (see review in Canadell et al., 2021 and Gruber et al., 2023), but also contributions from the North Atlantic and North Pacific (Landschützer et al., 2016, DeVries et al., 2019), or a global signal (McKinley et al., 2020) were proposed. The GOBM decomposition into climate and CO_2 effects emphasizes the dominance of the climate effect (that would include cooling signals from volcanic eruptions) over the CO_2 effect for the stagnation in the 1990s

https://doi.org/10.5194/essd-2026-895
Preprint. Discussion started: 10 November 2026
© Author(s) 2026. CC BY 4.0 License.



until 2002, which are seemingly more pronounced in the tropics and north than in the south (Figure S9). The atmospheric pCO_2 growth rate is a spatially uniform driver that amplifies with large-scale averaging, while climate exerts spatially heterogeneous effects that cancel with averaging. Thus, climate dominates small-scale flux variability, but is matched on the global mean by the impact of the pCO_2 growth rate (Fay et al., 2024).

The sink entered a phase of stagnation 2016 - 2022, largely in response to large inter-annual climate variability, but has continued to increase in the most recent years. The first-order effect of interannual variability stems from a stronger ocean sink during large El Niño events leading to a reduction in CO_2 outgassing from the Tropical Pacific (e.g., 1997/98, 2015/16) and a weaker sink in neutral years following El Niño (2017) and during La Niña events (2020-2022, Figure 10b; Rödenbeck et al., 2014, Hauck et al., 2020; McKinley et al. 2017). After the triple La Niña event 2020-2022, the ocean sink rebound in 2023 linked to the onset of an El Niño event. Warming in the extratropics, in particular in the Northern Hemisphere, however, weakened the overall increase in the ocean carbon sink (Müller et al., 2025). In the GOBMs, the ocean sink stagnation 2016-2022 is associated with a period of a stronger climate effect reducing the ocean sink, mostly stemming from the tropics, in line with the expected patterns from El Niño and La Niña (Figure S9). The CO_2 effect has also shown a lower growth rate 2016 - 2023 in line with the atmospheric CO_2 growth rate.

The ensemble means of GOBMs, and fCO_2-products (adjusted for the riverine flux) show a mean offset that was lower in the 1990s and 2000s (0.47 GtC yr^{-1}, 0.42 GtC yr^{-1}, respectively) than after 2010 (2010s: 0.57 GtC yr^{-1}, 2016-2025: 0.59 GtC yr^{-1}) . The offset is larger than in previous GCB versions in the early decades, because (i) fCO_2-products continue to be corrected for surface temperature effects, whereas a previously applied correction to the GOBMs is not applied this year (ii) two new fCO_2-products are included in GCB2026 (AOML-ET, SJTU-AVIT), while one fCO_2-product is not included this year (CSIR-ML6) and (iii) three fCO_2-products (UExP-FNN-U, JMA-MLR, AOML-ET), that use an adjusted version of the Surface Ocean CO_2 Atlas data (Ford et al., 2026b), are included in the GCB2026 fCO_2-product mean, which is one more than in GCB2025. In this version of the GCB, the positive trends in the ocean sink estimated by the GOBMs and the fCO_2-products diverges over time by a factor of 1.3 since 2002 (GOBMs: 0.27 ± 0.05 GtC yr^{-1} per decade, fCO_2-products: 0.36± 0.20 GtC yr^{-1} per decade, corrected S_{OCEAN}: 0.32 GtC yr^{-1} per decade), so the divergence shrinks with a lower fCO_2-product trend than in previous GCB releases, partly because the method with one of the strongest trend in past GCB releases (CSIR-ML6) is not included this year. A hybrid approach recently constrained the trend for 2000 to 2022 to 0.42 ± 0.06 GtC yr^{-1} $decade^{-1}$ (Mayot et al., 2024), which aligns with the updated trend of S_{OCEAN} (0.39 GtC yr^{-1} $decade^{-1}$), and the fCO_2-products (0.44 ± 0.04 GtC yr^{-1} $decade^{-1}$), while the GOBMs have a lower trend (0.33 ± 0.03 GtC yr^{-1} per decade) over the same period.

https://doi.org/10.5194/essd-2026-895
Preprint. Discussion started: 10 November 2026
© Author(s) 2026. CC BY 4.0 License.



Open Access Earth System Science Data Discussions

In the current budget, the discrepancy between the two types of estimates stems from a persistently larger ocean sink in the fCO_2-products in all large-scale latitudinal bands (Figure 14). Likely explanations for the discrepancy in the trends and decadal variability in the high latitudes are data sparsity and uneven data distribution (Bushinsky et al., 2019, Gloege et al., 2021, Hauck et al., 2023a, Mayot et al., 2024, Roobaert et al 2026, in review), whereas the discrepancy in the tropics may be related to the regional distribution of the river flux adjustment (Lacroix et al., 2020, Planchat et al., 2025). In particular, two fCO_2-products were shown to overestimate the Southern Ocean CO_2 flux trend by 50 and 130% based on current sampling in a model subsampling experiment (Hauck et al., 2023a) and the largest trends in the fCO_2-products occurred in a data devoid region in the North Pacific (Mayot et al., 2024). A study of Roobaert et al 2026, that extends an analysis presented in previous GCB releases based on model testbed analysis, confirms previously reported biases identified in Hauck et al. (2023a) within individual fCO_2-products, partly linked to data-sparsity, however, it also shows that the ensemble mean bias is significantly dampened. Similarly, a study using independent observations by McKinley et al. (2026) shows significant biases in the fCO_2-product mean (± 5µatm) and their seasonal cycle representation within large scale regions, again with individual methods having larger errors. In this respect it is highly worrisome that the coverage of fCO_2 observations has declined since 2016/17 (Dong et al., 2022, 2024b; Bakker et al., 2026b) and is now down to that of the mid-2000s (Figure 10b). The temperature correction applied products further worsens the agreement in trends between GOBMs and fCO_2-products. Similarly, model biases likely contribute to the discrepancy between GOBMs and fCO_2-products (as indicated by the comparison with Mayot et al., 2024, and by the large model spread in the South, Figure 14).

The S_{OCEAN} estimate is 2.8 ± 0.6 GtC yr^{-1} over the period 2004 to 2019, which agrees within the ranges of uncertainty with the ocean interior estimate of 3.2 ± 0.7 GtC yr^{-1} obtained with the MOBO-DIC approach (Keppler et al., 2023), which directly matches the definition of S_{OCEAN} used here (Hauck et al., 2020). Furthermore, the decadal S_{OCEAN} estimates agree well (mean offset < 0.1 GtC yr^{-1}) with the corresponding ocean interior estimates for all decades from the 1960s to the 2010s, which represent a composite estimate of three adjusted observation-based products (Table 6).

The S_{OCEAN} estimate agrees within uncertainties with other lines of evidence from atmospheric oxygen-based estimates, atmospheric inversions, and ocean interior observation-based constraints (Table 6). The atmospheric oxygen-based estimate shows a lower estimate than S_{OCEAN} in the 1990s, but a larger estimate over the 2016-2025 period, indicating a strong growth of >1.3 GtC yr^{-1} over that period. ESMs with data assimilation result in lower estimates of the ocean sink than all other estimates (Table 6). Also, the atmospheric inversion estimates of the ocean sink agree with S_{OCEAN} within 0.1 GtC yr^{-1} for all decades except the 2000s (0.15 GtC yr^{-1}) .

https://doi.org/10.5194/essd-2026-895
Preprint. Discussion started: 10 November 2026
© Author(s) 2026. CC BY 4.0 License.



Open Access Earth System Science Data Discussions

3.6.3 Final year 2025

The estimated ocean CO_2 sink is 3.2 ± 0.7 GtC for 2025. This is a small increase of <0.1 GtC compared to 2024 (Figure 4d and 10b), which is not significantly different from 2024. The small sink strengthening is related to rather neutral ENSO conditions in 2025 and the weaker increase in atmospheric CO_2 compared to 2024. A positive sink anomaly (stronger uptake) occurs throughout most of the Atlantic Ocean and in the North Pacific, whereas a negative sink anomaly (less uptake) is found in the tropical Pacific and in southern extratropics (Figure 11). Interestingly, the GOBMs suggest that the increase is driven by climate effects and dampened by CO_2 effects, suggesting a rebound effect after the strong atmospheric CO_2 growth rate of 2024 (Figure S9). GOBM and fCO_2-product ensemble mean estimates consistently result in an insignificant change in 2025 (GOBMs: +0.06 ±0.1 GtC, fCO_2-products: +0.00 ± 0.16 GtC yr^{-1}). Seven GOBMs and four fCO_2-products show an increase in S_{OCEAN}, while three GOBMs and six fCO_2-products show a decrease in S_{OCEAN}. The fCO_2-products have a larger uncertainty at the end of the reconstructed time series, potentially linked to uncertainties related to fewer available observations in the final year (see e.g. Watson et al 2020, Pérez et al 2024). Specifically, the fCO_2-products' estimate of the last year is regularly adjusted in the following release owing to the tail effect and an incrementally increasing data availability. While the monthly grid cells covered may have a lag of only about a year (Figure 10b inset), the values within grid cells may change with 1-5 years lag (see absolute number of observations plotted in previous GCB releases), potentially resulting in annual changes in the flux magnitude from fCO_2-products.

3.6.4 Year 2026 projection

Using a feed-forward neural network method (see Section 2.5.2) we project an ocean sink of 3.1 ±0.7 GtC for 2026, which is a declining sink of 0.1 GtC compared to 2025. As mentioned in Section 3.5.4 for the 2026 atmospheric growth rate,we do not predict an El-Niño initiated increase in the global carbon sink for 2026, but we expect to see the full El Niño effect on the ocean sink in 2027. For comparison, the set of ESMs predictions support this estimate with a 2026 ocean sink of around 3.1 [3.0, 3.2] GtC.

3.6.5 Evaluation of ocean models and fCO_2-products

The process-based model evaluation provides evidence for a good performance of the GOBM ensemble average. Although individual models have biases, these are typically averaged out in the ensemble mean and models close to the ensemble mean generally perform best in the evaluations (Figures S6 and S7). High sink models that appear to be closer to ocean interior estimates, atmospheric inversions and O_2:N_2 estimates do not perform better than the other models, but rather seem to ventilate too much and too deep (Figures S6 and S7).

https://doi.org/10.5194/essd-2026-895
Preprint. Discussion started: 10 November 2026
© Author(s) 2026. CC BY 4.0 License.



IOMB summarizes the GOBMs' performance across physical and biogeochemical data sets and various statistics relative to the GOBM ensemble (Figure S5). All GOBMs perform better in some variables compared to the other models, and worse in other variables. Models with an ocean sink close to the ensemble mean generally perform best in the IOMB evaluation. The Revelle factor and carbon uptake capacity scatter around the observational value of OceanSODA (Gregor and Gruber, 2021), and are also close to GLODAP (Supplement S3.3 and Table S12). Seven out of ten models are too salty in the Southern Ocean subpolar biome, and the Atlantic Meridional Overturning Circulation at 26°N is underestimated by 9 out of 10 GOBMs and overestimated by one GOBM.

The CFC analysis that is available for seven models further supports the ensemble average (Figure S6). GOBMs that have a high CFC inventory, indicating strong ventilation, also have a large ocean sink. Vice versa, a lower CFC inventory is associated with a lower ocean carbon sink. However, there are smaller deviations from this linear relationship that point to other drivers than ventilation. The ensemble mean of seven GOBMs simulates a CFC-11 inventory of 0.56 ± 0.11 Gmol, which hits the observational estimate of 0.55 ± 0.12 Gmol almost exactly (Willey et al., 2004). The CFC-11 inventory of OCIM (0.55 Gmol) with steady circulation (no climate change) confirms this value and extends the assessment until 2025. Other transient tracers (CFC-12, SF6) confirm this picture (not shown, as no observational estimate and fewer model simulations are available). OCIM has a higher deep ocean anthropogenic carbon inventory per CFC inventory, which may be partially explained by the earlier starting date of OCIM, which affects total anthropogenic carbon storage, but not the CFC inventory as CFCs only started to increase in the atmosphere in the 1930s. There is no obvious compensation of deep versus upper ocean CFC inventory biases that would suggest a too low accumulation of total C_{ant} inventory in the GOBMs.

The emergent constraint work (Terhaar et al., 2022), which accounts for model biases in ventilation and carbonate buffer capacity provides further evidence for a 0% scaling in the current suite of GOBMs (Figure S7) as ventilation biases from too high Southern Ocean salinities and too weak Atlantic Meridional Overturning Circulation (AMOC) largely compensate, while the simulated carbonate uptake capacity of surface ocean waters is on average similar to the observation-based one. The constraint yields 2.60 ± 0.22 GtC yr^{-1} for 2016-2025, compared with 2.67 ± 0.30 GtC yr^{-1} unconstrained (Table S13). The uncertainty is only moderately reduced because one model simulates excessive deep North Atlantic convection unrelated to the AMOC. The emergent constraint without this model would yield a similar value of 2.64 ± 0.11 GtC yr^{-1} (for more details, see Supplement S3.3). The same emergent constraint methodology leads to a higher estimate of the ocean sink from Earth System Models (Terhaar, 2025). One hypothesis is that this is related to the different spin-up strategies, with the GOBMs being spun-up with the earliest available reanalysis data (typically 1958 onwards) that already includes some anthropogenic warming. Hence, over the course of the simulation the GOBMs may underestimate warming and enhanced stratification (Huguenin et al., 2022; Takano et al., 2023;

https://doi.org/10.5194/essd-2026-895
Preprint. Discussion started: 10 November 2026
© Author(s) 2026. CC BY 4.0 License.



Hollitzer et al., 2024). On the other hand, Earth System Models were shown to overestimate stratification due to warming over the historical period (Danek and Hauck, 2026) and data-assimilating ESMs provide a lower ocean sink (Table 6).

The GOBMs estimate a lower S_{OCEAN} and interior carbon accumulation than the composite estimate averaging three observation-based reconstructions (Table 6 and S12). The deviation amounts to 0.25 and 0.23 GtC yr^{-1} in the 1990s and 2000s, respectively, and increases to 0.5 GtC yr^{-1} in the 2010s. The increasing deviation in the last decade is primarily due to the availability and inclusion of MOBO-DIC estimates from Keppler et al. (2023) only in this decade, which is the only observation-based reconstruction that aims to resolve changes in natural carbon storage and suggest a substantially higher accumulation rate than the OCIM and eMLR(C*) estimates from Devries (2022) and Müller et al. (2023). Comparing the GOBMs to individual ocean interior products, one finds that the GOBM ensemble average of anthropogenic carbon inventory changes are close to the interior observation-based estimate for the decade 2004-2014 from Müller et al. (2023) (GOBMs sim D minus sim A, 2.5 ± 0.4 GtC yr^{-1}, Müller et al. 2.7 ± 0.3 GtC yr^{-1}), but do not reproduce the supposedly higher anthropogenic carbon accumulation in the earlier period 1994-2004 (GOBMs sim D minus sim A, 2.1 ± 0.3 GtC yr^{-1}, Müller et al. 2.9 ± 0.3 GtC yr^{-1}). Four models fall within the range reported by Müller et al. (2023) for the 2004-2014 period (24.8-29.8 PgC), with one model simulating a higher, and five models a lower inventory change. All models simulate a lower inventory change than the range reported for the 1994-2004 period (26.8-31.8). The GOBMs match the regional interior ocean carbon distribution with roughly half of the accumulation in the tropics though with a slight overestimate of the relative accumulation in the north on the expense of the south, compared to Müller et al. (2023)(Table S12). For the decade 1994-2004 they match the N:T:S split almost exactly (GOBMs: 15:49:36%, obs: 12:49:39%), but they do not agree with the proposed shift towards the tropics for 2004-2014 (GOBMs: 16:47:37%, obs: 9:56:35%; Table S12).

Additional benchmarking of the fCO_2-products with independent data generally shows low and consistent biases and RMSEs, with the exception of the comparison with SOCAT flag E data in the tropics where the biases range from -6.4 µatm in JMA-MLR to -10.03 µatm in OceanSODA_ETHv2 , (Figure S8) and the Northern Hemisphere, where biases range from -3.09 µatm in VLIZ-SOMFFN to -26.03 µatm in UExP-FNN-U (Figure S8), although with few measurements covering the latter area. Generally, biases in the northern hemisphere have improved since GCB2025. This is broadly consistent with a study by McKinley et al (2026) that evaluated the bias of 10 fCO_2-products (8 contributing to GCB2026) and their seasonal representation in 5 large scale biome regions with independent datasets (see supplement S3).

Furthermore, an fCO_2-product testbed study by Roobaert et al 2026 (in review), examines mean biases and trend biases derived from a subset of 9 fCO_2-products by subsampling five GOBMs used in Friedlingstein et al. (2023) following the approach of Hauck et al. (2023a) and evaluating the air-sea

https://doi.org/10.5194/essd-2026-895
Preprint. Discussion started: 10 November 2026
© Author(s) 2026. CC BY 4.0 License.



CO_2 flux trend for the 2001-2021 period, i.e. the period of strong divergence in the air-sea CO_2 exchange excluding the tail effect, against trend biases identified by the GOBM reconstruction. Results, based on idealized model testbed experiments, indicate significant fCO_2-product biases regionally in individual reconstruction methods, when they reconstruct full model CO_2 fields and air-sea fluxes based on sparse real-world subsampling, consistent with Hauck et al 2023a and Gloege et al 2021. However, Roobaert et al 2026 (in review) also reveal that many of the regional biases are compensated at larger spatial scales and individual trend biases are partly compensated and in the ensemble average of multiple CO_2 products.

3.7 Land Sink

3.7.1 Historical period 1850-2025

Cumulated since 1850, the terrestrial carbon sink S_{LAND} amounts to 190 ± 40 GtC, 25% of total anthropogenic emissions, with nearly two thirds of this amount (125 ± 30 GtC) being taken up by the terrestrial ecosystems since 1959. Over the historical period, the land sink increased in pace with the anthropogenic emissions exponential increase (Figure 3).

3.7.2 Recent period 1959-2025

S_{LAND} increased from 1.0 ± 0.3 GtC yr^{-1} in the 1960s to 2.5 ± 0.7 GtC yr^{-1} during 2016-2025, with important interannual variations of up to 2 GtC yr^{-1} generally showing a decreased land sink during El Niño events (Figure 10a), responsible for the corresponding enhanced growth rate in atmospheric CO_2 concentration. The larger land CO_2 sink during 2016-2025 compared to the 1960s is reproduced by all the DGVMs in response to the increase in both atmospheric CO_2, nitrogen deposition, and the changes in climate, and is broadly consistent with the residual estimated from the other budget terms, that is $E_{FOS}+E_{LUC}-G_{ATM}-S_{OCEAN}$ which amounts to 2.9 ± 1.1 GtC yr-1 for the last decade (See Table 5). As described in section 2.6.1, S_{LAND} is now adjusted for the δL bias (see Supplement S4 for details).

Over the historical period, the increase in the global terrestrial CO_2 sink is largely attributed to the CO_2 fertilisation effect (Prentice et al., 2001, Piao et al., 2009, Schimel et al., 2015) and increased nitrogen deposition (Huntzinger et al., 2017, O'Sullivan et al., 2019), directly stimulating plant photosynthesis and increased plant water use in water limited systems, with a smaller negative contribution of climate change (Figure 12). There is a range of evidence to support a positive terrestrial carbon sink in response to increasing atmospheric CO_2 (Walker et al., 2021), including a new synthesis of free-air CO_2-enrichment experiments across forests and ages, which concluded that Net Primary Productivity increased by 22% for a common 41% CO_2 enrichment (Norby 2025). As expected from theory, the greatest CO_2 effect is simulated in the tropical forest regions, associated with warm temperatures and long growing seasons (Hickler et al., 2008) (Figure 12a). However, evidence from tropical intact forest

https://doi.org/10.5194/essd-2026-895
Preprint. Discussion started: 10 November 2026
© Author(s) 2026. CC BY 4.0 License.



plots indicate an overall decline in the land sink across Amazonia (1985-2011), attributed to enhanced mortality offsetting productivity gains (Brienen et al., 2015, Hubau et al., 2020). During 2016-2025 the land sink is positive in all regions (Figure 6d) with the exception of eastern Brazil, Bolivia, northern Venezuela, Southwest USA northern Mexico, North and South Africa, and western Australia, where the negative effects of climate variability and change (i.e. reduced rainfall and/or increased temperature) counterbalance CO_2 effects. This is clearly visible in Figure 12 where the effects of CO_2 (Figure 12a) and climate (Figure 12b) as simulated by the DGVMs are isolated (see also Figure S13). The negative effect of climate can be seen across the globe, and is particularly strong in most of South America, Central America, Southwest US, Central and Western Europe, western Sahel, central Africa, southern Africa, Southeast Asia and China, and eastern Australia (Figure 12b, Figure S13). Globally, over the 2016-2025 period, climate change reduces the land sink by 0.6 ± 0.5 GtC yr^{-1} (19% of the CO_2 effect, which is 3.3 ± 0.8 GtC yr^{-1} for the corresponding period).

Most DGVMs have similar S_{LAND} averaged over 2016-2025, and 20/23 models, when adjusted for δL and LOAC, fall within the 1σ range of the residual land sink [1.8 to 4.0 GtC yr^{-1}] (see Table 5), and all models are within the 2σ range [0.7 to 5.1 GtC yr^{-1}]. There are no direct global observations of the land sink (S_{LAND}), or the CO_2 fertilisation effect, and so we are not yet able to rule out models based on component fluxes if their net land sink (S_{LAND}-E_{LUC}) is within the observational uncertainty provided by O_2 measurements. The important role of non-living carbon pools in carbon budgets has also been recently highlighted from an Earth-observation (EO) perspective, where contrary to DGVMs, EO products do not show an increase in biomass, thus inferring a larger role of dead carbon in land carbon cycle dynamics (Bar-On et al., 2025). However EO-based carbon accumulation in mature forests may be underestimated (Ma et al., 2026).

Since 2020 the globe has experienced La Niña conditions which would be expected to lead to an increased land carbon sink. This 3-year long period of La Niña conditions came to an end by the second half of 2023 and transitioned to an El Niño which lasted until mid-2024. A clear transition from maximum to a minimum in the global land sink is evident in S_{LAND}, from 2022 to 2023 and we find that an El Niño-driven decrease in tropical land sink is offset by a smaller increase in the high-latitude land sink. In the past years several regions experienced record-setting fire events (see also section 3.8.3). While global burned area has declined over the past decades mostly due to declining fire activity in savannas (Andela et al., 2017), forest fire emissions are rising and have the potential to counter the negative fire trend in savannas (Zheng et al., 2021). Noteworthy extreme fire events include the 2019-2020 Black Summer event in Australia (emissions of roughly 0.2 GtC; van der Velde et al., 2021), Siberia in 2021, where emissions approached 0.4 GtC or three times the 1997-2020 average according to GFED4s, Canada in 2023 and 2024 (Byrne et al., 2024), and unprecedented wildfires in Brazil and Bolivia in 2024 (partly related to land-use activity, see Sec. 3.2.3 and 3.2.4) (Bourgoin et al., 2025), partially offset by a negative trend in wildfire over Northern Hemisphere Africa. Despite these regional

https://doi.org/10.5194/essd-2026-895
Preprint. Discussion started: 10 November 2026
© Author(s) 2026. CC BY 4.0 License.



negative effects of climate change on S_{LAND}, the efficiency of land to remove anthropogenic CO_2 emissions has remained broadly constant over the last six decades at around 23% (Figure S17).

The combined effect of climate change on S_{LAND} and S_{OCEAN} (assessed in Section 3.6.3), leads to a cumulative sink reduction of 27 ± 21 GtC since 1960 (relative to the counterfactuals that only accounts for the effect of atmospheric CO_2 increase), implying that the carbon-climate feedback has already contributed 7.3 ± 4.5 ppm (7%) to the observed increase in atmospheric CO_2 concentration since 1960.

3.7.3 Final year 2025

The terrestrial CO_2 sink from the DGVMs ensemble S_{LAND} was 3.6 ± 0.9 GtC in 2025, over 50% larger than the 2024 land sink (2.2 ± 0.9 GtC), and above the 2016-2025 average of 2.5 ± 0.7 GtC yr^{-1} (Figure 4e, Table 7). We estimate that the 2025 land sink is the highest on record. This is a combination of the positive long-term land sink trend in all three latitude bands, combined with a strong tropical recovery from the 2023/24 climate extremes and a stable northern sink, relative to 2024 (Figures 11 and 14). DGVM results are broadly consistent from those based on atmospheric inversions (Figure 14). We note that the S_{LAND} estimate for 2025 is in good agreement with the 4.1 ± 1.1 GtC yr^{-1} estimate from the residual sink from the global budget (E_{FOS}+E_{LUC}-G_{ATM}-S_{OCEAN}, Table 5).

3.7.4 Year 2026 projection

Calculating the land sink as the residual of the other projections for 2026, we project a land sink of 4.1 ± 0.7 GtC for 2026, 0.5 GtC larger than the 2025 estimate, potentially still recovering from the reduced land sink after the 2023/24 El Niño event. The ESMs do not provide an additional estimate of S_{LAND} as they only simulate the net atmosphere-land carbon flux (S_{LAND}-E_{LUC}).

3.7.5 Evaluation of land models

All DGVMs meet the three minimum-realism criteria described in Supplement S.4.2. We further evaluate the DGVMs and CARDAMOM against observational benchmarks for carbon and water cycle variables using the International Land Model Benchmarking system (ILAMB; Collier et al., 2018; Figure S10). The scores in Figure S10 are relative, showing how each model performs compared with the others rather than absolute skill. DGVM differences are often of similar magnitude to the range across observational datasets (Seiler et al., 2022), and a more comprehensive analysis of DGVM performance against benchmark data is given in Sitch et al. (2024).

On the combined hydrology and carbon cycle score, CABLE-POP, ORCHIDEEv4 and CARDAMOM perform best relative to the other models, with CARDAMOM constrained by the observations it assimilates. EDv3 has the lowest overall score, followed by JSBACH and LPJmL. No model performs uniformly well, and most have at least one variable with a low relative score: soil carbon for CLM6.0,

https://doi.org/10.5194/essd-2026-895
Preprint. Discussion started: 10 November 2026
© Author(s) 2026. CC BY 4.0 License.



CLM-FATES and GDSTEM, biomass for E3SM and ISAM, leaf area index for LPJmL, LPX-Bern and VISIT, GPP for EDv3 and LPJmL, and evapotranspiration or runoff for IBIS, IQJ, JSBACH and SDGVM. Performance in the carbon and water cycles is not always aligned: IQJ, for example, is among the best models for the ecosystem and carbon cycle but among the weakest for hydrology.

New to GCB2026, we also evaluate the net land flux of the 21 DGVMs that provide monthly NBP against atmospheric CO_2 measured at 38 NOAA stations, comparing the simulated and observed seasonal cycle, interannual variability (IAV) and trend in seasonal amplitude (Figures S11 and S12). Models errors in the simulated seasonal cycle are largest in the northern extratropics, ranging from 1.2 ppm (LPX-Bern) to 5.0 ppm (iMAPLE), and are mostly below 1 ppm in the tropics and Southern Hemisphere. IAV errors vary less between models, from 0.8-1.0 ppm in the north to 0.3-0.7 ppm elsewhere. At northern stations (north of 30°N), all models misrepresent the observed trend in seasonal amplitude somewhat, with median absolute errors across stations of 0.30-0.75 ppm decade^{-1} (Figure S12). The change in the amplitude of the seasonal cycle is a useful metric to track and help constrain environmental effects (particularly CO_2) on the biological activity of the northern hemisphere biosphere (McGuire et al, 2001, Graven et al., 2013, Forkel et al., 2016). Results suggest a wide performance among DGVMs with large bias at some stations indicative of a misrepresentation of the response of northern ecosystems to environmental change, such as CO_2 fertilisation, warming or land-use change. The ILAMB CO_2 score, which is based on the same emulated CO_2 (Figure S10), gives a consistent picture: LPX-Bern and VISIT-UT score best and CABLE-POP, DLEM and EDv3 score worst, matching the large northern seasonal-cycle errors of CABLE-POP and EDv3 and the large tropical and southern errors of DLEM. Model rankings nevertheless differ between the atmospheric CO_2 metrics and the flux and stock benchmarks. CABLE-POP has the highest overall ILAMB score among the DGVMs but one of the largest northern seasonal-cycle errors, while SDGVM has the smallest error in the amplitude trend but among the largest seasonal and interannual errors in the tropics and south.

3.8 Partitioning the carbon sinks

3.8.1 Global sinks and spread of estimates

In the period 2016-2025, the bottom-up view of global net ocean and land carbon sinks provided by the GCB, S_{OCEAN} for the ocean and S_{LAND}– E_{LUC} for the land, agree closely with the top-down global carbon sinks delivered by the atmospheric inversions. This is shown in Figure 13, which visualises the individual decadal mean atmosphere-land and atmosphere-ocean fluxes from each, along with the constraints on their sum offered by the global fossil CO_2 emissions flux minus the atmospheric growth rate (E_{FOS} – G_{ATM}, 4.6 ± 0.5 Gt C yr^{-1}, Table 7, shown as diagonal line in Figure 13). The GCB estimate for net atmosphere-to-surface flux (S_{OCEAN} + S_{LAND} - E_{LUC}) during 2016-2025 is 4.2 ± 1.2 Gt C yr^{-1} (Table 7), implying a budget imbalance (B_{IM}) of 0.4 Gt C yr^{-1} (see Section 3.9). The atmospheric inversions estimate of the net atmosphere-to-surface flux during 2016-2025 is 4.5 Gt C yr^{-1}, with a <

https://doi.org/10.5194/essd-2026-895
Preprint. Discussion started: 10 November 2026
© Author(s) 2026. CC BY 4.0 License.



0.1 GtC yr^{-1} imbalance, and thus scatter across the diagonal, with inverse models trading land for ocean fluxes in their solution. The independent constraint on the net atmosphere-to-surface flux based on atmospheric O_2 by design also closes the balance and is 4.6 ± 1.0 GtC yr^{-1} over the 2016-2025 period (orange symbol on Figure 13), while the ESMs estimate for the net atmosphere-to-surface flux over that period is 5.0 [2.2, 6.3] GtC yr^{-1} (Tables 5 and 6).

The distributions based on the individual models and fCO_2-products reveal substantial spread but converge near the decadal means quoted in Tables 5 to 7. Sink estimates for S_{OCEAN} are mostly non-Gaussian, while the ensemble of DGVMs and inverse models appears more normally distributed justifying the use of a multi-model mean and standard deviation for their errors in the budget. Noteworthy is that the tails of the distributions provided by the land and ocean bottom-up estimates would not agree with the global constraint provided by the fossil fuel emissions and the observed atmospheric CO_2 growth rate. This illustrates the power of the atmospheric joint constraint from the global CO_2 observation capacity.

3.8.1.1 Net atmosphere-to-land flux

The GCB estimate of the net atmosphere-to-land flux ($S_{LAND} - E_{LUC}$), calculated as the difference between S_{LAND} from the DGVMs and E_{LUC} from the bookkeeping models, amounts to a 1.2 ± 1.0 GtC yr^{-1} sink during 2016-2025 (Table 5). The estimate of net atmosphere-to-land flux ($S_{LAND} - E_{LUC}$) from the DGVMs alone (1.5 ± 0.6 GtC yr^{-1}, Table 5, green symbols on Figure 13) is slightly larger, although within the uncertainty of the GCB estimate and agrees well with the budget constraint ($E_{FOS} - G_{ATM} - S_{OCEAN}$, 1.6 ± 0.8 GtC yr^{-1}; Table 7). Also, for 2016-2025, the inversions estimate the net atmosphere-to-land flux is a 1.5 ± 0.3 GtC yr^{-1} sink, similar to the mean of the DGVMs estimates (purple versus grey symbols on Figure 13). The independent constraint based on atmospheric O_2 also aligns well with a net sink of 1.3 ± 0.9 GtC yr^{-1} (orange symbol in Figure 13). Last, the ESMs estimate for the net atmosphere-to-land flux during 2016-2025 is a 2.4 [-0.4, 3.9] GtC yr^{-1} sink, larger than all other estimates (Table 5).

As discussed in Section 3.5.3, the atmospheric growth rate of CO_2 derived from the NOAA surface stations was very high in 2024 (8.0 ± 0.2 GtC) but relatively low in 2025 (4.4 ± 0.2 GtC). Both DGVMs and inversions assign this small CO_2 growth rate to a strong land sink, in particular in the tropics (Figures 11 and 14). DGVMs simulate the 2025 global net atmosphere-to-land flux as a 2.7 ± 0.9 GtC yr^{-1} sink, while it was a 0.1 ± 0.9 GtC yr^{-1} source in 2024. The 2025 estimate is 80% greater than the 2016-2025 decadal mean (1.5 ± 0.6 GtC yr^{-1}). This is primarily driven by tropical recovery of S_{LAND} from the climate extremes in 2023/24, with E_{LUC} in 2025 similar to the decadal mean. The tropics (30°N-30°S) in DGVMs show a dramatic increase in the net atmosphere-to-land flux from a 0.1 GtC yr^{-1} source in 2024 to a 1.4 GtC yr^{-1} sink in 2025. The atmospheric inversions show the global net

https://doi.org/10.5194/essd-2026-895
Preprint. Discussion started: 10 November 2026
© Author(s) 2026. CC BY 4.0 License.



atmosphere-to-land flux going from near neutral (-0.3 GtC yr^{-1}) in 2024 to a strong sink (3.0 GtC yr^{-1}) in 2025, with tropical land fluxes nearly fully accounting for the extra carbon uptake (+2.7 GtC yr^{-1}).

3.8.1.2 Net atmosphere-to-ocean flux

For the 2016-2025 period, the GOBMs produce a lower estimate of the ocean sink of 2.7 ± 0.4 GtC yr^{-1} than the fCO_2-products with 3.3 ± 0.6 GtC yr^{-1}, which shows up in Figure 13 as separate peaks in the distribution from the GOBMs (dark blue symbols) and from the fCO_2-products (light blue symbols). Atmospheric inversions suggest an ocean uptake of 3.1 ± 0.3 GtC yr^{-1}, close to the average of the GOBMs and fCO_2-products for the recent decade (Table 6). The inversions are not fully independent as 9 out of 16 inversions covering the last decade use fCO_2-products as ocean priors and one uses a GOBM (Table S4). The independent constraint based on atmospheric O_2 (3.3 ± 0.65 GtC yr^{-1}) aligns well with the fCO_2-products and majority of the inversions. The large growth in the ocean carbon sink from O_2 is compatible with the GOBMs and fCO_2-products estimates when accounting for their uncertainty ranges. Lastly, the ESMs estimate, 2.5 [2.3, 3.0] GtC yr^{-1}, suggest a lower average ocean carbon sink than the other estimates. We caution that the riverine transport of carbon taken up on land and outgassing from the ocean, accounted for here, is a substantial (0.65 ± 0.3 GtC yr^{-1}) and uncertain term (Crisp et al., 2022; Gruber et al., 2023; DeVries et al., 2023) that separates the GOBMs, ESMs and oxygen-based estimates on the one hand from the fCO_2-products and atmospheric inversions on the other hand.

3.8.2 Regional partitioning

Figure 14 shows the latitudinal partitioning of the global atmosphere-to-ocean and atmosphere-to-land CO_2 fluxes, and their sum, according to the estimates from GOBMs and ocean fCO_2-products, DGVMs, and atmospheric inversions. The ocean fluxes consistently show S_{OCEAN}, so the preindustrial mean and riverine CO_2 fluxes are subtracted from the contemporary flux estimates from fCO_2-products and inversions (see methods). For $fCO2$-products and inversions, reported S_{OCEAN} uncertainties combine model spread and the uncertainty in the preindustrial mean ocean flux estimate (Table S14).

3.8.2.1 North

Despite being one of the most densely observed and studied regions of our globe, annual mean carbon atmosphere-to-surface flux estimates in the northern extra-tropics (north of 30°N) continue to differ. The atmospheric inversions suggest an anthropogenic (S_{LAND} - E_{LUC} + S_{OCEAN}) atmosphere-to-surface sink for 2016-2025 of 2.0 ± 0.5 GtC yr^{-1}, which is higher than the process models' estimate of 1.5 ± 0.4 GtC yr^{-1} (Figure 14). The GOBMs (0.5 ± 0.1 GtC yr^{-1}), fCO_2-products (0.6 ± 0.2 GtC yr^{-1}), and inversion systems (0.5 ± 0.2 GtC yr^{-1}) produce largely consistent estimates of the ocean sink. Thus, the

https://doi.org/10.5194/essd-2026-895
Preprint. Discussion started: 10 November 2026
© Author(s) 2026. CC BY 4.0 License.



difference mainly arises from the net land flux estimate, which is 1.0 ± 0.4 GtC yr^{-1} in the DGVMs compared to 1.5 ± 0.5 GtC yr^{-1} in the atmospheric inversions (Figure 14, second row).

Discrepancies in the northern land fluxes conform with persistent issues surrounding the quantification of the drivers of the global net land CO_2 flux (Arneth et al., 2017; Huntzinger et al., 2017; O'Sullivan et al., 2022) and the distribution of atmosphere-to-land fluxes between the tropics and high northern latitudes (Baccini et al., 2017; Schimel et al., 2015; Stephens et al., 2007; Ciais et al., 2019; Gaubert et al., 2019; O'Sullivan et al. 2024).

In the northern extra-tropics, the process models, inversions, and *f*CO_2-products consistently suggest that most of the interannual variability stems from the land (Figure 14). Inversions generally agree on the magnitude of interannual variations (IAV) over land, more so than DGVMs (0.25-0.35 vs 0.15-0.61 GtC yr^{-1}, averaged over 1990-2025).

3.8.2.2 Tropics

In the tropics (30°S-30°N), both the atmospheric inversions and process models estimate a substantial net anthropogenic (S_{LAND} - E_{LUC} + S_{OCEAN}) atmosphere-to-surface flux over the past decade (inversions: 1.3 ± 0.9 GtC yr^{-1}, process models: 1.5±0.7 GtC yr^{-1}). The GOBMs (1.0 ± 0.1 GtC yr^{-1}), *f*CO_2-products (1.3 ± 0.3 GtC yr^{-1}), and inversion systems (1.4 ± 0.3 GtC yr^{-1}) indicate a large S_{OCEAN} sink for the tropical ocean flux (see Figure 6c for spatial patterns). DGVMs indicate a sink for the net land flux of 0.5 ±0.4 GtC yr^{-1}, whereas the inversion systems indicate a small source although with larger model spread (-0.1 ± 0.6 GtC yr^{-1}, Figure 14, third row).

A continuing conundrum is the partitioning of the global atmosphere-land flux between the Northern Hemisphere land and the tropical land (Stephens et al., 2007; Pan et al., 2011; Gaubert et al., 2019; Stephens et al., 2026). It is of importance because each region has its own history of land-use change, climate drivers, and impact of increasing atmospheric CO_2 and nitrogen deposition. Quantifying the magnitude of each sink is a prerequisite to understanding how each individual driver impacts the tropical and mid/high-latitude carbon balance. We define the North-South (N-S) difference as net atmosphere-land flux north of 30°N minus the net atmosphere-land flux south of 30°N. For the inversions, the N-S difference is 1.7 ± 1.0 GtC yr^{-1} across this year's inversion ensemble. In the ensemble of DGVMs the N-S difference is 0.5 ± 0.6 GtC yr^{-1}, a much narrower range than the one from atmospheric inversions. The smaller spread across DGVMs than across inversions is to be expected as there is no correlation between Northern and Tropical land sinks in the DGVMs as opposed to the inversions where the sum of the two regions being well-constrained by atmospheric observations leads to an anti-correlation between these two regions.

https://doi.org/10.5194/essd-2026-895
Preprint. Discussion started: 10 November 2026
© Author(s) 2026. CC BY 4.0 License.



The tropical lands are the origin of most of the atmospheric CO_2 interannual variability (Ahlström et al., 2015), consistently among the process models and inversions (Figure 14). The interannual variability in the tropical ocean is similar among the ocean fCO_2-products (0.05-0.15 GtC yr^{-1}) the GOBMs (0.07-0.18 GtC yr^{-1}), and the atmospheric inversions (0.08-0.15 GtC yr^{-1}). The DGVMs and inversions indicate that atmosphere-to-land CO_2 fluxes are more variable than atmosphere-to-ocean CO_2 fluxes in the tropics, with interannual variability of 0.4 to 1.2 GtC yr-1 for DGVMs and 0.8 to 1.0 GtC yr^{-1} for inversions, for 1990-2025. The year 2024 saw the largest growth rate in the atmosphere so far, largely caused by reductions in the tropical land sink, similar to earlier extreme years, such as during the 2015-2016 El Niño period. The inversions seem to capture the response of the tropical land sink to a larger degree than the DGVMs, with a 2024 tropical land source of 1.7 ± 0.8 GtC yr^{-1} for the inversions versus a much smaller source of 0.1 ± 0.7 for the DGVMs. The year 2025 saw a return to more normal climate conditions which caused a rebound of the tropical land sink to 1.0 ± 0.9 GtC yr^{-1} for the inversions and 1.4 ± 0.5 GtC yr^{-1} for the DGVMs (Figure 14).

3.8.2.3 South

In the southern extra-tropics (south of 30°S), the atmospheric inversions suggest a net anthropogenic (S_{LAND} - E_{LUC} + S_{OCEAN}) atmosphere-to-surface sink for 2016-2025 of 1.2 ± 0.3 GtC yr^{-1}, in line with the process models' estimate of 1.2 ± 0.2 GtC yr^{-1} (Figure 14). An approximately neutral net land flux for the southern extra-tropics is estimated by both the DGVMs (0.04 ± 0.06 GtC yr^{-1}) and the inversion systems (0.03 ± 0.1 GtC yr^{-1}). This means nearly all carbon uptake is due to oceanic sinks south of 30°S. The Southern Ocean flux in the fCO_2-products (1.3 ± 0.3 GtC yr^{-1}), inversion estimates (1.2 ± 0.3 GtC yr^{-1}), and GOBMs (1.2 ± 0.2 GtC yr^{-1}) agree well (Figure 14, bottom row). This agreement is subject to the choice of the river flux adjustment (Lacroix et al., 2020, Hauck et al., 2023b, Planchat et al., 2025). Nevertheless, the time-series of atmospheric inversions and fCO_2-products diverge from the GOBMs. A substantial overestimation of the trends in the fCO_2-products has been suggested resulting from sparse and unevenly distributed observations, especially in wintertime (Figure S4; Hauck et al., 2023a; Gloege et al., 2021). Model biases likely contribute as well, although expected biases in mode water formation, stratification, and the chemical buffer capacity (Terhaar et al., 2021, Bourgeois et al., 2022, Terhaar et al., 2022) were not confirmed for the ensemble average of the suite of models used here (section 3.6.5 and Supplement S3.3, Figures S6 and S7). Recently, a high-resolution model study has shown that the Southern Ocean sink is 10% higher when spatial resolution is increased such that mesoscale eddies are resolved (Patara et al., 2026).

The interannual variability in the southern extra-tropics is low because of the dominance of ocean areas with low variability compared to land areas. The split between land (S_{LAND}-E_{LUC}) and ocean (S_{OCEAN}) shows a substantial contribution to variability in the south coming from the land, with no consistency between the DGVMs and the inversions or among inversions. This is expected due to the difficulty of

https://doi.org/10.5194/essd-2026-895
Preprint. Discussion started: 10 November 2026
© Author(s) 2026. CC BY 4.0 License.



Open Access Earth System Science Data Discussions

separating exactly the land and oceanic fluxes when viewed from atmospheric observations alone. The S_{OCEAN} interannual variability was found to be higher in the fCO_2-products (0.04-0.17 GtC yr^{-1}) compared to GOBMs (0.03 to 0.07 GtC yr^{-1}) in 1990-2025. Inversions give an interannual variability of 0.06 to 0.13 GtC yr^{-1}. Model subsampling experiments recently illustrated that fCO_2-products may overestimate decadal variability in the Southern Ocean carbon sink by 30% and the trend since 2000 by 50-130% due to data sparsity, based on one and two fCO_2-products with strong variability (Gloege et al., 2021, Hauck et al., 2023a). The trend benchmark test using the method of Hauck et al., (2023a) and a subset of 9 fCO_2-products confirms the sensitivity of the decadal trends in fCO_2-products to reconstruction biases, particularly in the Southern Ocean (Roobaert et al 2026). However, Roobaert et al (2026) also find compensating positive biases in the ensemble so that the ensemble mean bias is smaller than the bias from some individual fCO_2-products.

3.8.2.4 RECCAP2 regions

Aligning with the RECCAP-2 initiative (Ciais et al., 2022; Poulter et al., 2022; DeVries et al., 2023), we provide a breakdown of this GCB paper estimate of the E_{LUC}, S_{LAND}, Net land (S_{LAND} - E_{LUC}), and S_{OCEAN} fluxes over the 10 land, and 5 ocean RECCAP-2 regions, averaged over the period 2016-2025 (Figure 15). The DGVMs and inversions suggest a positive net land sink in all regions, except for South America, Africa, and Southeast Asia, where the inversions indicate a small net source of -0.11±0.45 GtC yr^{-1}, -0.22±0.30 GtC yr^{-1}, and -0.05±0.32 GtC yr^{-1}, respectively, compared to a small sink of 0.04±0.26 GtC yr^{-1}, 0.25±0.17 GtC yr^{-1}, and 0.08±0.11 GtC yr^{-1} for the DGVMs. The uncertainty in the sign of net tropical carbon fluxes is driven by opposing gross fluxes and relatively large uncertainty in the gross fluxes themselves. For South America, DGVMs estimate S_{LAND} of 0.45±0.29 GtC yr^{-1} and E_{LUC} of 0.42±0.13 GtC yr^{-1}. Bookkeeping models suggest a larger E_{LUC} source of 0.53±0.01 GtC yr^{-1}. Similarly, in Southeast Asia, the DGVMs estimate an E_{LUC} of 0.19±0.07 GtC yr^{-1}, compared with the bookkeeping model estimate of 0.32±0.02 GtC yr^{-1}. It is worth noting that emissions from peat fires (from GFED5) and drainage (from FAO, LPX-Bern, and ORCHIDEE-Peat) are added to bookkeeping model E_{LUC} estimates (see Supplement S2.2), which increases Southeast Asia E_{LUC} by 0.08 GtC yr^{-1}, over 2016-2025. Importantly, only 2 out of 23 DGVMs include peat fires and none of the DGVMs include peat drainage. Therefore, DGVMs may underestimate E_{LUC}, which could explain the net sink discrepancy with inversions. In Africa, E_{LUC} is similar for DGVMs and bookkeeping models (0.3-0.4 GtC yr^{-1}), and DGVMs estimate an S_{LAND} of 0.56±0.13 GtC yr^{-1}.

The inversions suggest the largest net land sinks are in North America (0.41±0.32 GtC yr^{-1}), Russia (0.60±0.27 GtC yr^{-1}), Europe (0.24±0.27 GtC yr^{-1}), and East Asia (0.27±0.32 GtC yr^{-1}). This agrees well with the DGVMs in North America (0.39±0.16 GtC yr^{-1}), which indicate a large natural land sink (S_{LAND}) of 0.44±0.16 GtC yr^{-1}, and small net land-use related carbon losses (0.05±0.07 GtC yr^{-1}). The

https://doi.org/10.5194/essd-2026-895
Preprint. Discussion started: 10 November 2026
© Author(s) 2026. CC BY 4.0 License.



DGVMs suggest a smaller net land sink in Russia compared to inversions (0.34±0.15 GtC yr^{-1}), and a similar net sink in East Asia (0.20±0.11 GtC yr^{-1}).

There is generally a higher level of agreement in the estimates of regional ocean anthropogenic carbon sink between the different data streams (GOBMs, fCO_2-products and atmospheric inversions) on decadal scale, compared to the agreement between the different land flux estimates. The data streams agree that the largest contribution to S_{OCEAN} stems from the Southern Ocean due to a combination of high flux density and large surface area, followed by the Pacific (large area) and Atlantic (high flux density) basins . In the Southern Ocean, GOBMs suggest a sink of 0.98±0.16 GtC yr^{-1}, in line with the fCO_2-products (1.03±0.31 GtC yr^{-1}) and atmospheric inversions (0.96±0.29 GtC yr^{-1}). There is also agreement within the uncertainties in the Pacific Ocean, with GOBMs, fCO_2-products, and atmospheric inversions indicating a sink of 0.83±0.10 GtC yr^{-1}, 1.04±0.25 GtC yr^{-1}, and 0.93±0.24 GtC yr^{-1}, respectively. However, in the Atlantic Ocean, GOBMs simulate a sink of 0.50±0.09 GtC yr^{-1}, noticeably lower than both the fCO_2-products (0.77±0.13 GtC yr^{-1}) and atmospheric inversions (0.77±0.14 GtC yr^{-1}). It is important to note the fCO_2-products and atmospheric inversions have a substantial and uncertain river flux adjustment in the Atlantic Ocean (0.3 GtC yr^{-1}) that also leads to a mean offset between GOBMs and fCO_2-products/inversions in the latitude band of the tropics (Figure 14). The Indian Ocean due its smaller size and the Arctic Ocean due to its size and sea-ice cover that prevents air-sea gas-exchange are responsible for smaller but non negligible S_{OCEAN} fluxes (Indian Ocean: 0.26±0.03 GtC yr^{-1}, 0.29±0.14 GtC yr^{-1}, and 0.31±0.14 GtC yr^{-1} for GOBMs, fCO_2-products, and atmospheric inversions, respectively, and Arctic Ocean: 0.05±0.02 GtC yr^{-1}, 0.13±0.07 GtC yr^{-1}, and 0.06±0.04 GtC yr^{-1} for GOBMs, fCO_2-products, and atmospheric inversions, respectively). Note that the S_{OCEAN} numbers presented here deviate from numbers reported in RECCAP-2 where the net air-sea CO_2 flux is reported (i.e. without river flux and preindustrial mean adjustment for fCO_2-products and inversions, and with river flux adjustment subtracted from GOBMs in most chapters, or comparing unadjusted datasets with discussion of uncertain regional riverine fluxes as major uncertainty, e.g. Sarma et al., 2023, DeVries et al., 2023).

3.8.3 Fire emissions in 2026

Fire emissions so far in 2026 have been close to the average of recent decades, with high emissions in Southeast Asia offset by relatively low emissions in several other major fire regions, particularly South America and North America. Figure S15 shows global and regional emissions estimates for the period 1 January-30 September in each year from 2003 to 2026. Estimates derive from the Global Fire Emissions Database version 5.1 (GFED5.1; van der Werf et al., 2025, Chen et al., 2026) and the Global Fire Assimilation System (GFAS; Kaiser et al., 2012). Because the transition to GFED5.1 has substantially revised absolute fire emissions estimates, we report absolute emissions from GFED5.1,

https://doi.org/10.5194/essd-2026-895
Preprint. Discussion started: 10 November 2026
© Author(s) 2026. CC BY 4.0 License.



Open Access Earth System Science Data Discussions

while relative anomalies are calculated independently for GFED5.1 and GFAS and reported separately, following Burton et al. (2026). GFED5.1 estimates that global fire emissions were 2.55 GtC during January-September 2026. Relative to the 2016-2025 average for the same months, global emissions were 8% below average in GFED5.1 but 3% above average in GFAS. Relative to the full 2003-2025 record, emissions were 7% below average in GFED5.1 and 5% below average in GFAS.

Global fire emissions in 2026 remained well below the high levels of 2023 and 2024, when GFED5.1 estimates January-September emissions of 3.17 and 3.41 GtC, respectively, but were slightly higher than the 2.49 GtC emitted during the same period in 2025. The high global emissions in 2023 and 2024 were associated with exceptionally high emissions in North America in 2023, principally in Canada, and in both North America and South America in 2024, principally in Canada and Brazil (Jones et al., 2024a; Kelley et al., 2025). In contrast, the global total in 2026 reflects a mixture of strong positive and negative regional anomalies rather than synchronously high emissions across several major fire regions.

The clearest positive regional anomaly in 2026 occurred in Southeast Asia, where GFED5.1 estimates January-September fire emissions of 0.34 GtC. Relative to the 2016-2025 average, emissions were 29% above average in GFED5.1 and 232% above average in GFAS; relative to the full 2003-2025 record, they were 12% above average in GFED5.1 and 131% above average in GFAS. Indonesia showed the strongest national-scale positive anomaly among the countries with high fire emissions shown in Figure S15, with GFED5.1 emissions of 0.13 GtC. Relative to the previous decade, emissions were 433% above average in GFED5.1 and 791% above average in GFAS. The substantially larger anomaly in GFAS may partly reflect differences in remote-sensing approach: GFAS is driven by active fire observations and fire radiative power, whereas GFED5.1 remains more strongly constrained by burned area detection. This distinction may be particularly important for Indonesian peat fires, where persistent and spatially fragmented burning can be difficult to capture completely from burned area but can generate repeated active fire detections, potentially making FRP-based estimates more sensitive to anomalously high fire activity (Mouillot et al., 2014; Wooster et al., 2021; Chen et al., 2024).

These positive anomalies were counterbalanced by low emissions in several other major fire regions. In South America, GFED5.1 estimates January-September fire emissions of 0.17 GtC, with emissions 50% below the 2016-2025 average in GFED5.1 and 29% below average in GFAS. Brazil emitted 0.094 GtC according to GFED5.1, with emissions 54% below average in GFED5.1 and 32% below average in GFAS. In North America, GFED5.1 estimates emissions of 0.22 GtC, 20% below the previous-decade average in GFED5.1 and 40% below average in GFAS. Canada emitted 0.14 GtC, with emissions 7% below average in GFED5.1 and 53% below average in GFAS. Emissions were also below the previous-decade average in Australasia, by 8% in GFED5.1 and 19% in GFAS, and across the Southern Hemisphere extratropics, by 26% in GFED5.1 and 44% in GFAS. Across the tropics, GFED5.1 estimates emissions of 1.94 GtC, 12% below the 2016-2025 average, whereas GFAS indicates emissions 16% above average.

https://doi.org/10.5194/essd-2026-895
Preprint. Discussion started: 10 November 2026
© Author(s) 2026. CC BY 4.0 License.



We caution that the fire emissions fluxes presented here should not be compared directly with other fluxes of the budget (e.g., S_{LAND} or E_{LUC}) due to incompatibilities between the observable fire emission fluxes and what is quantified in the S_{LAND} and E_{LUC} components of the budget. The fire emission estimates from global fire products relate to all fire types that can be observed in Earth Observations (Giglio et al., 2018; Randerson et al., 2012; Kaiser et al., 2012), including (i) fires occurring as part of natural disturbance-recovery cycles that would also have occurred in the pre-industrial period (Yue et al., 2016; Keeley and Pausas, 2019; Zou et al., 2019), (ii) fires occurring above and beyond natural disturbance-recovery cycle due to changes in climate, CO_2 and N fertilisation and to an increased frequency of extreme drought and heatwave events (Abatzoglou et al., 2019; Jones et al., 2022; Zheng et al., 2021; Burton et al., 2024), and (iii) fires occurring in relation to land use and land use change, such as deforestation fires and agricultural fires (van der Werf et al., 2010; Magi et al., 2012). In the context of the global carbon budget, fire emissions associated with (ii) should be included in the S_{LAND} component, fire emissions associated with (iii) should already be accounted for in the E_{LUC} component, while fire emissions associated with (i) should not be included in the global carbon budget as part of the natural carbon cycle. However, it is not currently possible to derive specific estimates for fluxes (i), (ii), and (iii) using global fire emission products such as GFED or GFAS. In addition, the fire emissions estimates from global fire emissions products represent a gross flux of carbon to the atmosphere, whereas the S_{LAND} component of the budget is a net flux that should also include post-fire recovery fluxes. Even if emissions from fires of type (ii) could be separated from those of type (i), these fluxes may be partially or wholly offset in subsequent years by post-fire fluxes as vegetation recovers, sequestering carbon from the atmosphere to the terrestrial biosphere (Yue et al., 2016; Jones et al., 2024b). Increases in forest fire emissions and severity (emissions per unit area) globally during the past two decades have highlighted the increasing potential for fire emissions fluxes to outweigh post-fire recovery fluxes, though long-term monitoring of vegetation recovery is required to quantify the net effect on terrestrial C storage (Jones et al., 2024b).

3.9 Closing the global carbon cycle

3.9.1 Partitioning of cumulative emissions and sink fluxes

Emissions during the period 1850-2025 amounted to 755 ± 55 GtC and were partitioned among the atmosphere (295 ± 5 GtC; 39%), ocean (200± 55 GtC; 26%), and land (190 ± 40 GtC; 25%). The cumulative land sink is lower than the cumulative land-use emissions (245 ± 50 GtC), making the global land a source of 55 ± 65 GtC over the whole 1850-2025 period (Table 8).

The use of nearly independent estimates for the individual terms of the global carbon budget shows a cumulative budget imbalance of 70 GtC (9% of total emissions) during 1850-2025 (Table 8), which suggests that emissions could be slightly too high by the same proportion or that the combined land and ocean sinks are underestimated (by up to 20%). A large part of the B_{IM} occurs over the first half of the

https://doi.org/10.5194/essd-2026-895
Preprint. Discussion started: 10 November 2026
© Author(s) 2026. CC BY 4.0 License.



20th century (Figure 3, red dashed line) and could originate from the estimation of significant increase in E_{FOS} and E_{LUC} between the mid 1920s and the mid 1960s which is unmatched by a similar growth in atmospheric CO_2 concentration as recorded in ice cores (Figure 3).

For the more recent 1959-2025 period where direct atmospheric CO_2 measurements are available, total emissions ($E_{FOS} + E_{LUC}$) amounted to 545 ± 50 GtC, of which 430 ± 20 GtC (79%) were caused by fossil CO_2 emissions, and 110 ± 45 GtC (21%) by land-use change (Table 8). The total emissions were partitioned among the atmosphere (235 ± 5 GtC; 43%), ocean (145 ± 40 GtC; 26%), and the land (125 ± 30 GtC; 23%), with a budget imbalance of 40 GtC (7% of total emissions). All components except land-use change emissions have significantly grown since the 1960s, with important interannual variability in the growth rate in atmospheric CO_2 concentration primarily mirrored in the land CO_2 sink (Figure 4), and some decadal variability in all terms (Table 7). Differences with previous budget releases are documented in Figure S16.

The global carbon budget averaged over the last decade (2016-2025) is shown in Figure 2 and Table 7. For this period, 88% of the total emissions ($E_{FOS} + E_{LUC}$) were from fossil CO_2 emissions (E_{FOS}), and 12% from land-use change (E_{LUC}). The total emissions were partitioned among the atmosphere (48%), ocean (27%) and land (22%), with a small positive budget imbalance (3%). For single years, the budget imbalance can be larger (Figure 4f).

3.9.2 Trend and variability in the carbon budget imbalance

The carbon budget imbalance (B_{IM}; Eq. 1, Figure 4f) quantifies the mismatch between the estimated total emissions and the estimated changes in the atmosphere, land, and ocean reservoirs. The budget imbalance from 1959 to 2025 is relatively small (40 GtC cumulated over the period, i.e. 0.6 GtC yr^{-1} on average) and shows no significant trend over the 1959-2025 period (Figure 4, Table 7). The process models (GOBMs and DGVMs) and fCO_2-products have been selected to match observational constraints in the 1990s, but no further constraints have been applied to their representation of trend and variability. Therefore, the small mean and trend in the budget imbalance can be seen as evidence of a coherent community understanding of the emissions and their partitioning on those time scales (Figure 4). However, the budget imbalance shows substantial variability of the order of ±1 GtC yr^{-1}, particularly over semi-decadal time scales, although most of the variability is within the uncertainty of the individual estimates of the global budget.

We cannot attribute the cause of the budget imbalance with our analysis, we only note that the budget imbalance is unlikely to be explained by errors in the emissions alone because of its large semi-decadal variability component, a variability that is atypical of emissions, and also because the budget imbalance has not increased in the past 60 years despite a near tripling in anthropogenic emissions (Figure 4). Errors in S_{LAND} and S_{OCEAN} are more likely to be the main cause for the budget imbalance, especially on

https://doi.org/10.5194/essd-2026-895
Preprint. Discussion started: 10 November 2026
© Author(s) 2026. CC BY 4.0 License.



interannual to semi-decadal timescales. For example, underestimation of the S_{LAND} by DGVMs has been reported following the eruption of Mount Pinatubo in 1991 possibly due to missing responses to changes in diffuse radiation (Mercado et al., 2009). Although we account for aerosol effects on solar radiation quantity and quality (diffuse vs direct), most DGVMs only used the former as input (i.e., total solar radiation) (Table S1). Thus, the ensemble mean may not capture the full effects of volcanic eruptions, i.e., associated with high light scattering sulphate aerosols, on the land carbon sink (O'Sullivan et al., 2021), potentially explaining the large positive B_{IM} in 1991-1992. DGVMs are suspected to underestimate the land sink reduction in response to El Niño events (drought, high temperature extremes, and fires) (see Section 3.7.3), which could explain the large negative B_{IM} in 1986-1987, 1997-1998 or 2023-2024. Few DGVMs have explicit representation of drought-mortality and only 6 from 23 include forest demography, although recent efforts are underway to fill these critical research gaps (Eckes-Shephard et al., 2025 Yao et al., 2022, 2023). Quasi-decadal variability in the ocean sink has also been reported, with all methods agreeing on smaller than expected ocean CO_2 sink in the 1990s and a larger than expected sink in the 2000s (Figure 10b; Landschützer et al., 2016, DeVries et al., 2019, Hauck et al., 2020, McKinley et al., 2020, Gruber et al., 2023) and the climate-driven variability could be substantial but is not well constrained (DeVries et al., 2023, Müller et al., 2023). Errors in sink estimates could also be partly driven by errors in the climatic forcing data, particularly precipitation for S_{LAND} and wind for S_{OCEAN}.

Further, we cannot exclude an overestimation of CO_2 emissions, particularly from land-use change, given their large uncertainty, as has been suggested elsewhere (Piao et al., 2018), and/or an underestimate of the land or ocean sinks. A larger estimate of the atmosphere-land CO_2 flux (S_{LAND}-E_{LUC}) over the extra-tropics would reconcile bottom-up model results with inversion estimates (Figure 14). Likewise, a larger S_{OCEAN} is also possible given the higher estimates from the fCO_2-products and the oxygen-based estimates (see Table 6 and Figure 10b), the underestimation of interior ocean anthropogenic carbon accumulation in the GOBMs (Section 3.6.5, Müller et al., 2023), or known biases of ocean models (e.g., Terhaar et al., 2022; 2024). More integrated use of observations in the global carbon budget, either on their own or for further constraining model results, should help resolve some of the budget imbalance.

4 Tracking progress towards mitigation targets

The average growth in global fossil CO_2 emissions peaked at nearly +3% per year during the 2000s, primarily driven by the rapid growth in emissions in China. In the last decade, however, the global growth rate has slowly declined, reaching a low +0.9% per year on average over 2016-2025. While this slowdown in global fossil CO_2 emissions growth is welcome, global fossil CO_2 emissions continued to grow, far from the rapid emission decreases needed to be consistent with the temperature goals of the Paris Agreement.

https://doi.org/10.5194/essd-2026-895
Preprint. Discussion started: 10 November 2026
© Author(s) 2026. CC BY 4.0 License.



Since the 1990s, the average growth rate of fossil CO_2 emissions has continuously declined across the group of developed countries of the Organisation for Economic Co-operation and Development (OECD), with emissions peaking in around 2005 and declining at 1.4% yr^{-1} in the decade 2015-2025, compared to a decline of 1.0% yr^{-1} during the 2006-2015 period (Table 9). In the non-OECD countries, emissions rose 4.1% yr^{-1} from 2006-2015, but growth has lowered to 2.1% yr^{-1} from 2016-2025.

In the decade 2016-2025, territorial fossil CO_2 emissions decreased significantly (at the 95% confidence level) in 40 countries whose gross domestic product (GDP) grew significantly (also at the 95% confidence level): Albania, Australia, Austria, Belarus, Belgium, Bosnia and Herzegovina, Bulgaria, Cameroon, Chile, Czechia, Denmark, Estonia, Finland, France, Germany, Greece, Hungary, Ireland, Italy, Japan, Latvia, Lithuania, Luxembourg, Netherlands, New Zealand, Norway, Poland, Portugal, Romania, Serbia, Slovakia, Slovenia, South Korea, Spain, Sweden, Switzerland, Thailand, United Kingdom, USA, Venezuela (updated from Le Quéré et al., 2019). Altogether, these 40 countries emitted 2.8 GtC yr^{-1} (10.1 $GtCO_2$ yr^{-1}) on average over the last decade, about 26% of 2025 global CO_2 fossil emissions. For comparison, over the previous decade (2006-2015), 22 countries showed a significant decrease in territorial fossil CO_2 emissions while significantly growing their GDP (Austria, Belgium, Bulgaria, Czechia, France, Germany, Lithuania, Luxembourg, Malta, Netherlands, North Macedonia, Poland, Romania, Serbia, Slovakia, Sweden, Switzerland, Tonga, Tuvalu, United Kingdom, USA, Uzbekistan). These 22 economies emitted an average 2.2 GtC yr^{-1} over 2006–2015, or 23% of 2015 global CO_2 fossil emissions. The number of countries reducing their emissions while growing their economies is clearly increasing, with emissions reductions expanding to 59 countries in all continents for the shorter 2019-2025 period, although not all of these trends are significant (Le Quéré et al., 2026).

By decomposing emission changes into the components of growth, a Kaya decomposition helps give an initial understanding of the drivers of emission changes (Peters et al., 2017b). The reduction in growth in global fossil CO_2 emissions in the last decade (2016-2025, 0.9% yr^{-1}) relative to the previous decade (2006-2015, 1.9% yr^{-1}) is due to slightly weaker economic growth (3.2% yr^{-1} to 2.8% yr^{-1}), a decline in CO_2 emissions per unit of energy (+0.3% yr^{-1} to -0.4% yr^{-1}), and steady declines in energy per unit of GDP (-1.5% yr^{-1} to -1.5% yr^{-1}) (Figure S18). The growth in solar and wind energy in electricity, and to a lesser extent the deployment of electric vehicles, are a dominant contribution to the reduction in emissions growth between the two decades (Le Quéré et al., 2026).

Fossil CO_2 emission declines in the USA and the EU27 are primarily driven by sustained or increasing declines in energy per GDP and CO_2 emissions per unit energy. China has seen emissions growth decline from 5.7% yr^{-1} in the 2006-2015 decade to 2.7% yr^{-1} from 2016-2025, driven by weaker economic growth (four percentage points), offset by a considerable weakening in the rate of reduction in the energy per GDP (two percentage points), with sustained improvements in CO_2 emissions per unit energy (Figure S18). India has had strong economic growth that is not offset by declines in energy per

https://doi.org/10.5194/essd-2026-895
Preprint. Discussion started: 10 November 2026
© Author(s) 2026. CC BY 4.0 License.



GDP or declines in CO_2 emissions per unit energy, driving up fossil CO_2 emissions. In the rest of the world, economic growth has slowed considerably in the last decade, and carbon intensity has increased, with declines in energy per GDP unable to counteract these increases leading to growing emissions. Despite the high deployment of renewables in some countries (e.g., China, India), fossil energy sources continue to grow to meet growing energy demand (Le Quéré et al., 2019, 2026). In summary, the carbon intensity of energy has consistently decreased over the past decade globally (-0.4% yr^{-1}), indicating decarbonisation of the global energy system, with declines in China (-0.8% yr^{-1}), the European Union (-1.3% yr^{-1}), the USA (-0.9% yr^{-1}), but no change in India. Carbon intensity in the Rest of the World combined, also declined (-0.3%). The global decarbonation trends have not been sufficient to offset the growth in global energy demand, with energy demand growing faster than expected due to weakening declines in energy per GDP in China, US, and globally.

The slower growth of global fossil CO_2 emissions in the last decade is due in part to the emergence of climate policy (Eskander and Fankhauser 2020; Le Quéré et al 2019; Hoppe et al., 2023) and technological change, which is leading to a shift from coal to gas and growth in renewable energies, and reduced expansion and utilisation of coal capacity in some countries. At the aggregated global level, decarbonisation shows a strong and growing signal in the last decade, with smaller contributions from lower economic growth and declines in energy per GDP. Altogether, current global fossil CO_2 emissions growth is far from the reductions needed to meet the ambitious climate goals of the UNFCCC Paris agreement.

Last, we update the remaining carbon budget (RCB) based on two studies, the IPCC AR6 (Canadell et al., 2021) and the revision of the IPCC AR6 estimates (Forster et al., 2026, Lamboll et al., 2023). We update the RCB assessed by the IPCC AR6 (Canadell et al., 2021), accounting for the 2020 to 2026 GCB estimated anthropogenic emissions from fossil combustion (E_{FOS}) and land use change (E_{LUC}). From January 2027, the IPCC AR6 RCB (50% likelihood) for limiting global warming to 1.5°C, 1.7°C and 2°C is estimated to amount to 55, 155, and 290 GtC (210, 560, 1060 $GtCO_2$). The Forster et al. (2026) study proposed a significantly lower RCB than IPCC AR6, primarily due to an update of the climate emulator (MAGICC) used to estimate the warming contribution of non-CO_2 agents, and to the warming (i.e. emissions) that occurred over the 2020-2025 period. We update the Forster et al., (2026) RCB accounting for our estimated anthropogenic emissions for 2026. From January 2027, the Forster et al., (2026) RCB (50% likelihood) for limiting global warming to 1.5°C, 1.7°C and 2°C is estimated to amount to 25, 125, and 275 GtC (85, 455, 1005 $GtCO_2$), significantly smaller than the updated IPCC AR6 estimate. Both the original IPCC AR6 and Forster et al. (2026) estimates include the Earth System uncertainty on the climate response to cumulative CO_2 emissions, which is reflected through the percent likelihood of exceeding the given temperature threshold, an additional uncertainty of ±220$GtCO_2$ due to alternative non-CO_2 emission scenarios, and other sources of uncertainties (see Canadell et al., 2021). The two sets of original estimates overlap when considering all uncertainties.

https://doi.org/10.5194/essd-2026-895
Preprint. Discussion started: 10 November 2026
© Author(s) 2026. CC BY 4.0 License.



Open Access Earth System Science Data Discussions

Here, we take the average of our update of both IPCC AR6 and Forster et al. (2025) estimates, giving a remaining carbon budget (50% likelihood) for limiting global warming to 1.5°C, 1.7°C and 2°C of respectively 40, 140, and 280 GtC (150, 510, 1035 $GtCO_2$) starting from January 2027. We emphasise the large uncertainties, particularly when close to the global warming limit of 1.5°C. These 1.5°C, 1.7°C and 2°C RCBs correspond respectively to about 3, 12 and 24 years from the beginning of 2027, at the 2026 level of total anthropogenic CO_2 emissions. Reaching net-zero CO_2 emissions by 2050 entails cutting total anthropogenic CO_2 emissions by about 0.5 GtC (1.8 $GtCO_2$, 4% of 2026 emissions), each year on average, comparable to the decrease in E_{FOS} observed in 2020 during the COVID-19 pandemic. However, such linear decrease between now and 2050 would lead to cumulative emissions of 140 GtC (515 $GtCO_2$), well above the 40 GtC remaining budget to limit global warming to 1.5°C, but still compatible to the 140 GtC budget to limit warming to 1.7°C (in phase with the "well below 2°C" ambition of the Paris Agreement).

5 Discussion

Each year when the global carbon budget is published, each flux component is updated for all previous years to consider revisions that are the result of further scrutiny and verification of the underlying data in the primary input datasets. Annual estimates may be updated with improvements in data quality and timeliness (e.g., to eliminate the need for extrapolation of forcing data such as land use). Of all terms in the global budget, only the fossil CO_2 emissions and the growth rate in atmospheric CO_2 concentration are based primarily on empirical inputs supporting annual estimates in this carbon budget. The carbon budget imbalance, yet an imperfect measure, provides a strong indication of the limitations in observations, in understanding and representing processes in models, and/or in the integration of the carbon budget components.

The persistent unexplained variability in the carbon budget imbalance limits our ability to verify reported emissions (Peters et al., 2017a) and suggests we do not yet have a complete understanding of the underlying carbon cycle dynamics on annual to decadal timescales. Resolving most of this unexplained variability should be possible through different and complementary approaches. First, as intended with our annual updates, the imbalance as an error term should be reduced by improvements of individual components of the global carbon budget that follow from improving the underlying data and statistics and by improving the models through the resolution of some of the key uncertainties detailed in Table 10. Second, additional clues to the origin and processes responsible for the variability in the budget imbalance could be obtained through a closer scrutiny of carbon variability in light of other Earth system data (e.g., heat balance, water balance), and the use of a wider range of biogeochemical observations to better understand the land-ocean partitioning of the carbon imbalance such as the constraint from atmospheric oxygen. Finally, additional information could also be obtained through better inclusion of process knowledge at the regional level. The limit for reducing the carbon

https://doi.org/10.5194/essd-2026-895
Preprint. Discussion started: 10 November 2026
© Author(s) 2026. CC BY 4.0 License.

budget imbalance is yet unclear, but most certainly not yet reached given the possibilities for improvements that lie ahead.

Estimates of global fossil CO_2 emissions from different datasets are in relatively good agreement when the different system boundaries of these datasets are considered (Andrew, 2020a). While estimates of E_{FOS} are derived from reported activity data requiring much fewer complex transformations than some other components of the budget, uncertainties remain, and one reason for the apparently low variation between datasets is precisely the reliance on the same underlying reported energy data. The budget excludes some sources of fossil CO_2 emissions, which available evidence suggests are relatively small (<1%) (see Supplement S.8.2). We include emissions from lime production in China and the US, but these are still absent in reporting from most other non-Annex I countries, and before 1990 in other Annex I countries.

Estimates of E_{LUC} suffer from a range of intertwined issues (Obermeier et al., 2025), including the poor knowledge of historical land-cover and land-use change (particularly before the 1960s when FAO reporting started), the rudimentary representation of management processes in most models, and the diversity in methodologies and boundary conditions used across methods (e.g., Arneth et al., 2017; Pongratz et al., 2014; Bastos et al., 2021). Uncertainties in current and historical carbon stocks in soils and vegetation also contribute to uncertainty in E_{LUC} estimates. Major efforts are thus necessary to resolve the different issues concerning E_{LUC} (Obermeier et al., 2025). The large uncertainty and limited reliability of E_{LUC} estimates are particularly concerning given the growing importance of E_{LUC} for climate mitigation strategies, and the large issues in the quantification of the cumulative emissions over the historical period that arise from large uncertainties in E_{LUC}.

By adding the natural land sink in managed forests estimated by DGVMs (part of S_{LAND} in this budget) to the budget E_{LUC} estimate, we reconcile most of the large gap between our E_{LUC} estimate and the land-use flux estimates from NGHGIs (Figure 8). This reconciliation (translation) can be used as potential adjustment in the policy context, for instance to help assess the collective countries' progress towards the goal of the Paris Agreement avoiding double-accounting for the natural sink in managed forests. In the absence of this translation, collective progress would appear better than it is (Grassi et al., 2021). A clear understanding of these implications is thus essential for policymakers for developing effective climate targets (Grassi et al., 2025). The application of this translation is also recommended in the UNFCCC Synthesis report for the first Global Stocktake (UNFCCC, 2022) whenever a comparison between LULUCF fluxes reported by countries and the global emission estimates of the IPCC is conducted. However, this translation should be seen as a short-term and pragmatic fix based on existing data, rather than a definitive solution to bridge the differences between global models and national inventories. Platforms for dataset comparisons (e.g., Melo et al., 2026) help strengthening the dialogue across communities and identify the additional steps needed to understand and reconcile the remaining

https://doi.org/10.5194/essd-2026-895
Preprint. Discussion started: 10 November 2026
© Author(s) 2026. CC BY 4.0 License.



differences, some of which are relevant at the country level (Grassi, et al., 2023, Schwingshackl, et al., 2022).

The comparison of GOBMs, fCO_2-products, and inversions highlights discrepancies in the temporal evolution of S_{OCEAN} in the Southern Ocean and northern high-latitudes (Figure 14, Hauck et al., 2023a) and in the mean S_{OCEAN} in the tropics. A large part of the uncertainty in the mean fluxes stems from the regional distribution of the river flux adjustment term. The current distribution simulates the largest share of the outgassing to occur in the tropics (Lacroix et al., 2020) whereas a new study suggests a more equal split between the regions (Planchat et al., 2025). The long-standing sparse data coverage of fCO_2 observations in the Southern compared to the Northern Hemisphere (e.g., Takahashi et al., 2009) continues to exist (Bakker et al., 2016, 2026a, Figure S4) and to lead to substantially higher uncertainty in the S_{OCEAN} estimate for the Southern Hemisphere (Watson et al., 2020, Gloege et al., 2021, Hauck et al., 2023a, Heimdal et al 2024, Behncke et al 2026). This discrepancy, which also hampers model improvement, points to the need for increased high-quality fCO_2 observations especially in the Southern Ocean. At the same time, model uncertainty is illustrated by the large spread of individual GOBM estimates (indicated by shading in Figure 14) and highlights the need for model improvement, now also supported by the IOMB benchmarking. The issue of diverging trends in S_{OCEAN} from different methods remains a matter of concern, although the magnitude is reduced in this version of the GCB. Recent and on-going work suggests that the fCO_2-products may overestimate the trend although biases in the fCO_2-product ensemble may partly cancel out (Supplement S3.4). A data-constrained model approach suggests that the GOBMs underestimate the amplitude of decadal variability, but that the fCO_2-products overestimate the trend (Mayot et al., 2024). All three process-based GOBM evaluation approaches reject the previous hypothesis that biases in ocean ventilation explain a low anthropogenic CO_2 uptake in the GOBMs. This reinforces the question of how the larger anthropogenic carbon accumulation in ocean interior estimates can be reconciled with the process models. A potential candidate could be the anthropogenic riverine fluxes. The various methods agree within uncertainties on the mean ocean sink in the last decade, although the independent estimate from atmospheric oxygen measurements still shows the largest sink estimate for the past decade and has a steeper trend (Table 6). However, the estimate is consistent within uncertainties with S_{OCEAN}, with the relatively larger ocean sink in the fCO_2-products and some of the GOBMs.

The assessment of the net land-atmosphere exchange from DGVMs and atmospheric inversions also shows substantial discrepancy, particularly for the estimate of the net land flux over the northern extra-tropic. This discrepancy highlights the difficulty to quantify complex processes (CO_2 fertilisation, nitrogen deposition and fertilisers, climate change and variability, land management, etc.) that collectively determine the net land CO_2 flux. Resolving the differences in the Northern Hemisphere land sink will require the consideration and inclusion of larger volumes of observations.

https://doi.org/10.5194/essd-2026-895
Preprint. Discussion started: 10 November 2026
© Author(s) 2026. CC BY 4.0 License.



We provide metrics for the evaluation of the ocean and land models and the atmospheric inversions (Figure S5-S14, Tables S12 and S13). These metrics expand the use of observations in the global carbon budget, helping 1) to support improvements in the ocean and land carbon models that produce the sink estimates, and 2) to constrain the representation of key underlying processes in the models and to allocate the regional partitioning of the CO_2 fluxes. The joint use of process-based metrics in an objective evaluation framework (IOMB) targeted to evaluate the simulation of S_{OCEAN} in the ocean biogeochemistry models together with the introduction of CFC inventories to evaluate the ocean ventilation and the emergent constraint approach is an important advance. This is another step in the endeavour to use a broader range of observations and more stringent model evaluation that we hope will support continued improvements in the models and in the annual estimates of the global carbon budget. We assessed before that a sustained decrease of –1% in global emissions could be detected at the 66% likelihood level after a decade only (Peters et al., 2017a). Similarly, a change in behaviour of the land and/or ocean carbon sink would take as long to detect, and much longer if it emerges more slowly. To continue reducing the carbon imbalance on annual to decadal time scales, regionalising the carbon budget, and integrating multiple variables are powerful ways to shorten the detection limit and ensure the research community can rapidly identify issues of concern in the evolution of the global carbon cycle under the current rapid and unprecedented changing environmental conditions.

6 Conclusions

The estimation of global CO_2 emissions and sinks is a major effort by the carbon cycle research community that requires a careful compilation and synthesis of measurements, statistical estimates, and model results. The delivery of an annual carbon budget serves two purposes. First, there is a large demand for up-to-date information on the state of the anthropogenic perturbation of the climate system and its underpinning causes. A broad stakeholder community relies on the datasets associated with the annual carbon budget including scientists, policy makers, businesses, journalists, and non-governmental organisations engaged in adapting to and mitigating human-driven climate change. Second, over the last decades we have seen unprecedented changes in the human and biophysical environments (e.g., changes in the growth of fossil fuel emissions, impact of COVID-19 pandemic, Earth's warming, extreme events, and strength of the carbon sinks), which call for frequent assessments of the state of the planet, a better quantification of the causes of changes in the contemporary global carbon cycle, and an improved capacity to anticipate its evolution in the future. Building this scientific understanding to meet the extraordinary climate mitigation challenge requires frequent, robust, transparent, and traceable datasets and methods that can be scrutinised and replicated. This paper via 'living data' helps to keep track of new budget updates.

https://doi.org/10.5194/essd-2026-895
Preprint. Discussion started: 10 November 2026
© Author(s) 2026. CC BY 4.0 License.



7 Data availability

The data presented here are made available in the belief that their wide dissemination will lead to greater understanding and new scientific insights of how the carbon cycle works, how humans are altering it, and how we can mitigate the resulting human-driven climate change. Full contact details and information on how to cite the data shown here are given at the top of each page in the accompanying database and summarised in Table 2.

The accompanying database includes three Excel files organised in the following spreadsheets:

File Global_Carbon_Budget_2026v1.0.xlsx includes the following:

1. Summary
2. The global carbon budget (1959-2025);
3. The historical global carbon budget (1750-2025);
4. Global CO_2 emissions from fossil fuels and cement production by fuel type, and the per-capita emissions (1850-2025);
5. CO_2 emissions from land-use change from the individual bookkeeping models (1959-2025);
6. Ocean CO_2 sink from the individual global ocean biogeochemistry models and fCO_2-products (1959-2025);
7. Terrestrial CO_2 sink from the individual DGVMs (1959-2025);
8. Cement carbonation CO_2 sink (1959-2025).

File National_Fossil_Carbon_Emissions_2026v1.0.xlsx includes the following:

1. Summary
2. Territorial country CO_2 emissions from fossil fuels and cement production (1850-2025);
3. Consumption country CO_2 emissions from fossil fuels and cement production and emissions transfer from the international trade of goods and services (1990-2020) using CDIAC/UNFCCC data as reference;
4. Emissions transfers (Consumption minus territorial emissions; 1990-2020);
5. Country definitions.

File National_LandUseChange_Carbon_Emissions_2026v1.0.xlsx includes the following:

https://doi.org/10.5194/essd-2026-895
Preprint. Discussion started: 10 November 2026
© Author(s) 2026. CC BY 4.0 License.



1. Summary

2. Territorial country CO_2 emissions from Land Use Change (1850-2025) from three bookkeeping models.

All three spreadsheets are published by the Integrated Carbon Observation System (ICOS) Carbon Portal and are available at https://doi.org/10.18160/GCP-2026 (Friedlingstein et al., 2026b) and via the Global Carbon Budget website (https://globalcarbonbudget.org/, Global Carbon Budget, 2026). National emissions data are also available at https://doi.org/10.5281/zenodo.5569234 (Andrew and Peters, 2026), from the Global Carbon Atlas (http://www.globalcarbonatlas.org/, Global Carbon Atlas, 2026) and from Our World in Data (https://ourworldindata.org/co2-emissions, Our World in Data, 2026).

We also make all gridded data available. Bookkeeping model data: https://doi.org/10.5281/zenodo.23528902 (Schwingshackl et al. 2026); DGVM data: https://doi.org/10.5281/zenodo.23532075 (O'Sullivan et al. 2026b); GOBM and fCO_2 data : https://doi.org/10.5281/zenodo.23723209 (Hauck et al., 2026);inversion models data: doi/10.18160/99Y6-6994 (Naus et al., 2026).

Author contributions

PF, MOS, RMA, JH, MWJ, PL, CLQ, HL, ITL, AO, GPP, WP, JP, CSc, and SS designed the study, conducted the analysis, and wrote the paper with input from JGC and PC. RMA, GPP, JIK and TK produced the fossil CO_2 emissions and their uncertainties and analysed the emissions data. ME and GM provided fossil fuel emission data. ZL provided the Carbon Monitor fossil emission projection. JP, CSc, TG, ZQ and GS provided the bookkeeping land-use change emissions with synthesis by JP and CSc. LC and QS provided estimates of emissions from peat drainage. GRvdW provided the GFED fire emissions. KH and JDM provided the estimates of non-vegetation CDR fluxes. SB, LB, MAC, NG, ÖG, TI, TJ, LR, JS and TT provided an update of the global ocean biogeochemical models, with quality control by SLC and an emergent constraint by JT; AFa, DJF, MG, LG, AJ, EL, MM, CR, JAT and JZ provided an update of the ocean fCO_2-data products, with synthesis on both models and products by JH, PL and AR. AR benchmarked the data products against independent observations. JDM and TD provided estimates of ocean interior carbon storage. SRA, NRB, KB, AB, CFB, MC, SEC, TE, MPE, KE, WE, AFs, TGk, SKL, NM, NMM, DRM, SN, CN, LO, XAP, DP, GR, EHS, IS, AJS, CSw, ST, BT, SJvdV and RW provided ocean fCO_2 measurements for the year 2025, with synthesis by AO and LK. KA, VA, DMB, EB, BF, AFo, JHe, AI, AKJ, EK, JK, SL, LM, TN, BP, RS, KSD, TLS, QS, HT, APW, XYa, WY and XYu provided an update of the Dynamic Global Vegetation Models, with synthesis by SS and MOS. FF, VL, WSL, JM and HiT provided estimates of land and ocean sinks from Earth System Models, as well as a projection of the atmospheric growth rate for 2026, with synthesis by HiL. FC, ARJ, FJ, ZJ, JL, SM,

https://doi.org/10.5194/essd-2026-895
Preprint. Discussion started: 10 November 2026
© Author(s) 2026. CC BY 4.0 License.



Open Access Earth System Science Data Discussions

RRN, PP, YQ, CR, AvdW, NZ, and BZ provided an updated atmospheric inversion; WP, FC, AvdW, and ITL developed the protocol and produced the synthesis and evaluation of the atmospheric inversions. EJM and RFK provided the atmospheric oxygen estimate of surface net carbon sinks. RMA provided projections of the 2026 fossil emissions and atmospheric CO_2 growth rate. PL provided the predictions of the 2026 ocean sink. IBMB, LPC, KKG, GCH and TMR provided forcing data for land-use change. FT, GG and SR provided data for the land-use change NGHGI and FAO comparison, and LC provided FAO estimates of emissions from organic soils. XL provided the surface atmospheric CO_2 data. SP provided the satellite-based atmospheric CO_2 growth rate (GRESO) from combined GOSAT and OCO-2 retrievals. TO and ARF provided the climate forcing data for the DGVMs. WH provided the nitrogen fertilizer forcing data for the DGVMs. MOS and NB produced the aerosol diffuse radiative forcing for the DGVMs. PCM provided the ILAMB evaluation of the DGVMs. MGS provided the IOMB evaluation of the GOBMs. MWJ provided the emissions prior for use in the inversion systems, with input from YQ to the GridFED fossil emissions prior. PF and MOS coordinated the effort, revised all figures, tables, text and numbers to ensure the update was clear from the 2025 edition and in line with https://globalcarbonatlas.org (last access: 30 October 2026).

Competing interests.

At least one of the authors is a member of the editorial board of Earth System Science Data

Acknowledgements

We thank all people and institutions who provided the data used in this global carbon budget 2026 and the Global Carbon Project members for their input throughout the development of this publication. We thank Christian Ethé, Olivier Torres, Xavier Perrot, Damian Loher, Fatemeh Chegini, Fabrice Lacroix, Yangyang Zhao, Paridhi Rustogi, Aurore Voldoire, Youcef Amar, Bertrand Decharme, Hiroyuki Tsujino, Yoshiteru Kitamura, Katsuya Toyama, Hideyuki Nakano, L. Shogo Urakawa, Philip Townsend, Nathaniel O. Collier, Min Xu, Galen A. McKinley, Jamie D. Shutler, Andrew J. Watson, T. Holding, I. G. C. Ashton, D. K. Woolf, Lonneke Goddijn-Murphy and Richard Sims for their involvement in the development, use, and analysis of the models and data products used here. ERA5 forcing (Hersbach et al., 2020) was downloaded from the Copernicus Climate Change Service (C3S) Climate Data Store; the results contain modified Copernicus Climate Change Service information 2020, and neither the European Commission nor ECMWF is responsible for any use that may be made of the Copernicus information or data it contains. We thank Leticia Barbero, Susan Hartman, Anita Flohr, Siyabulela Hamnca, and Melchor González-Dávila, Claire Lo Monaco who contributed to the provision of surface ocean CO2 observations for the year 2025 (see Table S8). We also thank Eugene Burger of NOAA's Pacific Marine Environmental Laboratory, Alex Kozyr of NOAA's National Centers for Environmental Information, and Steve Jones

https://doi.org/10.5194/essd-2026-895
Preprint. Discussion started: 10 November 2026
© Author(s) 2026. CC BY 4.0 License.



2348 and Sara Poelmans of the Flanders Marine Institute (VLIZ) for their contribution to surface ocean CO2
2349 data and metadata management. We thank the scientists, institutions, and funding agencies responsible
2350 for the collection and quality control of the data in SOCAT as well as the International Ocean Carbon
2351 Coordination Project (IOCCP) and the Surface Ocean Lower Atmosphere Study (SOLAS) program for
2352 their support. The Surface Ocean CO2 Observing Network (SOCONET), the Surface Ocean CO2 Atlas
2353 (SOCAT) and the Surface Ocean CO2 Mapping (SOCOM) program are linked international efforts that,
2354 along with additional critical data from satellites, models and re-analysis, enable the routine delivery of
2355 ocean carbon and carbonate system data products. The loss of any activity (SOCONET, SOCAT, or
2356 SOCOM) or data source (satellite, in situ, or re-analysis) would prevent delivery of data products to global
2357 or regional assessments (Global Carbon Budget, IPCC, and others) that guide policy decisions.
2358 SOCONET, SOCAT and SOCOM are endorsed by the International Ocean Carbon Coordination Project
2359 (IOCCP, an Infrastructural Project of the Scientific Committee on Oceanic Research) and the Global
2360 Ocean Observing System (GOOS) Biogeochemistry Panel. The many researchers, funders, and agencies
2361 responsible for these activities and data are thanked for their contributions. ITL and WP thank the
2362 CarbonTracker Europe team at Wageningen University, including Remco de Kok and Joram Hooghiem.
2363 The inverse modelling team thanks all data providers of atmospheric CO2 data provided through multiple
2364 ObsPack products. HL thanks Sebastian Brune and Kristina Frölich for helping with the MPI-ESM1-2-
2365 LR assimilation and providing the data. Zhangcai Qin thanks Ziwang Fu for contributing to the latest
2366 LUCE modeling. We thank Ram Alkama for helping in filtering SLAND data from DGVMs with
2367 managed forest area and Joana Melo for extracting and processing data from NGHGIs. FT and LC
2368 acknowledge support of member countries to the FAO regular budget and FAOSTAT. The conclusions
2369 in this paper are the authors' only and do not represent FAO views and position on the subject matter.
2370 The 2025 pCO2 measurements on RV Celtic Explorer were made possible thanks to the dedication of the
2371 ship's technicians, Lukasz Pawlikowski and Ruahri Strachan, and the support of the Instrumentation and
2372 IT section at P&O Maritime, Galway. WE thanks the Tula Foundation for funding support. pCO2
2373 measurements on the Marion Dufresne were collected in the frame of the French COOL/OISO long-term
2374 monitoring program with support from the National Institute of Sciences of the Universe (INSU), the
2375 French Polar Institute (IPEV) and the French Oceanographic Fleet (FOF). The measurements on RV
2376 Polarstern are only possible thanks to the dedication of the crew and of Mario Hoppema and Hauke
2377 Becker, whom we thank warmly; we also thank Toste Tanhua and skipper Nicolas Lueven for the data
2378 collection on Holcim-PRB during the Vendée Globe 2024. Underway data on the RV Sarmiento de
2379 Gamboa are collected through the collaboration of the Marine Technology Unit (UTM-CSIC) and the
2380 CSIC Interdisciplinary Thematic Platform PTI OCEANS+, together with the involvement of the principal
2381 investigators of the MORIA (Leopoldo D. Pena and Isabel Cacho) and DICHOSO (I. Emma Huertas and
2382 Antonio Tovar-Sánchez) projects. SJvdV thanks Andrew Marriner of Earth Sciences New Zealand for
2383 the maintenance and processing of the underway data collected on board the RV Tangaroa. CFB thanks
2384 INIDEP for support. PCM thanks T. Quaife and E. Robertson for support. FC thanks Adrien Martinez

https://doi.org/10.5194/essd-2026-895
Preprint. Discussion started: 10 November 2026
© Author(s) 2026. CC BY 4.0 License.



Open Access Earth System Science Data Discussions

who maintained the atmospheric transport model for the CAMS inversion. We acknowledge the contributions of Jeongmin Yun, Anthony Bloom, and Kevin Bowman to the CMS-Flux inversion submission. SM thanks Yosuke Niwa for his contribution to the development of NISMON-CO2. PP thanks Liang Feng for his contribution to the UoE inverse framework. We thank Stijn Naus for contributing to the production of CTE2026 and for the inverse model synthesis, and Joram Hooghiem for the development of CTE. Zhe Jin thanks Xiangjun Tian, Yilong Wang, Hongqin Zhang, Tao Wang, and Shilong Piao for their contributions to the GONGGA inversion system. NZ thanks Zhiqiang Liu, Yun Liu, Eugenia Kalnay, and Gassem Asrar for their contributions to the COLA system. CarbonTracker CT2026 results provided by NOAA GML, Boulder, Colorado, USA from the website at http://carbontracker.noaa.gov (last access: 30 October 2026). FJ thanks Weimin Ju for running the BEPS model. RRJ thanks Lorna Nayagam and Shamil Maksyutov for their contribution to the NTFVAR inversion. BZ acknowledges Yawen Kong from the Aerospace Information Research Institute for her contribution to the THU-GCDAS products. YQ acknowledges the help and support of Tianyu Li, Xinyou Chen, Wu Su, Xinru Ding, Shilong Piao and Song Xi Chen. SP thanks Christopher O'Dell for providing the ACOS XCO2 retrievals from OCO-2 and GOSAT used to calculate the GRESO CO_2 growth rates.

Financial and computing support

This research was supported by the following sources of funding:
INIDEP (Argentina); Joint Technical Commission of the Maritime Front (CTMFM) (Argentina-Uruguay); Australian National Environmental Science Program (NESP) (Australia); Integrated Marine Observing System (IMOS, enabled by the National Collaborative Research Infrastructure Strategy, NCRIS) (Australia); Tula Foundation (Canada); National Natural Science Foundation of China (grant no. 42525503); National Natural Science Foundation of China Major Program (grant No. 12292980); National Key Research and Development Program of China (grant no. 2023YFF0805400) (China); National Key R&D Program of China (2025YFF0516904); Ocean Negative Carbon Emissions (ONCE) Program. (China); European Space Agency (OceanSODA project, grant no. 4000112091/14/I-LG) (ESA); European Space Agency through the OCE Award #2333608. (ESA); THRAC3E (grant no. 4000149569/25/I-AG) (ESA); INFORMA (101060309) (EU); NextGenCarbon (101184989) (EU); SafeNet (101181981) (EU); GreenFeedBack (101056921) (EU); OptimESM (101081193) (EU); ERC-2022-STG OceanPeak (Grant 101077209). The work reflects only the authors' view; the European Commission and their executive agency are not responsible for any use that may be made. (EU); This work was funded by the European Union under grant agreement no. 101083922 (OceanICU) and UK Research and Innovation (UKRI) under the UK government's Horizon Europe funding guarantee [grant number 10054454, 10063673, 10064020, 10059241, 10079684, 10059012, 10048179]. Views and opinions expressed are however those of the author(s) only and do not necessarily reflect those of the European Union or European Research Executive Agency. Neither the European Union nor the granting authority can be held responsible for them. (EU); The Copernicus Marine Environment Monitoring

https://doi.org/10.5194/essd-2026-895
Preprint. Discussion started: 10 November 2026
© Author(s) 2026. CC BY 4.0 License.



Service implemented by Mercator Ocean on behalf of the European Commission (grant no. 83-CMEMSTAC-MOB). (EU); European Commission (COMFORT project, grant no. 820989) (EU); ClimTip (grant no. 101137601) (EU); GEORGE (Grant id. 101094716) (EU);
Agence Nationale de la Recherche - France 2030 as part of the PEPR TRACCS programme under grant number ANR-22-EXTR-0008 and ANR-22-EXTR-0009. (France); Agence Nationale de la Recherche - France 2030 as part of the PEPR TRACCS programme under grant number ANR-22-EXTR-0009 (France); INSU/CNRS (France); IPEV (France); IFREMER (France); FOF (France); OSU Ecce Terra (France); Deutsche Forschungsgemeinschaft (DFG, German Research Foundation) through TRR 410 WETSCAPES2.0 (grant no. 531801029) (Germany); Deutsches Klimarechenzentrum (DKRZ) (Project: bm0891) (Germany); Initiative and Networking Fund of the Helmholtz Association (no. VH-NG-19-33) (Germany); BMFTR and BMW (Germany); Helmholtz Association POF-IV (Germany); Icelandic Ministry for the Environment and Natural Resources (Iceland); Department of Agriculture, Food and the Marine (Ireland); Environment Research and Technology Development Fund (ERTDF) of ERCA by Ministry of the Environment of Japan (grant no. JPMEERF24S12206) (Japan); Meteorological Research Institute and the Environment Research and Technology Development Fund (JPMEERF24S12200) of the Environmental Restoration and Conservation Agency provided by Ministry of Environment of Japan. (Japan); NIES GOSAT-2 Project, GED (Global Environmental Database) Project and GCP Tsukuba International Office of NIES. (Japan); Global Environmental Research Coordination System, Ministry of the Environment (grant nos. MOE1751 and MOE2252) (Japan); Japan Meteorological Agency (Japan); JST CREST (grant no. JPMJCR23J4), JST PRESTO (grant no. JPMJPR23G7), and JSPS KAKENHI (grant no. 23H03516) (Japan); MBIE Strategic Science Investment Fund via the ESNZ Ocean-Climate Interaction programme (New Zeeland); Research Council of Norway (grant no. 352405) (Norway); Norwegian Research Council (grant no. 350390) (Norway); Norwegian Polar Institute (Norway); Research Council of Norway (ICOS-3, grant no. 350341) (Norway); Ministry of Science, Innovation and Universities (projects: MORIA (Grant PID2022-138010OB-I00), DICHOSO (Grant PID2021-125783OB-I00) and FICARAM+ (Grant PID2023-148924OB-I00)) (Spain); ETH Zürich (Switzerland); Schweizerischer Nationalfonds zur Förderung der Wissenschaftlichen Forschung (grant no. PZ00P2_209044 (ArcticECO)) (Switzerland); NERC NCEO (NE/R016518/1) (United Kingdom); Met Office Hadley Centre Climate Programme (HCCP) funded by the UK Department for Business, Innovation, Science and Trade (DBIST) (United Kingdom); National Centre for Atmospheric Science, a NERC collaborative centre (United Kingdom); Royal Society (grant no. RSRP\R\241002) (United Kingdom); NERC EXPLANATIONS (grant no. NE/Y005260/1) (United Kingdom); NERC Marine Frontiers (grant no. NE/V011103/1) (United Kingdom); Schmidt Sciences (projects CALIPSO, CLARiTy, and InMOS) (USA); Princeton University High Meadows Environmental Institute. We thank Princeton Research Computing, a consortium of groups including the Princeton Institute for Computational Science and Engineering (PICSciE) and the Office of Information Technology's High-Performance Computing Center and Visualization Laboratory at Princeton University. (USA); NOAA,

https://doi.org/10.5194/essd-2026-895
Preprint. Discussion started: 10 November 2026
© Author(s) 2026. CC BY 4.0 License.



2458 through a University of Miami subaward to the University of Santiago de Compostela under the project
2459 “Remote sensing and in situ observations for improved monitoring and forecasting in U.S. near-coastal
2460 regions” (Subaward OS00001891). (USA); NOAA grant NA24NESX432C0001 (Cooperative Institute
2461 for Satellite Earth System Studies - CISESS) at the University of Maryland/ESSIC (USA); NSF through
2462 the LEAP STC (Award #2019625) (USA); NSF National Center for Atmospheric Research, which is a
2463 major facility sponsored by the National Science Foundation under Cooperative Agreement No. 1852977
2464 (USA); NASA Land-Cover and Land-Use Change (LCLUC) Program (NASA Grant Nos.
2465 80NSSC24K0920 and 80NSSC25K7497). (USA);
2466 Future of Life Institute (CODEC project) (USA); NOAA Global Ocean Monitoring and Observing
2467 Program (Open Funder Registry no. 100018302) (USA); NOAA Ocean Acidification Program (Research
2468 Organization Registry (ROR): 02bfn4816) (USA); NOAA Pacific Marine Environmental Laboratory
2469 (ROR: 03crn0n59) (USA); NOAA Ocean Acidification Program and Alaska Ocean Observing System
2470 (NA21NOS0120094) (USA); NASA Carbon Monitoring System (grant no. 80NSSC25K7221) (USA);
2471 NASA Early Career Investigator Program in Earth Science (grant no. 80NSSC24K1632) (USA); NASA
2472 GEDI Competed Science Team (grant no. 80NSSC24K0599) (USA);
2473 ORNL Terrestrial Ecosystem Science SFA and Energy Exascale Earth System Model (E3SM) project,
2474 funded by the U.S. Department of Energy, Office of Science, Office of Biological and Environmental
2475 Research Earth Systems Model Development Program area of Earth and Environmental System
2476 Modeling. (USA). A portion of this research was carried out at the Jet Propulsion Laboratory, California
2477 Institute of Technology, under contract with the National Aeronautics and Space Administration
2478 (80NM0018D0004).

2479 We also acknowledge support from the following computing facilities:

2480 ACCESS-NRI and National Computational Infrastructure (NCI) (Australia); National Large Scientific
2481 and Technological Infrastructure: Earth System Numerical Simulation Facility (China); HPC resources
2482 from LSCE, IPSL, and GENCI-TGCC under grant 06328 from 2018 to 2026 (France); Deutsches
2483 Klimarechenzentrum (DKRZ) granted by its shareholder Max Planck Society under project ID 143
2484 (Germany); NIES Supercomputer system (Japan); UNINETT Sigma2, National Infrastructure for High
2485 Performance Computing and Data Storage in Norway (NN9560K/NS9560K) (Norway); Swiss National
2486 Supercomputing Centre (CSCS) under project ID s1323 on Alps (Switzerland); Edinburgh Compute and
2487 Data Facility (ECDF, http://www.ecdf.ed.ac.uk/) (United Kingdom); UEA High Performance Computing
2488 cluster (United Kingdom); CEDA JASMIN data analysis facility for environmental science (United
2489 Kingdom). This research used resources of the Compute and Data Environment for Science (CADES) at
2490 the Oak Ridge National Laboratory, which is supported by the Office of Science of the U.S. Department
2491 of Energy under Contract No. DE-AC05-00OR22725 (USA).

2492

https://doi.org/10.5194/essd-2026-895
Preprint. Discussion started: 10 November 2026
© Author(s) 2026. CC BY 4.0 License.



Open Access Earth System Science Data Discussions

2493

https://doi.org/10.5194/essd-2026-895
Preprint. Discussion started: 10 November 2026
© Author(s) 2026. CC BY 4.0 License.



References

Abatzoglou, J. T., Williams, A. P., and Barbero, R.: Global Emergence of Anthropogenic Climate Change in Fire Weather Indices, Geophys. Res. Lett., 46, 326–336, https://doi.org/10.1029/2018GL080959, 2019.

Ahlström, A., Raupach, M. R., Schurgers, G., Smith, B., Arneth, A., Jung, M., Reichstein, M., Canadell, J. G., Friedlingstein, P., Jain, A. K., Kato, E., Poulter, B., Sitch, S., Stocker, B. D., Viovy, N., Wang, Y. P., Wiltshire, A., Zaehle, S., and Zeng, N.: The dominant role of semi-arid ecosystems in the trend and variability of the land CO2 sink, Science, 348, 895–899, https://doi.org/10.1126/science.aaa1668, 2015.

Andela, N., Morton, D. C., Giglio, L., Chen, Y., van der Werf, G. R., Kasibhatla, P. S., DeFries, R. S., Collatz, G. J., Hantson, S., Kloster, S., Bachelet, D., Forrest, M., Lasslop, G., Li, F., Mangeon, S., Melton, J. R., Yue, C., and Randerson, J. T.: A human-driven decline in global burned area, Science, 356, 1356–1362, https://doi.org/10.1126/science.aal4108, 2017.

Andrew, R. M.: A comparison of estimates of global carbon dioxide emissions from fossil carbon sources, Earth Syst. Sci. Data, 12, 1437–1465, https://doi.org/10.5194/essd-12-1437-2020, 2020a.

Andrew, R. M.: Timely estimates of India's annual and monthly fossil CO2 emissions, Earth Syst. Sci. Data, 12, 2411–2421, https://doi.org/10.5194/essd-12-2411-2020, 2020b.

Andrew, R. M.: Towards near real-time, monthly fossil CO2 emissions estimates for the European Union with current-year projections, Atmospheric Pollution Research, 12, 101229, https://doi.org/10.1016/j.apr.2021.101229, 2021.

Andrew, R. M.: Global CO2 emissions from cement production (version 260830) [Data set]. Zenodo. https://doi.org/10.5281/ZENODO.831454, last access: 30 October 2026, 2026.

Andrew, R. M., & Peters, G. P.:The Global Carbon Project's fossil CO2 emissions dataset (version 2026v11) [Data set]. Zenodo. https://doi.org/10.5281/zenodo.5569234, last access: 30 October 2026, 2026.

Aragão, L. E. O. C., Anderson, L. O., Fonseca, M. G., Rosan, T. M., Vedovato, L. B., Wagner, F. H., Silva, C. V. J., Silva Junior, C. H. L., Arai, E., Aguiar, A. P., Barlow, J., Berenguer, E., Deeter, M. N., Domingues, L. G., Gatti, L., Gloor, M., Malhi, Y., Marengo, J. A., Miller, J. B., Phillips, O. L., and Saatchi, S.: 21st Century drought-related fires counteract the decline of Amazon deforestation carbon emissions, Nat Commun, 9, 536, https://doi.org/10.1038/s41467-017-02771-y, 2018.

Archer, D., Eby, M., Brovkin, V., Ridgwell, A., Cao, L., Mikolajewicz, U., Caldeira, K., Matsumoto, K., Munhoven, G., Montenegro, A., and Tokos, K.: Atmospheric Lifetime of Fossil Fuel Carbon Dioxide, Annu. Rev. Earth Planet. Sci., 37, 117–134, https://doi.org/10.1146/annurev.earth.031208.100206, 2009.

Arneth, A., Sitch, S., Pongratz, J., Stocker, B. D., Ciais, P., Poulter, B., Bayer, A. D., Bondeau, A., Calle, L., Chini, L. P., Gasser, T., Fader, M., Friedlingstein, P., Kato, E., Li, W., Lindeskog, M., Nabel, J. E. M. S., Pugh, T. A. M., Robertson, E., Viovy, N., Yue, C., and Zaehle, S.: Historical carbon dioxide emissions caused by land-use changes are possibly larger than assumed, Nature Geosci, 10, 79–84, https://doi.org/10.1038/ngeo2882, 2017.

Aumont, O., Orr, J. C., Monfray, P., Ludwig, W., Amiotte-Suchet, P., and Probst, J.-L.: Riverine-driven interhemispheric transport of carbon, Global Biogeochem. Cycles, 15, 393–405, https://doi.org/10.1029/1999GB001238, 2001.

Aumont, O., Ethé, C., Tagliabue, A., Bopp, L., and Gehlen, M.: PISCES-v2: an ocean biogeochemical model for carbon and ecosystem studies, 8, 2465–2513, https://doi.org/10.5194/gmd-8-2465-2015, 2015.

Babiker, M., G. Berndes, K. Blok, B. Cohen, A. Cowie, O. Geden, V. Ginzburg, A. Leip, P. Smith, M. Sugiyama, F. Yamba, Al Khourdajie, A., Arneth, A., Lima de Azevedo, I. M., Bataille, C., Beerling, D., Bezner Kerr, R., Bradley, J., Buck, H. J., Cabeza, L. F., Calvin, K., Campbell, D., Carnicer Cols, J., Daioglou, V., Harmsen, M., Höglund-Isaksson, L., House, J. I., Keller, D., de Kleijne, K., Kugelberg, S., Makarov, I., Meza, F., Minx, J. C., Morecroft, M., Nabuurs, G. J., Neufeldt, H., Novikova, A., Nugroho, S. B., Oschlies, A., Parmesan, C., Peters, G. P., Poore, J., Portugal-Pereira, J., Postigo, J. C., Pradhan, P., Renforth, P., Rivera-Ferre, M. G., Roe, S., Singh, P. K., Slade, R., Smith, S. M., Tirado von der Pahlen, M. C., and Toribio Ramirez, D.: Cross sectoral perspectives. In: Climate Change 2022: Mitigation of Climate Change. Contribution of Working Group III to the Sixth Assessment Report of the Intergovernmental Panel on Climate Change [P.R. Shukla, J. Skea, R. Slade, A. Al Khourdajie, R. van Diemen, D. McCollum, M. Pathak, S. Some, P. Vyas, R. Fradera, M. Belkacemi, A. Hasija, G. Lisboa, S. Luz,

https://doi.org/10.5194/essd-2026-895
Preprint. Discussion started: 10 November 2026
© Author(s) 2026. CC BY 4.0 License.



J. Malley, (eds.)]. Cambridge University Press, Cambridge, UK and New York, NY, USA. doi: 10.1017/9781009157926.014, 2022.

Baccini, A., Walker, W., Carvalho, L., Farina, M., Sulla-Menashe, D., and Houghton, R. A.: Tropical forests are a net carbon source based on aboveground measurements of gain and loss, Science, 358, 230–234, https://doi.org/10.1126/science.aam5962, 2017.

Bakker, D. C. E., Pfeil, B., Landa, C. S., Metzl, N., O'Brien, K. M., Olsen, A., Smith, K., Cosca, C., Harasawa, S., Jones, S. D., Nakaoka, S., Nojiri, Y., Schuster, U., Steinhoff, T., Sweeney, C., Takahashi, T., Tilbrook, B., Wada, C., Wanninkhof, R., Alin, S. R., Balestrini, C. F., Barbero, L., Bates, N. R., Bianchi, A. A., Bonou, F., Boutin, J., Bozec, Y., Burger, E. F., Cai, W.-J., Castle, R. D., Chen, L., Chierici, M., Currie, K., Evans, W., Featherstone, C., Feely, R. A., Fransson, A., Goyet, C., Greenwood, N., Gregor, L., Hankin, S., Hardman-Mountford, N. J., Harlay, J., Hauck, J., Hoppema, M., Humphreys, M. P., Hunt, C. W., Huss, B., Ibánhez, J. S. P., Johannessen, T., Keeling, R., Kitidis, V., Körtzinger, A., Kozyr, A., Krasakopoulou, E., Kuwata, A., Landschützer, P., Lauvset, S. K., Lefèvre, N., Lo Monaco, C., Manke, A., Mathis, J. T., Merlivat, L., Millero, F. J., Monteiro, P. M. S., Munro, D. R., Murata, A., Newberger, T., Omar, A. M., Ono, T., Paterson, K., Pearce, D., Pierrot, D., Robbins, L. L., Saito, S., Salisbury, J., Schlitzer, R., Schneider, B., Schweitzer, R., Sieger, R., Skjelvan, I., Sullivan, K. F., Sutherland, S. C., Sutton, A. J., Tadokoro, K., Telszewski, M., Tuma, M., van Heuven, S. M. A. C., Vandemark, D., Ward, B., Watson, A. J., and Xu, S.: A multi-decade record of high-quality CO2 data in version 3 of the Surface Ocean CO2 Atlas (SOCAT), Earth Syst. Sci. Data, 8, 383–413, https://doi.org/10.5194/essd-8-383-2016, 2016.

Bakker, D. C. E., Alin, S. R., Bates, N. R., Ehmen, T., Gkritzalis, T., Jones, S. D., Kamb, L., Kozyr, A., Lauvset, S. K., Macovei, V. A., Metzl, N., Nakaoka, S.-i., O'Brien, K. M., Olsen, A., Pierrot, D., Poelmans, S., Steinhoff, T., Sutton, A. J., Sweeney, C., Takao, S., Telszewski, M., Theetaert, H., Tilbrook, B., Wada, C., Wanninkhof, R., Akl, J., Aramaki, T., Arbilla, L. A., Àvila, R. A., Baier, B. C., Barbero, L., Battisti, R., Beatty, C. M., Becker, H., Benoit-Cattin, A., Berghoff, C. F., Bittig, H. C., Bonin, J. A., Bozzano, R., Burger, E. F., Cai, W.-J., Cantoni, C., Castelli, G., Castro, A., Chambers, D. P., Chierici, M., Cronin, M., Cubiella, Á. H., Curbelo, D., Curless, S. E., Czyz, C., Diverrès, D., Dougherty, S., Enochs, I., Enright, M. P., Enyo, K., Evans, W., Feely, R. A., Flohr, A., Fragiacomo, E., Frangoulis, C., Fransson, A., Gehrung, M., Glockzin, M., González, A. G., González-Dávila, M., González-Santana, D., Hales, B., Hamnca, S., Hartman, S. E., Hermes, R., Herndon, J., Hoppema, M., Howard, E., Huertas, E., Kerr, R., Kristensen, T. O., Landschützer, P., Lee, C. M., Lee, H., Lefèvre, N., Leseurre, C., Lo Monaco, C., Luchetta, A., Maenner Jones, S. M., Manalang, D., McAuliffe, A. M., Mdokwana, B. W., Monacci, N. M., Monteiro, P. M. S., Morell, J. M., Munro, D. R., Neill, C., Newberger, T., Nickford, S., Nillson, E., Noakes, S., Noh, J.-H., Noisel, C., O'Brien, C., Olivier, L., Omar, A., Orselli, I., Padin, A., Pena, L. D., Pensieri, S., Pryterch, J., Rehder, G., Rutgersson, A., Sabine, C. L., Sallée, J.-B., Sanders, R., Santana-Casiano, J. M., Sarpe, D., Schirnik, C., Schlitzer, R., Shadwick, E., Skjelvan, I., T'Jampens, M., Tamsitt, V., Toledo Aboy, A. E., Tovar-Sanchez, A., Tsanwani, M., Van de Velde, S., Van Ooijen, E., Vandemark, D., Veccia, M. H., Voynova, Y. G., Williams, N. L., and Xu, Y.: Surface Ocean CO2 Atlas Database Version 2026 (SOCATv2026) (NCEI Accession 0315110), NOAA National Centers for Environmental Information [data set], https://doi.org/10.25921/8dba-fr90, 2026a.

Bakker, D. C. E., Alin, S. R., Bates, N. R., Ehmen, T., Gkritzalis, T., Jones, S. D., Kamb, L., Kozyr, A., Lauvset, S. K., Macovei, V. A., Metzl, N., Nakaoka, S.-i., O'Brien, K. M., Olsen, A., Pierrot, D., Poelmans, S., Steinhoff, T., Sutton, A. J., Sweeney, C., Takao, S., Telszewski, M., Theetaert, H., Tilbrook, B., Wada, C., and Wanninkhof, R.: SOCAT version 2026: High-quality synthesis products for ocean CO2 sink quantification, https://socat.info/index.php/posters/, Poster published on 16/06/2026. Last access 30 October 2026, 2026b

Ballantyne, A. P., Alden, C. B., Miller, J. B., Tans, P. P., and White, J. W. C.: Increase in observed net carbon dioxide uptake by land and oceans during the past 50 years, Nature, 488, 70–72, https://doi.org/10.1038/nature11299, 2012.

Ballantyne, A. P., Andres, R., Houghton, R., Stocker, B. D., Wanninkhof, R., Anderegg, W., Cooper, L. A., DeGrandpre, M., Tans, P. P., Miller, J. B., Alden, C., and White, J. W. C.: Audit of the global carbon budget: estimate errors and their impact on uptake uncertainty, Biogeosciences, 12, 2565–2584, https://doi.org/10.5194/bg-12-2565-2015, 2015.

Bar-On, Y. M.,Li, X., O'Sullivan, M., Wigneron, J-P., Sitch, S., Ciais, P., Frankenberg, C., Fischer, W. W.: Recent gains in global terrestrial carbon stocks are mostly stored in nonliving pools, Science 387, 1291–1295, 2025.

https://doi.org/10.5194/essd-2026-895
Preprint. Discussion started: 10 November 2026
© Author(s) 2026. CC BY 4.0 License.



2595 Bastos, A., Hartung, K., Nützel, T. B., Nabel, J. E. M. S., Houghton, R. A., and Pongratz, J.: Comparison of
2596 uncertainties in land-use change fluxes from bookkeeping model parameterisation, 12, 745–762,
2597 https://doi.org/10.5194/esd-12-745-2021, 2021.

2598 Battle, M. O., Raynor, R., Kesler, S., and Keeling, R.: Technical Note: The impact of industrial activity on the
2599 amount of atmospheric O2, Atmospheric Chem. Phys. Discuss., 1–17, https://doi.org/10.5194/acp-2022-765, 2023.

2600 Behncke, J., Ilyina, T., Chegini, F., and Landschützer, P.: Improved air-sea CO2 flux estimates from sailboat
2601 measurements, Sci. Adv., 12, eadz1502, https://doi.org/10.1126/sciadv.adz1502, 2026.

2602 Bellenger, H., Bopp, L., Ethé, C., Ho, D., Duvel, J. P., Flavoni, S., Guez, L., Kataoka, T., Perrot, X., Parc, L., and
2603 Watanabe, M.: Sensitivity of the Global Ocean Carbon Sink to the Ocean Skin in a Climate Model, J. Geophys.
2604 Res. Oceans, 128, e2022JC019479, https://doi.org/10.1029/2022JC019479, 2023.

2605 Bennington, V., Gloege, L., and McKinley, G. A.: Variability in the Global Ocean Carbon Sink From 1959 to 2020
2606 by Correcting Models with Observations, Geophys. Res. Lett., 49, e2022GL098632,
2607 https://doi.org/10.1029/2022GL098632, 2022.

2608 Bernardello, R., Sicardi, V., Lapin, V., Ortega, P., Ruprich-Robert, Y., Tourigny, E. and Ferrer, E.: Ocean
2609 biogeochemical reconstructions to estimate historical ocean CO 2 uptake. Earth System Dynamics, 15(5), pp.1255-
2610 1275, https://doi.org/10.5194/esd-15-1255-2024, 2024.

2611 Bethke, I., Wang, Y., Counillon, F., Keenlyside, N., Kimmritz, M., Fransner, F., Samuelsen, A., Langehaug, H.,
2612 Svendsen, L., Chiu, P.-G., Passos, L., Bentsen, M., Guo, C., Gupta, A., Tjiputra, J., Kirkevåg, A., Olivié, D.,
2613 Seland, Ø., Solsvik Vågane, J., Fan, Y., and Eldevik, T.: NorCPM1 and its contribution to CMIP6 DCPP, Geosci.
2614 Model Dev., 14, 7073–7116, https://doi.org/10.5194/gmd-14-7073-2021, 2021.

2615 Betts, R. A., Jones, C. D., Knight, J. R., Keeling, R. F., and Kennedy, J. J.: El Niño and a record CO2 rise, Nat.
2616 Clim. Change, 6, 806–810, https://doi.org/10.1038/nclimate3063, 2016.

2617 Bilbao, R., Wild, S., Ortega, P., Acosta-Navarro, J., Arsouze, T., Bretonnière, P.A., Caron, L.P., Castrillo, M.,
2618 Cruz-García, R., Cvijanovic, I. and Doblas-Reyes, F.J.: Assessment of a full-field initialised decadal climate
2619 prediction system with the CMIP6 version of EC-Earth. Earth System Dynamics Discussions, 2020, pp.1-30,
2620 https://doi.org/10.5194/esd-12-173-2021, 2021.

2621 Bloom, A. A. and Williams, M.: Constraining ecosystem carbon dynamics in a data-limited world: integrating
2622 ecological "common sense" in a model–data fusion framework, Biogeosciences, 12, 1299–1315,
2623 https://doi.org/10.5194/bg-12-1299-2015, 2015.

2624 Bloom, A. A., Exbrayat, J.-F., van der Velde, I. R., Feng, L., and Williams, M.: The decadal state of the terrestrial
2625 carbon cycle: Global retrievals of terrestrial carbon allocation, pools, and residence times, Proc. Natl. Acad. Sci.,
2626 113, 1285–1290, https://doi.org/10.1073/pnas.1515160113, 2016.

2627 Boer, G. J., Smith, D. M., Cassou, C., Doblas-Reyes, F., Danabasoglu, G., Kirtman, B., Kushnir, Y., Kimoto, M.,
2628 Meehl, G. A., Msadek, R., Mueller, W. A., Taylor, K. E., Zwiers, F., Rixen, M., Ruprich-Robert, Y., and Eade, R.:
2629 The Decadal Climate Prediction Project (DCPP) contribution to CMIP6, Geosci. Model Dev., 9, 3751–3777,
2630 https://doi.org/10.5194/gmd-9-3751-2016, 2016.

2631 Boucher, O., Servonnat, J., Albright, A. L., Aumont, O., Balkanski, Y., Bastrikov, V., Bekki, S., Bonnet, R., Bony,
2632 S., Bopp, L., Braconnot, P., Brockmann, P., Cadule, P., Caubel, A., Cheruy, F., Codron, F., Cozic, A., Cugnet, D.,
2633 D'Andrea, F., Davini, P., de Lavergne, C., Denvil, S., Deshayes, J., Devilliers, M., Ducharne, A., Dufresne, J.-L.,
2634 Dupont, E., Éthé, C., Fairhead, L., Falletti, L., Flavoni, S., Foujols, M.-A., Gardoll, S., Gastineau, G., Ghattas, J.,
2635 Grandpeix, J.-Y., Guenet, B., Guez, E., Lionel, Guilyardi, E., Guimberteau, M., Hauglustaine, D., Hourdin, F.,
2636 Idelkadi, A., Joussaume, S., Kageyama, M., Khodri, M., Krinner, G., Lebas, N., Levavasseur, G., Lévy, C., Li, L.,
2637 Lott, F., Lurton, T., Luyssaert, S., Madec, G., Madeleine, J.-B., Maignan, F., Marchand, M., Marti, O., Mellul, L.,
2638 Meurdesoif, Y., Mignot, J., Musat, I., Ottlé, C., Peylin, P., Planton, Y., Polcher, J., Rio, C., Rochetin, N., Rousset,
2639 C., Sepulchre, P., Sima, A., Swingedouw, D., Thiéblemont, R., Traore, A. K., Vancoppenolle, M., Vial, J., Vialard,
2640 J., Viovy, N., and Vuichard, N.: Presentation and Evaluation of the IPSL-CM6A-LR Climate Model, J. Adv.
2641 Model. Earth Syst., 12, e2019MS002010, https://doi.org/10.1029/2019MS002010, 2020.

2642 Bourgeois, T., Goris, N., Schwinger, J., and Tjiputra, J. F.: Stratification constrains future heat and carbon uptake
2643 in the Southern Ocean between 30°S and 55°S, Nat. Commun., 13, 340, https://doi.org/10.1038/s41467-022-
2644 27979-5, 2022.

https://doi.org/10.5194/essd-2026-895
Preprint. Discussion started: 10 November 2026
© Author(s) 2026. CC BY 4.0 License.



2645 Bourgoin, C., Beuchle, R., Branco, A., Carreiras, J., Ceccherini, G., Oom, D., San-Miguel-Ayanz, J., and Sedano,
2646 F.: Extensive fire-driven degradation in 2024 marks worst Amazon forest disturbance in over 2 decades,
2647 Biogeosciences, 22, 5247–5256, https://doi.org/10.5194/bg-22-5247-2025, 2025.

2648 Bray, E.: 2017 Minerals Yearbook: Aluminum [Advance Release], Tech. rep., U.S. Geological Survey, https://d9-
2649 wret.s3-us-west-2.amazonaws.com/assets/palladium/production/atoms/files/myb1-2017-alumi.pdf, 2020.

2650 Brienen, R. J. W., Caldwell, L., Duchesne, L., Voelker, S., Barichivich, J., Baliva, M., Ceccantini, G., Di Filippo,
2651 A., Helama, S., Locosselli, G. M., Lopez, L., Piovesan, G., Schöngart, J., Villalba, R., and Gloor, E.: Forest carbon
2652 sink neutralized by pervasive growth-lifespan trade-offs, Nat. Commun., 11, 4241, https://doi.org/10.1038/s41467-
2653 020-17966-z, 2020.

2654 Brienen, R. J. W., Phillips, O. L., Feldpausch, T. R., Gloor, E., Baker, T. R., Lloyd, J., Lopez-Gonzalez, G.,
2655 Monteagudo-Mendoza, A., Malhi, Y., Lewis, S. L., Vásquez Martinez, R., Alexiades, M., Álvarez Dávila, E.,
2656 Alvarez-Loayza, P., Andrade, A., Aragão, L. E. O. C., Araujo-Murakami, A., Arets, E. J. M. M., Arroyo, L.,
2657 Aymard C., G. A., Bánki, O. S., Baraloto, C., Barroso, J., Bonal, D., Boot, R. G. A., Camargo, J. L. C., Castilho, C.
2658 V., Chama, V., Chao, K. J., Chave, J., Comiskey, J. A., Cornejo Valverde, F., da Costa, L., de Oliveira, E. A., Di
2659 Fiore, A., Erwin, T. L., Fauset, S., Forsthofer, M., Galbraith, D. R., Grahame, E. S., Groot, N., Hérault, B.,
2660 Higuchi, N., Honorio Coronado, E. N., Keeling, H., Killeen, T. J., Laurance, W. F., Laurance, S., Licona, J.,
2661 Magnussen, W. E., Marimon, B. S., Marimon-Junior, B. H., Mendoza, C., Neill, D. A., Nogueira, E. M., Núñez, P.,
2662 Pallqui Camacho, N. C., Parada, A., Pardo-Molina, G., Peacock, J., Peña-Claros, M., Pickavance, G. C., Pitman, N.
2663 C. A., Poorter, L., Prieto, A., Quesada, C. A., Ramírez, F., Ramírez-Angulo, H., Restrepo, Z., Roopsind, A., Rudas,
2664 A., Salomão, R. P., Schwarz, M., Silva, N., Silva-Espejo, J. E., Silveira, M., Stropp, J., Talbot, J., ter Steege, H.,
2665 Teran-Aguilar, J., Terborgh, J., Thomas-Caesar, R., Toledo, M., Torello-Raventos, M., Umetsu, R. K., van der
2666 Heijden, G. M. F., van der Hout, P., Guimarães Vieira, I. C., Vieira, S. A., Vilanova, E., Vos, V. A., and Zagt, R.
2667 J.: Long-term decline of the Amazon carbon sink, 519, 344–348, https://doi.org/10.1038/nature14283, 2015.

2668 Bruno, M. and Joos, F.: Terrestrial carbon storage during the past 200 years: A Monte Carlo Analysis of CO 2 data
2669 from ice core and atmospheric measurements, Global Biogeochem. Cycles, 11, 111–124,
2670 https://doi.org/10.1029/96GB03611, 1997.

2671 Burrows, S. M., Maltrud, M., Yang, X., Zhu, Q., Jeffery, N., Shi, X., Ricciuto, D., Wang, S., Bisht, G., Tang, J.,
2672 Wolfe, J., Harrop, B. E., Singh, B., Brent, L., Baldwin, S., Zhou, T., Cameron-Smith, P., Keen, N., Collier, N., Xu,
2673 M., Hunke, E. C., Elliott, S. M., Turner, A. K., Li, H., Wang, H., Golaz, J.-C., Bond-Lamberty, B., Hoffman, F. M.,
2674 Riley, W. J., Thornton, P. E., Calvin, K., and Leung, L. R.: The DOE E3SM v1.1 Biogeochemistry Configuration:
2675 Description and Simulated Ecosystem-Climate Responses to Historical Changes in Forcing, J. Adv. Model. Earth
2676 Syst., 12, e2019MS001766, https://doi.org/10.1029/2019MS001766, 2020.

2677 Bunsen, F., Nissen, C., and Hauck, J.: The Impact of Recent Climate Change on the Global Ocean Carbon Sink.
2678 Geophysical Research Letters, 51(4), e2023GL107030, https://doi.org/10.1029/2023GL107030, 2024.

2679 Burton, C., Betts, R., Cardoso, M., Feldpausch, T. R., Harper, A., Jones, C. D., Kelley, D. I., Robertson, E., and
2680 Wiltshire, A.: Representation of fire, land-use change and vegetation dynamics in the Joint UK Land Environment
2681 Simulator vn4.9 (JULES), Geosci. Model Dev., 12, 179–193, https://doi.org/10.5194/gmd-12-179-2019, 2019.

2682 Burton, C., Lampe, S., Kelley, D. I., Thiery, W., Hantson, S., Christidis, N., Gudmundsson, L., Forrest, M., Burke,
2683 E., Chang, J., Huang, H., Ito, A., Kou-Giesbrecht, S., Lasslop, G., Li, W., Nieradzik, L., Li, F., Chen, Y.,
2684 Randerson, J., Reyer, C. P. O., and Mengel, M.: Global burned area increasingly explained by climate change,
2685 Nature Climate Change, https://doi.org/10.1038/s41558-024-02140-w, 2024.

2686 Burton, C., Di Giuseppe, F., Jones, M. W., Kelley, D. I., Barbosa, M. L. F., McNorton, J., Potts, R., Segura-Garcia,
2687 C., Abatzoglou, J. T., Alin Rosu, I., Andela, N., Anderson, L. O., Archibald, S., Brambleby, E., Chuvieco, E.,
2688 Ciavarella, A., Clarke, H., De La Barrera, F., Di Bella, C. M., Di Tomaso, E., Dintwe, K., Doherty, T. S., Donovan,
2689 V. M., Eden, J. M., Fernandes, P. M., Fiedler, L., Giglio, L., Haas, O., Hamilton, D., Hantson, S., Harris, S.,
2690 Hartley, A. J., Keeping, T. R., Kolden, C. A., Kouassi, J.-L., Kukavskaya, E., Lampe, S., Liu, Z., Mataveli, G.,
2691 Meier, S., Oom, D., Parrington, M., Qu, Y., Resco De Dios, V., Ruffault, J., Sadegh, M., Santín, C., Sedano, F.,
2692 Shuman, J. K., Silva, P. S., Spuler, F. R., Steinmann, C. B., Tanpipat, V., Torres-Vazquez, M. Á., Turco, M., Van
2693 Der Werf, G. R., Van Wees, D., Veraverbeke, S., Wessel, J. B., and Zheng, B.: State of Wildfires 2025–2026,
2694 https://doi.org/10.5194/essd-2026-587, 3 August 2026., 2026.

2695 Bushinsky, S. M., Landschützer, P., Rödenbeck, C., Gray, A. R., Baker, D., Mazloff, M. R., Resplandy, L.,
2696 Johnson, K. S., and Sarmiento, J. L.: Reassessing Southern Ocean Air-Sea CO 2 Flux Estimates With the Addition
2697 of Biogeochemical Float Observations, Global Biogeochem. Cycles, 33, 1370–1388,
2698 https://doi.org/10.1029/2019GB006176, 2019.

https://doi.org/10.5194/essd-2026-895
Preprint. Discussion started: 10 November 2026
© Author(s) 2026. CC BY 4.0 License.



2699 Byrne, B., Liu, J., Bowman, K.W., Pascolini-Campbell, M., Chatterjee, A., Pandey, S., Miyazaki, K., van der Werf,
2700 G.R., Wunch, D., Wennberg, P.O., Roehl, C.M., and Sinha, S.: Carbon emissions from the 2023 Canadian
2701 wildfires. Nature, 633, 835–839, https://doi.org/10.1038/s41586-024-07878-z, 2024.

2702 Canadell, J. G., Le Quere, C., Raupach, M. R., Field, C. B., Buitenhuis, E. T., Ciais, P., Conway, T. J., Gillett, N.
2703 P., Houghton, R. A., and Marland, G.: Contributions to accelerating atmospheric CO2 growth from economic
2704 activity, carbon intensity, and efficiency of natural sinks, Proceedings of the National Academy of Sciences, 104,
2705 18866–18870, https://doi.org/10.1073/pnas.0702737104, 2007.

2706 Canadell, J. G., Monteiro, P. M. S., Costa, M. H., Cotrim da Cunha, L., Cox, P. M., Eliseev, A. V., Henson, S.,
2707 Ishii, M., Jaccard, S., Koven, C., Lohila, A., Patra, P. K., Piao, S., Rogelj, J., Syampungani, S., Zaehle, S., and
2708 Zickfeld, K.: Global Carbon and other Biogeochemical Cycles and Feedbacks. In: Climate Change 2021: The
2709 Physical Science Basis. Contribution of Working Group I to the Sixth Assessment Report of the Intergovernmental
2710 Panel on Climate Change [Masson-Delmotte, V., P. Zhai, A. Pirani, S. L. Connors, C. Péan, S. Berger, N. Caud, Y.
2711 Chen, L. Goldfarb, M. I. Gomis, M. Huang, K. Leitzell, E. Lonnoy, J.B.R. Matthews, T. K. Maycock, T.
2712 Waterfield, O. Yelekçi, R. Yu and B. Zhou (eds.)]. Cambridge University Press, Cambridge, United Kingdom and
2713 New York, NY, USA, pp. 673–816, https://doi.org/10.1017/9781009157896.007., 2021.

2714 Cao, Z., Myers, R. J., Lupton, R. C., Duan, H., Sacchi, R., Zhou, N., Reed Miller, T., Cullen, J. M., Ge, Q., and
2715 Liu, G.: The sponge effect and carbon emission mitigation potentials of the global cement cycle, Nat Commun, 11,
2716 3777, https://doi.org/10.1038/s41467-020-17583-w, 2020.

2717 Carbon Monitor: Year in Review: Global carbon emissions and decarbonization in 2025, available at:
2718 https://carbonmonitor.org/ , last access: 30 October 2026, 2026.

2719 Chau, T. T. T., Gehlen, M., and Chevallier, F.: A seamless ensemble-based reconstruction of surface ocean pCO2
2720 and air–sea CO2 fluxes over the global coastal and open oceans, Biogeosciences, 19, 1087–1109,
2721 https://doi.org/10.5194/bg-19-1087-2022, 2022.

2722 Chau, T.-T.-T., Gehlen, M., Metzl, N., and Chevallier, F.: CMEMS-LSCE: a global, 0.25°, monthly reconstruction
2723 of the surface ocean carbonate system, Earth Syst. Sci. Data, 16, 121–160, https://doi.org/10.5194/essd-16-121-
2724 2024, 2024.

2725 Chen, Y., Morton, D.C., Andela, N. Giglio, L., Van Der Werf, G. R., and Randerson, J. T.: A pan-tropical cascade
2726 of fire driven by El Niño/Southern Oscillation. *Nature Clim Change* **7**, 906–911. https://doi.org/10.1038/s41558-
2727 017-0014-8, 2017.

2728 Chen, Y., Hall, J., Van Wees, D., Andela, N., Hantson, S., Giglio, L., Van Der Werf, G. R., Morton, D. C., and
2729 Randerson, J. T.: Multi-decadal trends and variability in burned area from the fifth version of the Global Fire
2730 Emissions Database (GFED5), Earth Syst. Sci. Data, 15, 5227–5259, https://doi.org/10.5194/essd-15-5227-2023,
2731 2023.

2732 Chen, Y., Morton, D. C., and Randerson, J. T.: Remote sensing for wildfire monitoring: Insights into burned area,
2733 emissions, and fire dynamics, One Earth, 7, 1022–1028, https://doi.org/10.1016/j.oneear.2024.05.014, 2024.

2734 Chen, Y., Van Der Werf, G. R., Mu, M., Van Wees, D., Hall, J. V., Giglio, L., Vernooij, R., Morton, D. C., Xu, L.,
2735 Liu, T., Scholten, R. C., Coffield, S. R., Follette-Cook, M. B., Ott, L., and Randerson, J. T.: Tracking recent
2736 extremes and interannual variability of global fire emissions using a near-real-time extension to the Global Fire
2737 Emissions Database, Earth Syst. Sci. Data, 18, 7535–7555, https://doi.org/10.5194/essd-18-7535-2026, 2026.

2738 Chevallier, F., Fisher, M., Peylin, P., Serrar, S., Bousquet, P., Bréon, F.-M., Chédin, A., and Ciais, P.: Inferring CO
2739 2 sources and sinks from satellite observations: Method and application to TOVS data, J. Geophys. Res., 110,
2740 D24309, https://doi.org/10.1029/2005JD006390, 2005.

2741 Chevallier, F., Martinez, A., Lloret, Z., Takache, S., and Cozic, A.: Offline Atmospheric Transport on a Global
2742 Mesh of Hexagons, JGR Atmospheres, 130, e2025JD043579, https://doi.org/10.1029/2025JD043579, 2025.

2743 Ciais, P., Sabine, C., Bala, G., Bopp, L., Brovkin, V., Canadell, J. G., Chhabra, A., DeFries, R., Galloway, J.,
2744 Heimann, M., Jones, C., Le Quéré, C., Myneni, R., Piao, S., Thornton, P., Willem, J., Friedlingstein, P., and
2745 Munhoven, G.: Carbon and Other Biogeochemical Cycles, in Climate Change 2013: The Physical Science Basis,
2746 Contribution of Working Group I to the Fifth Assessment Report of the Intergovernmental Panel on Climate
2747 Change, edited by: Intergovernmental Panel on Climate Change, Cambridge University Press, Cambridge, United
2748 Kingdom and New York, NY, USA, https://doi.org/10.1017/CBO9781107415324.015, 2013.

https://doi.org/10.5194/essd-2026-895
Preprint. Discussion started: 10 November 2026
© Author(s) 2026. CC BY 4.0 License.



2749 Ciais, P., Tan, J., Wang, X., Roedenbeck, C., Chevallier, F., Piao, S.-L., Moriarty, R., Broquet, G., Le Quéré, C.,
2750 Canadell, J. G., Peng, S., Poulter, B., Liu, Z., and Tans, P.: Five decades of northern land carbon uptake revealed
2751 by the interhemispheric CO2 gradient, Nature, 568, 221–225, https://doi.org/10.1038/s41586-019-1078-6, 2019.

2752

2753 Ciais, P., Bastos, A., Chevallier, F., Lauerwald, R., Poulter, B., Canadell, P., Hugelius, G., Jackson, R. B., Jain, A.,
2754 Jones, M., Kondo, M., Luijkx, I. T., Patra, P. K., Peters, W., Pongratz, J., Petrescu, A. M. R., Piao, S., Qiu, C., Von
2755 Randow, C., Regnier, P., Saunois, M., Scholes, R., Shvidenko, A., Tian, H., Yang, H., Wang, X., and Zheng, B.:
2756 Definitions and methods to estimate regional land carbon fluxes for the second phase of the REgional Carbon
2757 Cycle Assessment and Processes Project (RECCAP-2), Geosci. Model Dev., 15, 1289–1316,
2758 https://doi.org/10.5194/gmd-15-1289-2022, 2022.

2759 Collier, N., Hoffman, F. M., Lawrence, D. M., Keppel-Aleks, G., Koven, C. D., Riley, W. J., Mu, M., and
2760 Randerson, J. T.: The International Land Model Benchmarking (ILAMB) System: Design, Theory, and
2761 Implementation, J. Adv. Model. Earth Syst., 10, 2731–2754, https://doi.org/10.1029/2018MS001354, 2018.

2762 Conchedda, G. and Tubiello, F. N.: Drainage of organic soils and GHG emissions: Validation with country data,
2763 Biosphere – Biogeosciences, https://doi.org/10.5194/essd-2020-202, 2020.

2764 Cox, P. M., Pearson, D., Booth, B. B., Friedlingstein, P., Huntingford, C., Jones, C. D., and Luke, C. M.:
2765 Sensitivity of tropical carbon to climate change constrained by carbon dioxide variability, Nature, 494, 341–344,
2766 https://doi.org/10.1038/nature11882, 2013.

2767 Crisp, D., Dolman, H., Tanhua, T., McKinley, G. A., Hauck, J., Bastos, A., Sitch, S., Eggleston, S., and Aich, V.:
2768 How Well Do We Understand the Land-Ocean-Atmosphere Carbon Cycle?, Reviews of Geophysics, 60,
2769 e2021RG000736, https://doi.org/10.1029/2021RG000736, 2022.

2770 Danek, C. and Hauck, J.: Contrasting high-latitude mixed layer depth trends in Earth System Models and data
2771 products and their impact on temporal pCO2 variability, Clim Dyn, 64, 211, https://doi.org/10.1007/s00382-026-
2772 08109-z, 2026.

2773 De Kauwe, M. G., Medlyn, B. E., Zaehle, S., Walker, A. P., Dietze, M. C., Wang, Y.-P., Luo, Y., Jain, A. K., El-
2774 Masri, B., Hickler, T., Wårlind, D., Weng, E., Parton, W. J., Thornton, P. E., Wang, S., Prentice, I. C., Asao, S.,
2775 Smith, B., McCarthy, H. R., Iversen, C. M., Hanson, P. J., Warren, J. M., Oren, R., and Norby, R. J.: Where does
2776 the carbon go? A model–data intercomparison of vegetation carbon allocation and turnover processes at two
2777 temperate forest free-air CO2 enrichment sites, New Phytol., 203, 883–899, https://doi.org/10.1111/nph.12847,
2778 2014.

2779 Decharme, B., Delire, C., Minvielle, M., Colin, J., Vergnes, J.-P., Alias, A., Saint-Martin, D., Séférian, R., Sénési,
2780 S., and Voldoire, A.: Recent Changes in the ISBA-CTRIP Land Surface System for Use in the CNRM-CM6
2781 Climate Model and in Global Off-Line Hydrological Applications, Journal of Advances in Modeling Earth
2782 Systems, 11, 1207–1252, https://doi.org/10.1029/2018MS001545, 2019.

2783 Delire, C., Séférian, R., Decharme, B., Alkama, R., Calvet, J.-C., Carrer, D., Gibelin, A.-L., Joetzjer, E., Morel, X.,
2784 Rocher, M., and Tzanos, D.: The Global Land Carbon Cycle Simulated With ISBA-CTRIP: Improvements Over
2785 the Last Decade, J. Adv. Model. Earth Syst., 12, e2019MS001886, https://doi.org/10.1029/2019MS001886, 2020.

2786 Denman, K. L., Brasseur, G., Chidthaisong, A., Ciais, P., Cox, P. M., Dickinson, R. E., Hauglustaine, D., Heinze,
2787 C., Holland, E., Jacob, D., Lohmann, U., Ramachandran, S., Leite da Silva Dias, P., Wofsy, S. C., and Zhang, X.:
2788 Couplings Between Changes in the Climate System and Biogeochemistry, in: Climate Change 2007: The Physical
2789 Science Basis. Contribution of Working Group I to the Fourth Assessment Report of the Intergovernmental Panel
2790 on Climate Change, edited by: Solomon, S., Qin, D., Manning, M., Marquis, M., Averyt, K., Tignor, M. M. B.,
2791 Miller, H. L., and Chen, Z. L., Cambridge University Press, Cambridge, UK and New York, USA, 499–587, ISBN:
2792 9780521705967, 2007.

2793 Denvil-Sommer, A., Gehlen, M., and Vrac, M.: Observation system simulation experiments in the Atlantic Ocean
2794 for enhanced surface ocean pCO2 reconstructions, Ocean Sci., 17, 1011–1030, https://doi.org/10.5194/os-17-1011-
2795 2021, 2021.

2796 DeVries, T., Holzer, M., and Primeau, F.: Recent increase in oceanic carbon uptake driven by weaker upper-ocean
2797 overturning, Nature, 542, 215–218, https://doi.org/10.1038/nature21068, 2017.

2798 DeVries, T.: The oceanic anthropogenic CO 2 sink: Storage, air-sea fluxes, and transports over the industrial era,
2799 Global Biogeochem. Cycles, 28, 631–647, https://doi.org/10.1002/2013GB004739, 2014.

https://doi.org/10.5194/essd-2026-895
Preprint. Discussion started: 10 November 2026
© Author(s) 2026. CC BY 4.0 License.



2800 DeVries, T., Quéré, C. L., Andrews, O., Berthet, S., Hauck, J., Ilyina, T., Landschützer, P., Lenton, A., Lima, I. D.,
2801 Nowicki, M., Schwinger, J., and Séférian, R.: Decadal trends in the ocean carbon sink, PNAS, 116, 11646–11651,
2802 https://doi.org/10.1073/pnas.1900371116, 2019.

2803 DeVries, T.: Atmospheric CO2 and Sea Surface Temperature Variability Cannot Explain Recent Decadal
2804 Variability of the Ocean CO2 Sink, Geophysical Research Letters, 49, e2021GL096018,
2805 https://doi.org/10.1029/2021GL096018, 2022.

2806 DeVries, T., Yamamoto, K., Wanninkhof, R., Gruber, N., Hauck, J., Müller, J. D., Bopp, L., Carroll, D., Carter, B.,
2807 Chau, T.-T.-T., Doney, S. C., Gehlen, M., Gloege, L., Gregor, L., Henson, S., Kim, J. H., Iida, Y., Ilyina, T.,
2808 Landschützer, P., Le Quéré, C., Munro, D., Nissen, C., Patara, L., Pérez, F. F., Resplandy, L., Rodgers, K. B.,
2809 Schwinger, J., Séférian, R., Sicardi, V., Terhaar, J., Triñanes, J., Tsujino, H., Watson, A., Yasunaka, S., and Zeng,
2810 J.: Magnitude, trends, and variability of the global ocean carbon sink from 1985-2018, Glob. Biogeochem. Cycles,
2811 n/a, e2023GB007780, https://doi.org/10.1029/2023GB007780, 2023.

2812 Döscher, R., Acosta, M., Alessandri, A., Anthoni, P., Arneth, A., Arsouze, T., Bergmann, T., Bernadello, R.,
2813 Bousetta, S., Caron, L.P. and Carver, G.: The EC-earth3 Earth system model for the climate model intercomparison
2814 project 6. Geoscientific Model Development Discussions, 2021, pp.1-90, https://doi.org/10.5194/gmd-15-2973-
2815 2022, 2021.

2816 Doney, S. C., Lima, I., Feely, R. A., Glover, D. M., Lindsay, K., Mahowald, N., Moore, J. K., and Wanninkhof, R.:
2817 Mechanisms governing interannual variability in upper-ocean inorganic carbon system and air–sea CO2 fluxes:
2818 Physical climate and atmospheric dust, Deep Sea Research Part II: Topical Studies in Oceanography, 56, 640–655,
2819 https://doi.org/10.1016/j.dsr2.2008.12.006, 2009.

2820 Dong, Y., Bakker, D. C. E., Bell, T. G., Huang, B., Landschützer, P., Liss, P. S., and Yang, M.: Update on the
2821 Temperature Corrections of Global Air-Sea CO2 Flux Estimates, Glob. Biogeochem. Cycles, 36, e2022GB007360,
2822 https://doi.org/10.1029/2022GB007360, 2022.

2823 Dong, Y., Bakker, D. C. E., Bell, T. G., Yang, M., Landschützer, P., Hauck, J., Rödenbeck, C., Kitidis, V.,
2824 Bushinsky, S. M., and Liss, P. S.: Direct observational evidence of strong CO2 uptake in the Southern Ocean, Sci.
2825 Adv., 10, eadn5781, https://doi.org/10.1126/sciadv.adn5781, 2024a.

2826 Dong, Y., Bakker, D. C. E., and Landschützer, P.: Accuracy of ocean CO2 uptake estimates at a risk by a reduction
2827 in the data collection, Geophys. Res. Lett., 51, e2024GL108502, https://doi.org/10.1029/2024GL108502, 2024b.

2828 Dorgeist, L., Schwingshackl, C., Bultan, S., and Pongratz, J.: A consistent budgeting of terrestrial carbon fluxes.
2829 Nature Communications, 15(1), 7426, https://doi.org/10.1038/s41467-024-51126-x, 2024.

2830 Eckes-Shephard, A. H., Argles, A. P. K., Brzeziecki, B., Cox, P. M., De Kauwe, M. G., Esquivel-Muelbert, A.,
2831 Fisher, R. A., Hurtt, G. C., Knauer, J., Koven, C. D., Lehtonen, A., Luyssaert, S., Marqués, L., Ma, L., Marie, G.,
2832 Moore, J. R., Needham, J. F., Olin, S., Peltoniemi, M., Piltz, K., Sato, H., Sitch, S., Stocker, B. D., Weng, E.,
2833 Zuleta, D., and Pugh, T. A. M. Pugh: Demography, dynamics and data: building confidence for simulating changes
2834 in the world's forests, New Phytologist, doi: 10.1111/nph.70643, 2025.

2835 Edwards, M., Geden, O., Gidden, M., Lamb, W. F., Minx, J., Nemet, G. F., Smith, S., Bellamy, R., Brutschin, E.,
2836 Anadon, L. D., Fuss, S., Grassi, G., Injy Johnstone, Lebling, K., Lunstrum, A., Müller-Hansen, F., Portugal-
2837 Pereira, J., Probst, B. S., and Vaughan, N.: The State of Carbon Dioxide Removal - 3rd Edition (2026),
2838 https://doi.org/10.17605/OSF.IO/ZRD65, 2026.

2839 EIA: Short-Term Energy Outlook: March 2026. U.S. Energy Information Administration [Data set]. Available at:
2840 http://www.eia.gov/forecasts/steo/outlook.cfm, last access: 23 March 2026, 2026.

2841 Erb, K.-H., Kastner, T., Luyssaert, S., Houghton, R. A., Kuemmerle, T., Olofsson, P., and Haberl, H.: Bias in the
2842 attribution of forest carbon sinks, Nature Clim Change, 3, 854–856, https://doi.org/10.1038/nclimate2004, 2013.

2843 Erb, K.-H., Kastner, T., Plutzar, C., Bais, A. L. S., Carvalhais, N., Fetzel, T., Gingrich, S., Haberl, H., Lauk, C.,
2844 Niedertscheider, M., Pongratz, J., Thurner, M., and Luyssaert, S.: Unexpectedly large impact of forest management
2845 and grazing on global vegetation biomass, Nature, 553, 73–76, https://doi.org/10.1038/nature25138, 2018.

2846 Erb, M. and Marland, G.: Global carbon dioxide emissions from 1750 to 2022: the CDIAC-FF annual product,
2847 Carbon Res., 5, 65, https://doi.org/10.1007/s44246-026-00304-1, 2026a.

https://doi.org/10.5194/essd-2026-895
Preprint. Discussion started: 10 November 2026
© Author(s) 2026. CC BY 4.0 License.



2848 Erb, M. and Marland, G.: Global, Regional, and National Fossil-Fuel CO2 Emissions: 1751-2023 CDIAC-FF,
2849 Research Institute for Environment, Energy, and Economics, Appalachian State University,
2850 https://rieee.appstate.edu/projects-programs/cdiac/ (last access: 30 October 2026), 2026b.

2851 Eskander, S. M. S. U. and Fankhauser, S.: Reduction in greenhouse gas emissions from national climate legislation,
2852 Nat. Clim. Chang., 10, 750–756, https://doi.org/10.1038/s41558-020-0831-z, 2020.

2853 Etheridge, D. M., Steele, L. P., Langenfelds, R. L., Francey, R. J., Barnola, J.-M., and Morgan, V. I.: Natural and
2854 anthropogenic changes in atmospheric CO 2 over the last 1000 years from air in Antarctic ice and firn, J. Geophys.
2855 Res., 101, 4115–4128, https://doi.org/10.1029/95JD03410, 1996.

2856 Fan, Y., Miguez-Macho, G., Jobbágy, E. G., Jackson, R. B., and Otero-Casal, C.: Hydrologic regulation of plant
2857 rooting depth, Proc. Natl. Acad. Sci. U.S.A., 114, 10572–10577, https://doi.org/10.1073/pnas.1712381114, 2017.

2858 FAO: Land statistics 2001–2023 – Global, regional and country trends. FAOSTAT Analytical Briefs, No.107.
2859 Rome, available at: https://doi.org/10.4060/cd5765en, last access: 30 October 2026, 2025.

2860 FAO: FAOSTAT Emissions from drained organic soils. Available at http://www.fao.org/faostat/en/#data/GV, last
2861 access: 30 October 2026, 2026a.

2862 FAO: FAOSTAT Land Use. Available at http://www.fao.org/faostat/en/#data/RL, last access: 30 October 2026,
2863 2026b.

2864 FAO: FAOSTAT Emissions totals database, available at https://faostat.fao.org/internal/en/#data/GT, last access: 14
2865 October 2026, FAO2026c.

2866 Fay, A. R., Gregor, L., Landschützer, P., McKinley, G. A., Gruber, N., Gehlen, M., Iida, Y., Laruelle, G. G.,
2867 Rödenbeck, C., Roobaert, A., and Zeng, J.: SeaFlux: harmonization of air–sea CO2 fluxes from surface pCO2 data
2868 products using a standardized approach, Earth System Science Data, 13, 4693–4710, https://doi.org/10.5194/essd-
2869 13-4693-2021, 2021.

2870 Fay, A. R., McKinley, G. A., Lovenduski, N. S., Eddebbar, Y., Levy, M. N., Long, M. C., Olivarez, H. C., and
2871 Rustagi, R. R.: Immediate and Long-Lasting Impacts of the Mt. Pinatubo Eruption on Ocean Oxygen and Carbon
2872 Inventories. Global Biogeochemical Cycles, 37(2). https://doi.org/10.1029/2022gb007513, 2023.

2873 Fay, A. R., Carroll, D., McKinley, G. A., Menemenlis, D., and Zhang, H.: Scale-Dependent Drivers of Air-Sea
2874 CO2 Flux Variability, Geophysical Research Letters, 51, e2024GL111911, https://doi.org/10.1029/2024GL111911,
2875 2024.

2876 Felzer, B. S.: Carbon, nitrogen, and water response to climate and land use changes in Pennsylvania during the
2877 20th and 21st centuries, Ecological Modelling, 240, 49–63, https://doi.org/10.1016/j.ecolmodel.2012.05.003, 2012.

2878 Felzer, B. S. and Jiang, M.: Effect of Land Use and Land Cover Change in Context of Growth Enhancements in the
2879 United States Since 1700: Net Source or Sink?, JGR Biogeosciences, 123, 3439–3457,
2880 https://doi.org/10.1029/2017JG004378, 2018.

2881 Felzer, B. S., Cronin, T. W., Melillo, J. M., Kicklighter, D. W., and Schlosser, C. A.: Importance of carbon-
2882 nitrogen interactions and ozone on ecosystem hydrology during the 21st century, J. Geophys. Res., 114,
2883 2008JG000826, https://doi.org/10.1029/2008JG000826, 2009.

2884 Felzer, B. S., Cronin, T. W., Melillo, J. M., Kicklighter, D. W., Schlosser, C. A., and Dangal, S. R. S.: Nitrogen
2885 effect on carbon-water coupling in forests, grasslands, and shrublands in the arid western United States, J.
2886 Geophys. Res., 116, G03023, https://doi.org/10.1029/2010JG001621, 2011.

2887 Feng, L., Palmer, P. I., Parker, R. J., Deutscher, N. M., Feist, D. G., Kivi, R., Morino, I., and Sussmann, R.:
2888 Estimates of European uptake of CO2 inferred from GOSAT XCO2 retrievals: sensitivity to measurement bias
2889 inside and outside Europe, Atmos. Chem. Phys., 16, 1289–1302, https://doi.org/10.5194/acp-16-1289-2016, 2016.

2890 Fernández-Blanco, R., Rodríguez-Gómez, N., Pozo, D., Costescu, A., and Bolado-Lavín, R.: Natural gas
2891 consumption estimation in the European Union, Energy Reports, 11, 558–566,
2892 https://doi.org/10.1016/j.egyr.2023.12.011, 2024.

2893 Fisher, R. A., Muszala, S., Verteinstein, M., Lawrence, P., Xu, C., McDowell, N. G., Knox, R. G., Koven, C.,
2894 Holm, J., Rogers, B. M., Spessa, A., Lawrence, D., and Bonan, G.: Taking off the training wheels: the properties of
2895 a dynamic vegetation model without climate envelopes, CLM4.5(ED), Geosci. Model Dev., 8, 3593–3619,
2896 https://doi.org/10.5194/gmd-8-3593-2015, 2015.

https://doi.org/10.5194/essd-2026-895
Preprint. Discussion started: 10 November 2026
© Author(s) 2026. CC BY 4.0 License.



Flanagan, D.: 2017 Minerals Yearbook: Copper [Advance Release], Tech. rep., U.S. Geological Survey, https://pubs.usgs.gov/myb/vol1/2017/myb1-2017-copper.pdf, 2021.

Ford, D. J., Blannin, J., Watts, J., Watson, A. J., Landschützer, P., Jersild, A., and Shutler, J. D.: A Comprehensive Analysis of Air-Sea CO2 Flux Uncertainties Constructed From Surface Ocean Data Products, Global Biogeochemical Cycles, 38, e2024GB008188, https://doi.org/10.1029/2024GB008188, 2024.

Ford, D.J., Shutler, J.D., Blanco-Sacristán, J. et al. Enhanced ocean CO2 uptake due to near-surface temperature gradients. Nat. Geosci. 17, 1135–1140 . https://doi.org/10.1038/s41561-024-01570-7, 2024a

Ford, D. J., Shutler, J. D., Holding, T., Sims, R. P., Ashton, I., Woolf, D. K., Goddijn-Murphy, L., Bakker, D. C. E., Sabine, C., Merchant, C. J., Embury, O., Dong, Y., and Wanninkhof, R.: Recalculating the Surface Ocean CO2 Atlas (SOCAT) to a sea surface temperature climate data record, Sci Data, 13, 1329, https://doi.org/10.1038/s41597-026-07532-5, 2026a.

Ford, D. J., Shutler, J. D., Ashton, I., Sims, R. P., and Holding, T.: Recalculated (depth and temperature consistent) surface ocean CO_2 atlas (SOCAT) version 2026 (v0-1) [Data set], Zenodo, https://doi.org/10.5281/ZENODO.20757579, 2026b.

Forkel, M., Carvalhais, N., Rödenbeck, C., Keeling, R., Heimann, M., Thonicke, K., Zaehle, S., and Reichstein, M.: Enhanced seasonal CO2 exchange caused by amplified plant productivity in northern ecosystems, Science, 351, 696–699, https://doi.org/10.1126/science.aac4971, 2016.

Forster, P. M., Smith, C., Walsh, T., Lamb, W. F., Lamboll, R., Cassou, C., Hauser, M., Hausfather, Z., Lee, J.-Y., Palmer, M. D., Von Schuckmann, K., Slangen, A. B. A., Szopa, S., Trewin, B., Yun, J., Gillett, N. P., Jenkins, S., Matthews, H. D., Raghavan, K., Ribes, A., Rogelj, J., Rosen, D., Zhang, X., Allen, M., Aleluia Reis, L., Andrew, R. M., Betts, R. A., Borger, A., Broersma, J. A., Burgess, S. N., Cheng, L., Friedlingstein, P., Domingues, C. M., Gambarini, M., Gasser, T., Gütschow, J., Ishii, M., Kadow, C., Kennedy, J., Killick, R. E., Krummel, P. B., Liné, A., Monselesan, D. P., Morice, C., Mühle, J., Naik, V., Peters, G. P., Pirani, A., Pongratz, J., Minx, J. C., Rigby, M., Rohde, R., Savita, A., Seneviratne, S. I., Thorne, P., Wells, C., Western, L. M., Van Der Werf, G. R., Wijffels, S. E., Masson-Delmotte, V., and Zhai, P.: Indicators of Global Climate Change 2024: annual update of key indicators of the state of the climate system and human influence, Earth Syst. Sci. Data, 17, 2641–2680, https://doi.org/10.5194/essd-17-2641-2025, 2025.

Forster, P. M., Walsh, T., Smith, C., Lamb, W. F., Lamboll, R., Cassou, C., Hauser, M., Hausfather, Z., Lee, J.-Y., Palmer, M. D., Von Schuckmann, K., Slangen, A. B. A., Szopa, S., Trewin, B., Yun, J., Gillett, N. P., Jenkins, S., Matthews, H. D., Raghavan, K., Ribes, A., Rogelj, J., Rosen, D., Zhang, X., Allen, M., Andrew, R. M., Atkinson, C., Betts, R. A., Bombelli, A., Burgess, S. N., Cheng, L., Claxton, H. E., Friedlingstein, P., Frölicher, T. L., Domingues, C. M., Gasser, T., Gregory, C. H., Hoesly, R. M., Huppmann, D., Ishii, M., Kadow, C., Karwat, A., Kennedy, J., Killick, R. E., Kovilakam, M. V. M., Krummel, P. B., Lan, X., Lamarque, J.-F., Liné, A., Martín-Míguez, B., Monselesan, D. P., Morice, C., Mühle, J., Mussak, P., Peters, G. P., Pirani, A., Pongratz, J., Rigby, M., Rohde, R., Savita, A., Seneviratne, S. I., Smith, S. J., Taha, G., Tassone, C., Thorne, P., Wells, C., Western, L. M., Van Der Werf, G. R., Wijffels, S. E., Zecchetto, M., Zhong, J., Zhang, X.-Y., Masson-Delmotte, V., and Zhai, P.: Indicators of Global Climate Change 2025: annual update of key indicators of the state of the climate system and human influence, Earth Syst. Sci. Data, 18, 3889–3933, https://doi.org/10.5194/essd-18-3889-2026, 2026.

Friedlingstein, P., Houghton, R. A., Marland, G., Hackler, J., Boden, T. A., Conway, T. J., Canadell, J. G., Raupach, M. R., Ciais, P., and Le Quéré, C.: Update on CO2 emissions, Nature Geosci, 3, 811–812, https://doi.org/10.1038/ngeo1022, 2010.

Friedlingstein, P., Andrew, R. M., Rogelj, J., Peters, G. P., Canadell, J. G., Knutti, R., Luderer, G., Raupach, M. R., Schaeffer, M., van Vuuren, D. P., and Le Quéré, C.: Persistent growth of CO2 emissions and implications for reaching climate targets, Nature Geosci, 7, 709–715, https://doi.org/10.1038/ngeo2248, 2014.

Friedlingstein, P., Jones, M. W., O'Sullivan, M., Andrew, R. M., Hauck, J., Peters, G. P., Peters, W., Pongratz, J., Sitch, S., Le Quéré, C., Bakker, D. C. E., Canadell, J. G., Ciais, P., Jackson, R. B., Anthoni, P., Barbero, L., Bastos, A., Bastrikov, V., Becker, M., Bopp, L., Buitenhuis, E., Chandra, N., Chevallier, F., Chini, L. P., Currie, K. I., Feely, R. A., Gehlen, M., Gilfillan, D., Gkritzalis, T., Goll, D. S., Gruber, N., Gutekunst, S., Harris, I., Haverd, V., Houghton, R. A., Hurtt, G., Ilyina, T., Jain, A. K., Joetzjer, E., Kaplan, J. O., Kato, E., Klein Goldewijk, K., Korsbakken, J. I., Landschützer, P., Lauvset, S. K., Lefèvre, N., Lenton, A., Lienert, S., Lombardozzi, D., Marland, G., McGuire, P. C., Melton, J. R., Metzl, N., Munro, D. R., Nabel, J. E. M. S., Nakaoka, S.-I., Neill, C., Omar, A. M., Ono, T., Peregon, A., Pierrot, D., Poulter, B., Rehder, G., Resplandy, L., Robertson, E., Rödenbeck, C., Séférian, R., Schwinger, J., Smith, N., Tans, P. P., Tian, H., Tilbrook, B., Tubiello, F. N., van der Werf, G. R.,

https://doi.org/10.5194/essd-2026-895
Preprint. Discussion started: 10 November 2026
© Author(s) 2026. CC BY 4.0 License.



2950 Wiltshire, A. J., and Zaehle, S.: Global Carbon Budget 2019, Earth Syst. Sci. Data, 11, 1783–1838,
2951 https://doi.org/10.5194/essd-11-1783-2019, 2019.

2952 Friedlingstein, P., O'Sullivan, M., Jones, M. W., Andrew, R. M., Hauck, J., Olsen, A., Peters, G. P., Peters, W.,
2953 Pongratz, J., Sitch, S., Le Quéré, C., Canadell, J. G., Ciais, P., Jackson, R. B., Alin, S., Aragão, L. E. O. C., Arneth,
2954 A., Arora, V., Bates, N. R., Becker, M., Benoit-Cattin, A., Bittig, H. C., Bopp, L., Bultan, S., Chandra, N.,
2955 Chevallier, F., Chini, L. P., Evans, W., Florentie, L., Forster, P. M., Gasser, T., Gehlen, M., Gilfillan, D.,
2956 Gkritzalis, T., Gregor, L., Gruber, N., Harris, I., Hartung, K., Haverd, V., Houghton, R. A., Ilyina, T., Jain, A. K.,
2957 Joetzjer, E., Kadono, K., Kato, E., Kitidis, V., Korsbakken, J. I., Landschützer, P., Lefèvre, N., Lenton, A., Lienert,
2958 S., Liu, Z., Lombardozzi, D., Marland, G., Metzl, N., Munro, D. R., Nabel, J. E. M. S., Nakaoka, S.-I., Niwa, Y.,
2959 O'Brien, K., Ono, T., Palmer, P. I., Pierrot, D., Poulter, B., Resplandy, L., Robertson, E., Rödenbeck, C.,
2960 Schwinger, J., Séférian, R., Skjelvan, I., Smith, A. J. P., Sutton, A. J., Tanhua, T., Tans, P. P., Tian, H., Tilbrook,
2961 B., van der Werf, G., Vuichard, N., Walker, A. P., Wanninkhof, R., Watson, A. J., Willis, D., Wiltshire, A. J.,
2962 Yuan, W., Yue, X., and Zaehle, S.: Global Carbon Budget 2020, Earth Syst. Sci. Data, 12, 3269–3340,
2963 https://doi.org/10.5194/essd-12-3269-2020, 2020.

2964 Friedlingstein, P., Jones, M. W., O'Sullivan, M., Andrew, R. M., Bakker, D. C. E., Hauck, J., Le Quéré, C., Peters,
2965 G. P., Peters, W., Pongratz, J., Sitch, S., Canadell, J. G., Ciais, P., Jackson, R. B., Alin, S. R., Anthoni, P., Bates, N.
2966 R., Becker, M., Bellouin, N., Bopp, L., Chau, T. T. T., Chevallier, F., Chini, L. P., Cronin, M., Currie, K. I.,
2967 Decharme, B., Djeutchouang, L. M., Dou, X., Evans, W., Feely, R. A., Feng, L., Gasser, T., Gilfillan, D.,
2968 Gkritzalis, T., Grassi, G., Gregor, L., Gruber, N., Gürses, Ö., Harris, I., Houghton, R. A., Hurtt, G. C., Iida, Y.,
2969 Ilyina, T., Luijkx, I. T., Jain, A., Jones, S. D., Kato, E., Kennedy, D., Klein Goldewijk, K., Knauer, J., Korsbakken,
2970 J. I., Körtzinger, A., Landschützer, P., Lauvset, S. K., Lefèvre, N., Lienert, S., Liu, J., Marland, G., McGuire, P. C.,
2971 Melton, J. R., Munro, D. R., Nabel, J. E. M. S., Nakaoka, S.-I., Niwa, Y., Ono, T., Pierrot, D., Poulter, B., Rehder,
2972 G., Resplandy, L., Robertson, E., Rödenbeck, C., Rosan, T. M., Schwinger, J., Schwingshackl, C., Séférian, R.,
2973 Sutton, A. J., Sweeney, C., Tanhua, T., Tans, P. P., Tian, H., Tilbrook, B., Tubiello, F., van der Werf, G. R.,
2974 Vuichard, N., Wada, C., Wanninkhof, R., Watson, A. J., Willis, D., Wiltshire, A. J., Yuan, W., Yue, C., Yue, X.,
2975 Zaehle, S., and Zeng, J.: Global Carbon Budget 2021, Earth Syst. Sci. Data, 14, 1917–2005,
2976 https://doi.org/10.5194/essd-14-1917-2022, 2022a.

2977 Friedlingstein, P., O'Sullivan, M., Jones, M. W., Andrew, R. M., Gregor, L., Hauck, J., Le Quéré, C., Luijkx, I. T.,
2978 Olsen, A., Peters, G. P., Peters, W., Pongratz, J., Schwingshackl, C., Sitch, S., Canadell, J. G., Ciais, P., Jackson, R.
2979 B., Alin, S. R., Alkama, R., Arneth, A., Arora, V. K., Bates, N. R., Becker, M., Bellouin, N., Bittig, H. C., Bopp,
2980 L., Chevallier, F., Chini, L. P., Cronin, M., Evans, W., Falk, S., Feely, R. A., Gasser, T., Gehlen, M., Gkritzalis, T.,
2981 Gloege, L., Grassi, G., Gruber, N., Gürses, Ö., Harris, I., Hefner, M., Houghton, R. A., Hurtt, G. C., Iida, Y., Ilyina,
2982 T., Jain, A. K., Jersild, A., Kadono, K., Kato, E., Kennedy, D., Klein Goldewijk, K., Knauer, J., Korsbakken, J. I.,
2983 Landschützer, P., Lefèvre, N., Lindsay, K., Liu, J., Liu, Z., Marland, G., Mayot, N., McGrath, M. J., Metzl, N.,
2984 Monacci, N. M., Munro, D. R., Nakaoka, S., Niwa, Y., O'Brien, K., Ono, T., Palmer, P. I., Pan, N., Pierrot, D.,
2985 Pocock, K., Poulter, B., Resplandy, L., Robertson, E., Rödenbeck, C., Rodriguez, C., Rosan, T. M., Schwinger, J.,
2986 Séférian, R., Shutler, J. D., Skjelvan, I., Steinhoff, T., Sun, Q., Sutton, A. J., Sweeney, C., Takao, S., Tanhua, T.,
2987 Tans, P. P., Tian, X., Tian, H., Tilbrook, B., Tsujino, H., Tubiello, F., van der Werf, G. R., Walker, A. P.,
2988 Wanninkhof, R., Whitehead, C., Willstrand Wranne, A., Wright, R., Yuan, W., Yue, C., Yue, X., Zaehle, S., Zeng,
2989 J., and Zheng, B.: Global Carbon Budget 2022, Earth Syst. Sci. Data, 14, 4811–4900, https://doi.org/10.5194/essd-
2990 14-4811-2022, 2022b.

2991 Friedlingstein, P., O'Sullivan, M., Jones, M. W., Andrew, R. M., Bakker, D. C. E., Hauck, J., Landschützer, P., Le
2992 Quéré, C., Luijkx, I. T., Peters, G. P., Peters, W., Pongratz, J., Schwingshackl, C., Sitch, S., Canadell, J. G., Ciais,
2993 P., Jackson, R. B., Alin, S. R., Anthoni, P., Barbero, L., Bates, N. R., Becker, M., Bellouin, N., Decharme, B.,
2994 Bopp, L., Brasika, I. B. M., Cadule, P., Chamberlain, M. A., Chandra, N., Chau, T.-T.-T., Chevallier, F., Chini, L.
2995 P., Cronin, M., Dou, X., Enyo, K., Evans, W., Falk, S., Feely, R. A., Feng, L., Ford, D. J., Gasser, T., Ghattas, J.,
2996 Gkritzalis, T., Grassi, G., Gregor, L., Gruber, N., Gürses, Ö., Harris, I., Hefner, M., Heinke, J., Houghton, R. A.,
2997 Hurtt, G. C., Iida, Y., Ilyina, T., Jacobson, A. R., Jain, A. K., Jarníková, T., Jersild, A., Jiang, F., Jin, Z., Joos, F.,
2998 Kato, E., Keeling, R. F., Kennedy, D., Klein Goldewijk, K., Knauer, J., Korsbakken, J. I., Körtzinger, A., Lan, X.,
2999 Lefèvre, N., Li, H., Liu, J., Liu, Z., Ma, L., Marland, G., Mayot, N., McGuire, P. C., McKinley, G. A., Meyer, G.,
3000 Morgan, E. J., Munro, D. R., Nakaoka, S., Niwa, Y., O'Brien, K. M., Olsen, A., Omar, A. M., Ono, T., Paulsen, M.,
3001 Pierrot, D., Pocock, K., Poulter, B., Powis, C. M., Rehder, G., Resplandy, L., Robertson, E., Rödenbeck, C., Rosan,
3002 T. M., Schwinger, J., Séférian, R., Smallman, T. L., Smith, S. M., Sospedra-Alfonso, R., Sun, Q., Sutton, A. J.,
3003 Sweeney, C., Takao, S., Tans, P. P., Tian, H., Tilbrook, B., Tsujino, H., Tubiello, F., van der Werf, G. R., van
3004 Ooijen, E., Wanninkhof, R., Watanabe, M., Wimart-Rousseau, C., Yang, D., Yang, X., Yuan, W., Yue, X., Zaehle,
3005 S., Zeng, J., and Zheng, B.: Global Carbon Budget 2023, Earth Syst. Sci. Data, 15, 5301–5369,
3006 https://doi.org/10.5194/essd-15-5301-2023, 2023.

https://doi.org/10.5194/essd-2026-895
Preprint. Discussion started: 10 November 2026
© Author(s) 2026. CC BY 4.0 License.



3007 Friedlingstein, P., O'Sullivan, M., Jones, M. W., Andrew, R. M., Hauck, J., Landschützer, P., Le Quéré, C., Li, H.,
3008 Luijkx, I. T., Olsen, A., Peters, G. P., Peters, W., Pongratz, J., Schwingshackl, C., Sitch, S., Canadell, J. G., Ciais,
3009 P., Jackson, R. B., Alin, S. R., Arneth, A., Arora, V., Bates, N. R., Becker, M., Bellouin, N., Berghoff, C. F., Bittig,
3010 H. C., Bopp, L., Cadule, P., Campbell, K., Chamberlain, M. A., Chandra, N., Chevallier, F., Chini, L. P., Colligan,
3011 T., Decayeux, J., Djeutchouang, L. M., Dou, X., Duran Rojas, C., Enyo, K., Evans, W., Fay, A. R., Feely, R. A.,
3012 Ford, D. J., Foster, A., Gasser, T., Gehlen, M., Gkritzalis, T., Grassi, G., Gregor, L., Gruber, N., Gürses, Ö., Harris,
3013 I., Hefner, M., Heinke, J., Hurtt, G. C., Iida, Y., Ilyina, T., Jacobson, A. R., Jain, A. K., Jarníková, T., Jersild, A.,
3014 Jiang, F., Jin, Z., Kato, E., Keeling, R. F., Klein Goldewijk, K., Knauer, J., Korsbakken, J. I., Lan, X., Lauvset, S.
3015 K., Lefèvre, N., Liu, Z., Liu, J., Ma, L., Maksyutov, S., Marland, G., Mayot, N., McGuire, P. C., Metzl, N.,
3016 Monacci, N. M., Morgan, E. J., Nakaoka, S.-I., Neill, C., Niwa, Y., Nützel, T., Olivier, L., Ono, T., Palmer, P. I.,
3017 Pierrot, D., Qin, Z., Resplandy, L., Roobaert, A., Rosan, T. M., Rödenbeck, C., Schwinger, J., Smallman, T. L.,
3018 Smith, S. M., Sospedra-Alfonso, R., Steinhoff, T., Sun, Q., Sutton, A. J., Séférian, R., Takao, S., Tatebe, H., Tian,
3019 H., Tilbrook, B., Torres, O., Tourigny, E., Tsujino, H., Tubiello, F., van der Werf, G., Wanninkhof, R., Wang, X.,
3020 Yang, D., Yang, X., Yu, Z., Yuan, W., Yue, X., Zaehle, S., Zeng, N., and Zeng, J.: Global Carbon Budget 2024,
3021 Earth Syst. Sci. Data, 17, 965–1039, https://doi.org/10.5194/essd-17-965-2025, 2025a.

3022 Friedlingstein, P. ,Le Quéré, C., O'Sullivan, M., Hauck, J., Landschützer, P., Luijkx, I.T., Li, H., van der Woude,
3023 A., Schwingshackl, C., Pongratz, P., Regnier, P., Andrew, R.M., Bakker, D.C.E., Canadell, J.G., Ciais, P., Gasser,
3024 T., Jones, M.W., Lan, X., Morgan, E., Olsen, A., Peters, G.P., Peters, W., Sitch, S., and Tian, H.: Emerging climate
3025 impact on carbon sinks in a consolidated carbon budget, Nature, https://doi.org/10.1038/s41586-025-09802-5,
3026 2025b.

3027 Friedlingstein, P., O'Sullivan, M., Jones, M. W., Andrew, R. M., Bakker, D. C. E., Hauck, J., Landschützer, P., Le
3028 Quéré, C., Li, H., Luijkx, I. T., Peters, G. P., Peters, W., Pongratz, J., Schwingshackl, C., Sitch, S., Canadell, J. G.,
3029 Ciais, P., Aas, K., Alin, S. R., Anthoni, P., Barbero, L., Bates, N. R., Bellouin, N., Benoit-Cattin, A., Berghoff, C.
3030 F., Bernardello, R., Bopp, L., Brasika, I. B. M., Chamberlain, M. A., Chandra, N., Chevallier, F., Chini, L. P.,
3031 Collier, N. O., Colligan, T. H., Cronin, M., Djeutchouang, L. M., Dou, X., Enright, M. P., Enyo, K., Erb, M.,
3032 Evans, W., Feely, R. A., Feng, L., Ford, D. J., Foster, A., Fransner, F., Gasser, T., Gehlen, M., Gkritzalis, T.,
3033 Goncalves De Souza, J., Grassi, G., Gregor, L., Gruber, N., Guenet, B., Gürses, Ö., Harrington, K., Harris, I.,
3034 Heinke, J., Hurtt, G. C., Iida, Y., Ilyina, T., Ito, A., Jacobson, A. R., Jain, A. K., Jarníková, T., Jersild, A., Jiang, F.,
3035 Jones, S. D., Kato, E., Keeling, R. F., Klein Goldewijk, K., Knauer, J., Kong, Y., Korsbakken, J. I., Koven, C.,
3036 Kunimitsu, T., Lan, X., Liu, J., Liu, Z., Liu, Z., Lo Monaco, C., Ma, L., Marland, G., McGuire, P. C., McKinley,
3037 G. A., Melton, J. R., Monacci, N., Monier, E., Morgan, E. J., Munro, D. R., Müller, J. D., Nakaoka, S.-I.,
3038 Nayagam, L. R., Niwa, Y., Nutzel, T., Olsen, A., Omar, A. M., Pan, N., Pandey, S., Pierrot, D., Qin, Z., Regnier,
3039 P., Rehder, G., Resplandy, L., Roobaert, A., Rosan, T. M., Rödenbeck, C., Schwinger, J., Skjelvan, I., Smallman,
3040 T. L., Spada, V., Sreeush, M. G., Sun, Q., Sutton, A. J., Sweeney, C., Swingedouw, D., Séférian, R., Takao, S.,
3041 Tatebe, H., Tian, H., Tian, X., Tilbrook, B., Tsujino, H., Tubiello, F., Van Ooijen, E., Van Der Werf, G. R., Van
3042 De Velde, S. J., Walker, A. P., Wanninkhof, R., Yang, X., Yuan, W., Yue, X., and Zeng, J.: Global Carbon Budget
3043 2025, Earth Syst. Sci. Data, 18, 3211–3288, https://doi.org/10.5194/essd-18-3211-2026, 2026a.

3044 Friedlingstein, P., O'Sullivan, M., Andrew, R. M., Hauck, J., Jones, M. W., Landschützer, P., Le Quéré, C., Li, H.,
3045 Luijkx, I. T., Olsen, A., Peters, G. P., Peters, W., Pongratz, J., Schwingshackl, C., Sitch, S., Canadell, J. G., Ciais,
3046 P., Aas, K., Alin, S. R., Arora, V., Bates, N. R., Bedard, K., Martin Belda, D., Bellouin, N., Benoit-Cattin, A.,
3047 Berghoff, C. F., Berthet, S., Bopp, L., Brasika, I. B. M., Burke, E., Casse, L., Chamberlain, M. A., Chevallier, F.,
3048 Chini, L. P., Cronin, M., Curless, S. E., DeVries, T., Ehmen, T., Enright, M. P., Enyo, K., Erb, M., Evans, W., Fay,
3049 A. R., Felzer, B., Ford, D. J., Foster, A., Fransner, F., Fransson, A., Friedman, A., Gasser, T., Gehlen, M.,
3050 Gkritzalis, T., Grassi, G., Gregor, L., Gruber, N., Gürses, Ö., Hao, W., Harrington, K., Heinke, J., Hurtt, G. C.,
3051 Ilyina, T., Ito, A., Jacobson, A. R., Jain, A. K., Janardanan, R. R., Jarníková, T., Jersild, A., Jiang, F., Jin, Z.,
3052 Kamb, L., Kato, E., Keeling, R. F., Klein Goldewijk, K., Knauer, J., Korsbakken, J. I., Kunimitsu, T., Lan, X.,
3053 Lapin, V., Lauvset, S. K., Le Chevère, S., Lee, W.-S., Liao, E., Liu, J., Liu, Z., Luyssaert, S., Ma, L., Maity, S.,
3054 Marland, G., McGuire, P. C., Metzl, N., Mignot, J., Monacci, N. M., Morgan, E. J., Müller, J. D., Munro, D. R.,
3055 Muramatsu, M., Nakaoka, S.-I., Neill, C., Nützel, T., Olivier, L., Osborn, T., Padín, X. A., Palmer, P. I., Pandey,
3056 S., Pierrot, D., Poulter, B., Qin, Z., Qiu, Y., Rehder, G., Resplandy, L., Rödenbeck, C., Roobaert, A., Rosan, T. M.,
3057 Rossi, S., Schwinger, J., Seeberg, G., Séférian, R., Shadwick, E. H., Skjelvan, I., Slominska-Durdasiak, K.,
3058 Smallman, T. L., Sreeush, M. G., Sun, Q., Sutton, A. J., Sweeney, C., Takao, S., Tatebe, H., Terhaar, J., Tian, H.,
3059 Tilbrook, B., Toyoda, T., Triñanes, J. A., Tubiello, F., van der Werf, G. R., van der Woude, A. M., van de Velde,
3060 S. J., Walker, A. P., Wanninkhof, R., Yang, X., Yuan, W., Yue, X., Zeng, J., Zheng, N., and Zheng, B.:
3061 Supplemental data of the Global Carbon Budget 2026, ICOS-ERIC Carbon Portal [data set],
3062 https://doi.org/10.18160/GCP-2026, 2026b.

3063 Fu, W., Moore, J. K., Primeau, F., Collier, N., Ogunro, O. O., Hoffman, F. M., and Randerson, J. T.: Evaluation of
3064 Ocean Biogeochemistry and Carbon Cycling in CMIP Earth System Models With the International Ocean Model

https://doi.org/10.5194/essd-2026-895
Preprint. Discussion started: 10 November 2026
© Author(s) 2026. CC BY 4.0 License.



3065 Benchmarking (IOMB) Software System, JGR Oceans, 127, e2022JC018965,
3066 https://doi.org/10.1029/2022JC018965, 2022.

3067 Ganzenmüller, R., Bultan, S., Winkler, K., Fuchs, R., Zabel, F., and Pongratz, J.: Land-use change emissions based
3068 on high-resolution activity data substantially lower than previously estimated, Environ. Res. Lett., 17, 064050,
3069 https://doi.org/10.1088/1748-9326/ac70d8, 2022.

3070 Gasser, T., Crepin, L., Quilcaille, Y., Houghton, R. A., Ciais, P., and Obersteiner, M.: Historical CO2 emissions
3071 from land use and land cover change and their uncertainty, Biogeosciences, 17, 4075–4101,
3072 https://doi.org/10.5194/bg-17-4075-2020, 2020.

3073 Gaubert, B., Stephens, B. B., Basu, S., Chevallier, F., Deng, F., Kort, E. A., Patra, P. K., Peters, W., Rödenbeck,
3074 C., Saeki, T., Schimel, D., Van der Laan-Luijkx, I., Wofsy, S., and Yin, Y.: Global atmospheric CO2 inverse
3075 models converging on neutral tropical land exchange, but disagreeing on fossil fuel and atmospheric growth rate,
3076 Biogeosciences, 16, 117–134, https://doi.org/10.5194/bg-16-117-2019, 2019.

3077 Gauthier, C. B., Melton, J. R., Meyer, G., Raj Deepak, S. N., and Sonnentag, O.: Parameter Optimization for
3078 Global Soil Carbon Simulations: Not a Simple Problem, J Adv Model Earth Syst, 17, e2024MS004577,
3079 https://doi.org/10.1029/2024MS004577, 2025.

3080 GCP: The Global Carbon Budget 2007, available at: http://www.
3081 globalcarbonproject.org/carbonbudget/archive.htm, last access: 30 October 2026, 2008.

3082 Giglio, L., Schroeder, W., and Justice, C. O.: The collection 6 MODIS active fire detection algorithm and fire
3083 products, Remote Sensing of Environment, 178, 31–41, https://doi.org/10.1016/j.rse.2016.02.054, 2016.

3084 Giglio, L., Boschetti, L., Roy, D. P., Humber, M. L., and Justice, C. O.: The Collection 6 MODIS burned area
3085 mapping algorithm and product, Remote Sensing of Environment, 217, 72–85,
3086 https://doi.org/10.1016/j.rse.2018.08.005, 2018.

3087 Gitz V, Ciais P. Amplifying effects of land-use change on future atmospheric CO2 levels. Global Biogeochemical
3088 Cycles. https://doi.org/10.1029/2002GB001963, 2003.

3089 Gloege, L., McKinley, G. A., Landschützer, P., Fay, A. R., Frölicher, T. L., Fyfe, J. C., Ilyina, T., Jones, S.,
3090 Lovenduski, N. S., Rodgers, K. B., Schlunegger, S., and Takano, Y.: Quantifying Errors in Observationally Based
3091 Estimates of Ocean Carbon Sink Variability, Global Biogeochem. Cy., 35, e2020GB006788,
3092 https://doi.org/10.1029/2020GB006788, 2021.

3093 Gloege, L., Yan, M., Zheng, T., and McKinley, G. A.: Improved Quantification of Ocean Carbon Uptake by Using
3094 Machine Learning to Merge Global Models and pCO2 Data, J. Adv. Model. Earth Syst., 14, e2021MS002620,
3095 https://doi.org/10.1029/2021MS002620, 2022.

3096 Goris, N., Tjiputra, J. F., Olsen, A., Schwinger, J., Lauvset, S. K., and Jeansson, E.: Constraining Projection-Based
3097 Estimates of the Future North Atlantic Carbon Uptake, J. Clim., 31, 3959–3978, https://doi.org/10.1175/JCLI-D-
3098 17-0564.1, 2018.

3099 Grassi, G., House, J., Kurz, W. A., Cescatti, A., Houghton, R. A., Peters, G. P., Sanz, M. J., Viñas, R. A., Alkama,
3100 R., Arneth, A., Bondeau, A., Dentener, F., Fader, M., Federici, S., Friedlingstein, P., Jain, A. K., Kato, E., Koven,
3101 C. D., Lee, D., Nabel, J. E. M. S., Nassikas, A. A., Perugini, L., Rossi, S., Sitch, S., Viovy, N., Wiltshire, A., and
3102 Zaehle, S.: Reconciling global-model estimates and country reporting of anthropogenic forest CO2 sinks, Nature
3103 Clim Change, 8, 914–920, https://doi.org/10.1038/s41558-018-0283-x, 2018.

3104 Grassi, G., Stehfest, E., Rogelj, J., van Vuuren, D., Cescatti, A., House, J., Nabuurs, G.-J., Rossi, S., Alkama, R.,
3105 Viñas, R. A., Calvin, K., Ceccherini, G., Federici, S., Fujimori, S., Gusti, M., Hasegawa, T., Havlik, P.,
3106 Humpenöder, F., Korosuo, A., Perugini, L., Tubiello, F. N., and Popp, A.: Critical adjustment of land mitigation
3107 pathways for assessing countries' climate progress, Nat. Clim. Chang., 11, 425–434,
3108 https://doi.org/10.1038/s41558-021-01033-6, 2021.

3109 Grassi, G., Schwingshackl, C., Gasser, T., Houghton, R. A., Sitch, S., Canadell, J. G., Cescatti, A., Ciais, P.,
3110 Federici, S., Friedlingstein, P., Kurz, W. A., Sanz Sanchez, M. J., Abad Viñas, R., Alkama, R., Bultan, S.,
3111 Ceccherini, G., Falk, S., Kato, E., Kennedy, D., Knauer, J., Korosuo, A., Melo, J., McGrath, M. J., Nabel, J. E. M.
3112 S., Poulter, B., Romanovskaya, A. A., Rossi, S., Tian, H., Walker, A. P., Yuan, W., Yue, X., and Pongratz, J.:
3113 Harmonising the land-use flux estimates of global models and national inventories for 2000–2020, Earth Syst. Sci.
3114 Data, 15, 1093–1114, https://doi.org/10.5194/essd-15-1093-2023, 2023.

https://doi.org/10.5194/essd-2026-895
Preprint. Discussion started: 10 November 2026
© Author(s) 2026. CC BY 4.0 License.



Grassi, G., Peters, G. P., Canadell, J. G., Cescatti, A., Federici, S., Gidden, M. J., Harris, N., Herold, M., Krug, T., O'Sullivan, M., Pongratz, J., Sanz, M. J., Schwingshackl, C., and Van Vuuren, D.: Improving land-use emission estimates under the Paris Agreement, Nat Sustain, 8, 579–581, https://doi.org/10.1038/s41893-025-01565-1, 2025.

Graven, H. D., Keeling, R. F., Piper, S. C., Patra, P. K., Stephens, B. B., Wofsy, S. C., Welp, L. R., Sweeney, C., Tans, P. P., Kelley, J. J., Daube, B. C., Kort, E. A., Santoni, G. W., and Bent, J. D.: Enhanced Seasonal Exchange of CO2 by Northern Ecosystems Since 1960, Science, 341, 1085–1089, https://doi.org/10.1126/science.1239207, 2013.

Gregor, L., Lebehot, A. D., Kok, S., and Scheel Monteiro, P. M.: A comparative assessment of the uncertainties of global surface ocean CO2 estimates using a machine-learning ensemble (CSIR-ML6 version 2019a)–have we hit the wall?. Geoscientific Model Development, 12(12), 5113-5136, https://doi.org/10.5194/gmd-12-5113-2019, 2019.

Gregor, L. and Gruber, N.: OceanSODA-ETHZ: a global gridded data set of the surface ocean carbonate system for seasonal to decadal studies of ocean acidification, Earth System Science Data, 13, 777–808, https://doi.org/10.5194/essd-13-777-2021, 2021.

Gregor, L., Shutler, J., and Gruber, N.: High-resolution variability of the ocean carbon sink. Global Biogeochemical Cycles, 38(8), e2024GB008127, https://doi.org/10.1029/2024GB008127, 2024.

Gruber, N., Gloor, M., Mikaloff Fletcher, S. E., Doney, S. C., Dutkiewicz, S., Follows, M. J., Gerber, M., Jacobson, A. R., Joos, F., Lindsay, K., Menemenlis, D., Mouchet, A., Müller, S. A., Sarmiento, J. L., and Takahashi, T.: Oceanic sources, sinks, and transport of atmospheric CO2, Global Biogeochemical Cycles, 23, GB1005, https://doi.org/10.1029/2008GB003349, 2009.

Gruber, N., Bakker, D. C. E., DeVries, T., Gregor, L., Hauck, J., Landschützer, P., McKinley, G. A., and Müller, J. D.: Trends and variability in the ocean carbon sink, Nat. Rev. Earth Environ., 4, 119–134, https://doi.org/10.1038/s43017-022-00381-x, 2023.

Gruber, N., Clement, D., Carter, B. R., Feely, R. A., van Heuven, S., Hoppema, M., Ishii, M., Key, R. M., Kozyr, A., Lauvset, S. K., Lo Monaco, C., Mathis, J. T., Murata, A., Olsen, A., Perez, F. F., Sabine, C. L., Tanhua, T., and Wanninkhof, R.: The oceanic sink for anthropogenic CO2 from 1994 to 2007, 363, 1193–1199, https://doi.org/10.1126/science.aau5153, 2019.

Guan, D., Liu, Z., Geng, Y., Lindner, S., and Hubacek, K.: The gigatonne gap in China's carbon dioxide inventories, Nature Clim Change, 2, 672–675, https://doi.org/10.1038/nclimate1560, 2012.

Gulev, S. K., Thorne, P. W., Ahn, J., Dentener, F. J., Domingues, C. M., Gerland, S., Gong, D. S., Kaufman, S., Nnamchi, H. C., Quaas, J., Rivera, J. A., Sathyendranath, S., Smith, S. L., Trewin, B., von Shuckmann, K., and Vose, R. S.: Changing State of the Climate System. In: Climate Change 2021: The Physical Science Basis. Contribution of Working Group I to the Sixth Assessment Report of the Intergovernmental Panel on Climate Change [Masson-Delmotte, V., Zhai, P., Pirani, A., Connors, S. L., Péan, C., Berger, S., Caud, N., Chen, Y., Goldfarb, L., Gomis, M. I., Huang, M., Leitzell, K., Lonnoy, E., Matthews, J.B.R., Maycock, T.K., Waterfield, T., Yelekçi, O., Yu, R. and Zhou, B. (eds.)]. Cambridge University Press, Cambridge, United Kingdom and New York, NY, USA, pp. 287–422, https://doi.org/10.1017/9781009157896.004, 2021.

Gürses, Ö., Oziel, L., Karakuş, O., Sidorenko, D., Völker, C., Ye, Y., Zeising, M., Butzin, M., and Hauck, J.: Ocean biogeochemistry in the coupled ocean–sea ice–biogeochemistry model FESOM2.1–REcoM3, Geosci. Model Dev., 16, 4883–4936, https://doi.org/10.5194/gmd-16-4883-2023, 2023.

Gütschow, J., Jeffery, M. L., Gieseke, R., Gebel, R., Stevens, D., Krapp, M., and Rocha, M.: The PRIMAP-hist national historical emissions time series, 8, 571–603, https://doi.org/10.5194/essd-8-571-2016, 2016.

Gütschow, J. and Pflüger, M.: The PRIMAP-hist national historical emissions time series (1750-2025) v2.8 (v2.8) [Data set], Zenodo, https://doi.org/10.5281/ZENODO.22876287, 2026.

Hall, B. D., Crotwell, A. M., Kitzis, D. R., Mefford, T., Miller, B. R., Schibig, M. F., and Tans, P. P.: Revision of the World Meteorological Organization Global Atmosphere Watch (WMO/GAW) CO2 calibration scale, 14, 3015–3032, https://doi.org/10.5194/amt-14-3015-2021, 2021.

Hansis, E., Davis, S. J., and Pongratz, J.: Relevance of methodological choices for accounting of land use change carbon fluxes, Global Biogeochem. Cycles, 29, 1230–1246, https://doi.org/10.1002/2014GB004997, 2015.

https://doi.org/10.5194/essd-2026-895
Preprint. Discussion started: 10 November 2026
© Author(s) 2026. CC BY 4.0 License.



3164 Hauck, J., Nissen, C., Landschützer, P., Rödenbeck, C., Bushinsky, S., and Olsen, A.: Sparse observations induce
3165 large biases in estimates of the global ocean CO2 sink: an ocean model subsampling experiment, Philos. Trans. R.
3166 Soc. Math. Phys. Eng. Sci., 381, 20220063, https://doi.org/10.1098/rsta.2022.0063, 2023a.

3167 Hauck, J., Gregor, L., Nissen, C., Patara, L., Hague, M., Mongwe, P., Bushinsky, S., Doney, S. C., Gruber, N., Le
3168 Quéré, C., Manizza, M., Mazloff, M., Monteiro, P. M. S., and Terhaar, J.: The Southern Ocean Carbon Cycle
3169 1985–2018: Mean, Seasonal Cycle, Trends, and Storage. Global Biogeochemical Cycles, 37(11), e2023GB007848,
3170 https://doi.org/10.1029/2023GB007848, 2023b.

3171 Hauck, J., Zeising, M., Le Quéré, C., Gruber, N., Bakker, D. C. E., Bopp, L., Chau, T. T. T., Gürses, Ö., Ilyina, T.,
3172 Landschützer, P., Lenton, A., Resplandy, L., Rödenbeck, C., Schwinger, J., and Séférian, R.: Consistency and
3173 Challenges in the Ocean Carbon Sink Estimate for the Global Carbon Budget, Front. Mar. Sci., 7, 571720,
3174 https://doi.org/10.3389/fmars.2020.571720, 2020.

3175 Hauck, J., Landschützer, P., Le Chevere, S., Roobaert, A., Berthet, S., Bopp, Laurent ., Chamberlain, M., DeVries,
3176 T., Fay, A., Ford, D. J., Gehlen, M., Gregor, L., Gruber, N., Gürses, Ö., Ilyina, T., Jarnikova, T., Jersild, A., Liao,
3177 E., Muramatsu, M., Resplandy, L., Rödenbeck, C., Schwinger, J., Takahiro, T., Triñanes, J., Zeng, J.: Global
3178 Carbon Budget Ocean - Models and data sets for the ocean sink estimate in the Global Carbon Budget 2026
3179 [Dataset]. Zenodo. https://doi.org/10.5281/zenodo.23723209, 2026.

3180 Haverd, V., Smith, B., Nieradzik, L., Briggs, P. R., Woodgate, W., Trudinger, C. M., Canadell, J. G., and Cuntz,
3181 M.: A new version of the CABLE land surface model (Subversion revision r4601) incorporating land use and land
3182 cover change, woody vegetation demography, and a novel optimisation-based approach to plant coordination of
3183 photosynthesis, Geosci. Model Dev., 11, 2995–3026, https://doi.org/10.5194/gmd-11-2995-2018, 2018.

3184 Heimdal, T. H., McKinley, G. A., Sutton, A. J., Fay, A. R., and Gloege, L.: Assessing improvements in global
3185 ocean p CO2 machine learning reconstructions with Southern Ocean autonomous sampling, Biogeosciences, 21,
3186 2159–2176, https://doi.org/10.5194/bg-21-2159-2024, 2024.

3187 Heinke, J., Rolinski, S., and Müller, C.: Modelling the role of livestock grazing in C and N cycling in grasslands
3188 with LPJmL5.0-grazing, Geosci. Model Dev., 16, 2455–2475, https://doi.org/10.5194/gmd-16-2455-2023, 2023.

3189 Heinke, J., Schaphoff, S., Wirth, S. B., and Müller, C.: Revised nitrogen balance for plant photosynthesis and
3190 growth in the dynamic global vegetation, hydrology and agriculture model LPJmL (5.10),
3191 https://doi.org/10.5194/egusphere-2026-4549, 28 September 2026., 2026.

3192 Hersbach, H., Bell, B., Berrisford, P., Hirahara, S., Horányi, A., Muñoz-Sabater, J., Nicolas, J., Peubey, C., Radu,
3193 R., Schepers, D., Simmons, A., Soci, C., Abdalla, S., Abellan, X., Balsamo, G., Bechtold, P., Biavati, G., Bidlot, J.,
3194 Bonavita, M., Chiara, G., Dahlgren, P., Dee, D., Diamantakis, M., Dragani, R., Flemming, J., Forbes, R., Fuentes,
3195 M., Geer, A., Haimberger, L., Healy, S., Hogan, R. J., Hólm, E., Janisková, M., Keeley, S., Laloyaux, P., Lopez,
3196 P., Lupu, C., Radnoti, G., Rosnay, P., Rozum, I., Vamborg, F., Villaume, S., and Thépaut, J.: The ERA5 global
3197 reanalysis, Q.J.R. Meteorol. Soc., 146, 1999–2049, https://doi.org/10.1002/qj.3803, 2020.

3198 Hickler, T., Smith, B., Prentice, I. C., Mjöfors, K., Miller, P., Arneth, A., and Sykes, M. T.: CO2 fertilization in
3199 temperate FACE experiments not representative of boreal and tropical forests, Glob. Change Biol., 14, 1531–1542,
3200 https://doi.org/10.1111/j.1365-2486.2008.01598.x, 2008.

3201 Hoesly, R., Smith, S. J., Ahsan, H., Prime, N., O'Rourke, P., Crippa, M., Klimont, Z., Guizzardi, D., Feng, L.,
3202 Harkins, C., MCDONALD, B., and Wang, S.: CEDS v_2025_03_18 Aggregate Data (v_2025_03_18) [Data set],
3203 Zenodo, https://doi.org/10.5281/ZENODO.15059443, 2025.

3204 Hollitzer, H. A. L., Patara, L., Terhaar, J., and Oschlies, A.: Competing effects of wind and buoyancy forcing on
3205 ocean oxygen trends in recent decades, Nat Commun, 15, 9264, https://doi.org/10.1038/s41467-024-53557-y,
3206 2024.

3207 Holzer, M., DeVries, T., and De Lavergne, C.: Diffusion controls the ventilation of a Pacific Shadow Zone above
3208 abyssal overturning, Nat Commun, 12, 4348, https://doi.org/10.1038/s41467-021-24648-x, 2021.

3209 Hong, C., Burney, J. A., Pongratz, J., Nabel, J. E. M. S., Mueller, N. D., Jackson, R. B., and Davis, S. J.: Global
3210 and regional drivers of land-use emissions in 1961–2017, Nature, 589, 554–561, https://doi.org/10.1038/s41586-
3211 020-03138-y, 2021.

3212 Hoppe, J., Hinder, B., Rafaty, R., Patt, A., and Grubb, M.: Three Decades of Climate Mitigation Policy: What Has
3213 It Delivered?, Annu. Rev. Environ. Resour., 48, 615–650, https://doi.org/10.1146/annurev-environ-112321-
3214 103821, 2023.

https://doi.org/10.5194/essd-2026-895
Preprint. Discussion started: 10 November 2026
© Author(s) 2026. CC BY 4.0 License.



3215 Houghton, R. A., House, J. I., Pongratz, J., van der Werf, G. R., DeFries, R. S., Hansen, M. C., Le Quéré, C., and
3216 Ramankutty, N.: Carbon emissions from land use and land-cover change, Biogeosciences, 9, 5125–5142,
3217 https://doi.org/10.5194/bg-9-5125-2012, 2012.

3218 Huang, B., Thorne, P. W., Banzon, V. F., Boyer, T., Chepurin, G., Lawrimore, J. H., Menne, M. J., Smith, T. M.,
3219 Vose, R. S., and Zhang, H.-M.: NOAA Extended Reconstructed Sea Surface Temperature (ERSST), Version 5,
3220 National Centers for Environmental Information [data set], https://doi.org/10.7289/V5T72FNM, 2017.

3221 Hubau, W., Lewis, S.L., Phillips, O.L., Affum-Baffoe, K., Beeckman, H., Cuní-Sanchez, A., Daniels, A.K.,
3222 Ewango, C.E.N., Fauset, S., Mukinzi, J.M., Sheil, D., Sonké, B., Sullivan, M.J.P., Sunderland, T.C.H., Taedoumg,
3223 H., Thomas, S.C., White, L.J.T., Abernethy, K.A., Adu-Bredu, S., Amani, C.A., Baker, T.R., Banin, L.F., Baya, F.,
3224 Begne, S.K., Bennett, A.C., Benedet, F., Bitariho, R., Bocko, Y.E., Boeckx, P., Boundja, P., Brienen, R.J.W.,
3225 Brncic, T., Chezeaux, E., Chuyong, G.B., Clark, C.J., Collins, M., Comiskey, J.A., Coomes, D.A., Dargie, G.C., de
3226 Haulleville, T., Kamdem, M.N.D., Doucet, J.-L., Esquivel-Muelbert, A., Feldpausch, T.R., Fofanah, A., Foli, E.G.,
3227 Gilpin, M., Gloor, E., Gonmadje, C., Gourlet-Fleury, S., Hall, J.S., Hamilton, A.C., Harris, D.J., Hart, T.B.,
3228 Hockemba, M.B.N., Hladik, A., Ifo, S.A., Jeffery, K.J., Jucker, T., Yakusu, E.K., Kearsley, E., Kenfack, D., Koch,
3229 A., Leal, M.E., Levesley, A., Lindsell, J.A., Lisingo, J., Lopez-Gonzalez, G., Lovett, J.C., Makana, J.-R., Malhi,
3230 Y., Marshall, A.R., Martin, J., Martin, E.H., Mbayu, F.M., Medjibe, V.P., Mihindou, V., Mitchard, E.T.A., Moore,
3231 S., Munishi, P.K.T., Bengone, N.N., Ojo, L., Ondo, F.E., Peh, K.S.-H., Pickavance, G.C., Poulsen, A.D., Poulsen,
3232 J.R., Qie, L., Reitsma, J., Rovero, F., Swaine, M.D., Talbot, J., Taplin, J., Taylor, D.M., Thomas, D.W., Toirambe,
3233 B., Mukendi, J.T., Tuagben, D., Umunay, P.M., van der Heijden, G.M.F., Verbeeck, H., Vleminckx, J., Willcock,
3234 S., Wöll, H., Woods, J.T., Zemagho, L.: Asynchronous carbon sink saturation in African and Amazonian tropical
3235 forests, Nature, 579, 80–87, https://doi.org/10.1038/s41586-020-2035-0, 2020.

3236 Huguenin, M. F., Holmes, R. M., and England, M. H.: Drivers and distribution of global ocean heat uptake over the
3237 last half century, Nat Commun, 13, 4921, https://doi.org/10.1038/s41467-022-32540-5, 2022.Humphrey, V.,
3238 Zscheischler, J., Ciais, P., Gudmundsson, L., Sitch, S., and Seneviratne, S. I.: Sensitivity of atmospheric CO2
3239 growth rate to observed changes in terrestrial water storage, Nature, 560, 628–631, https://doi.org/10.1038/s41586-
3240 018-0424-4, 2018.

3241 Humphrey, V., Berg, A., Ciais, P., Gentine, P., Jung, M., Reichstein, M., Seneviratne, S. I., and Frankenberg, C.:
3242 Soil moisture–atmosphere feedback dominates land carbon uptake variability, Nature, 592, 65–69,
3243 https://doi.org/10.1038/s41586-021-03325-5, 2021.

3244 Huntzinger, D. N., Michalak, A. M., Schwalm, C., Ciais, P., King, A. W., Fang, Y., Schaefer, K., Wei, Y., Cook,
3245 R. B., Fisher, J. B., Hayes, D., Huang, M., Ito, A., Jain, A. K., Lei, H., Lu, C., Maignan, F., Mao, J., Parazoo, N.,
3246 Peng, S., Poulter, B., Ricciuto, D., Shi, X., Tian, H., Wang, W., Zeng, N., and Zhao, F.: Uncertainty in the response
3247 of terrestrial carbon sink to environmental drivers undermines carbon-climate feedback predictions, Sci Rep, 7,
3248 4765, https://doi.org/10.1038/s41598-017-03818-2, 2017.

3249 Iida, Y., Takatani, Y., Kojima, A., and Ishii, M.: Global trends of ocean CO2 sink and ocean acidification: an
3250 observation-based reconstruction of surface ocean inorganic carbon variables, J Oceanogr, 77, 323–358,
3251 https://doi.org/10.1007/s10872-020-00571-5, 2021.

3252 Ilyina, T., Li, H., Spring, A., Müller, W. A., Bopp, L., Chikamoto, M. O., Danabasoglu, G., Dobrynin, M., Dunne,
3253 J., Fransner, F., Friedlingstein, P., Lee, W., Lovenduski, N. S., Merryfield, W. j., Mignot, J., Park, J. y., Séférian,
3254 R., Sospedra-Alfonso, R., Watanabe, M., and Yeager, S.: Predictable Variations of the Carbon Sinks and
3255 Atmospheric CO2 Growth in a Multi-Model Framework, Geophys. Res. Lett., 48, e2020GL090695,
3256 https://doi.org/10.1029/2020GL090695, 2021.

3257 IMF: International Monetary Fund: World Economic Outlook, available at: http://www.imf.org, last access: 30
3258 October 2026, 2026.

3259 Inoue, M., Morino, I., Uchino, O., Nakatsuru, T., Yoshida, Y., Yokota, T., Wunch, D., Wennberg, P. O., Roehl, C.
3260 M., Griffith, D. W. T., Velazco, V. A., Deutscher, N. M., Warneke, T., Notholt, J., Robinson, J., Sherlock, V.,
3261 Hase, F., Blumenstock, T., Rettinger, M., Sussmann, R., Kyrö, E., Kivi, R., Shiomi, K., Kawakami, S., De Mazière,
3262 M., Arnold, S. G., Feist, D. G., Barrow, E. A., Barney, J., Dubey, M., Schneider, M., Iraci, L. T., Podolske, J. R.,
3263 Hillyard, P. W., Machida, T., Sawa, Y., Tsuboi, K., Matsueda, H., Sweeney, C., Tans, P. P., Andrews, A. E.,
3264 Biraud, S. C., Fukuyama, Y., Pittman, J. V., Kort, E. A., and Tanaka, T.: Bias corrections of GOSAT SWIR
3265 XCO₂ and XCH₄ with TCCON data andtheir evaluation using
3266 aircraft measurement data, Atmos. Meas. Tech., 9, 3491–3512, https://doi.org/10.5194/amt-9-3491-2016, 2016.

https://doi.org/10.5194/essd-2026-895
Preprint. Discussion started: 10 November 2026
© Author(s) 2026. CC BY 4.0 License.



Ito, A.: Disequilibrium of terrestrial ecosystem CO2 budget caused by disturbance-induced emissions and non-CO2 carbon export flows: a global model assessment, Earth Syst. Dynam., 10, 685–709, https://doi.org/10.5194/esd-10-685-2019, 2019.

Ito, A. and Inatomi, M.: Use of a process-based model for assessing the methane budgets of global terrestrial ecosystems and evaluation of uncertainty, 9, 759–773, https://doi.org/10.5194/bg-9-759-2012, 2012.

Jackson, R. B., Canadell, J. G., Le Quéré, C., Andrew, R. M., Korsbakken, J. I., Peters, G. P., and Nakicenovic, N.: Reaching peak emissions, Nature Clim Change, 6, 7–10, https://doi.org/10.1038/nclimate2892, 2016.

Jackson, R. B., Le Quéré, C., Andrew, R. M., Canadell, J. G., Korsbakken, J. I., Liu, Z., Peters, G. P., and Zheng, B.: Global energy growth is outpacing decarbonization, Environ. Res. Lett., 13, 120401, https://doi.org/10.1088/1748-9326/aaf303, 2018.

Jackson, R. B., Friedlingstein, P., Andrew, R. M., Canadell, J. G., Le Quéré, C., and Peters, G. P.: Persistent fossil fuel growth threatens the Paris Agreement and planetary health, Environ. Res. Lett., 14, 121001, https://doi.org/10.1088/1748-9326/ab57b3, 2019.

Jackson, R. B., Friedlingstein, P., Quéré, C. L., Abernethy, S., Andrew, R. M., Canadell, J. G., Ciais, P., Davis, S. J., Deng, Z., Liu, Z., Korsbakken, J. I., and Peters, G. P.: Global fossil carbon emissions rebound near pre-COVID-19 levels, Environ. Res. Lett., 17, 031001, https://doi.org/10.1088/1748-9326/ac55b6, 2022.

Jacobson, A. R., Schuldt, K. N., Miller, J. B., Pera, A., Kaushik, A., Andrews, A., Basu, S., Triñanes, J., Landschützer, P., Mund, J., Weir, B., Ott, L., Aalto, T., Aaltonen, H., Abshire, J. B., Aikin, K., Allen, G., Andrade, M., Apadula, F., Arnold, S., Baier, B., Bakwin, P., Bartyzel, J., Bentz, G., Bergamaschi, P., Beyersdorf, A., Biermann, T., Biraud, S. C., Blanc, P.-E., Boenisch, H., Bowling, D., Brailsford, G., Brand, W. A., Brunner, D., Bui, T. P. V., Burban, B., Bäni, L., Calzolari, F., Chang, C. S., Chen, G., Chen, H., Chmura, L., St. Clair, J. M., Clark, S., Climadat, S., Della Coletta, J., Colomb, A., Commane, R., Condori, L., Conen, F., Conil, S., Couret, C., Cristofanelli, P., Cuevas, E., Curcoll, R., Daube, B., Davis, K. J., De Mazière, M., de Souza, R. A. F., De Wekker, S., Dean-Day, J. M., Delmotte, M., Di Iorio, T., di Sarra, A. G., Dickerson, R., DiGangi, E., DiGangi, J. P., Elsasser, M., Emmenegger, L., Fang, S., Fischer, M. L., Forster, G., France, J., Frumau, A., Fuente-Lastra, M., Galkowski, M., Gatti, L. V., Gehrlein, T., Gerbig, C., Gheusi, F., Gloor, E., Goto, D., Griffis, T., Hammer, S., Hanisco, T. F., Hanson, C., Hashimoto, S., Haszpra, L., Hatakka, J., Heimann, M., Heliasz, M., Heltai, D., Henne, S., Hensen, A., Hermans, C., Hermansen, O., Higgs, J., Hintsa, E., Hoheisel, A., Holst, J., Iraci, L. T., Ivakhov, V., Jaffe, D. A., Joly, L., Jordan, A., Joubert, W., Kang, H.-Y., Karion, A., Kawa, S. R., Kazan, V., Keeling, R. F., Ishijima, K., Keronen, P., Kim, J., Klausen, J., Kneuer, T., Ko, M.-Y., Kolari, P., Komínková, K., Kort, E., Kozlova, E., Krummel, P., Kubistin, D., Kulawik, S. S., Kumps, N., Labuschagne, C., Lam, D. H. Y., Lan, X., Langenfelds, R. L., Lanza, A., Larmanou, E., Laurent, O., Lauvaux, T., Lavric, J., Law, B. E., Lee, C.-H., Lee, J., Lehner, I., Lehtinen, K., Leppert, R., Leskinen, A., Leuenberger, M., Leung, W. H., Levin, I., Levula, J., Lin, J., Lindauer, M., Lindroth, A., Loh, Z., Lopez, M., Lueker, T. J., Luijkx, I. T., Lunder, C. R., Machida, T., Mammarella, I., Manca, G., Manning, A., Manning, A., Marek, M. V., Marklund, P., Marrero, J. E., Martin, D., Martin, M. Y., Martins, G. A., Matsueda, H., McAuliffe, A., McKain, K., Meijer, H., Meinhardt, F., Merchant, L., Metzger, J.-M., Mihalopoulos, N., Miles, N. L., Miller, C. E., Mitchell, L., Mölder, M., Müller-Williams, J., Monteiro, V., Montzka, S., Moossen, H., Moreno, C., Morgan, E., Morgui, J.-A., Morimoto, S., Mukai, H., Munger, J. W., Munro, D., Mutuku, M., Lund Myhre, C., Nakaoka, S.-I., Necki, J., Newberger, T., Newman, S., Nichol, S., Nisbet, E., Niwa, Y., Njiru, D. M., Noe, S. M., Nojiri, Y., Obersteiner, F., O'Doherty, S., Paplawsky, B., Parworth, C. L., Peischl, J., Peltola, O., Peters, W., Philippon, C., Piacentino, S., Pichon, J.-M., Pickers, P., Piper, S., Pitt, J., Plass-Dülmer, C., Platt, S. M., Prinzivalli, S., Ramonet, M., Ramos, R., Ren, X., Reyes-Sanchez, E., Richardson, S. J., Rigouleau, L.-J., Riris, H., Rivas, P. P., Rothe, M., Roulet, Y.-A., Ryerson, T., Ryoo, J.-M., Sargent, M., Sasakawa, M., Scheeren, B., Schmidt, M., Schuck, T., Schumacher, M., Seibel, J., Seifert, T., Sha, M. K., Shepson, P., Shin, D., Shook, M., Sloop, C. D., Smale, D., Spain, G., Stavert, A., Steger, D., Steinbacher, M., Stephens, B., Sweeney, C., Sørensen, L. L., Taipale, R., Takatsuji, S., Tans, P., Terao, Y., Thoning, K., Timas, H., Torn, M., Trisolino, P., Tørseth, K., Turnbull, J., van den Bulk, P., Vermeulen, A., Viner, B., Vitkova, G., Walker, S., Watson, A., Weiss, R., Weyrauch, D., Wofsy, S. C., Wolter, S., Worsey, J., Worthy, D., Xueref-Remy, I., Yates, E. L., Young, D., Yver-Kwok, C., Zaehle, S., Zahn, A., Zellweger, C., Zimnoch, M.: CarbonTracker CT2026 [Data set], NOAA, https://doi.org/10.25925/hqp0-rk68, 2026.

Jain, A. K., Meiyappan, P., Song, Y., and House, J. I.: CO2 emissions from land-use change affected more by nitrogen cycle, than by the choice of land-cover data, Global Change Biology, 19, 2893–2906, https://doi.org/10.1111/gcb.12207, 2013.

Janssens-Maenhout, G., Crippa, M., Guizzardi, D., Muntean, M., Schaaf, E., Dentener, F., Bergamaschi, P., Pagliari, V., Olivier, J. G. J., Peters, J. A. H. W., van Aardenne, J. A., Monni, S., Doering, U., Petrescu, A. M. R.,

https://doi.org/10.5194/essd-2026-895
Preprint. Discussion started: 10 November 2026
© Author(s) 2026. CC BY 4.0 License.



3322 Solazzo, E., and Oreggioni, G. D.: EDGAR v4.3.2 Global Atlas of the three major greenhouse gas emissions for
3323 the period 1970–2012, Earth Syst. Sci. Data, 11, 959–1002, https://doi.org/10.5194/essd-11-959-2019, 2019.

3324 Jiang, F., Wang, H., Chen, J. M., Ju, W., Tian, X., Feng, S., Li, G., Chen, Z., Zhang, S., Lu, X., Liu, J., Wang, H.,
3325 Wang, J., He, W., and Wu, M.: Regional CO2 fluxes from 2010 to 2015 inferred from GOSAT XCO2 retrievals
3326 using a new version of the Global Carbon Assimilation System, Atmospheric Chem. Phys., 21, 1963–1985,
3327 https://doi.org/10.5194/acp-21-1963-2021, 2021.

3328 Jin, Y., Keeling, R. F., Stephens, B. B., Long, M. C., Patra, P. K., Rödenbeck, C., Morgan, E. J., Kort, E. A., and
3329 Sweeney, C.: Improved atmospheric constraints on Southern Ocean CO 2 exchange. Proceedings of the National
3330 Academy of Sciences, 121(6), e2309333121, https://doi.org/10.1073/pnas.2309333121, 2024.

3331 Jin, Z., Wang, T., Zhang, H., Wang, Y., Ding, J., and Tian, X.: Constraint of satellite CO2 retrieval on the global
3332 carbon cycle from a Chinese atmospheric inversion system, Sci. China Earth Sci., 66, 609–618,
3333 https://doi.org/10.1007/s11430-022-1036-7, 2023.

3334 Joos, F. and Spahni, R.: Rates of change in natural and anthropogenic radiative forcing over the past 20,000 years,
3335 Proceedings of the National Academy of Sciences, 105, 1425–1430, https://doi.org/10.1073/pnas.0707386105,
3336 2008.

3337 Jones, M. W., Abatzoglou, J. T., Veraverbeke, S., Andela, N., Lasslop, G., Forkel, M., Smith, A. J. P., Burton, C.,
3338 Betts, R. A., van der Werf, G. R., Sitch, S., Canadell, J. G., Santín, C., Kolden, C., Doerr, S. H., and Le Quéré, C.:
3339 Global and Regional Trends and Drivers of Fire Under Climate Change, Rev. Geophys., 60, e2020RG000726,
3340 https://doi.org/10.1029/2020RG000726, 2022.

3341 Jones, M. W., Andrew, R. M., Peters, G. P., Janssens-Maenhout, G., De-Gol, A. J., Ciais, P., Patra, P. K.,
3342 Chevallier, F., and Le Quéré, C.: Gridded fossil CO2 emissions and related O2 combustion consistent with national
3343 inventories 1959–2018, Sci Data, 8, 2, https://doi.org/10.1038/s41597-020-00779-6, 2021.

3344 Jones, M. W., Andrew, R. M., Peters, G. P., Janssens-Maenhout, G., De-Gol, A. J., Dou, X., Liu, Z., Pickers, P.,
3345 Ciais, P., Patra, P. K., Chevallier, F., and Le Quéré, C.: Gridded fossil CO2 emissions and related O2 combustion
3346 consistent with national inventories, Zenodo [Data set], https://doi.org/10.5281/zenodo.17467681, 2025.

3347 Jones, M. W., Kelley, D. I., Burton, C. A., Di Giuseppe, F., Barbosa, M. L. F., Brambleby, E., Hartley, A. J.,
3348 Lombardi, A., Mataveli, G., McNorton, J. R., Spuler, F. R., Wessel, J. B., Abatzoglou, J. T., Anderson, L. O.,
3349 Andela, N., Archibald, S., Armenteras, D., Burke, E., Carmenta, R., Chuvieco, E., Clarke, H., Doerr, S. H.,
3350 Fernandes, P. M., Giglio, L., Hamilton, D. S., Hantson, S., Harris, S., Jain, P., Kolden, C. A., Kurvits, T., Lampe,
3351 S., Meier, S., New, S., Parrington, M., Perron, M. M. G., Qu, Y., Ribeiro, N. S., Saharjo, B. H., San-Miguel-Ayanz,
3352 J., Shuman, J. K., Tanpipat, V., van der Werf, G. R., Veraverbeke, S., and Xanthopoulos, G.: State of Wildfires
3353 2023–2024, Earth System Science Data, 16, 3601–3685, https://doi.org/10.5194/essd-16-3601-2024, 2024a.

3354 Jones, M.W., Veraverbeke, S., Andela, N., Doerr, S.H., Kolden, C., Mataveli, G., Pettinari, M.L., Le Quéré, C.,
3355 Rosan, T.M., van der Werf, G.R. and van Wees, D.: Global rise in forest fire emissions linked to climate change in
3356 the extratropics. Science, 386(6719), p.eadl5889, 2024b.

3357 Jung, M., Reichstein, M., Schwalm, C. R., Huntingford, C., Sitch, S., Ahlström, A., Arneth, A., Camps-Valls, G.,
3358 Ciais, P., Friedlingstein, P., Gans, F., Ichii, K., Jain, A. K., Kato, E., Papale, D., Poulter, B., Raduly, B.,
3359 Rödenbeck, C., Tramontana, G., Viovy, N., Wang, Y.-P., Weber, U., Zaehle, S., and Zeng, N.: Compensatory
3360 water effects link yearly global land CO2 sink changes to temperature, Nature, 541, 516–520,
3361 https://doi.org/10.1038/nature20780, 2017.

3362 Kaiser, J. W., Heil, A., Andreae, M. O., Benedetti, A., Chubarova, N., Jones, L., Morcrette, J.-J., Razinger, M.,
3363 Schultz, M. G., Suttie, M., and van der Werf, G. R.: Biomass burning emissions estimated with a global fire
3364 assimilation system based on observed fire radiative power, Biogeosciences, 9, 527–554,
3365 https://doi.org/10.5194/bg-9-527-2012, 2012.

3366 Kato, E., Kinoshita, T., Ito, A., Kawamiya, M., and Yamagata, Y.: Evaluation of spatially explicit emission
3367 scenario of land-use change and biomass burning using a process-based biogeochemical model, J. Land Use Sci., 8,
3368 104–122, https://doi.org/10.1080/1747423X.2011.628705, 2013.

3369 Keeley, J. E. and Pausas, J. G.: Distinguishing disturbance from perturbations in fire-prone ecosystems, Int. J.
3370 Wildland Fire, 28, 282–287, https://doi.org/10.1071/WF18203, 2019.

https://doi.org/10.5194/essd-2026-895
Preprint. Discussion started: 10 November 2026
© Author(s) 2026. CC BY 4.0 License.



3371 Keeling, C. D., Bacastow, R. B., Bainbridge, A. E., Ekdahl, C. A., Guenther, P. R., Waterman, L. S., and Chin, J.
3372 F. S.: Atmospheric carbon dioxide variations at Mauna Loa Observatory, Hawaii, Tellus A., 28, 538–551,
3373 https://doi.org/10.1111/j.2153-3490.1976.tb00701.x, 1976.

3374 Keeling R.F.: Development of an Interferometric Oxygen Analyzer for Precise Measurement of the Atmospheric
3375 O2 Mole Fraction, PhD thesis, Harvard University, Cambridge, Massachusetts, available at:
3376 https://bluemoon.ucsd.edu/publications/ralph/34_PhDthesis.pdf, last access: 30 October 2026, 1988.

3377 Keeling, R. F., Manning, A. C., Paplawsky, W. J., and Cox, A. C.: On the long-term stability of reference gases for
3378 atmospheric O2/N2 and CO2 measurements, Tellus B Chem. Phys. Meteorol., 59, 3–14,
3379 https://doi.org/10.1111/j.1600-0889.2006.00196.x, 2007.

3380 Keeling, R. F. and Manning, A. C.: 5.15 - Studies of Recent Changes in Atmospheric O2 Content, in: Treatise on
3381 Geochemistry (Second Edition), edited by: Holland, H. D. and Turekian, K. K., Elsevier, Oxford, 385–404,
3382 https://doi.org/10.1016/B978-0-08-095975-7.00420-4, 2014.

3383 Kelley, D. I., Burton, C., Di Giuseppe, F., Jones, M. W., Barbosa, M. L. F., Brambleby, E., McNorton, J. R., Liu,
3384 Z., Bradley, A. S. I., Blackford, K., Burke, E., Ciavarella, A., Di Tomaso, E., Eden, J., Ferreira, I. J. M., Fiedler, L.,
3385 Hartley, A. J., Keeping, T. R., Lampe, S., Lombardi, A., Mataveli, G., Qu, Y., Silva, P. S., Spuler, F. R.,
3386 Steinmann, C. B., Torres-Vázquez, M. Á., Veiga, R., Van Wees, D., Wessel, J. B., Wright, E., Bilbao, B.,
3387 Bourbonnais, M., Gao, C., Di Bella, C. M., Dintwe, K., Donovan, V. M., Harris, S., Kukavskaya, E. A., N'Dri, A.
3388 B., Santín, C., Selaya, G., Sjöström, J., Abatzoglou, J. T., Andela, N., Carmenta, R., Chuvieco, E., Giglio, L.,
3389 Hamilton, D. S., Hantson, S., Meier, S., Parrington, M., Sadegh, M., San-Miguel-Ayanz, J., Sedano, F., Turco, M.,
3390 Van Der Werf, G. R., Veraverbeke, S., Anderson, L. O., Clarke, H., Fernandes, P. M., and Kolden, C. A.: State of
3391 Wildfires 2024–2025, Earth Syst. Sci. Data, 17, 5377–5488, https://doi.org/10.5194/essd-17-5377-2025, 2025.

3392 Keppler, L. and Landschützer, P.: Regional Wind Variability Modulates the Southern Ocean Carbon Sink, Sci Rep,
3393 9, 7384, https://doi.org/10.1038/s41598-019-43826-y, 2019.

3394 Keppler, L., Landschützer, P., Lauvset, S. K., and Gruber, N.: Recent Trends and Variability in the Oceanic
3395 Storage of Dissolved Inorganic Carbon, Global Biogeochemical Cycles, 37, e2022GB007677,
3396 https://doi.org/10.1029/2022GB007677, 2023.

3397 Kharin, V. V., Boer, G. J., Merryfield, W. J., Scinocca, J. F., and Lee, W. -S.: Statistical adjustment of decadal
3398 predictions in a changing climate, Geophysical Research Letters, 39, 2012GL052647,
3399 https://doi.org/10.1029/2012GL052647, 2012.

3400 Khatiwala, S., Primeau, F., and Hall, T.: Reconstruction of the history of anthropogenic CO2 concentrations in the
3401 ocean, Nature, 462, 346–349, https://doi.org/10.1038/nature08526, 2009.

3402 Khatiwala, S., Tanhua, T., Mikaloff Fletcher, S., Gerber, M., Doney, S. C., Graven, H. D., Gruber, N., McKinley,
3403 G. A., Murata, A., Ríos, A. F., and Sabine, C. L.: Global ocean storage of anthropogenic carbon, Biogeosciences,
3404 10, 2169–2191, https://doi.org/10.5194/bg-10-2169-2013, 2013.

3405 Kong, Y., Zheng, B., Zhang, Q., and He, K.: Global and regional carbon budget for 2015–2020 inferred from
3406 OCO-2 based on an ensemble Kalman filter coupled with GEOS-Chem, Atmospheric Chem. Phys., 22, 10769–
3407 10788, https://doi.org/10.5194/acp-22-10769-2022, 2022.

3408 Kou-Giesbrecht, S. and Arora, V. K.: Representing the Dynamic Response of Vegetation to Nitrogen Limitation
3409 via Biological Nitrogen Fixation in the CLASSIC Land Model, Global Biogeochemical Cycles, 36,
3410 e2022GB007341, https://doi.org/10.1029/2022GB007341, 2022.

3411 Korsbakken, J. I., Peters, G. P., and Andrew, R. M.: Uncertainties around reductions in China's coal use and CO2
3412 emissions, Nature Clim Change, 6, 687–690, https://doi.org/10.1038/nclimate2963, 2016.

3413 Koven, C. D., Knox, R. G., Fisher, R. A., Chambers, J. Q., Christoffersen, B. O., Davies, S. J., Detto, M., Dietze,
3414 M. C., Faybishenko, B., Holm, J., Huang, M., Kovenock, M., Kueppers, L. M., Lemieux, G., Massoud, E.,
3415 McDowell, N. G., Muller-Landau, H. C., Needham, J. F., Norby, R. J., Powell, T., Rogers, A., Serbin, S. P.,
3416 Shuman, J. K., Swann, A. L. S., Varadharajan, C., Walker, A. P., Wright, S. J., and Xu, C.: Benchmarking and
3417 parameter sensitivity of physiological and vegetation dynamics using the Functionally Assembled Terrestrial
3418 Ecosystem Simulator (FATES) at Barro Colorado Island, Panama, Biogeosciences, 17, 3017–3044,
3419 https://doi.org/10.5194/bg-17-3017-2020, 2020.

https://doi.org/10.5194/essd-2026-895
Preprint. Discussion started: 10 November 2026
© Author(s) 2026. CC BY 4.0 License.



3420 Krol, M., Houweling, S., Bregman, B., van den Broek, M., Segers, A., van Velthoven, P., Peters, W., Dentener, F.,
3421 and Bergamaschi, P.: The two-way nested global chemistry-transport zoom model TM5: algorithm and
3422 applications, Atmospheric Chemistry and Physics, 5, 417–432, https://doi.org/10.5194/acp-5-417-2005, 2005.

3423 Kunimitsu, T. and Andrew, R. M.: Monthly-updated territorial fossil CO2 emissions estimates for Japan
3424 [Accepted], Earth System Science Data Discussions, https://doi.org/10.5194/essd-2026-417, 2026.

3425 Lacroix, F., Ilyina, T., and Hartmann, J.: Oceanic CO2 outgassing and biological production hotspots induced by
3426 pre-industrial river loads of nutrients and carbon in a global modeling approach, Biogeosciences, 17, 55–88,
3427 https://doi.org/10.5194/bg-17-55-2020, 2020.

3428 Lacroix, F., Ilyina, T., Mathis, M., Laruelle, G. G., and Regnier, P.: Historical increases in land-derived nutrient
3429 inputs may alleviate effects of a changing physical climate on the oceanic carbon cycle, Glob Change Biol, 27,
3430 5491–5513, https://doi.org/10.1111/gcb.15822, 2021.

3431 Lamboll, R. D., Nicholls, Z. R. J., Smith, C. J., Kikstra, J. S., Byers, E., and Rogelj, J.: Assessing the size and
3432 uncertainty of remaining carbon budgets, Nat. Clim. Change, https://doi.org/10.1038/s41558-023-01848-5, 2023.

3433 Lan, X., Tans, P. and Thoning, K.: NOAA Greenhouse Gas Marine Boundary Layer Reference - CO2 [Data set].
3434 NOAA Global Monitoring Laboratory, https://doi.org/10.15138/DVNP-F961, 2024.Lan, X., Tans, P. and K.W.
3435 Thoning: Trends in globally-averaged CO2 determined from NOAA Global Monitoring Laboratory measurements
3436 (Version 2026-09) [Data set], NOAA, https://doi.org/10.15138/9N0H-ZH07, 2026.

3437 Landschützer, P., Gruber, N., Haumann, F. A., Rödenbeck, C., Bakker, D. C. E., van Heuven, S., Hoppema, M.,
3438 Metzl, N., Sweeney, C., Takahashi, T., Tilbrook, B., and Wanninkhof, R.: The reinvigoration of the Southern
3439 Ocean carbon sink, Science, 349, 1221–1224, https://doi.org/10.1126/science.aab2620, 2015.

3440 Landschützer, P., Gruber, N., and Bakker, D. C. E.: Decadal variations and trends of the global ocean carbon sink:
3441 decadal air-sea CO2 flux variability, Global Biogeochem. Cycles, 30, 1396–1417,
3442 https://doi.org/10.1002/2015GB005359, 2016.

3443 Lapola, D. M., Pinho, P., Barlow, J., Aragão, L. E. O. C., Berenguer, E., Carmenta, R., Liddy, H. M., Seixas, H.,
3444 Silva, C. V. J., Silva-Junior, C. H. L., Alencar, A. A. C., Anderson, L. O., Armenteras, D., Brovkin, V., Calders,
3445 K., Chambers, J., Chini, L., Costa, M. H., Faria, B. L., Fearnside, P. M., Ferreira, J., Gatti, L., Gutierrez-Velez, V.
3446 H., Han, Z., Hibbard, K., Koven, C., Lawrence, P., Pongratz, J., Portela, B. T. T., Rounsevell, M., Ruane, A. C.,
3447 Schaldach, R., da Silva, S. S., von Randow, C., Walker, W. S.: The drivers and impacts of Amazon forest
3448 degradation. Science, 379(6630), p.eabp8622, https://doi.org/10.1126/science.abp8622, 2023.

3449 Law, R. M., Ziehn, T., Matear, R. J., Lenton, A., Chamberlain, M. A., Stevens, L. E., Wang, Y.-P., Srbinovsky, J.,
3450 Bi, D., Yan, H., and Vohralik, P. F.: The carbon cycle in the Australian Community Climate and Earth System
3451 Simulator (ACCESS-ESM1) – Part 1: Model description and pre-industrial simulation, Geosci. Model Dev., 10,
3452 2567–2590, https://doi.org/10.5194/gmd-10-2567-2017, 2017.

3453 Laughner, J. L., Roche, S., Kiel, M., Toon, G. C., Wunch, D., Baier, B. C., Biraud, S., Chen, H., Kivi, R.,
3454 Laemmel, T., McKain, K., Quéhé, P.-Y., Rousogenous, C., Stephens, B. B., Walker, K., and Wennberg, P. O.: A
3455 new algorithm to generate a priori trace gas profiles for the GGG2020 retrieval algorithm, Atmos. Meas. Tech., 16,
3456 1121–1146, https://doi.org/10.5194/amt-16-1121-2023, 2023.

3457 Lauvset, S. K., Lange, N., Tanhua, T., Bittig, H. C., Olsen, A., Kozyr, A., Álvarez, M., Azetsu-Scott, K., Brown, P.
3458 J., Carter, B. R., Cotrim Da Cunha, L., Hoppema, M., Humphreys, M. P., Ishii, M., Jeansson, E., Murata, A.,
3459 Müller, J. D., Pérez, F. F., Schirnick, C., Steinfeldt, R., Suzuki, T., Ulfsbo, A., Velo, A., Woosley, R. J., and Key,
3460 R. M.: The annual update GLODAPv2.2023: the global interior ocean biogeochemical data product, Earth Syst.
3461 Sci. Data, 16, 2047–2072, https://doi.org/10.5194/essd-16-2047-2024, 2024.

3462 Lawrence, D. M., Fisher, R. A., Koven, C. D., Oleson, K. W., Swenson, S. C., Bonan, G., Collier, N., Ghimire, B.,
3463 van Kampenhout, L., Kennedy, D., Kluzek, E., Lawrence, P. J., Li, F., Li, H., Lombardozzi, D., Riley, W. J.,
3464 Sacks, W. J., Shi, M., Vertenstein, M., Wieder, W. R., Xu, C., Ali, A. A., Badger, A. M., Bisht, G., van den
3465 Broeke, M., Brunke, M. A., Burns, S. P., Buzan, J., Clark, M., Craig, A., Dahlin, K., Drewniak, B., Fisher, J. B.,
3466 Flanner, M., Fox, A. M., Gentine, P., Hoffman, F., Keppel-Aleks, G., Knox, R., Kumar, S., Lenaerts, J., Leung, L.
3467 R., Lipscomb, W. H., Lu, Y., Pandey, A., Pelletier, J. D., Perket, J., Randerson, J. T., Ricciuto, D. M., Sanderson,
3468 B. M., Slater, A., Subin, Z. M., Tang, J., Thomas, R. Q., Val Martin, M., and Zeng, X.: The Community Land
3469 Model Version 5: Description of New Features, Benchmarking, and Impact of Forcing Uncertainty, J. Adv. Model
3470 Earth, Sy., 11, 4245–4287, https://doi.org/10.1029/2018MS001583, 2019.

https://doi.org/10.5194/essd-2026-895
Preprint. Discussion started: 10 November 2026
© Author(s) 2026. CC BY 4.0 License.



3471 Le Quéré, C., Rödenbeck, C., Buitenhuis, E. T., Conway, T. J., Langenfelds, R., Gomez, A., Labuschagne, C.,
3472 Ramonet, M., Nakazawa, T., Metzl, N., Gillett, N., and Heimann, M.: Saturation of the Southern Ocean CO2 Sink
3473 Due to Recent Climate Change, Science, 316, 1735–1738, https://doi.org/10.1126/science.1136188, 2007.

3474 Le Quéré, C., Raupach, M. R., Canadell, J. G., Marland, G., Bopp, L., Ciais, P., Conway, T. J., Doney, S. C., Feely,
3475 R. A., Foster, P., Friedlingstein, P., Gurney, K., Houghton, R. A., House, J. I., Huntingford, C., Levy, P. E., Lomas,
3476 M. R., Majkut, J., Metzl, N., Ometto, J. P., Peters, G. P., Prentice, I. C., Randerson, J. T., Running, S. W.,
3477 Sarmiento, J. L., Schuster, U., Sitch, S., Takahashi, T., Viovy, N., van der Werf, G. R., and Woodward, F. I.:
3478 Trends in the sources and sinks of carbon dioxide, Nature Geosci, 2, 831–836, https://doi.org/10.1038/ngeo689,
3479 2009.

3480 Le Quéré, C., Takahashi, T., Buitenhuis, E. T., Rödenbeck, C., and Sutherland, S. C.: Impact of climate change and
3481 variability on the global oceanic sink of CO2, Global Biogeochemical Cycles, 24,
3482 https://doi.org/10.1029/2009GB003599, 2010.

3483 Le Quéré, C., Andres, R. J., Boden, T., Conway, T., Houghton, R. A., House, J. I., Marland, G., Peters, G. P., van
3484 der Werf, G. R., Ahlström, A., Andrew, R. M., Bopp, L., Canadell, J. G., Ciais, P., Doney, S. C., Enright, C.,
3485 Friedlingstein, P., Huntingford, C., Jain, A. K., Jourdain, C., Kato, E., Keeling, R. F., Klein Goldewijk, K., Levis,
3486 S., Levy, P., Lomas, M., Poulter, B., Raupach, M. R., Schwinger, J., Sitch, S., Stocker, B. D., Viovy, N., Zaehle,
3487 S., and Zeng, N.: The global carbon budget 1959–2011, Earth Syst. Sci. Data, 5, 165–185,
3488 https://doi.org/10.5194/essd-5-165-2013, 2013.

3489 Le Quéré, C., Peters, G. P., Andres, R. J., Andrew, R. M., Boden, T. A., Ciais, P., Friedlingstein, P., Houghton, R.
3490 A., Marland, G., Moriarty, R., Sitch, S., Tans, P., Arneth, A., Arvanitis, A., Bakker, D. C. E., Bopp, L., Canadell, J.
3491 G., Chini, L. P., Doney, S. C., Harper, A., Harris, I., House, J. I., Jain, A. K., Jones, S. D., Kato, E., Keeling, R. F.,
3492 Klein Goldewijk, K., Körtzinger, A., Koven, C., Lefèvre, N., Maignan, F., Omar, A., Ono, T., Park, G.-H., Pfeil,
3493 B., Poulter, B., Raupach, M. R., Regnier, P., Rödenbeck, C., Saito, S., Schwinger, J., Segschneider, J., Stocker, B.
3494 D., Takahashi, T., Tilbrook, B., van Heuven, S., Viovy, N., Wanninkhof, R., Wiltshire, A., and Zaehle, S.: Global
3495 carbon budget 2013, Earth Syst. Sci. Data, 6, 235–263, https://doi.org/10.5194/essd-6-235-2014, 2014.

3496 Le Quéré, C., Moriarty, R., Andrew, R. M., Peters, G. P., Ciais, P., Friedlingstein, P., Jones, S. D., Sitch, S., Tans,
3497 P., Arneth, A., Boden, T. A., Bopp, L., Bozec, Y., Canadell, J. G., Chini, L. P., Chevallier, F., Cosca, C. E., Harris,
3498 I., Hoppema, M., Houghton, R. A., House, J. I., Jain, A. K., Johannessen, T., Kato, E., Keeling, R. F., Kitidis, V.,
3499 Klein Goldewijk, K., Koven, C., Landa, C. S., Landschützer, P., Lenton, A., Lima, I. D., Marland, G., Mathis, J. T.,
3500 Metzl, N., Nojiri, Y., Olsen, A., Ono, T., Peng, S., Peters, W., Pfeil, B., Poulter, B., Raupach, M. R., Regnier, P.,
3501 Rödenbeck, C., Saito, S., Salisbury, J. E., Schuster, U., Schwinger, J., Séférian, R., Segschneider, J., Steinhoff, T.,
3502 Stocker, B. D., Sutton, A. J., Takahashi, T., Tilbrook, B., van der Werf, G. R., Viovy, N., Wang, Y.-P.,
3503 Wanninkhof, R., Wiltshire, A., and Zeng, N.: Global carbon budget 2014, Earth Syst. Sci. Data, 7, 47–85,
3504 https://doi.org/10.5194/essd-7-47-2015, 2015a.

3505 Le Quéré, C., Moriarty, R., Andrew, R. M., Canadell, J. G., Sitch, S., Korsbakken, J. I., Friedlingstein, P., Peters,
3506 G. P., Andres, R. J., Boden, T. A., Houghton, R. A., House, J. I., Keeling, R. F., Tans, P., Arneth, A., Bakker, D. C.
3507 E., Barbero, L., Bopp, L., Chang, J., Chevallier, F., Chini, L. P., Ciais, P., Fader, M., Feely, R. A., Gkritzalis, T.,
3508 Harris, I., Hauck, J., Ilyina, T., Jain, A. K., Kato, E., Kitidis, V., Klein Goldewijk, K., Koven, C., Landschützer, P.,
3509 Lauvset, S. K., Lefèvre, N., Lenton, A., Lima, I. D., Metzl, N., Millero, F., Munro, D. R., Murata, A., Nabel, J. E.
3510 M. S., Nakaoka, S., Nojiri, Y., O'Brien, K., Olsen, A., Ono, T., Pérez, F. F., Pfeil, B., Pierrot, D., Poulter, B.,
3511 Rehder, G., Rödenbeck, C., Saito, S., Schuster, U., Schwinger, J., Séférian, R., Steinhoff, T., Stocker, B. D.,
3512 Sutton, A. J., Takahashi, T., Tilbrook, B., van der Laan-Luijkx, I. T., van der Werf, G. R., van Heuven, S.,
3513 Vandemark, D., Viovy, N., Wiltshire, A., Zaehle, S., and Zeng, N.: Global Carbon Budget 2015, Earth Syst. Sci.
3514 Data, 7, 349–396, https://doi.org/10.5194/essd-7-349-2015, 2015b.

3515 Le Quéré, C., Andrew, R. M., Canadell, J. G., Sitch, S., Korsbakken, J. I., Peters, G. P., Manning, A. C., Boden, T.
3516 A., Tans, P. P., Houghton, R. A., Keeling, R. F., Alin, S., Andrews, O. D., Anthoni, P., Barbero, L., Bopp, L.,
3517 Chevallier, F., Chini, L. P., Ciais, P., Currie, K., Delire, C., Doney, S. C., Friedlingstein, P., Gkritzalis, T., Harris,
3518 I., Hauck, J., Haverd, V., Hoppema, M., Klein Goldewijk, K., Jain, A. K., Kato, E., Körtzinger, A., Landschützer,
3519 P., Lefèvre, N., Lenton, A., Lienert, S., Lombardozzi, D., Melton, J. R., Metzl, N., Millero, F., Monteiro, P. M. S.,
3520 Munro, D. R., Nabel, J. E. M. S., Nakaoka, S., O'Brien, K., Olsen, A., Omar, A. M., Ono, T., Pierrot, D., Poulter,
3521 B., Rödenbeck, C., Salisbury, J., Schuster, U., Schwinger, J., Séférian, R., Skjelvan, I., Stocker, B. D., Sutton, A. J.,
3522 Takahashi, T., Tian, H., Tilbrook, B., van der Laan-Luijkx, I. T., van der Werf, G. R., Viovy, N., Walker, A. P.,
3523 Wiltshire, A. J., and Zaehle, S.: Global Carbon Budget 2016, Earth Syst. Sci. Data, 8, 605–649,
3524 https://doi.org/10.5194/essd-8-605-2016, 2016.

3525 Le Quéré, C., Andrew, R. M., Friedlingstein, P., Sitch, S., Pongratz, J., Manning, A. C., Korsbakken, J. I., Peters,
3526 G. P., Canadell, J. G., Jackson, R. B., Boden, T. A., Tans, P. P., Andrews, O. D., Arora, V. K., Bakker, D. C. E.,

https://doi.org/10.5194/essd-2026-895
Preprint. Discussion started: 10 November 2026
© Author(s) 2026. CC BY 4.0 License.



3527 Barbero, L., Becker, M., Betts, R. A., Bopp, L., Chevallier, F., Chini, L. P., Ciais, P., Cosca, C. E., Cross, J.,
3528 Currie, K., Gasser, T., Harris, I., Hauck, J., Haverd, V., Houghton, R. A., Hunt, C. W., Hurtt, G., Ilyina, T., Jain, A.
3529 K., Kato, E., Kautz, M., Keeling, R. F., Klein Goldewijk, K., Körtzinger, A., Landschützer, P., Lefèvre, N., Lenton,
3530 A., Lienert, S., Lima, I., Lombardozzi, D., Metzl, N., Millero, F., Monteiro, P. M. S., Munro, D. R., Nabel, J. E. M.
3531 S., Nakaoka, S., Nojiri, Y., Padin, X. A., Peregon, A., Pfeil, B., Pierrot, D., Poulter, B., Rehder, G., Reimer, J.,
3532 Rödenbeck, C., Schwinger, J., Séférian, R., Skjelvan, I., Stocker, B. D., Tian, H., Tilbrook, B., Tubiello, F. N., van
3533 der Laan-Luijkx, I. T., van der Werf, G. R., van Heuven, S., Viovy, N., Vuichard, N., Walker, A. P., Watson, A. J.,
3534 Wiltshire, A. J., Zaehle, S., and Zhu, D.: Global Carbon Budget 2017, Earth Syst. Sci. Data, 10, 405–448,
3535 https://doi.org/10.5194/essd-10-405-2018, 2018a.

3536 Le Quéré, C., Andrew, R. M., Friedlingstein, P., Sitch, S., Hauck, J., Pongratz, J., Pickers, P. A., Korsbakken, J. I.,
3537 Peters, G. P., Canadell, J. G., Arneth, A., Arora, V. K., Barbero, L., Bastos, A., Bopp, L., Chevallier, F., Chini, L.
3538 P., Ciais, P., Doney, S. C., Gkritzalis, T., Goll, D. S., Harris, I., Haverd, V., Hoffman, F. M., Hoppema, M.,
3539 Houghton, R. A., Hurtt, G., Ilyina, T., Jain, A. K., Johannessen, T., Jones, C. D., Kato, E., Keeling, R. F., Klein
3540 Goldewijk, K., Landschützer, P., Lefèvre, N., Lienert, S., Liu, Z., Lombardozzi, D., Metzl, N., Munro, D. R.,
3541 Nabel, J. E. M. S., Nakaoka, S., Neill, C., Olsen, A., Ono, T., Patra, P., Peregon, A., Peters, W., Peylin, P., Pfeil,
3542 B., Pierrot, D., Poulter, B., Rehder, G., Resplandy, L., Robertson, E., Rocher, M., Rödenbeck, C., Schuster, U.,
3543 Schwinger, J., Séférian, R., Skjelvan, I., Steinhoff, T., Sutton, A., Tans, P. P., Tian, H., Tilbrook, B., Tubiello, F.
3544 N., van der Laan-Luijkx, I. T., van der Werf, G. R., Viovy, N., Walker, A. P., Wiltshire, A. J., Wright, R., Zaehle,
3545 S., and Zheng, B.: Global Carbon Budget 2018, Earth Syst. Sci. Data, 10, 2141–2194, https://doi.org/10.5194/essd-
3546 10-2141-2018, 2018b.

3547 Le Quéré, C., Korsbakken, J. I., Wilson, C., Tosun, J., Andrew, R., Andres, R. J., Canadell, J. G., Jordan, A.,
3548 Peters, G. P., and van Vuuren, D. P.: Drivers of declining CO2 emissions in 18 developed economies, Nat. Clim.
3549 Chang., 9, 213–217, https://doi.org/10.1038/s41558-019-0419-7, 2019.

3550 Le Quéré, C., Peters, G. P., Friedlingstein, P., Andrew, R. M., Canadell, J. G., Davis, S. J., Jackson, R. B., and
3551 Jones, M. W.: Fossil CO2 emissions in the post-COVID-19 era, Nat. Clim. Chang., 11, 197–199,
3552 https://doi.org/10.1038/s41558-021-01001-0, 2021.

3553 Le Quéré, C., Andrew, R.M., Candela, J.G., Friedlingstein, P, Jackson, R.B, & Peters, G.P.: A further acceleration
3554 of clean energy is needed for global CO_2 emissions to peak and decline. *Nature Climate Change*
3555 https://dx.doi.org/10.1038/s41558-026-02821-8, 2026.

3556 Levitus, S., Antonov, J. I., Boyer, T. P., Baranova, O. K., Garcia, H. E., Locarnini, R. A., Mishonov, A. V.,
3557 Reagan, J. R., Seidov, D., Yarosh, E. S., and Zweng, M. M.: World ocean heat content and thermosteric sea level
3558 change (0–2000 m), 1955–2010, Geophys. Res. Lett., 39, https://doi.org/10.1029/2012GL051106, 2012.

3559 Li, H., Ilyina, T., Müller, W. A., and Sienz, F.: Decadal predictions of the North Atlantic CO2 uptake, Nat.
3560 Commun., 7, 11076, https://doi.org/10.1038/ncomms11076, 2016.

3561 Li, H., Ilyina, T., Müller, W. A., and Landschützer, P.: Predicting the variable ocean carbon sink, Sci. Adv., 5,
3562 eaav6471, https://doi.org/10.1126/sciadv.aav6471, 2019.

3563 Li, H., Ilyina, T., Loughran, T., Spring, A., and Pongratz, J.: Reconstructions and predictions of the global carbon
3564 budget with an emission-driven Earth system model, Earth Syst. Dyn., 14, 101–119, https://doi.org/10.5194/esd-
3565 14-101-2023, 2023.

3566 Li, W., Ciais, P., Peng, S., Yue, C., Wang, Y., Thurner, M., Saatchi, S. S., Arneth, A., Avitabile, V., Carvalhais, N.,
3567 Harper, A. B., Kato, E., Koven, C., Liu, Y. Y., Nabel, J. E. M. S., Pan, Y., Pongratz, J., Poulter, B., Pugh, T. A. M.,
3568 Santoro, M., Sitch, S., Stocker, B. D., Viovy, N., Wiltshire, A., Yousefpour, R., and Zaehle, S.: Land-use and land-
3569 cover change carbon emissions between 1901 and 2012 constrained by biomass observations, Biogeosciences, 14,
3570 5053–5067, https://doi.org/10.5194/bg-14-5053-2017, 2017.

3571 Li, H., Ilyina, T., Dunkl, I., Brune, S., Müller, W. A., Bernardello, R., Bethke, I., Bopp, L., Fransner, F.,
3572 Friedlingstein, P., Lapin, V., Merryfield, W. J., Mignot, J., O'Sullivan, M., Sospedra-Alfonso, R., Swingedouw, D.,
3573 Tatebe, H., Tjiputra, J., Torres, O., and Tourigny, E.: Multimodel Reconstructions and Predictions of the CO2
3574 Fluxes and Atmospheric CO2 Variations, Bulletin of the American Meteorological Society, 107, E1352–E1369,
3575 https://doi.org/10.1175/BAMS-D-25-0139.1, 2026.

3576 Lienert, S. and Joos, F.: A Bayesian ensemble data assimilation to constrain model parameters and land-use carbon
3577 emissions, Biogeosciences, 15, 2909–2930, https://doi.org/10.5194/bg-15-2909-2018, 2018.

https://doi.org/10.5194/essd-2026-895
Preprint. Discussion started: 10 November 2026
© Author(s) 2026. CC BY 4.0 License.



3578 Liu, J., Baskaran, L., Bowman, K., Schimel, D., Bloom, A. A., Parazoo, N. C., Oda, T., Carroll, D., Menemenlis,
3579 D., Joiner, J., Commane, R., Daube, B., Gatti, L. V., McKain, K., Miller, J., Stephens, B. B., Sweeney, C., and
3580 Wofsy, S.: Carbon Monitoring System Flux Net Biosphere Exchange 2020 (CMS-Flux NBE 2020), 13, 299–330,
3581 https://doi.org/10.5194/essd-13-299-2021, 2021.

3582 Liu, Z., Guan, D., Wei, W., Davis, S. J., Ciais, P., Bai, J., Peng, S., Zhang, Q., Hubacek, K., Marland, G., Andres,
3583 R. J., Crawford-Brown, D., Lin, J., Zhao, H., Hong, C., Boden, T. A., Feng, K., Peters, G. P., Xi, F., Liu, J., Li, Y.,
3584 Zhao, Y., Zeng, N., and He, K.: Reduced carbon emission estimates from fossil fuel combustion and cement
3585 production in China, Nature, 524, 335–338, https://doi.org/10.1038/nature14677, 2015.

3586 Liu, Z., Zeng, N., Liu, Y., Kalnay, E., Asrar, G., Wu, B., Cai, Q., Liu, D., and Han, P.: Improving the joint
3587 estimation of CO2 and surface carbon fluxes using a constrained ensemble Kalman filter in COLA (v1.0), Geosci.
3588 Model Dev., 15, 5511–5528, https://doi.org/10.5194/gmd-15-5511-2022, 2022.

3589 Liu, Z., Ciais, P., Deng, Z., Lei, R., Davis, S. J., Feng, S., Zheng, B., Cui, D., Dou, X., Zhu, B., Guo, R., Ke, P.,
3590 Sun, T., Lu, C., He, P., Wang, Y., Yue, X., Wang, Y., Lei, Y., Zhou, H., Cai, Z., Wu, Y., Guo, R., Han, T., Xue, J.,
3591 Boucher, O., Boucher, E., Chevallier, F., Tanaka, K., Wei, Y., Zhong, H., Kang, C., Zhang, N., Chen, B., Xi, F.,
3592 Liu, M., Bréon, F.-M., Lu, Y., Zhang, Q., Guan, D., Gong, P., Kammen, D. M., He, K., and Schellnhuber, H. J.:
3593 Near-real-time monitoring of global CO2 emissions reveals the effects of the COVID-19 pandemic, Nat Commun,
3594 11, 5172, https://doi.org/10.1038/s41467-020-18922-7, 2020a.

3595 Liu, Z., Ciais, P., Deng, Z., Davis, S. J., Zheng, B., Wang, Y., Cui, D., Zhu, B., Dou, X., Ke, P., Sun, T., Guo, R.,
3596 Zhong, H., Boucher, O., Bréon, F.-M., Lu, C., Guo, R., Xue, J., Boucher, E., Tanaka, K., and Chevallier, F.:
3597 Carbon Monitor, a near-real-time daily dataset of global CO2 emission from fossil fuel and cement production, Sci
3598 Data, 7, 392, https://doi.org/10.1038/s41597-020-00708-7, 2020b.

3599 Lovenduski, N. S., Bonan, G. B., Yeager, S. G., Lindsay, K., and Lombardozzi, D. L.: High predictability of
3600 terrestrial carbon fluxes from an initialized decadal prediction system, Environ. Res. Lett., 14, 124074,
3601 https://doi.org/10.1088/1748-9326/ab5c55, 2019a.

3602 Lovenduski, N. S., Yeager, S. G., Lindsay, K., and Long, M. C.: Predicting near-term variability in ocean carbon
3603 uptake, Earth Syst. Dyn., 10, 45–57, https://doi.org/10.5194/esd-10-45-2019, 2019b.

3604 Lutz, F., Herzfeld, T., Heinke, J., Rolinski, S., Schaphoff, S., von Bloh, W., Stoorvogel, J. J., and Müller, C.:
3605 Simulating the effect of tillage practices with the global ecosystem model LPJmL (version 5.0-tillage), Geosci.
3606 Model Dev., 12, 2419–2440, https://doi.org/10.5194/gmd-12-2419-2019, 2019.

3607 Ma, L., Hurtt, G., Ott, L., Sahajpal, R., Fisk, J., Lamb, R., Tang, H., Flanagan, S., Chini, L., Chatterjee, A., and
3608 Sullivan, J.: Global evaluation of the Ecosystem Demography model (ED v3.0), Geosci. Model Dev., 15, 1971–
3609 1994, https://doi.org/10.5194/gmd-15-1971-2022, 2022.

3610 Ma, L., Hurtt, G., Tang, H., Hao, D., Ciais, P., Pan, Y., Sitch, S., Friedlingstein, P., Dubayah, R., Nunes, M. H.,
3611 and Wei, X.: Widespread carbon accumulation in mature forests remains underestimated by satellite observations,
3612 Nat Ecol Evol, 10, 1864–1872, https://doi.org/10.1038/s41559-026-03151-w, 2026.

3613 Madec, G., Bell, M., Blaker, A., Bricaud, C., Bruciaferri, D., Castrillo, M., Calvert, D., Chanut, J., Clementi, E.,
3614 Coward, A., Epicoco, I., Éthé, C., Ganderton, J., Harle, J., Hutchinson, K., Iovino, D., Lea, D., Lovato, T., Martin,
3615 M., Martin, N., Mele, F., Martins, D., Masson, S., Mathiot, P., Mele, F., Mocavero, S., Müller, S., Nurser, A. J. G.,
3616 Paronuzzi, S., Peltier, M., Person, R., Rousset, C., Rynders, S., Samson, G., Téchené, S., Vancoppenolle, M.,
3617 Wilson, C. (2023). NEMO Ocean Engine Reference Manual. In Scientific Notes of IPSL Climate Modelling Center
3618 (Version v4.2). Zenodo. https://doi.org/10.5281/zenodo.8167700, 2023.Magi, B. I., Rabin, S., Shevliakova, E., and
3619 Pacala, S.: Separating agricultural and non-agricultural fire seasonality at regional scales, Biogeosciences, 9, 3003–
3620 3012, https://doi.org/10.5194/bg-9-3003-2012, 2012.

3621 Maity, S., Niwa, Y., Saeki, T., Someya, Y., and Yoshida, Y.: Drivers of 2023–2024 Atmospheric CO2 Growth:
3622 Role of Northern Mid-to-High Latitude Land Carbon Cycle, Geophysical Research Letters, 53, e2026GL122221,
3623 https://doi.org/10.1029/2026GL122221, 2026.

3624 Maksyutov, S., Oda, T., Saito, M., Janardanan, R., Belikov, D., Kaiser, J. W., Zhuravlev, R., Ganshin, A., Valsala,
3625 V. K., Andrews, A., Chmura, L., Dlugokencky, E., Haszpra, L., Langenfelds, R. L., Machida, T., Nakazawa, T.,
3626 Ramonet, M., Sweeney, C., and Worthy, D.: Technical note: A high-resolution inverse modelling technique for
3627 estimating surface CO2 fluxes based on the NIES-TM–FLEXPART coupled transport model and its adjoint,
3628 Atmos. Chem. Phys., 21, 1245–1266, https://doi.org/10.5194/acp-21-1245-2021, 2021.

https://doi.org/10.5194/essd-2026-895
Preprint. Discussion started: 10 November 2026
© Author(s) 2026. CC BY 4.0 License.



3629 Masarie, K. A. and Tans, P. P.: Extension and integration of atmospheric carbon dioxide data into a globally
3630 consistent measurement record, J. Geophys. Res., 100, 11593, https://doi.org/10.1029/95JD00859, 1995.

3631 Mather, A. S.: The transition from deforestation to reforestation in Europe, in: Agricultural technologies and
3632 tropical deforestation (eds. Angelsen, A.; Kaimowitz, D.), CABI in association with centre for international
3633 Forestry Research, 35–52, 2001.

3634 Matsumoto, K., Sarmiento, J. L., Key, R. M., Aumont, O., Bullister, J. L., Caldeira, K., Campin, J. -M., Doney, S.
3635 C., Drange, H., Dutay, J. -C., Follows, M., Gao, Y., Gnanadesikan, A., Gruber, N., Ishida, A., Joos, F., Lindsay, K.,
3636 Maier-Reimer, E., Marshall, J. C., Matear, R. J., Monfray, P., Mouchet, A., Najjar, R., Plattner, G. -K., Schlitzer,
3637 R., Slater, R., Swathi, P. S., Totterdell, I. J., Weirig, M. -F., Yamanaka, Y., Yool, A., and Orr, J. C.: Evaluation of
3638 ocean carbon cycle models with data-based metrics, Geophysical Research Letters, 31, 2003GL018970,
3639 https://doi.org/10.1029/2003GL018970, 2004.

3640 Mauritsen, T., Bader, J., Becker, T., Behrens, J., Bittner, M., Brokopf, R., Brovkin, V., Claussen, M., Crueger, T.,
3641 Esch, M., Fast, I., Fiedler, S., Fläschner, D., Gayler, V., Giorgetta, M., Goll, D. S., Haak, H., Hagemann, S.,
3642 Hedemann, C., Hohenegger, C., Ilyina, T., Jahns, T., Jimenéz-de-la-Cuesta, D., Jungclaus, J., Kleinen, T., Kloster,
3643 S., Kracher, D., Kinne, S., Kleberg, D., Lasslop, G., Kornblueh, L., Marotzke, J., Matei, D., Meraner, K.,
3644 Mikolajewicz, U., Modali, K., Möbis, B., Müller, W. A., Nabel, J. E. M. S., Nam, C. C. W., Notz, D., Nyawira, S.-
3645 S., Paulsen, H., Peters, K., Pincus, R., Pohlmann, H., Pongratz, J., Popp, M., Raddatz, T. J., Rast, S., Redler, R.,
3646 Reick, C. H., Rohrschneider, T., Schemann, V., Schmidt, H., Schnur, R., Schulzweida, U., Six, K. D., Stein, L.,
3647 Stemmler, I., Stevens, B., von Storch, J.-S., Tian, F., Voigt, A., Vrese, P., Wieners, K.-H., Wilkenskjeld, S.,
3648 Winkler, A., and Roeckner, E.: Developments in the MPI-M Earth System Model version 1.2 (MPI-ESM1.2) and
3649 Its Response to Increasing CO2, J. Adv. Model Earth Sy., 11, 998–1038, https://doi.org/10.1029/2018MS001400,
3650 2019.

3651 Mayot, N., Buitenhuis, E. T., Wright, R. M., Hauck, J., Bakker, D. C. E., and Le Quéré, C.: Constraining the trend
3652 in the ocean CO2 sink during 2000–2022. Nat Commun 15, 8429, https://doi.org/10.1038/s41467-024-52641-7,
3653 2024.

3654 McGrath, M. J., Luyssaert, S., Meyfroidt, P., Kaplan, J. O., Bürgi, M., Chen, Y., Erb, K., Gimmi, U., McInerney,
3655 D., Naudts, K., Otto, J., Pasztor, F., Ryder, J., Schelhaas, M.-J., and Valade, A.: Reconstructing European forest
3656 management from 1600 to 2010, 12, 4291–4316, https://doi.org/10.5194/bg-12-4291-2015, 2015.

3657 McGuire, A. D., Sitch, S., Clein, J. S., Dargaville, R., Esser, G., Foley, J., Heimann, M., Joos, F., Kaplan, J.,
3658 Kicklighter, D. W., Meier, R. A., Melillo, J. M., Moore, B., Prentice, I. C., Ramankutty, N., Reichenau, T., Schloss,
3659 A., Tian, H., Williams, L. J., and Wittenberg, U.: Carbon balance of the terrestrial biosphere in the Twentieth
3660 Century: Analyses of CO2 , climate and land use effects with four process-based ecosystem models, Global
3661 Biogeochemical Cycles, 15, 183–206, https://doi.org/10.1029/2000GB001298, 2001.

3662 McKinley, G. A., Fay, A. R., Eddebbar, Y. A., Gloege, L., and Lovenduski, N. S.: External Forcing Explains
3663 Recent Decadal Variability of the Ocean Carbon Sink, AGU Advances, 1, e2019AV000149,
3664 https://doi.org/10.1029/2019AV000149, 2020.

3665 McKinley, G. A., Fay, A. R., Lovenduski, N. S., and Pilcher, D. J.: Natural Variability and Anthropogenic Trends
3666 in the Ocean Carbon Sink, Annu. Rev. Mar. Sci., 9, 125–150, https://doi.org/10.1146/annurev-marine-010816-
3667 060529, 2017.

3668 McKinley, G. A., Fay, A., Heimdal, T. H., Moseley, L., and Shaum, A.: How well do global ocean approaches
3669 constrain local fCO2?, Environ. Res. Lett., 21, 134011, https://doi.org/10.1088/1748-9326/ae803e, 2026.

3670 Meiyappan, P., Jain, A. K., and House, J. I.: Increased influence of nitrogen limitation on CO 2 emissions from
3671 future land use and land use change, Global Biogeochem. Cycles, 29, 1524–1548,
3672 https://doi.org/10.1002/2015GB005086, 2015.

3673 Melo, J., Rossi, S., Achard, F., Alkama, R., Canadell, J. G., Federici, S., Friedlingstein, P., Gibbs, D., Harris, N.,
3674 Heinrich, V., O'Sullivan, M., Peters, G., Pongratz, J., Rose, M., Roman-Cuesta, R., Sanz Sanchez, M. J.,
3675 Schwingshackl, C., Sitch, S., and Grassi, G.: The LULUCF Data Hub: translating global land use emissions
3676 estimates into the national GHG inventory framework (Version 4.0.0, 2026 NGHGI release) (4.0.0) [Dataset],
3677 Zenodo. https://doi.org/10.5281/ZENODO.17140775, 2026.

3678 Melton, J. R., Arora, V. K., Wisernig-Cojoc, E., Seiler, C., Fortier, M., Chan, E., and Teckentrup, L.: CLASSIC
3679 v1.0: the open-source community successor to the Canadian Land Surface Scheme (CLASS) and the Canadian
3680 Terrestrial Ecosystem Model (CTEM) – Part 1: Model framework and site-level performance, Geosci. Model Dev.,
3681 13, 2825–2850, https://doi.org/10.5194/gmd-13-2825-2020, 2020.

https://doi.org/10.5194/essd-2026-895
Preprint. Discussion started: 10 November 2026
© Author(s) 2026. CC BY 4.0 License.



3682 Mercado, L. M., Bellouin, N., Sitch, S., Boucher, O., Huntingford, C., Wild, M., and Cox, P. M.: Impact of
3683 changes in diffuse radiation on the global land carbon sink, Nature, 458, 1014–1017,
3684 https://doi.org/10.1038/nature07949, 2009.

3685 Moorcroft, P. R., Hurtt, G. C., and Pacala, S. W.: A Method for Scaling Vegetation Dynamics: The Ecosystem
3686 Demography Model (ed), Ecol. Monogr., 71, 557–586, https://doi.org/10.1890/0012-
3687 9615(2001)071[0557:AMFSVD]2.0.CO;2, 2001.

3688 Mouillot, F., Schultz, M. G., Yue, C., Cadule, P., Tansey, K., Ciais, P., and Chuvieco, E.: Ten years of global
3689 burned area products from spaceborne remote sensing—A review: Analysis of user needs and recommendations for
3690 future developments, International Journal of Applied Earth Observation and Geoinformation, 26, 64–79,
3691 https://doi.org/10.1016/j.jag.2013.05.014, 2014.

3692 Müller, J. D., Gruber, N., Carter, B., Feely, R., Ishii, M., Lange, N., Lauvset, S. K., Murata, A., Olsen, A., Pérez, F.
3693 F., Sabine, C., Tanhua, T., Wanninkhof, R., and Zhu, D.: Decadal Trends in the Oceanic Storage of Anthropogenic
3694 Carbon From 1994 to 2014, AGU Adv., 4, e2023AV000875, https://doi.org/10.1029/2023AV000875, 2023.

3695 Müller, J. D., Gruber, N., Schneuwly, A., Bakker, D. C. E., Gehlen, M., Gregor, L., Hauck, J., Landschützer, P.,
3696 and McKinley, G. A.: Unexpected decline in the ocean carbon sink under record-high sea surface temperatures in
3697 2023, Nat. Clim. Chang., 15, 978–985, https://doi.org/10.1038/s41558-025-02380-4, 2025.

3698 Müller, J. and Joos, F.: Committed and projected future changes in global peatlands – continued transient model
3699 simulations since the Last Glacial Maximum, Biogeosciences, 18, 3657–3687, https://doi.org/10.5194/bg-18-3657-
3700 2021, 2021.

3701 Naudts, K., Ryder, J., McGrath, M. J., Otto, J., Chen, Y., Valade, A., Bellasen, V., Berhongaray, G., Bönisch, G.,
3702 Campioli, M., Ghattas, J., De Groote, T., Haverd, V., Kattge, J., MacBean, N., Maignan, F., Merilä, P., Penuelas,
3703 J., Peylin, P., Pinty, B., Pretzsch, H., Schulze, E. D., Solyga, D., Vuichard, N., Yan, Y., and Luyssaert, S.: A
3704 vertically discretised canopy description for ORCHIDEE (SVN r2290) and the modifications to the energy, water
3705 and carbon fluxes, Geosci. Model Dev., 8, 2035–2065, https://doi.org/10.5194/gmd-8-2035-2015, 2015.

3706 Naus, S., Peters, W., Hooghiem, J., van der Woude, A., Luijkx, I., Rödenbeck, C., Chevallier, F., Martinez, A.,
3707 Niwa, Y., Maity, S., Jacobson, A.R., Liu, J., Bowman, K., Yun, J., Bloom, A., Jin, Z., Tian, X., Piao, S., Wang, Y.,
3708 Zhang, H.., Wang, T., Liu, Z., Zeng, N., Jiang, F.., Feng, L., Palmer, P., Maksyutov, S., Nayagam, L., Janardanan,
3709 R., Kong, Y., Zheng, B. Qiu, Y "Global gridded CO2 fluxes and simulated mole fractions from the sixteen inverse
3710 models in the Global Carbon Budget 2026" DOI:10.18160/99Y6-6994, 2026.

3711 NCEP: National Centers for Environmental Prediction. ONI Index. Cold & Warm Episodes by Season [Data set],
3712 NOAA, available at: https://www.cpc.ncep.noaa.gov/products/analysis_monitoring/ensostuff/ONI_v5.php, last
3713 access: 30 October 2026, 2026.

3714 Nayagam, L., Maksyutov, S., Janardanan, R., Oda, T., Tiwari, Y. K., Sreenivas, G., Datye, A., Jain, C. D., Ratnam,
3715 M. V., Sinha, V., Hakkim, H., Terao, Y., Naja, M., Ahmed, Md. K., Mukai, H., Zeng, J., Kaiser, J. W., Someya,
3716 Y., Yoshida, Y., and Matsunaga, T.: Indian Land Carbon Sink Estimated from Surface and GOSAT Observations,
3717 Remote Sensing, 17, 450, https://doi.org/10.3390/rs17030450, 2025.

3718 Nevison, C.D., Mahowald, N.M., Doney, S.C., Lima, I.D. and Cassar, N.:. Impact of variable air-sea O 2 and CO 2
3719 fluxes on atmospheric potential oxygen (APO) and land-ocean carbon sink partitioning. Biogeosciences, 5(3),
3720 pp.875-889, https://doi.org/10.5194/bg-5-875-2008, 2008.

3721 Niu, L., Wu, S., Andrew, R. M., Shao, Z., Wang, J., and Xi, F.: Global and national CO2 uptake by cement
3722 carbonation from 1928 to 2024, Earth Syst. Sci. Data, 17, 2231–2247, https://doi.org/10.5194/essd-17-2231-2025,
3723 2025.

3724 Niwa, Y., Ishijima, K., Ito, A., and Iida, Y.: Toward a long-term atmospheric CO2 inversion for elucidating natural
3725 carbon fluxes: technical notes of NISMON-CO2 v2021.1, Prog. Earth Planet Sci., 9, 42,
3726 https://doi.org/10.1186/s40645-022-00502-6, 2022.

3727 Niwa, Y., Fujii, Y., Sawa, Y., Iida, Y., Ito, A., Satoh, M., Imasu, R., Tsuboi, K., Matsueda, H., and Saigusa, N.: A
3728 4D-Var inversion system based on the icosahedral grid model (NICAM-TM 4D-Var v1.0) – Part 2: Optimization
3729 scheme and identical twin experiment of atmospheric CO₂ inversion, Geosci. Model Dev.,
3730 10, 2201–2219, https://doi.org/10.5194/gmd-10-2201-2017, 2017.

3731 Norby, R.J.: Forest productivity response to elevated CO2 in free-air CO2 enrichment experiments: the 23 percent
3732 solution, revisited, New Phytologist, https://doi.org/10.1111/nph.70162, 2025.

https://doi.org/10.5194/essd-2026-895
Preprint. Discussion started: 10 November 2026
© Author(s) 2026. CC BY 4.0 License.



3733 Obermeier, W. A., Nabel, J. E. M. S., Loughran, T., Hartung, K., Bastos, A., Havermann, F., Anthoni, P., Arneth,
3734 A., Goll, D. S., Lienert, S., Lombardozzi, D., Luyssaert, S., McGuire, P. C., Melton, J. R., Poulter, B., Sitch, S.,
3735 Sullivan, M. O., Tian, H., Walker, A. P., Wiltshire, A. J., Zaehle, S., and Pongratz, J.: Modelled land use and land
3736 cover change emissions – a spatio-temporal comparison of different approaches, 12, 635–670,
3737 https://doi.org/10.5194/esd-12-635-2021, 2021.

3738 Obermeier, W. A., Schwingshackl, C., Ganzenmüller, R., Grassi, G., Heinrich, V., Luijkx, I. T., Bastos, A., Ciais,
3739 P., Sitch, S., and Pongratz, J.: Differences and uncertainties in land-use CO2 flux estimates, Nat Rev Earth
3740 Environ, https://doi.org/10.1038/s43017-025-00730-6, 2025.

3741 Obli-Laryea, G. and Tubiello, F.: FAO net Forest Emissions/removals 1990-2025 [Dataset], Zenodo.
3742 https://doi.org/10.5281/ZENODO.21489542, 2026.

3743 O'Dell, C. W., Eldering, A., Wennberg, P. O., Crisp, D., Gunson, M. R., Fisher, B., Frankenberg, C., Kiel, M.,
3744 Lindqvist, H., Mandrake, L., Merrelli, A., Natraj, V., Nelson, R. R., Osterman, G. B., Payne, V. H., Taylor, T. E.,
3745 Wunch, D., Drouin, B. J., Oyafuso, F., Chang, A., McDuffie, J., Smyth, M., Baker, D. F., Basu, S., Chevallier, F.,
3746 Crowell, S. M. R., Feng, L., Palmer, P. I., Dubey, M., García, O. E., Griffith, D. W. T., Hase, F., Iraci, L. T., Kivi,
3747 R., Morino, I., Notholt, J., Ohyama, H., Petri, C., Roehl, C. M., Sha, M. K., Strong, K., Sussmann, R., Te, Y.,
3748 Uchino, O., and Velazco, V. A.: Improved retrievals of carbon dioxide from Orbiting Carbon Observatory-2 with
3749 the version 8 ACOS algorithm, Atmos. Meas. Tech., 11, 6539–6576, https://doi.org/10.5194/amt-11-6539-2018,
3750 2018.

3751 O'Sullivan, M., Zhang, Y., Bellouin, N., Harris, I., Mercado, L. M., Sitch, S., Ciais, P., and Friedlingstein, P.:
3752 Aerosol–light interactions reduce the carbon budget imbalance, Environ. Res. Lett., 16, 124072,
3753 https://doi.org/10.1088/1748-9326/ac3b77, 2021.

3754 O'Sullivan, M., Friedlingstein, P., Sitch, S., Anthoni, P., Arneth, A., Arora, V. K., Bastrikov, V., Delire, C., Goll,
3755 D. S., Jain, A., Kato, E., Kennedy, D., Knauer, J., Lienert, S., Lombardozzi, D., McGuire, P. C., Melton, J. R.,
3756 Nabel, J. E. M. S., Pongratz, J., Poulter, B., Séférian, R., Tian, H., Vuichard, N., Walker, A. P., Yuan, W., Yue, X.,
3757 and Zaehle, S.: Process-oriented analysis of dominant sources of uncertainty in the land carbon sink, Nat.
3758 Commun., 13, 4781, https://doi.org/10.1038/s41467-022-32416-8, 2022.

3759 O'Sullivan, M., Spracklen, D. V., Batterman, S. A., Arnold, S. R., Gloor, M., and Buermann, W.: Have Synergies
3760 Between Nitrogen Deposition and Atmospheric CO2 Driven the Recent Enhancement of the Terrestrial Carbon
3761 Sink?, Glob. Biogeochem. Cycles, 33, 163–180, https://doi.org/10.1029/2018GB005922, 2019.

3762 O'Sullivan, M., Sitch, S., Friedlingstein, P., Luijkx, I. T., Peters, W., Rosan, T. M., Arneth, A., Arora, V. K.,
3763 Chandra, N., Chevallier, F., Ciais, P., Falk, S., Feng, L., Gasser, T., Houghton, R. A., Jain, A. K., Kato, E.,
3764 Kennedy, D., Knauer, J., McGrath, M. J., Niwa, Y., Palmer, P. I., Patra, P. K., Pongratz, J., Poulter, B., Rödenbeck,
3765 C., Schwingshackl, C., Sun, Q., Tian, H., Walker, A. P., Yang, D., Yuan, W., Yue, X., and Zaehle, S.: The key role
3766 of forest disturbance in reconciling estimates of the northern carbon sink. Commun Earth Environ 5, 705,
3767 https://doi.org/10.1038/s43247-024-01827-4, 2024.

3768 O'Sullivan, M., Friedlingstein, P., Sitch, S., Pongratz, J., Schwingshackl, C., Gasser, T., Ciais, P., Arora, V., Kato,
3769 E., Knauer, J., Monier, E., Nützel, T., Sun, Q., Yuan, W., Yue, X., and Zaehle, S.: An improved approach to
3770 estimate the natural land carbon sink, npj Clim Atmos Sci, 9, 29, https://doi.org/10.1038/s41612-025-01302-7,
3771 2026a.

3772 O'Sullivan, M., Sitch, S., Friedlingstein, P., Smallman, T. L., Knauer, J., Arora, V., Foster, A., Aas, K., Tian, H.,
3773 Ma, L., Yang, X., Felzer, B., Yuan, W., Yue, X., Jain, A. K., Nutzel, T., Burke, E., Belda, D., Poulter, B., Heinke,
3774 J., Sun, Q., Luyssaert, S., Slominska-Durdasiak, K., Walker, A., Kato, E., Ito, A., Séférian, R.: TRENDY Land
3775 Model Output for the Global Carbon Budget 2026 [Dataset]. Zenodo. https://doi.org/10.5281/zenodo.23561904,
3776 2026b.

3777 Palmer, P. I., Feng, L., Baker, D., Chevallier, F., Bösch, H., and Somkuti, P.: Net carbon emissions from African
3778 biosphere dominate pan-tropical atmospheric CO2 signal, Nat Commun, 10, 3344, https://doi.org/10.1038/s41467-
3779 019-11097-w, 2019.

3780 Pan, Y., Birdsey, R. A., Fang, J., Houghton, R., Kauppi, P. E., Kurz, W. A., Phillips, O. L., Shvidenko, A., Lewis,
3781 S. L., Canadell, J. G., Ciais, P., Jackson, R. B., Pacala, S. W., McGuire, A. D., Piao, S., Rautiainen, A., Sitch, S.,
3782 and Hayes, D.: A Large and Persistent Carbon Sink in the World's Forests, Science, 333, 988–993,
3783 https://doi.org/10.1126/science.1201609, 2011.

3784 Pandey, S., Miller, J. B., Basu, S., Liu, J., Weir, B., Byrne, B., Chevallier, F., Bowman, K. W., Liu, Z., Deng, F.,
3785 O'Dell, C. W., and Chatterjee, A.: Toward Low-Latency Estimation of Atmospheric CO2 Growth Rates Using

https://doi.org/10.5194/essd-2026-895
Preprint. Discussion started: 10 November 2026
© Author(s) 2026. CC BY 4.0 License.



3786 Satellite Observations: Evaluating Sampling Errors of Satellite and In Situ Observing Approaches, AGU Advances,
3787 5, e2023AV001145, https://doi.org/10.1029/2023AV001145, 2024.

3788 Pandey, S., Chevallier, F., Rödenbeck, C., Byrne, B., Chatterjee, A., Liu, J., and Frankenberg, C.: Reduction in
3789 Earth's carbon budget imbalance, Nat Commun, 16, 6818, https://doi.org/10.1038/s41467-025-61588-2, 2025.

3790 Patara, L., Rieck, J. K., Hauck, J., Ödalen, M., Oschlies, A., and Gürses, Ö.: Stronger Southern Ocean
3791 Anthropogenic Carbon Uptake in Eddying Ocean Simulations, Journal of Climate, 39, 2017–2037,
3792 https://doi.org/10.1175/JCLI-D-25-0198.1, 2026.

3793 Pendrill, F., Persson, U. M., Godar, J., Kastner, T., Moran, D., Schmidt, S., and Wood, R.: Agricultural and
3794 forestry trade drives large share of tropical deforestation emissions, Global Environmental Change, 56, 1–10,
3795 https://doi.org/10.1016/j.gloenvcha.2019.03.002, 2019.

3796 Pérez, F. F., Becker, M., Goris, N., Gehlen, M., López-Mozos, M., Tjiputra, J., Olsen, A., Müller, J. D., Huertas, I.
3797 E., Chau, T. T. T., Cainzos, V., Velo, A., Benard, G., Hauck, J., Gruber, N., and Wanninkhof, R.: An Assessment
3798 of CO 2 Storage and Sea-Air Fluxes for the Atlantic Ocean and Mediterranean Sea Between 1985 and 2018. Global
3799 Biogeochemical Cycles, 38(4), e2023GB007862, https://doi.org/10.1029/2023GB007862, 2024.

3800 Peters, G. P., Minx, J. C., Weber, C. L., and Edenhofer, O.: Growth in emission transfers via international trade
3801 from 1990 to 2008, Proceedings of the National Academy of Sciences, 108, 8903–8908,
3802 https://doi.org/10.1073/pnas.1006388108, 2011.

3803 Peters, G. P., Marland, G., Le Quéré, C., Boden, T., Canadell, J. G., and Raupach, M. R.: Rapid growth in CO2
3804 emissions after the 2008–2009 global financial crisis, Nature Clim Change, 2, 2–4,
3805 https://doi.org/10.1038/nclimate1332, 2012a.

3806 Peters, G. P., Andrew, R. M., Boden, T., Canadell, J. G., Ciais, P., Le Quéré, C., Marland, G., Raupach, M. R., and
3807 Wilson, C.: The challenge to keep global warming below 2 °C, Nature Clim Change, 3, 4–6,
3808 https://doi.org/10.1038/nclimate1783, 2013.

3809 Peters, G. P., Le Quéré, C., Andrew, R. M., Canadell, J. G., Friedlingstein, P., Ilyina, T., Jackson, R. B., Joos, F.,
3810 Korsbakken, J. I., McKinley, G. A., Sitch, S., and Tans, P.: Towards real-time verification of CO2 emissions,
3811 Nature Clim Change, 7, 848–850, https://doi.org/10.1038/s41558-017-0013-9, 2017a.

3812 Peters, G. P., Andrew, R. M., Canadell, J. G., Fuss, S., Jackson, R. B., Korsbakken, J. I., Le Quéré, C. and
3813 Nakicenovic, N.: Key indicators to track current progress and future ambition of the Paris Agreement, 7, 118–122,
3814 https://doi.org/10.1038/nclimate3202, 2017b.

3815 Peters, G. P., Andrew, R. M., Canadell, J. G., Friedlingstein, P., Jackson, R. B., Korsbakken, J. I., Le Quéré, C.,
3816 and Peregon, A.: Carbon dioxide emissions continue to grow amidst slowly emerging climate policies, Nat. Clim.
3817 Chang., 10, 3–6, https://doi.org/10.1038/s41558-019-0659-6, 2020.

3818 Petrescu, A. M. R., Peters, G. P., Janssens-Maenhout, G., Ciais, P., Tubiello, F. N., Grassi, G., Nabuurs, G.-J.,
3819 Leip, A., Carmona-Garcia, G., Winiwarter, W., Höglund-Isaksson, L., Günther, D., Solazzo, E., Kiesow, A.,
3820 Bastos, A., Pongratz, J., Nabel, J. E. M. S., Conchedda, G., Pilli, R., Andrew, R. M., Schelhaas, M.-J., and Dolman,
3821 A. J.: European anthropogenic AFOLU greenhouse gas emissions: a review and benchmark data, Earth Syst. Sci.
3822 Data, 12, 961–1001, https://doi.org/10.5194/essd-12-961-2020, 2020.

3823 Pfeil, B., Olsen, A., Bakker, D. C. E., Hankin, S., Koyuk, H., Kozyr, A., Malczyk, J., Manke, A., Metzl, N., Sabine,
3824 C. L., Akl, J., Alin, S. R., Bates, N., Bellerby, R. G. J., Borges, A., Boutin, J., Brown, P. J., Cai, W.-J., Chavez, F.
3825 P., Chen, A., Cosca, C., Fassbender, A. J., Feely, R. A., González-Dávila, M., Goyet, C., Hales, B., Hardman-
3826 Mountford, N., Heinze, C., Hood, M., Hoppema, M., Hunt, C. W., Hydes, D., Ishii, M., Johannessen, T., Jones, S.
3827 D., Key, R. M., Körtzinger, A., Landschützer, P., Lauvset, S. K., Lefèvre, N., Lenton, A., Lourantou, A., Merlivat,
3828 L., Midorikawa, T., Mintrop, L., Miyazaki, C., Murata, A., Nakadate, A., Nakano, Y., Nakaoka, S., Nojiri, Y.,
3829 Omar, A. M., Padin, X. A., Park, G.-H., Paterson, K., Perez, F. F., Pierrot, D., Poisson, A., Ríos, A. F., Santana-
3830 Casiano, J. M., Salisbury, J., Sarma, V. V. S. S., Schlitzer, R., Schneider, B., Schuster, U., Sieger, R., Skjelvan, I.,
3831 Steinhoff, T., Suzuki, T., Takahashi, T., Tedesco, K., Telszewski, M., Thomas, H., Tilbrook, B., Tjiputra, J.,
3832 Vandemark, D., Veness, T., Wanninkhof, R., Watson, A. J., Weiss, R., Wong, C. S., and Yoshikawa-Inoue, H.: A
3833 uniform, quality controlled Surface Ocean CO2 Atlas (SOCAT), Earth Syst. Sci. Data, 5, 125–143,
3834 https://doi.org/10.5194/essd-5-125-2013, 2013.

3835 Piao, S., Ciais, P., Friedlingstein, P., de Noblet-Ducoudré, N., Cadule, P., Viovy, N., and Wang, T.: Spatiotemporal
3836 patterns of terrestrial carbon cycle during the 20th century, Global Biogeochem. Cy., 23, GB4026,
3837 https://doi.org/10.1029/2008GB003339, 2009.

https://doi.org/10.5194/essd-2026-895
Preprint. Discussion started: 10 November 2026
© Author(s) 2026. CC BY 4.0 License.



3838 Piao, S., Huang, M., Liu, Z., Wang, X., Ciais, P., Canadell, J. G., Wang, K., Bastos, A., Friedlingstein, P.,
3839 Houghton, R. A., Le Quéré, C., Liu, Y., Myneni, R. B., Peng, S., Pongratz, J., Sitch, S., Yan, T., Wang, Y., Zhu, Z.,
3840 Wu, D., and Wang, T.: Lower land-use emissions responsible for increased net land carbon sink during the slow
3841 warming period, Nature Geosci, 11, 739–743, https://doi.org/10.1038/s41561-018-0204-7, 2018.

3842 Planchat, A., Bopp, L., and Kwiatkowski, L.: A fresh look at the pre-industrial air–sea carbon flux using the
3843 alkalinity budget, Biogeosciences, 22, 6017–6055, https://doi.org/10.5194/bg-22-6017-2025, 2025.

3844 Pongratz, J., Reick, C.H., Raddatz, T. and Claussen, M.: Effects of anthropogenic land cover change on the carbon
3845 cycle of the last millennium. Global Biogeochemical Cycles, 23(4), doi:10.1029/2009GB003488, 2009.

3846 Pongratz, J., Reick, C. H., Houghton, R. A., and House, J. I.: Terminology as a key uncertainty in net land use and
3847 land cover change carbon flux estimates, Earth Syst. Dynam., 5, 177–195, https://doi.org/10.5194/esd-5-177-2014,
3848 2014.

3849 Poulter, B., Bastos, A., Canadell, J., Ciais, P., Gruber, N., Hauck, J., Jackson, R., Ishii, M., Müller, J., Patra, P., and
3850 Tian, H.: Inventorying Earth's Land and Ocean Greenhouse Gases, Eos, 103,
3851 https://doi.org/10.1029/2022EO179084, 2022.

3852 Poulter, B., Frank, D. C., Hodson, E. L., and Zimmermann, N. E.: Impacts of land cover and climate data selection
3853 on understanding terrestrial carbon dynamics and the CO2 airborne fraction, Biogeosciences, 8, 2027–2036,
3854 https://doi.org/10.5194/bg-8-2027-2011, 2011.

3855 Powis, C. M., Smith, S. M., Minx, J. C., and Gasser, T.: Quantifying global carbon dioxide removal deployment,
3856 Environ. Res. Lett., 18, 024022, https://doi.org/10.1088/1748-9326/acb450, 2023.

3857 Prentice, I. C., Farquhar, G. D., Fasham, M. J. R., Goulden, M. L., Heimann, M., Jaramillo, V. J., Kheshgi, H. S.,
3858 Le Quéré, C., Scholes, R. J., and Wallace, D. W. R.: The Carbon Cycle and Atmospheric Carbon Dioxide, in
3859 Climate Change 2001: The Scientific Basis. Contribution of Working Group I to the Third Assessment Report of
3860 the Intergovernmental Panel on Climate Change, edited by: Houghton, J. T., Ding, Y., Griggs, D. J., Noguer, M.,
3861 van der Linden, P. J., Dai, X., Maskell, K., and Johnson, C. A., Cambridge University Press, Cambridge, United
3862 Kingdom and New York, NY, USA, 183–237, ISBN: 978-0521014953, 2001.

3863 Price, J. T. and Warren, R.: Literature Review of the Potential of "Blue Carbon" Activities to Reduce Emissions,
3864 available at: https://avoid-net-uk.cc.ic.ac.uk/wp-content/uploads/delightful-downloads/2016/03/Literature-review-
3865 of-the-potential-of-blue-carbon-activities-to-reduce-emissions-AVOID2-WPE2.pdf, last access: 30 October 2026,
3866 2016.

3867 Qin, Y., Xiao, X., Wigneron, J.-P., Ciais, P., Brandt, M., Fan, L., Li, X., Crowell, S., Wu, X., Doughty, R., Zhang,
3868 Y., Liu, F., Sitch, S., and Moore, B.: Carbon loss from forest degradation exceeds that from deforestation in the
3869 Brazilian Amazon, Nat. Clim. Chang., 11, 442–448, https://doi.org/10.1038/s41558-021-01026-5, 2021.

3870 Qin, Z., Zhu, Y., Canadell, J.G., Chen, M., Li, T., Mishra, U. and Yuan, W.: Global spatially explicit carbon
3871 emissions from land-use change over the past six decades (1961–2020). One Earth, 7(5), pp.835-847,
3872 https://doi.org/10.1016/j.oneear.2024.04.002, 2024.

3873 Qiu, C., Ciais, P., Zhu, D., Guenet, B., Peng, S., Petrescu, A. M. R., Lauerwald, R., Makowski, D., Gallego-Sala,
3874 A. V., Charman, D. J., and Brewer, S. C.: Large historical carbon emissions from cultivated northern peatlands,
3875 Sci. Adv., 7, eabf1332, https://doi.org/10.1126/sciadv.abf1332, 2021.

3876 Randerson, J. T., Chen, Y., van der Werf, G. R., Rogers, B. M., and Morton, D. C.: Global burned area and
3877 biomass burning emissions from small fires: BURNED AREA FROM SMALL FIRES, J. Geophys. Res.
3878 Biogeosciences, 117, n/a-n/a, https://doi.org/10.1029/2012JG002128, 2012.

3879 Randerson, J. T., Li, Y., Fu, W., Primeau, F., Kim, J. E., Mu, M., Hoffman, F. M., Trugman, A. T., Yang, L., Wu,
3880 C., Wang, J. A., Anderegg, W. R. L., Baccini, A., Friedl, M. A., Saatchi, S. S., Denning, A. S., and Goulden, M. L.:
3881 The weak land carbon sink hypothesis, Sci. Adv., 11, eadr5489, https://doi.org/10.1126/sciadv.adr5489, 2025.

3882 Raupach, M. R., Marland, G., Ciais, P., Le Quere, C., Canadell, J. G., Klepper, G., and Field, C. B.: Global and
3883 regional drivers of accelerating CO2 emissions, Proceedings of the National Academy of Sciences, 104, 10288–
3884 10293, https://doi.org/10.1073/pnas.0700609104, 2007.

3885 Regnier, P., Resplandy, L., Najjar, R. G., and Ciais, P.: The land-to-ocean loops of the global carbon cycle, Nature,
3886 603, 401–410, https://doi.org/10.1038/s41586-021-04339-9, 2022.

https://doi.org/10.5194/essd-2026-895
Preprint. Discussion started: 10 November 2026
© Author(s) 2026. CC BY 4.0 License.



3887 Reick, C. H., Gayler, V., Goll, D., Hagemann, S., Heidkamp, M., Nabel, J. E. M. S., Raddatz, T., Roeckner, E.,
3888 Schnur, R., 110 and Wilkenskjeld, S.: JSBACH 3 – The land component of the MPI Earth System Model:
3889 documentation of version 3.2, available at: https://doi.org/10.17617/2.3279802, 2021.

3890 Remaud, M., Chevallier, F., Cozic, A., Lin, X., and Bousquet, P.: On the impact of recent developments of the
3891 LMDz atmospheric general circulation model on the simulation of CO2 transport, 11, 4489,
3892 https://doi.org/10.5194/gmd-11-4489-2018, 2018.

3893 Resplandy, L., Keeling, R. F., Eddebbar, Y., Brooks, M., Wang, R., Bopp, L., Long, M. C., Dunne, J. P., Koeve,
3894 W., and Oschlies, A.: Quantification of ocean heat uptake from changes in atmospheric O2 and CO2 composition,
3895 Scientific Reports, 9, 20244, https://doi.org/10.1038/s41598-019-56490-z, 2019.

3896 Rödenbeck, C., Bakker, D. C. E., Metzl, N., Olsen, A., Sabine, C., Cassar, N., Reum, F., Keeling, R. F., and
3897 Heimann, M.: Interannual sea–air CO2 flux variability from an observation-driven ocean mixed-layer scheme, 11,
3898 4599–4613, https://doi.org/10.5194/bg-11-4599-2014, 2014.

3899 Rödenbeck, C., Zaehle, S., Keeling, R., and Heimann, M.: History of El Niño impacts on the global carbon cycle
3900 1957–2017: a quantification from atmospheric CO2 data, 373, 20170303, https://doi.org/10.1098/rstb.2017.0303,
3901 2018.

3902 Rödenbeck, C., DeVries, T., Hauck, J., Le Quéré, C., and Keeling, R. F.: Data-based estimates of interannual sea–
3903 air CO2 flux variations 1957–2020 and their relation to environmental drivers, Biogeosciences, 19, 2627–2652,
3904 https://doi.org/10.5194/bg-19-2627-2022, 2022.

3905 Roobaert, A., Ford, D. J., Sreeush, M. G., McKinley, G. A., Hauck, J., Fay, A. R., Heimdal, T. H., Gruber, N.,
3906 Bopp, L., Chevallier, F., Djeutchouang, L. M., Gehlen, M., Gregor, L., Iida, Y., Jersild, A., Rödenbeck, C.,
3907 Rogerson, J., Schwinger, J., Shaum, C. A., Tsujino, H., Watson, A., Zeng, J., Shutler, J. D., and Landschützer, P.:
3908 Reconciling ocean carbon uptake estimates: a multi-model assessment of surface ocean CO2 reconstruction skill
3909 within the SOCOMv2 initiative, https://doi.org/10.22541/essoar.15003624/v1, 20 May 2026., 2026.

3910 Rosan, T. M., Sitch, S., O'Sullivan, M., Basso, L. S., Wilson, C., Silva, C., Gloor, E., Fawcett, D., Heinrich, V.,
3911 Souza, J. G. and Bezerra, F.G.S.: Synthesis of the land carbon fluxes of the Amazon region between 2010 and
3912 2020. Communications Earth & Environment, 5(1), p.46. https://doi.org/10.1038/s43247-024-01205-0, 2024.

3913 Sarma, V. V. S. S., Sridevi, B., Metzl, N., Patra, P. K., Lachkar, Z., Chakraborty, K., Goyet, C., Levy, M., Mehari,
3914 M., and Chandra, N.: Air-Sea Fluxes of CO2 in the Indian Ocean Between 1985 and 2018: A Synthesis Based on
3915 Observation-Based Surface CO2, Hindcast and Atmospheric Inversion Models, Glob. Biogeochem. Cycles, 37,
3916 e2023GB007694, https://doi.org/10.1029/2023GB007694, 2023.

3917 Schaphoff, S., von Bloh, W., Rammig, A., Thonicke, K., Biemans, H., Forkel, M., Gerten, D., Heinke, J.,
3918 Jägermeyr, J., Knauer, J., Langerwisch, F., Lucht, W., Müller, C., Rolinski, S., and Waha, K.: LPJmL4 – a dynamic
3919 global vegetation model with managed land – Part 1: Model description, Geosci. Model Dev., 11, 1343–1375,
3920 https://doi.org/10.5194/gmd-11-1343-2018, 2018.

3921 Schimel, D., Alves, D., Enting, I. G., Heimann, M., Joos, F., Raynaud, D., Wigley, T., Prater, M., Derwent, R.,
3922 Ehhalt, D., Fraser, P., Sanhueza, E., Zhou, X., Jonas, P., Charlson, R., Rodhe, H., Sadasivan, S., Shine, K. P.,
3923 Fouquart, Y., Ramaswamy, V., Solomon, S., Srinivasan, J., Albritton, D., Derwent, R., Isaksen, I., Lal, M., and
3924 Wuebbles, D.: Radiative Forcing of Climate Change, in: Climate Change 1995: The Science of Climate Change,
3925 Contribution of Working Group I to the Second Assessment Report of the Intergovernmental Panel on Climate
3926 Change [Houghton, J. T., Meira Rilho, L. G., Callander, B. A., Harris, N., Kattenberg, A., and Maskell, K. (eds.)],
3927 Cambridge University Press, Cambridge, United Kingdom and New York, NY, USA, ISBN: 978-0521559621,
3928 1995.

3929 Schimel, D., Stephens, B. B., and Fisher, J. B.: Effect of increasing CO 2 on the terrestrial carbon cycle, Proc Natl
3930 Acad Sci USA, 112, 436–441, https://doi.org/10.1073/pnas.1407302112, 2015.

3931 Schuh, A. E., Jacobson, A. R., Basu, S., Weir, B., Baker, D., Bowman, K., Chevallier, F., Crowell, S., Davis, K. J.,
3932 Deng, F., Denning, S., Feng, L., Jones, D., Liu, J., and Palmer, P. I.: Quantifying the Impact of Atmospheric
3933 Transport Uncertainty on CO 2 Surface Flux Estimates, Global Biogeochem. Cycles, 33, 484–500,
3934 https://doi.org/10.1029/2018GB006086, 2019.

3935 Schuldt, K. N., Mund, J., Aalto, T., Abshire, J. B., Aikin, K., Allen, G., Andrade, M., Andrews, A., Apadula, F.,
3936 Arnold, S., Baier, B., Bakwin, P., Bartyzel, J., Bentz, G., Bergamaschi, P., Beyersdorf, A., Biermann, T., Biraud, S.
3937 C., Blanc, P.-E., Boenisch, H., Bowling, D., Brailsford, G., Brand, W. A., Brunner, D., Bui, T. P., Burban, B.,
3938 Bäni, L., Calzolari, F., Chang, C. S., Chen, H., Chen, G., Chmura, L., Clark, S., Climadat, S., Colomb, A.,

https://doi.org/10.5194/essd-2026-895
Preprint. Discussion started: 10 November 2026
© Author(s) 2026. CC BY 4.0 License.



3939 Commane, R., Condori, L., Conen, F., Conil, S., Couret, C., Cristofanelli, P., Cuevas, E., Curcoll, R., Daube, B.,
3940 Davis, K. J., De Mazière, M., De Wekker, S., Dean-Day, J. M., Della Coletta, J., Delmotte, M., Di Iorio, T.,
3941 DiGangi, E., DiGangi, J. P., Dickerson, R., Elsasser, M., Emmenegger, L., Fang, S., Forster, G., France, J.,
3942 Frumau, A., Fuente-Lastra, M., Galkowski, M., Gatti, L. V., Gehrlein, T., Gerbig, C., Gheusi, F., Gloor, E., Goto,
3943 D., Griffis, T., Hammer, S., Hanisco, T. F., Hanson, C., Haszpra, L., Hatakka, J., Heimann, M., Heliasz, M., Heltai,
3944 D., Henne, S., Hensen, A., Hermans, C., Hermansen, O., Hintsa, E., Hoheisel, A., Holst, J., Iraci, L. T., Ivakhov,
3945 V., Jaffe, D. A., Jordan, A., Joubert, W., Kang, H.-Y., Karion, A., Kawa, S. R., Kazan, V., Keeling, R. F., Keronen,
3946 P., Kim, J., Klausen, J., Kneuer, T., Ko, M.-Y., Kolari, P., Kominkova, K., Kort, E., Kozlova, E., Krummel, P. B.,
3947 Kubistin, D., Kulawik, S. S., Kumps, N., Labuschagne, C., Lam, D. H., Lan, X., Langenfelds, R. L., Lanza, A.,
3948 Laurent, O., Laurila, T., Lauvaux, T., Lavric, J., Law, B. E., Lee, C.-H., Lee, J., Lehner, I., Lehtinen, K., Leppert,
3949 R., Leskinen, A., Leuenberger, M., Leung, W. H., Levin, I., Levula, J., Lin, J., Lindauer, M., Lindroth, A., Loh, Z.
3950 M., Lopez, M., Lunder, C. R., Löfvenius, M. O., Machida, T., Mammarella, I., Manca, G., Manning, A., Manning,
3951 A., Marek, M. V., Marklund, P., Marrero, J. E., Martin, M. Y., Martin, D., Martins, G. A., Matsueda, H., McKain,
3952 K., Meijer, H., Meinhardt, F., Merchant, L., Metzger, J.-M., Mihalopoulos, N., Miles, N. L., Miller, C. E., Miller, J.
3953 B., Mitchell, L., Monteiro, V., Montzka, S., Moossen, H., Moreno, C., Morgan, E., Morgui, J.-A., Morimoto, S.,
3954 Munger, J. W., Munro, D., Mutuku, M., Myhre, C. L., Mölder, M., Müller-Williams, J., Nakaoka, S.-I., Necki, J.,
3955 Newman, S., Nichol, S., Nisbet, E., Niwa, Y., Njiru, D. M., Noe, S. M., Nojiri, Y., O'Doherty, S., Obersteiner, F.,
3956 Paplawsky, B., Parworth, C. L., Peischl, J., Peltola, O., Peters, W., Philippon, C., Piacentino, S., Pichon, J. M.,
3957 Pickers, P., Piper, S., Pitt, J., Plass-Dülmer, C., Platt, S. M., Prinzivalli, S., Ramonet, M., Ramos, R., Ren, X.,
3958 Reyes-Sanchez, E., Richardson, S. J., Rigouleau, L.-J., Riris, H., Rivas, P. P., Rothe, M., Roulet, Y.-A., Ryerson,
3959 T., Ryoo, J.-M., Sargent, M., Sasakawa, M., Schaefer, H., Scheeren, B., Schmidt, M., Schuck, T., Schumacher, M.,
3960 Seibel, J., Seifert, T., Sha, M. K., Shepson, P., Shin, D., Shook, M., Sloop, C. D., Smale, D., Smith, P. D., Spain,
3961 G., St. Clair, J. M., Steger, D., Steinbacher, M., Stephens, B., Sweeney, C., Sørensen, L. L., Taipale, R., Takatsuji,
3962 S., Tans, P., Thoning, K., Timas, H., Torn, M., Trisolino, P., Turnbull, J., Vermeulen, A., Viner, B., Vitkova, G.,
3963 Walker, S., Watson, A., Weiss, R., Weyrauch, D., Wofsy, S. C., Worsey, J., Worthy, D., Xueref-Remy, I., Yates,
3964 E. L., Young, D., Yver-Kwok, C., Zaehle, S., Zahn, A., Zellweger, C., Zimnoch, M., de Souza, R. A., di Sarra, A.
3965 G., van Dinther, D., van den Bulk, P.: Multi-laboratory compilation of atmospheric carbon dioxide data for the
3966 period 1957-2023; obspack_co2_1_GLOBALVIEWplus_v10.1_2024-11-13, https://doi.org/10.25925/20241101,
3967 2024.

3968 Schuldt, K. N., Jacobson, A. R., Aalto, T., Aaltonen, H., Andrews, A., Apadula, F., Arnold, S., Bakwin, P.,
3969 Bartyzel, J., Bergamaschi, P., Biermann, T., Biraud, S. C., Blanc, P.-E., Brunner, D., Bäni, L., Calzolari, F., Chen,
3970 H., Chmura, L., Colomb, A., Condori, L., Conen, F., Conil, S., Couret, C., Cristofanelli, P., Cuevas, E., De
3971 Mazière, M., De Wekker, S., Della Coletta, J., Delmotte, M., Di Iorio, T., Elsasser, M., Emmenegger, L., Forster,
3972 G., Frumau, A., Fuente-Lastra, M., Galkowski, M., Gheusi, F., Hammer, S., Haszpra, L., Hatakka, J., Heliasz, M.,
3973 Heltai, D., Henne, S., Hensen, A., Hermans, C., Hermansen, O., Hoheisel, A., Holst, J., Jaffe, D. A., Karion, A.,
3974 Kazan, V., Keronen, P., Kneuer, T., Kolari, P., Kominkova, K., Krummel, P. B., Kubistin, D., Kumps, N., Lan, X.,
3975 Langenfelds, R. L., Lanza, A., Laurent, O., Lee, J., Lehner, I., Lehtinen, K., Leskinen, A., Leuenberger, M., Levin,
3976 I., Levula, J., Lindauer, M., Lindroth, A., Loh, Z. M., Lopez, M., Lunder, C. R., Löfvenius, M. O., Mammarella, I.,
3977 Manca, G., Manning, A., Manning, A., Marek, M. V., Marklund, P., McKain, K., Meijer, H., Meinhardt, F.,
3978 Metzger, J.-M., Miller, J. B., Miller, C. E., Myhre, C. L., Mölder, M., Müller-Williams, J., Necki, J., Noe, S. M.,
3979 O'Doherty, S., Peltola, O., Philippon, C., Piacentino, S., Pichon, J. M., Pickers, P., Pitt, J., Plass-Dülmer, C., Platt,
3980 S. M., Ramonet, M., Ramos, R., Reyes-Sanchez, E., Rigouleau, L.-J., Rivas, P. P., Roulet, Y.-A., Scheeren, B.,
3981 Schmidt, M., Schumacher, M., Sha, M. K., Sloop, C. D., Smith, P. D., Steger, D., Steinbacher, M., Sweeney, C.,
3982 Sørensen, L. L., Taipale, R., Tans, P., Thoning, K., Trisolino, P., Vermeulen, A., Viner, B., Vitkova, G., Weyrauch,
3983 D., Worthy, D., Xueref-Remy, I., Young, D., Yver-Kwok, C., Zimnoch, M., di Sarra, A. G., van den Bulk, P.:
3984 Multi-laboratory compilation of atmospheric carbon dioxide data for the year 2024;
3985 obspack_co2_1_NRT_v10.1_2025-02-07, https://doi.org/10.25925/20250101, 2025.

3986 Schwinger, J., Goris, N., Tjiputra, J. F., Kriest, I., Bentsen, M., Bethke, I., Ilicak, M., Assmann, K. M., and Heinze,
3987 C.: Evaluation of NorESM-OC (versions 1 and 1.2), the ocean carbon-cycle stand-alone configuration of the
3988 Norwegian Earth System Model (NorESM1), Geosci. Model Dev., 9, 2589–2622, https://doi.org/10.5194/gmd-9-
3989 2589-2016, 2016.

3990 Schwingshackl, C., Obermeier, W. A., Bultan, S., Grassi, G., Canadell, J. G., Friedlingstein, P., Gasser, T.,
3991 Houghton, R. A., Kurz, W. A., Sitch, S., and Pongratz, J.: Differences in land-based mitigation estimates
3992 reconciled by separating natural and land-use CO2 fluxes at the country level, One Earth, 5, 1367–1376,
3993 https://doi.org/10.1016/j.oneear.2022.11.009, 2022.

3994 Schwingshackl, C., Gasser, T., Qin, Z., Seeberg, G., Fu, Z., & Pongratz, J. (2026). Land-use change CO2 emissions
3995 (ELUC) data for the Global Carbon Budget 2026 (Version 1.0) [Data set]. Zenodo.
3996 https://doi.org/10.5281/zenodo.23528902, 2026.

https://doi.org/10.5194/essd-2026-895
Preprint. Discussion started: 10 November 2026
© Author(s) 2026. CC BY 4.0 License.



3997 Séférian, R., Nabat, P., Michou, M., Saint-Martin, D., Voldoire, A., Colin, J., Decharme, B., Delire, C., Berthet, S.,
3998 Chevallier, M., Sénési, S., Franchisteguy, L., Vial, J., Mallet, M., Joetzjer, E., Geoffroy, O., Guérémy, J.-F., Moine,
3999 M.-P., Msadek, R., Ribes, A., Rocher, M., Roehrig, R., Salas-y-Mélia, D., Sanchez, E., Terray, L., Valcke, S.,
4000 Waldman, R., Aumont, O., Bopp, L., Deshayes, J., Éthé, C., and Madec, G.: Evaluation of CNRM Earth System
4001 Model, CNRM-ESM2-1: Role of Earth System Processes in Present-Day and Future Climate, Journal of Advances
4002 in Modeling Earth Systems, 11, 4182–4227, https://doi.org/10.1029/2019MS001791, 2019.

4003 Seiler, C., Melton, J. R., Arora, V. K., Sitch, S., Friedlingstein, P., Anthoni, P., Goll, D., Jain, A. K., Joetzjer, E.,
4004 Lienert, S., Lombardozzi, D., Luyssaert, S., Nabel, J. E. M. S., Tian, H., Vuichard, N., Walker, A. P., Yuan, W.,
4005 and Zaehle, S.: Are Terrestrial Biosphere Models Fit for Simulating the Global Land Carbon Sink?, J. Adv. Model.
4006 Earth Syst., 14, e2021MS002946, https://doi.org/10.1029/2021MS002946, 2022.

4007 Sellar, A. A., Jones, C. G., Mulcahy, J. P., Tang, Y., Yool, A., Wiltshire, A., O'Connor, F. M., Stringer, M., Hill,
4008 R., Palmieri, J., Woodward, S., Mora, L., Kuhlbrodt, T., Rumbold, S. T., Kelley, D. I., Ellis, R., Johnson, C. E.,
4009 Walton, J., Abraham, N. L., Andrews, M. B., Andrews, T., Archibald, A. T., Berthou, S., Burke, E., Blockley, E.,
4010 Carslaw, K., Dalvi, M., Edwards, J., Folberth, G. A., Gedney, N., Griffiths, P. T., Harper, A. B., Hendry, M. A.,
4011 Hewitt, A. J., Johnson, B., Jones, A., Jones, C. D., Keeble, J., Liddicoat, S., Morgenstern, O., Parker, R. J., Predoi,
4012 V., Robertson, E., Siahaan, A., Smith, R. S., Swaminathan, R., Woodhouse, M. T., Zeng, G., and Zerroukat, M.:
4013 UKESM1: Description and Evaluation of the U.K. Earth System Model, J. Adv. Model. Earth Syst., 11, 4513–
4014 4558, https://doi.org/10.1029/2019MS001739, 2019.

4015 Shu, S., Jain, A. K., Koven, C. D., and Mishra, U.: Estimation of Permafrost SOC Stock and Turnover Time Using
4016 a Land Surface Model With Vertical Heterogeneity of Permafrost Soils, Global Biogeochem. Cy., 34,
4017 e2020GB006585, https://doi.org/10.1029/2020GB006585, 2020.

4018 Sitch, S., V. Brovkin, W. von Bloh, D. Van Vuuren, B. Eickhout, and Ganopolski, A.: Impacts of future land cover
4019 on atmospheric CO2 and climate. Global Biogeochemical Cycles, 19, GB2013. doi:10.1029/2004GB002311, 2005.

4020 Sitch, S., O'Sullivan, M., Robertson, E., Friedlingstein, P., Albergel, C., Anthoni, P., Arneth, A., Arora, V. K.,
4021 Bastos, A., Bastrikov, V., Bellouin, N., Canadell, J. G., Chini, L., Ciais, P., Falk, S., Harris, I., Hurtt, G., Ito, A.,
4022 Jain, A. K., Jones, M. W., Joos, F., Kato, E., Kennedy, D., Klein Goldewijk, K., Kluzek, E., Knauer, J., Lawrence,
4023 P. J., Lombardozzi, D., Melton, J. R., Nabel, J. E. M. S., Pan, N., Peylin, P., Pongratz, J., Poulter, B., Rosan, T. M.,
4024 Sun, Q., Tian, H., Walker, A. P., Weber, U., Yuan, W., Yue, X., Zaehle, S.: Trends and Drivers of Terrestrial
4025 Sources and Sinks of Carbon Dioxide: An Overview of the TRENDY Project, Global Biogeochemical Cycles,
4026 38(7), e2024GB008102, https://doi.org/10.1029/2024GB008102, 2024.

4027 Smallman, T. L., Milodowski, D. T., Neto, E. S., Koren, G., Ometto, J., and Williams, M.: Parameter uncertainty
4028 dominates C-cycle forecast errors over most of Brazil for the 21st century, Earth Syst. Dyn., 12, 1191–1237,
4029 https://doi.org/10.5194/esd-12-1191-2021, 2021.

4030 Smith, B., Wårlind, D., Arneth, A., Hickler, T., Leadley, P., Siltberg, J., and Zaehle, S.: Implications of
4031 incorporating N cycling and N limitations on primary production in an individual-based dynamic vegetation model,
4032 Biogeosciences, 11, 2027–2054, https://doi.org/10.5194/bg-11-2027-2014, 2014.

4033 Smith, S., Grassi, G., Harrington, K., Schwingshackl, C., Pilli, R., Gupta, S., and Rink, A.: Chapter 7: Current
4034 levels of CDR, The State of Carbon Dioxide Removal - 3rd Edition (2026),
4035 https://doi.org/10.17605/OSF.IO/VH7U6, 2026.

4036 Sospedra-Alfonso, R., Merryfield, W. J., Boer, G. J., Kharin, V. V., Lee, W.-S., Seiler, C., and Christian, J. R.:
4037 Decadal climate predictions with the Canadian Earth System Model version 5 (CanESM5), Geosci. Model Dev.,
4038 14, 6863–6891, https://doi.org/10.5194/gmd-14-6863-2021, 2021.

4039 Steele, L. P., Dlugokencky, E. J., Lang, P. M., Tans, P. P., Martin, R. C., and Masarie, K. A.: Slowing down of the
4040 global accumulation of atmospheric methane during the 1980s, Nature 358, 313–316,
4041 https://doi.org/10.1038/358313a0, 1992.

4042 Stephens, B. B., Gurney, K. R., Tans, P. P., Sweeney, C., Peters, W., Bruhwiler, L., Ciais, P., Ramonet, M.,
4043 Bousquet, P., Nakazawa, T., Aoki, S., Machida, T., Inoue, G., Vinnichenko, N., Lloyd, J., Jordan, A., Heimann,
4044 M., Shibistova, O., Langenfelds, R. L., Steele, L. P., Francey, R. J., and Denning, A. S.: Weak Northern and Strong
4045 Tropical Land Carbon Uptake from Vertical Profiles of Atmospheric CO2, Science, 316, 1732–1735,
4046 https://doi.org/10.1126/science.1137004, 2007.

4047 Stephens, B. B., Keeling, R. F., Heimann, M., Six, K. D., Murnane, R., and Caldeira, K.: Testing global ocean
4048 carbon cycle models using measurements of atmospheric O2 and CO2 concentration, Glob. Biogeochem. Cycles,
4049 12, 213–230, https://doi.org/10.1029/97GB03500, 1998.

https://doi.org/10.5194/essd-2026-895
Preprint. Discussion started: 10 November 2026
© Author(s) 2026. CC BY 4.0 License.



4050 Stephens, B. B., Jin, Y., Sweeney, C., McKain, K., Gaubert, B., Baker, D. F., Basu, S., Bertolacci, M., Chevallier,
4051 F., Commane, R., Crowell, S., Deng, F., Johnson, M. S., Keeling, R. F., Liu, J., Liu, Z., Maity, S., Morgan, E. J.,
4052 Patra, P., Philip, S., Wofsy, S. C., and Zammit-Mangion, A.: Improved latitudinal carbon budgets from global
4053 airborne surveys, Proc. Natl. Acad. Sci. U.S.A., 123, e2523984123, https://doi.org/10.1073/pnas.2523984123,
4054 2026.

4055 Stock, C. A., Dunne, J. P., Luo, J. Y., Ross, A. C., Van Oostende, N., Zadeh, N., Cordero, T. J., Liu, X., and Teng,
4056 Y.: Photoacclimation and Photoadaptation Sensitivity in a Global Ocean Ecosystem Model, J Adv Model Earth
4057 Syst, 17, e2024MS004701, https://doi.org/10.1029/2024MS004701, 2025.

4058 Stocker, T., Qin, D., and Platner, G.-K.: Climate Change 2013: The Physical Science Basis. Contribution of
4059 Working Group I to the Fifth Assessment Report of the Intergovernmental Panel on Climate Change
4060 [Intergovernmental Panel on Climate Change (eds.)], Cambridge University Press, Cambridge, ISBN:
4061 9789291691388, 2013.

4062 Su, W., Wang, B., Chen, H., Zhu, L., Zheng, X., and Chen, S. X.: A new global carbon flux estimation
4063 methodology by assimilation of both in situ and satellite CO2 observations, npj Clim Atmos Sci, 7, 287,
4064 https://doi.org/10.1038/s41612-024-00824-w, 2024.

4065 Swart, N. C., Cole, J. N. S., Kharin, V. V., Lazare, M., Scinocca, J. F., Gillett, N. P., Anstey, J., Arora, V.,
4066 Christian, J. R., Hanna, S., Jiao, Y., Lee, W. G., Majaess, F., Saenko, O. A., Seiler, C., Seinen, C., Shao, A.,
4067 Sigmond, M., Solheim, L., von Salzen, K., Yang, D., and Winter, B.: The Canadian Earth System Model version 5
4068 (CanESM5.0.3), Geosci. Model Dev., 12, 4823–4873, https://doi.org/10.5194/gmd-12-4823-2019, 2019.

4069 Takahashi, T., Sutherland, S. C., Wanninkhof, R., Sweeney, C., Feely, R. A., Chipman, D. W., Hales, B.,
4070 Friederich, G., Chavez, F., Sabine, C., Watson, A., Bakker, D. C. E., Schuster, U., Metzl, N., Yoshikawa-Inoue, H.,
4071 Ishii, M., Midorikawa, T., Nojiri, Y., Körtzinger, A., Steinhoff, T., Hoppema, M., Olafsson, J., Arnarson, T. S.,
4072 Tilbrook, B., Johannessen, T., Olsen, A., Bellerby, R., Wong, C. S., Delille, B., Bates, N. R., and de Baar, H. J. W.:
4073 Climatological mean and decadal change in surface ocean pCO2, and net sea–air CO2 flux over the global oceans,
4074 Deep Sea Research Part II: Topical Studies in Oceanography, 56, 554–577,
4075 https://doi.org/10.1016/j.dsr2.2008.12.009, 2009.

4076 Takano, Y., Ilyina, T., Tjiputra, J., Eddebbar, Y. A., Berthet, S., Bopp, L., Buitenhuis, E., Butenschön, M.,
4077 Christian, J. R., Dunne, J. P., Gröger, M., Hayashida, H., Hieronymus, J., Koenigk, T., Krasting, J. P., Long, M. C.,
4078 Lovato, T., Nakano, H., Palmieri, J., Schwinger, J., Séférian, R., Suntharalingam, P., Tatebe, H., Tsujino, H.,
4079 Urakawa, S., Watanabe, M., and Yool, A.: Simulations of ocean deoxygenation in the historical era: insights from
4080 forced and coupled models, Front. Mar. Sci., 10, 1139917, https://doi.org/10.3389/fmars.2023.1139917, 2023.

4081 Taylor, T. E., O'Dell, C. W., Chang, A., Chatterjee, A., Cheng, C., Dang, L., et al.: The OCO-2 and OCO-3 ACOS
4082 version 11 XCO2 data products: A benchmark record for space-based global carbon cycle research. Earth and
4083 Space Science, 13, e2026EA005360. https://doi.org/10.1029/2026EA005360, 2026.

4084 Terhaar, J., Frölicher, T. L., and Joos, F.: Southern Ocean anthropogenic carbon sink constrained by sea surface
4085 salinity, Sci. Adv., 7, eabd5964, https://doi.org/10.1126/sciadv.abd5964, 2021.

4086 Terhaar, J., Frölicher, T. L., and Joos, F.: Observation-constrained estimates of the global ocean carbon sink from
4087 Earth system models, Biogeosciences, 19, 4431–4457, https://doi.org/10.5194/bg-19-4431-2022, 2022.

4088 Terhaar, J.: Drivers of decadal trends in the ocean carbon sink in the past, present, and future in Earth system
4089 models, Biogeosciences, 21, 3903–3926, https://doi.org/10.5194/bg-21-3903-2024, 2024.

4090 Terhaar, J., Goris, N., Müller, J. D., DeVries, T., Gruber, N., Hauck, J., Perez, F. F., and Séférian, R.: Assessment
4091 of Global Ocean Biogeochemistry Models for Ocean Carbon Sink Estimates in RECCAP2 and Recommendations
4092 for Future Studies. Journal of Advances in Modeling Earth Systems, 16(3), e2023MS003840,
4093 https://doi.org/10.1029/2023MS003840, 2024.

4094 Terhaar, J.: Composite model-based estimate of the ocean carbon sink from 1959 to 2022, Biogeosciences, 22,
4095 1631–1649, https://doi.org/10.5194/bg-22-1631-2025, 2025.

4096 Tian, H., Xu, X., Lu, C., Liu, M., Ren, W., Chen, G., Melillo, J., and Liu, J.: Net exchanges of CO2, CH4, and
4097 N2O between China's terrestrial ecosystems and the atmosphere and their contributions to global climate warming,
4098 J. Geophys. Res. Biogeosciences, 116, G02011, https://doi.org/10.1029/2010JG001393, 2011.

https://doi.org/10.5194/essd-2026-895
Preprint. Discussion started: 10 November 2026
© Author(s) 2026. CC BY 4.0 License.



4099 Thum, T., Caldararu, S., Engel, J., Kern, M., Pallandt, M., Schnur, R., Yu, L., and Zaehle, S.: A new model of the
4100 coupled carbon, nitrogen, and phosphorus cycles in the terrestrial biosphere (QUINCY v1.0; revision 1996),
4101 Geosci. Model Dev., 12, 4781–4802, https://doi.org/10.5194/gmd-12-4781-2019, 2019.

4102 Tjiputra, J. F., Schwinger, J., Bentsen, M., Morée, A. L., Gao, S., Bethke, I., Heinze, C., Goris, N., Gupta, A., He,
4103 Y.-C., Olivié, D., Seland, Ø., and Schulz, M.: Ocean biogeochemistry in the Norwegian Earth System Model
4104 version 2 (NorESM2), Geosci. Model Dev., 13, 2393–2431, https://doi.org/10.5194/gmd-13-2393-2020, 2020.

4105 Torres, R., Waldman, R., Madec, G., De Lavergne, C., Séférian, R., and Mak, J.: An Energetically and
4106 Observationally Constrained Mesoscale Parameterization for Ocean Climate Models, J Adv Model Earth Syst, 17,
4107 e2025MS005394, https://doi.org/10.1029/2025MS005394, 2025.

4108 Tsujino, H., Nakano, H., Sakamoto, K., Urakawa, L. S., Toyama, K., Kosugi, N., Kitamura, Y., Ishii, M.,
4109 Nishikawa, S., Nishikawa, H., Sugiyama, T., and Ishikawa, Y.: Impact of Increased Horizontal Resolution of an
4110 Ocean Model on Carbon Circulation in the North Pacific Ocean, J Adv Model Earth Syst, 16, e2023MS003720,
4111 https://doi.org/10.1029/2023MS003720, 2024.

4112 Tubiello, F. N., Branthomme, A., Obli-Laryea, G., Piccoli, M., Ramadan, N., Condor, R. D., Wanner, N., Brivio,
4113 R., Jonsson, Ö., Conchedda, G., and Pekkarinen, A.: FAO estimates of net forest emissions and removals, 1990–
4114 2025, Earth Syst. Sci. Data, 18, 6799–6813, https://doi.org/10.5194/essd-18-6799-2026, 2026.

4115 Tuck, C.: 2022 Mineral Commodity Summary: Iron Ore, Tech. rep., U.S. Geological Survey,
4116 https://pubs.usgs.gov/periodicals/mcs2022/mcs2022-iron-ore.pdf, 2022.

4117 UNFCCC: Synthesis report for the technical assessment component of the first global stocktake, available at:
4118 https://unfccc.int/documents/461466, last access: 30 October 2026, 2022.

4119 Van Den Berg, A.-W., Hooghiem, J. J. D., Van Der Woude, A. M., Rijsdijk, P., Vernooij, R., Botía, S., Van Der
4120 Werf, G. R., Miller, J. B., Luijkx, I. T., Krol, M. C., and Peters, W.: Fire carbon emission constraints from space-
4121 based carbon monoxide retrievals during the 2019 intense burning season in Brazil, Atmos. Chem. Phys., 26,
4122 13929–13958, https://doi.org/10.5194/acp-26-13929-2026, 2026.

4123 van der Laan-Luijkx, I. T., van der Velde, I. R., van der Veen, E., Tsuruta, A., Stanislawska, K., Babenhauserheide,
4124 A., Zhang, H. F., Liu, Y., He, W., Chen, H., Masarie, K. A., Krol, M. C., and Peters, W.: The CarbonTracker Data
4125 Assimilation Shell (CTDAS) v1.0: implementation and global carbon balance 2001–2015, Geosci. Model Dev., 10,
4126 2785–2800, https://doi.org/10.5194/gmd-10-2785-2017, 2017.

4127 van der Velde, I. R., van der Werf, G. R., Houweling, S., Maasakkers, J. D., Borsdorff, T., Landgraf, J., Tol, P.,
4128 van Kempen, T. A., van Hees, R., Hoogeveen, R., Veefkind, J. P., and Aben, I.: Vast CO2 release from Australian
4129 fires in 2019–2020 constrained by satellite, Nature, 597, 366–369, https://doi.org/10.1038/s41586-021-03712-y,
4130 2021.

4131 van der Werf, G. R., Randerson, J. T., Giglio, L., Collatz, G. J., Mu, M., Kasibhatla, P. S., Morton, D. C., DeFries,
4132 R. S., Jin, Y., and van Leeuwen, T. T.: Global fire emissions and the contribution of deforestation, savanna, forest,
4133 agricultural, and peat fires (1997–2009), Atmospheric Chem. Phys., 10, 11707–11735, https://doi.org/10.5194/acp-
4134 10-11707-2010, 2010.

4135 van der Werf, G. R., Randerson, J. T., Giglio, L., van Leeuwen, T. T., Chen, Y., Rogers, B. M., Mu, M., van Marle,
4136 M. J. E., Morton, D. C., Collatz, G. J., Yokelson, R. J., and Kasibhatla, P. S.: Global fire emissions estimates
4137 during 1997–2016, Earth Syst. Sci. Data, 9, 697–720, https://doi.org/10.5194/essd-9-697-2017, 2017.

4138 van der Werf, G. R., Randerson, J. T., Van Wees, D., Chen, Y., Giglio, L., Hall, J., Vernooij, R., Mu, M., Binte
4139 Shahid, S., Barsanti, K. C., Yokelson, R., and Morton, D. C.: Landscape fire emissions from the 5th version of the
4140 Global Fire Emissions Database (GFED5), Sci Data, 12, 1870, https://doi.org/10.1038/s41597-025-06127-w, 2025.

4141 van Wees, D., van der Werf, G. R., Randerson, J. T., Andela, N., Chen, Y., and Morton, D. C.: The role of fire in
4142 global forest loss dynamics, Glob. Change Biol., 27, 2377–2391, https://doi.org/10.1111/gcb.15591, 2021.

4143 von Bloh, W., Schaphoff, S., Müller, C., Rolinski, S., Waha, K., and Zaehle, S.: Implementing the nitrogen cycle
4144 into the dynamic global vegetation, hydrology, and crop growth model LPJmL (version 5.0), Geosci. Model Dev.,
4145 11, 2789–2812, https://doi.org/10.5194/gmd-11-2789-2018, 2018.

4146 Vaittinada Ayar, P., Bopp, L., Christian, J. R., Ilyina, T., Krasting, J. P., Séférian, R., Tsujino, H., Watanabe, M.,
4147 Yool, A., and Tjiputra, J.: Contrasting projections of the ENSO-driven CO2 flux variability in the equatorial

https://doi.org/10.5194/essd-2026-895
Preprint. Discussion started: 10 November 2026
© Author(s) 2026. CC BY 4.0 License.



4148 Pacific under high-warming scenario, Earth Syst. Dynam., 13, 1097–1118, https://doi.org/10.5194/esd-13-1097-
4149 2022, 2022.

4150 Vuichard, N., Messina, P., Luyssaert, S., Guenet, B., Zaehle, S., Ghattas, J., Bastrikov, V., and Peylin, P.:
4151 Accounting for carbon and nitrogen interactions in the global terrestrial ecosystem model ORCHIDEE (trunk
4152 version, rev 4999): multi-scale evaluation of gross primary production, Geosci. Model Dev., 12, 4751–4779,
4153 https://doi.org/10.5194/gmd-12-4751-2019, 2019.

4154 Walker, A. P., Quaife, T., Bodegom, P. M., De Kauwe, M. G., Keenan, T. F., Joiner, J., Lomas, M. R., MacBean,
4155 N., Xu, C., Yang, X., and Woodward, F. I.: The impact of alternative trait-scaling hypotheses for the maximum
4156 photosynthetic carboxylation rate (V cmax) on global gross primary production, New Phytol., 215, 1370–1386,
4157 https://doi.org/10.1111/nph.14623, 2017.

4158 Walker, A. P., De Kauwe, M. G., Bastos, A., Belmecheri, S., Georgiou, K., Keeling, R. F., McMahon, S. M.,
4159 Medlyn, B. E., Moore, D. J. P., Norby, R. J., Zaehle, S., Anderson-Teixeira, K. J., Battipaglia, G., Brienen, R. J.
4160 W., Cabugao, K. G., Cailleret, M., Campbell, E., Canadell, J. G., Ciais, P., Craig, M. E., Ellsworth, D. S., Farquhar,
4161 G. D., Fatichi, S., Fisher, J. B., Frank, D. C., Graven, H., Gu, L., Haverd, V., Heilman, K., Heimann, M., Hungate,
4162 B. A., Iversen, C. M., Joos, F., Jiang, M., Keenan, T. F., Knauer, J., Körner, C., Leshyk, V. O., Leuzinger, S., Liu,
4163 Y., MacBean, N., Malhi, Y., McVicar, T. R., Penuelas, J., Pongratz, J., Powell, A. S., Riutta, T., Sabot, M. E. B.,
4164 Schleucher, J., Sitch, S., Smith, W. K., Sulman, B., Taylor, B., Terrer, C., Torn, M. S., Treseder, K. K., Trugman,
4165 A. T., Trumbore, S. E., van Mantgem, P. J., Voelker, S. L., Whelan, M. E., and Zuidema, P. A.: Integrating the
4166 evidence for a terrestrial carbon sink caused by increasing atmospheric CO2, New Phytol., 229, 2413–2445,
4167 https://doi.org/10.1111/nph.16866, 2021.

4168 Walker, A. P., Obermeier, W. A., Pongratz, J., Friedlingstein, P., Koven, C. D., Schwingshackl, C., Sitch, S., and
4169 O'Sullivan, M.: Harmonizing direct and indirect anthropogenic land carbon fluxes indicates a substantial missing
4170 sink in the global carbon budget since the early 20th century, Plants People Planet, 7, 1123–1136,
4171 https://doi.org/10.1002/ppp3.10619, 2025.

4172 Wanninkhof, R., Triñanes, J., Pierrot, D., Munro, D. R., Sweeney, C., and Fay, A. R.: Trends in Sea-Air CO2
4173 Fluxes and Sensitivities to Atmospheric Forcing Using an Extremely Randomized Trees Machine Learning
4174 Approach, Global Biogeochemical Cycles, 39, e2024GB008315, https://doi.org/10.1029/2024GB008315, 2025.

4175 Watanabe, M., Tatebe, H., Koyama, H., Hajima, T., Watanabe, M., and Kawamiya, M.: Importance of El Niño
4176 reproducibility for reconstructing historical CO2 flux variations in the equatorial Pacific, Ocean Sci., 16, 1431–
4177 1442, https://doi.org/10.5194/os-16-1431-2020, 2020.

4178 Watson, A. J., Schuster, U., Shutler, J. D., Holding, T., Ashton, I. G. C., Landschützer, P., Woolf, D. K., and
4179 Goddijn-Murphy, L.: Revised estimates of ocean-atmosphere CO2 flux are consistent with ocean carbon inventory,
4180 Nat Commun, 11, 4422, https://doi.org/10.1038/s41467-020-18203-3, 2020.

4181 Watson, R. T., Rohde, H., Oeschger, H., and Siegenthaler, U.: Greenhouse Gases and Aerosols, in: Climate
4182 Change: The IPCC Scientific Assessment. Intergovernmental Panel on Climate Change (IPCC), edited by:
4183 Houghton, J. T., Jenkins, G. J., and Ephraums, J. J., Cambridge University Press, Cambridge, ISBN: 978-
4184 0521403603, 1990.

4185 Wenzel, S., Cox, P. M., Eyring, V., and Friedlingstein, P.: Projected land photosynthesis constrained by changes in
4186 the seasonal cycle of atmospheric CO2, Nature, 538, 499–501, https://doi.org/10.1038/nature19772, 2016.

4187 Wilkenskjeld, S., Kloster, S., Pongratz, J., Raddatz, T., and Reick, C. H.: Comparing the influence of net and gross
4188 anthropogenic land-use and land-cover changes on the carbon cycle in the MPI-ESM, Biogeosciences, 11, 4817–
4189 4828, https://doi.org/10.5194/bg-11-4817-2014, 2014.

4190 Willey, D. A., Fine, R. A., Sonnerup, R. E., Bullister, J. L., Smethie, W. M., and Warner, M. J.: Global oceanic
4191 chlorofluorocarbon inventory, Geophysical Research Letters, 31, 2003GL018816,
4192 https://doi.org/10.1029/2003GL018816, 2004.

4193 Wiltshire, A. J., Burke, E. J., Chadburn, S. E., Jones, C. D., Cox, P. M., Davies-Barnard, T., Friedlingstein, P.,
4194 Harper, A. B., Liddicoat, S., Sitch, S., and Zaehle, S.: JULES-CN: a coupled terrestrial carbon–nitrogen scheme
4195 (JULES vn5.1), 14, 2161–2186, https://doi.org/10.5194/gmd-14-2161-2021, 2021.

4196 Woodward, F. I. and Lomas, M. R.: Vegetation dynamics – simulating responses to climatic change, Biol. Rev., 79,
4197 643–670, https://doi.org/10.1017/S1464793103006419, 2004.

https://doi.org/10.5194/essd-2026-895
Preprint. Discussion started: 10 November 2026
© Author(s) 2026. CC BY 4.0 License.



4198 Wooster, M. J., Roberts, G. J., Giglio, L., Roy, D. P., Freeborn, P. H., Boschetti, L., Justice, C., Ichoku, C.,
4199 Schroeder, W., Davies, D., Smith, A. M. S., Setzer, A., Csiszar, I., Strydom, T., Frost, P., Zhang, T., Xu, W., De
4200 Jong, M. C., Johnston, J. M., Ellison, L., Vadrevu, K., Sparks, A. M., Nguyen, H., McCarty, J., Tanpipat, V.,
4201 Schmidt, C., and San-Miguel-Ayanz, J.: Satellite remote sensing of active fires: History and current status,
4202 applications and future requirements, Remote Sensing of Environment, 267, 112694,
4203 https://doi.org/10.1016/j.rse.2021.112694, 2021.

4204 Wright, R. M., Le Quéré, C., Buitenhuis, E., Pitois, S., and Gibbons, M. J.: Role of jellyfish in the plankton
4205 ecosystem revealed using a global ocean biogeochemical model, 18, 1291–1320, https://doi.org/10.5194/bg-18-
4206 1291-2021, 2021.

4207 Wunch, D., Wennberg, P. O., Osterman, G., Fisher, B., Naylor, B., Roehl, C. M., O'Dell, C., Mandrake, L., Viatte,
4208 C., Kiel, M., Griffith, D. W. T., Deutscher, N. M., Velazco, V. A., Notholt, J., Warneke, T., Petri, C., De Maziere,
4209 M., Sha, M. K., Sussmann, R., Rettinger, M., Pollard, D., Robinson, J., Morino, I., Uchino, O., Hase, F.,
4210 Blumenstock, T., Feist, D. G., Arnold, S. G., Strong, K., Mendonca, J., Kivi, R., Heikkinen, P., Iraci, L., Podolske,
4211 J., Hillyard, P. W., Kawakami, S., Dubey, M. K., Parker, H. A., Sepulveda, E., García, O. E., Te, Y., Jeseck, P.,
4212 Gunson, M. R., Crisp, D., and Eldering, A.: Comparisons of the Orbiting Carbon Observatory-2 (OCO-2) X CO2
4213 measurements with TCCON, Atmos. Meas. Tech., 10, 2209–2238, https://doi.org/10.5194/amt-10-2209-2017,
4214 2017.

4215 Xia, X., Ren, P., Wang, X., Liu, D., Chen, X., Dan, L., He, B., He, H., Ju, W., Liang, M., Lu, X., Peng, J., Qin, Z.,
4216 Xia, J., Zheng, B., Wei, J., Yue, X., Yu, G., Piao, S., and Yuan, W.: The carbon budget of China: 1980–2021,
4217 Science Bulletin, 69, 114–124, https://doi.org/10.1016/j.scib.2023.11.016, 2024.

4218 Xiao, R., Prentice, D., Sarkar, M., Kumar, A., Rosner, F., Neithalath, N., La Plante, E., Bauchy, M., and Sant, G.:
4219 Ambient concrete carbonation is a trivial contributor in mitigating carbon dioxide emissions from cement
4220 production, Commun. Sustain., 1, 118, https://doi.org/10.1038/s44458-026-00116-9, 2026.

4221 Yang, X., Thornton, P., Ricciuto, D., Wang, Y., and Hoffman, F.: Global evaluation of terrestrial biogeochemistry
4222 in the Energy Exascale Earth System Model (E3SM) and the role of the phosphorus cycle in the historical
4223 terrestrial carbon balance, Biogeosciences, 20, 2813–2836, https://doi.org/10.5194/bg-20-2813-2023, 2023.

4224 Yao, Y., Joetzjer, E., Ciais, P., Viovy, N., Cresto Aleina, F., Chave, J., Sack, L., Bartlett, M., Meir, P., Fisher, R.,
4225 and Luyssaert, S.: Forest fluxes and mortality response to drought: model description (ORCHIDEE-CAN-NHA
4226 r7236) and evaluation at the Caxiuanã drought experiment, Geosci. Model Dev., 15, 7809–7833,
4227 https://doi.org/10.5194/gmd-15-7809-2022, 2022.

4228 Yao, Y., Ciais, P., Viovy, N., Joetzjer, E. and Chave, J.: How drought events during the last century have impacted
4229 biomass carbon in Amazonian rainforests. Global Change Biology, 29(3), pp.747-762,
4230 https://doi.org/10.1111/gcb.16504, 2023.

4231 You, Y., Tian, H., Pan, S., Shi, H., Bian, Z., Gurgel, A., Huang, Y., Kicklighter, D., Liang, X.-Z., Lu, C., Melillo,
4232 J., Miao, R., Pan, N., Reilly, J., Ren, W., Xu, R., Yang, J., Yu, Q., and Zhang, J.: Incorporating dynamic crop
4233 growth processes and management practices into a terrestrial biosphere model for simulating crop production in the
4234 United States: Toward a unified modeling framework, Agricultural and Forest Meteorology, 325, 109144,
4235 https://doi.org/10.1016/j.agrformet.2022.109144, 2022.

4236 Yu, Z., Ciais, P., Piao, S., Houghton, R. A., Lu, C., Tian, H., Agathokleous, E., Kattel, G. R., Sitch, S., Goll, D.,
4237 Yue, X., Walker, A., Friedlingstein, P., Jain, A. K., Liu, S., and Zhou, G.: Forest expansion dominates China's land
4238 carbon sink since 1980, Nat. Commun., 13, 5374, https://doi.org/10.1038/s41467-022-32961-2, 2022.

4239 Yue, X., Zhou, H., Tian, C., Ma, Y., Hu, Y., Gong, C., Zheng, H., and Liao, H.: Development and evaluation of the
4240 interactive Model for Air Pollution and Land Ecosystems (iMAPLE) version 1.0, Geosci. Model Dev., 17, 4621–
4241 4642, https://doi.org/10.5194/gmd-17-4621-2024, 2024.

4242 Yue, C., Ciais, P., Zhu, D., Wang, T., Peng, S. S., and Piao, S. L.: How have past fire disturbances contributed to
4243 the current carbon balance of boreal ecosystems?, Biogeosciences, 13, 675–690, https://doi.org/10.5194/bg-13-675-
4244 2016, 2016.

4245 Zaehle, S., Ciais, P., Friend, A. D., and Prieur, V.: Carbon benefits of anthropogenic reactive nitrogen offset by
4246 nitrous oxide emissions, Nature Geosci, 4, 601–605, https://doi.org/10.1038/ngeo1207, 2011.

4247 Zaehle, S., Medlyn, B. E., De Kauwe, M. G., Walker, A. P., Dietze, M. C., Hickler, T., Luo, Y., Wang, Y.-P., El-
4248 Masri, B., Thornton, P., Jain, A., Wang, S., Warlind, D., Weng, E., Parton, W., Iversen, C. M., Gallet-Budynek, A.,
4249 McCarthy, H., Finzi, A., Hanson, P. J., Prentice, I. C., Oren, R., and Norby, R. J.: Evaluation of 11 terrestrial

https://doi.org/10.5194/essd-2026-895
Preprint. Discussion started: 10 November 2026
© Author(s) 2026. CC BY 4.0 License.



carbon–nitrogen cycle models against observations from two temperate Free-Air CO2 Enrichment studies, New Phytol., 202, 803–822, https://doi.org/10.1111/nph.12697, 2014.

Zeng, J., Iida, Y., Matsunaga, T., and Shirai, T.: Surface ocean CO2 concentration and air-sea flux estimate by machine learning with modelled variable trends, Front. Mar. Sci., 9, https://doi.org/10.3389/fmars.2022.989233, 2022.

Zhang, X., Liao, E., Lu, W., Wu, Z., Wang, G., Zhu, X., and Liang, S.: A surface ocean p CO2 product with improved representation of interannual variability using a vision transformer-based model, Earth Syst. Sci. Data, 17, 6071–6095, https://doi.org/10.5194/essd-17-6071-2025, 2025.

Zheng, B., Ciais, P., Chevallier, F., Chuvieco, E., Chen, Y., and Yang, H.: Increasing forest fire emissions despite the decline in global burned area, Sci. Adv., 7, eabh2646, https://doi.org/10.1126/sciadv.abh2646, 2021.

Zhu, Y., Xia, X., Canadell, J. G., Piao, S., Lu, X., Mishra, U., Wang, X., Yuan, W., and Qin, Z.: China's carbon sinks from land-use change underestimated, Nat. Clim. Chang., 15, 428–435, https://doi.org/10.1038/s41558-025-02296-z, 2025.

Zou, Y., Wang, Y., Ke, Z., Tian, H., Yang, J., and Liu, Y.: Development of a REgion-Specific Ecosystem Feedback Fire (RESFire) Model in the Community Earth System Model, J. Adv. Model. Earth Syst., 11, 417–445, https://doi.org/10.1029/2018MS001368, 2019.

Zscheischler, J., Mahecha, M. D., Avitabile, V., Calle, L., Carvalhais, N., Ciais, P., Gans, F., Gruber, N., Hartmann, J., Herold, M., Ichii, K., Jung, M., Landschützer, P., Laruelle, G. G., Lauerwald, R., Papale, D., Peylin, P., Poulter, B., Ray, D., Regnier, P., Rödenbeck, C., Roman-Cuesta, R. M., Schwalm, C., Tramontana, G., Tyukavina, A., Valentini, R., van der Werf, G., West, T. O., Wolf, J. E., and Reichstein, M.: Reviews and syntheses: An empirical spatiotemporal description of the global surface–atmosphere carbon fluxes: opportunities and data limitations, Biogeosciences, 14, 3685–3703, https://doi.org/10.5194/bg-14-3685-2017, 2017.

https://doi.org/10.5194/essd-2026-895
Preprint. Discussion started: 10 November 2026
© Author(s) 2026. CC BY 4.0 License.



4274 **Tables**

4275

4276 **Table 1.** Factors used to convert carbon in various units (by convention, Unit 1 = Unit 2 × conversion).

Unit 1	Unit 2	Conversion	Source
GtC (gigatonnes of carbon)	ppm (parts per million) (a)	2.124 (b)	Ballantyne et al. (2012)
GtC (gigatonnes of carbon)	PgC (petagrams of carbon)	1	SI unit conversion
GtCO2 (gigatonnes of carbon dioxide)	GtC (gigatonnes of carbon)	3.664	44.01/12.011 in mass equivalent
(a) Measurements of atmospheric CO_2 concentration have units of dry-air mole fraction. 'ppm' is an abbreviation for micromole/mol, dry air.			
(b) The use of a factor of 2.124 assumes that all the atmosphere is well mixed within one year. In reality, only the troposphere is well mixed and the growth rate of CO_2 concentration in the less well-mixed stratosphere is not measured by sites from the NOAA network. Using a factor of 2.124 makes the approximation that the growth rate of CO_2 concentration in the stratosphere equals that of the troposphere on a yearly basis.			

4277

https://doi.org/10.5194/essd-2026-895
Preprint. Discussion started: 10 November 2026
© Author(s) 2026. CC BY 4.0 License.



4278 **Table 2.** How to cite the individual components of the global carbon budget presented here.

Component	Primary reference
Global and national fossil CO2 emissions (EFOS), total and by fuel type	This paper and Andrew and Peters (2026)
National consumption-based fossil CO2 emissions (EFOS) by country (consumption)	Peters et al. (2011) updated as described in this paper
Net land-use change flux (ELUC)	This paper and Schwingshackl et al. (2026); see also Table 4 for individual model references
Growth rate in atmospheric CO2 concentration (GATM)	Lan et al. (2026), Pandey et al (2024)
Atmospheric inversions	This paper and Naus et al (2026); see also Table 4 for individual model references
Ocean CO2 sinks (SOCEAN)	This paper and Hauck et al (2026); see also Table 4 for individual model and data products references
Land CO2 sinks (SLAND)	This paper and O'Sullivan et al (2026a); see also Table 4 for individual model references

4279

https://doi.org/10.5194/essd-2026-895
Preprint. Discussion started: 10 November 2026
© Author(s) 2026. CC BY 4.0 License.



Open Access Earth System Science Data Discussions

4280 **Table 3.** Main methodological changes in the global carbon budget this year (GCB2026). Empty cells mean
4281 there were no methodological changes introduced that year. Table S10 lists methodological changes from the
4282 first global carbon budget publication up to 2025.

Fossil fuel emissions		**LUC emissions**	**Reservoirs**			**Other changes**
Global	Country (territorial)		Atmosphere	Ocean	Land	
	Canada: Added emissions from historical (1923-1989) lime production USA: Switched to NIR published by Center for Global Sustainability at the University of Maryland Argentina: Added pre-1950 oil trade	Component 'other transitions' split into contributions from clearing and (re-)growth of shrub and herbaceous vegetation and from transitions between cropland, pasture, and urban areas. Update in land-use data (HYDE3.6). Update to GFED5 for fire emissions.	Satellite-based growth rate (GRESO) now uses combined GOSAT and OCO-2 retrievals from 2010 onward.	Updated ocean uncertainty estimate. Accounting for pre-industrial (natural steady state) carbon fluxes in fCO2-products and inversions to determine SOCEAN regionally.	Include the δL adjustment. Extended evaluation for DGVMs.	

4283

https://doi.org/10.5194/essd-2026-895
Preprint. Discussion started: 10 November 2026
© Author(s) 2026. CC BY 4.0 License.



4284 **Table 4.** References for the process models, bookkeeping models, ocean data products, and atmospheric
4285 inversions. All models and products are updated with new data to the end of year 2025.

Model/data name	Reference	Change from Global Carbon Budget 2025 (Friedlingstein et al., 2026a)
Bookkeeping models for land-use change emissions		
BLUE	Hansis et al. (2015)	No change
OSCAR	Gasser et al. (2020)	No change
LUCE	Qin et al. (2024)	No change
Dynamic global vegetation models		
CABLE-POP	Haverd et al. (2018)	No change
CLASSIC	Melton et al. (2020), Kou-Giesbrecht and Arora (2022), Gauthier et al. (2025)	Compared to TRENDY 2025, exponential distribution of saturated hydraulic conductivity with depth is turned on, and dry surface layer parameterization which reduces soil evaporation is turned off.
CLM-FATES	Fisher et al. (2015), Koven et al. (2020)	Updated parameters
CLM6.0	Lawrence et al. (2019)	Parameter updates, new wetland scheme
DLEM	Tian et al. (2015), You et al. (2022)	No change
E3SM	Yang et al.(2023), Burrows et al.(2020)	No change
EDv3	Moorcroft et al. (2001), Ma et al. (2022)	Recalibrated fire submodule
GDSTEM	Felzer et al. (2009), Felzer et al. (2011), Felzer (2012), Felzer and Jiang (2018)	No change
IBIS	Xia et al., (2024)	No change
iMAPLE	Yue et al. (2024)	No change.
IQJ	Thum et al. (2019)	Include representation of agriculture, pasture and sylviculture (wood harvest), land-use change as well as update to fully consistent treatment of physical processes as in the JSBACH model + representation of skin surface temperature, update of model parameters
ISAM	Jain et al. (2013), Meiyappan et al. (2015), Shu et al. (2020)	Vertically resolved soil biogeochemistry (carbon and nitrogen) module, following Shu et al. (2020)
ISBA-CTRIP	Delire et al. (2020); Decharme et al. (2019)	no change wrt 2024 contribution

https://doi.org/10.5194/essd-2026-895
Preprint. Discussion started: 10 November 2026
© Author(s) 2026. CC BY 4.0 License.



JSBACH	Mauritsen et al. (2019), Reick et al. (2021)	No change
JULES	Wiltshire et al. (2021), Sellar et al. (2019), Burton et al. (2019)	No change.
LPJ-EOSIM	Poulter et al. (2011) (d)	Used original implementation of respiration temperature response, with no acclimation
LPJ-GUESS	Smith et al. (2014)	Correction in the Burned Area Fraction estimation method to eliminate land cover adjustment during post-processing
LPJmL	Schaphoff et al. (2018), von Bloh et al. (2018), Lutz et al., (2019), Heinke et al. (2023), Heinke et al. (2026)	Updated livestock density input
LPX-Bern	Lienert and Joos (2018)	No change
ORCHIDEEv4	Naudts et al. (2015), Vuichard et al. (2019)	Switch from v3.0 to v4.3.1 incorporating new albedo scheme, forest demography, forest management, soil insulation, biogeochemistry of permafrost, vertical discretisation of snow and ice, and updating river routing and model parameters.
SDGVM	Woodward and Lomas (2004), Walker et al. (2017)	No change
VISIT	Ito and Inatomi (2012), Kato et al. (2013)	Improve wood harvesting process. Revised the LAI accounting processes.
VISIT-UT	Ito (2019)	Refinement of carbon mass balance including revision of land-use emissions. Additional parameter calibration.
Intermediate complexity land carbon cycle model		
CARDAMOM	Bloom et al. (2016), Smallman et al. (2021)	Linear AGB trend from CCI Biomass (v6) added as additional constraint. Maximum rooting depth prior added (Fan et al., 2017). Extended to 2025
Global ocean biogeochemistry models		
NEMO-PlankTOM12	Wright et all (2021)	model physics version switch from NEMO3.6 to NEMO5.0, update of biogeochemical tuning to Wright et al (in prep), temperature correction to ERA5 atmospheric forcing
NEMO4.2-PISCES (IPSL)	Aumont et al. (2015)	No change
MICOM-HAMOCC (NorESM1-OCv1.2)	Schwinger et al. (2016)	No change
MPIOM-HAMOCC6	Lacroix et al. (2021)	No change

https://doi.org/10.5194/essd-2026-895
Preprint. Discussion started: 10 November 2026
© Author(s) 2026. CC BY 4.0 License.



NEMO4.2.3-PISCESv2-gas (CNRM)	Séférian et al. (2019), Madec et al. (2023)	Ocean model version has been updated from NEMO 3.6 to NEMO 4.2.3 (Madec et al 2023) and an improved mesoscale parameterization (Torres et al, 2025) has been activated. PISCESv2-gas remains unchanged and is described in Séférian et al (2019). Forcings have been switched to ERA5 (instead of JRA55-do). Spin-up (1848-1958) has been re-run with ERA5 based on a 10-years loop (1959-1968). A,B,C,D simulations have been re-run with ERA5, starting from the new ERA5 spin-up (i.e. from 1850 onwards).
FESOM2.7-REcoM3	Gürses et al. (2023)	Updated physical model version from FESOM2.1 to 2.7. A third zooplankton group and ballasting routines are added in REcoM. ERA5 is used for spin-up and simulations A, B C, D are started from this spinup.
MOM6-COBALTv3 (Princeton)	Stock et al., (2025)	Updated configuraton of MOM6-COBALTv3 with ~0.5° horizontal resolution (720x576)
CESM-ETHZ	Doney et al. (2009)	No change.
MRI-ESM2-4	Tsujino et al. (2026)	No change.
ACCESS (CSIRO)	Law et al. (2017)	Minor changes in model since 2025 submission: reduced the timescale for surface salinity restoring from 60 to 30 days and provided SF6 output. Extended the spinup another 200+ years.
fCO2-products		
VLIZ-SOMFFN	Landschützer et al. (2016)	Time period extended to 2025
Jena-MLS	Rödenbeck et al. (2014) updated to Rödenbeck et al (2022)	Time period extended to 2025; replaced prior based on OCIM by an adjustable trend in the ocean-interior sources/sinks; some small technical corrections
CMEMS-LSCE-FFNNv2	Chau et al. (2022) and Chau et al. (2024)	Time period extended to 2025
UExP-FNN-U	Watson et al. (2020) and Ford et al. (2024)	Updated to recalculated SOCATv2026 dataset (Ford et al. 2026b). Updated SOM to a probability based approach. Adds chlorophyll-a as predictor in FNN stage. Updates NOAA-COARE to v3.6. Updated time period to 1980 to 2025
NIES-ML3	Zeng et al. (2022)	Time period extended to 2025.
JMA-MLR	Iida et al. (2021)	Time period extended to 2025. Updated to recalculated SOCATv2026 dataset (Ford et al. 2026b)
OceanSODA-ETHZv2	Gregor et al. (2024)	Time period extended to 2025. High latitude winter chloropyll values set to 0 instead of filling with interpolated values.

https://doi.org/10.5194/essd-2026-895
Preprint. Discussion started: 10 November 2026
© Author(s) 2026. CC BY 4.0 License.



LDEO-HPD	Gloege et al. (2022) and Bennington et al. (2022)	Time period extended to 2025
AOML-ET	Wanninkhof et al. (2025)	New product for GCB 2026. The published AOML-ET framework was updated to a hybrid GAM + two-stage Extremely Randomized Trees architecture, trained with SOCATv2026 recalculated fCO2 and extended to 1982-2025.
SJTU-AVIT	Zhang et al. (2025)	Time period extended to 2025. Method unchanged from Zhang et al. (2025).
Ocean interior product		
Ocean inverse model OCIM-48L	Holzer et al. (2019), DeVries (2022)	New this year
Atmospheric inversions		
CarboScope	Rödenbeck et al. (2018) & Stephens et al. (2007).	Slight change in station set. Update of the prior fluxes and assimilated observations.
CarbonTracker Europe (CTE-insitu)	van der Laan-Luijkx et al. (2017), van den Berg et al (2026), Stroo et al (2026)	Changed statevector (split temporal domain), in-situ data only in 2nd step for land-fluxes with 3-day filter. Transport model at 1x1 degrees globally. Data selection expanded to use more sites
CarbonTracker Europe (CTE-satellite)	van der Laan-Luijkx et al. (2017), van den Berg et al (2026), Stroo et al (2026)	Same as above, but with only OCO2 column data in 2nd step with 2x5-day smoother
NISMON-CO2	Niwa et al. (2022), Niwa et al. (2017).	Used climatological mean flux for land, derived from NISMON-CO2_SRF ver.2025.1. Vertical structure switched from 40 terrain following layers to 78 hybrid layers. Meteorological data prepared by NICAM were nudged by UV & T (previously, only UV).
CT-NOAA	Jacobson et al. (2026), Byrne et al. (2023), Krol et al. (2005)	Switch to mean of two inversions with different sets of priors. Revision of fossil fuel emissions. New land and wildfire priors. Revised air-sea gas exchange including two new pCO2 prior models. A new Kalman filer time-propagation model. Physical parallelization of the analysis period.
CMS-Flux	Liu et al. (2021)	Update of prior fluxes and assimilated observations.

https://doi.org/10.5194/essd-2026-895
Preprint. Discussion started: 10 November 2026
© Author(s) 2026. CC BY 4.0 License.



CAMS-Insitu	Chevallier et al. (2005) and Chevallier et al. (2025)	Update of the prior fluxes and assimilated observations.
CAMS-Satellite	Chevallier et al. (2005) and Chevallier et al. (2025)	Update of the prior fluxes and assimilated observations.
GONGGA	Jin et al. (2024)	Update of the prior fluxes and assimilated observations.
COLA	Liu et al. (2022)	Update of the prior fluxes and assimilated observations.
GCASv2	Jiang et al. (2021) & Emmons et al. (2010)	Update of the prior fluxes and assimilated observations.
UoE	Feng et al. (2016) & Palmer et al. (2019)	Update of the prior fluxes and assimilated observations.
NTFVAR	Nayagam et al. (2025) & Maksyutov et al. (2021)	Update of prior fluxes and assimilated observations.
THU	Kong et al. (2022)	New this year, after missing out 1 year. Compared to the previous submission: update of prior fluxes and assimilated observations.
NISMON-CO2_GOSAT	Niwa et al. (2022), Niwa et al. (2017), Maity et al. (2026)	Used climatological mean flux for land, derived from NISMON-CO2_SRF ver.2025.1. GOSAT NIES ver.0305 retrievals over land assimilated.
YanDong	Su et al (2024) & Nassar et al. (2010)	First submission.
Earth System Models		
CanESM5	Swart et al. (2019), Sospedra-Alfonso et al. (2021)	No change
EC-Earth3-CC	Döscher et al. (2021), Bilbao et al. (2021), Bernardello et al. (2024)	No change
IPSL-CM6A-CO2-LR	Boucher et al. (2020)	No change
MIROC-ES2L	Watanabe et al. (2020)	No change
MPI-ESM1-2-LR	Mauritsen et al. (2019), Li et al. (2023)	No change
NorCPM-CC	Tjiputra et al. (2020), Bethke et al. (2021)	No change

https://doi.org/10.5194/essd-2026-895
Preprint. Discussion started: 10 November 2026
© Author(s) 2026. CC BY 4.0 License.



Open Access Earth System Science Data Discussions

Table 5. Comparison of results from the bookkeeping method and budget residuals with results from the DGVMs, as well as additional estimates from atmospheric oxygen, atmospheric inversions and Earth System Models (ESMs) for different periods, the last decade, and the last year available. All values are in GtC yr^{-1}. The best estimate for GCB2026 (E_{LUC}) is calculated with the bookkeeping models (1a) and used in the budget Table 7, see Section 2 and Figure 7 for description of the bookkeeping component fluxes. The best estimate for GCB2026 (S_{LAND}) is calculated with the DGVMs including the δL adjustment (2b), and used in the budget Table 7. The DGVM uncertainties represent ±1σ of the decadal or annual (for 2025) estimates from the individual DGVMs. For the inverse systems the mean and range of available results is given when the number of systems is less than 10, otherwise the ±1σ is provided. All values are rounded to the nearest 0.1 GtC.

Mean (GtC/yr)

		1960s	1970s	1980s	1990s	2000s	2010s	2016-2025	2025
Land-use change emissions (E_{LUC})	Bookkeeping (BK) Net flux (1a)	1.8±0.7	1.7±0.7	1.6±0.7	1.8±0.7	1.7±0.7	1.6±0.7	1.3±0.7	1.2±0.7
	BK - deforestation and clearing of other vegetation (total)	2.3 [2,2.7]	2.2 [2,2.5]	2.1 [2,2.3]	2.3 [2.1,2.5]	2.4 [2.1,2.6]	2.4 [2.1,2.6]	2.2 [1.9,2.5]	2.1 [1.8,2.5]
	BK - (re-)growth of forest and other vegetation (total)	-1.1 [-1.3,-0.8]	-1.1 [-1.3,-0.9]	-1.1 [-1.3,-0.9]	-1.3 [-1.4,-1.1]	-1.4 [-1.6,-1.3]	-1.6 [-1.8,-1.4]	-1.6 [-1.8,-1.4]	-1.6 [-1.7,-1.4]
	BK - cropland–pasture–urban transitions	0 [0,0]	0 [0,0]	0 [0,0]	0 [0,0]	0 [0,0.1]	0.1 [0.1,0.1]	0.1 [0,0.1]	0 [0,0]
	BK - peat drainage & peat fires	0.2 [0.1,0.2]	0.2 [0.1,0.2]	0.2 [0.2,0.3]	0.3 [0.3,0.4]	0.3 [0.2,0.3]	0.3 [0.3,0.3]	0.2 [0.2,0.3]	0.2 [0.2,0.3]
	BK - wood harvest & other management	0.4 [0.1,0.6]	0.4 [0.1,0.6]	0.5 [0.1,0.6]	0.5 [0.1,0.7]	0.4 [0.1,0.6]	0.4 [0.1,0.7]	0.4 [0.1,0.7]	0.4 [0.1,0.7]
	DGVMs-net flux (1b)†	1.5±0.4	1.3±0.4	1.2±0.4	1.3±0.3	1.3±0.3	1.2±0.3	1±0.3	0.9±0.3
Terrestrial sink (S_{LAND})	Residual sink from global budget (E_{FOS}+E_{LUC}(1a)-G_{ATM}-S_{OCEAN}) (2a)	1.8±0.8	1.9±0.8	1.7±0.9	2.8±0.9	3.0±0.9	3.3±0.9	2.9±0.9	4.1±1
	DGVMs (2b)†+	1.0±0.3	1.7±0.5	1.5±0.5	2±0.4	2.3±0.4	2.6±0.6	2.5±0.7	3.6±0.9
Net land fluxes (S_{LAND}-E_{LUC})	GCB2026 Budget (2b-1a)	-0.8±0.8	0±0.9	-0.2±0.9	0.2±0.8	0.6±0.8	0.9±0.9	1.2±1	2.4±1.1
	Atmospheric O_2	---	---	---	1.3±0.6	0.9±0.7	1.0±0.8	0.7±0.8	-

https://doi.org/10.5194/essd-2026-895
Preprint. Discussion started: 10 November 2026
© Author(s) 2026. CC BY 4.0 License.



		1960s	1970s	1980s	1990s	2000s	2010s	2016-2025	2025
	DGVMs-net (2b-1b)[+]	-0.4±0.5	0.4±0.6	0.2±0.5	0.7±0.4	0.9±0.3	1.3±0.5	1.5±0.6	2.7±0.9
	Inversions[*]	- [-,-]	- [-,-]	0.4 [0.1,0.7] (2)	0.8 [0.6,1.2] (3)	1.4 [1.2,1.6] (4)	1.5 [1.3,1.9] (8)	1.5±0.3 (16)	3±0.6 (16)
	ESMs	0 [-0.7,0.5]	1.5 [1.2,2]	1.1 [0.5,1.4]	1.8 [1.2,2.4]	1.8 [0.4,2.7]	2 [0.7,3]	2.4 [-0.4,3.9]	3.5 [0.1-4.9]

[†]The mean DGVM estimates for S_{LAND} and E_{LUC} are adjusted by δL (estimated by the bookkeeping models), which represents the interaction between land-use change and changing environmental conditions, excluding the direct land-use change effect. See Section S.4.1 for details.

[+]The mean DGVM estimate of S_{LAND} is further reduced by 0.07 GtC/yr to account for the lateral carbon (LOAC) flux for 2016-2025 and for 2025.

[*]Estimates are adjusted for the pre-industrial influence of river fluxes, for the cement carbonation sink, and adjusted to common E_{FOS} (Sect. 2.7). The ranges given include varying numbers (in parentheses) of inversions in each decade (Table S4)

https://doi.org/10.5194/essd-2026-895
Preprint. Discussion started: 10 November 2026
© Author(s) 2026. CC BY 4.0 License.



Open Access Earth System Science Data Discussions

Table 6: Comparison of results for the ocean sinks from the fCO_2-products (without warm layer/cool skin correction), from global ocean biogeochemistry models (GOBMs), the best estimate for GCB2026 (adjusted S_{OCEAN}) calculated from fCO_2-products and GOBMs and used in the budget Table 7, as well as additional estimates from ocean interior observation-based changes in the dissolved inorganic carbon (DIC) inventory, atmospheric oxygen, atmospheric inversions and Earth System Models (ESMs) for different periods, the last decade, and the last year available. All values are in GtC yr^{-1}. Uncertainties represent ±1σ of the estimates from the GOBMs and inversions (n>10) and range of ensemble members is given for ensembles with n<10 (inversions prior to 2015, ocean interior, ESMs). The uncertainty of the GCB2026 S_{OCEAN} estimate is based on expert judgement (Section 2.5 and Supplement S3) and for oxygen it is the standard deviation of a Monte Carlo ensemble (Section 2.8). Note that river flux adjustments were applied to the fCO_2-products and two of the ocean interior estimates to match the definition of S_{OCEAN}, and the ocean interior estimates from Müller et al. (2023) were scaled to the closest full decade in proportion to the atmospheric CO_2 increase (see section 2.5.1 and S3.6).

Mean (GtC/yr)

Product	1960s	1970s	1980s	1990s	2000s	2010s	2016-2025	2025
GCB2026 Budget	1.3±0.4	1.6±0.4	2±0.4	2.3±0.4	2.4±0.4	2.9±0.4	3±0.4	3.2±0.4
fCO_2-products	---	---	---	2.4 [2,3]	2.6 [2.3,3]	3.1 [2.7,3.4]	3.3 [2.8,3.9]	3.4 [2.6,4.2]
GOBMs	1.1±0.2	1.3±0.2	1.7±0.2	2±0.2	2.2±0.3	2.5±0.3	2.7±0.3	2.9±0.4
Atmospheric O_2	---	---	---	2±0.4	2.8±0.4	3.4±0.5	3.5±0.5	-
Inversions	- [-,-]	- [-,-]	1.7 [1.4,2.1] (2)	2.3 [1.9,2.6] (3)	2.3 [2.1,2.5] (4)	2.9 [2.6,3.1] (8)	3.1±0.3 (16)	3.3±0.4 (16)
Ocean interior	1.1 [-,-]	1.4 [-,-]	1.8 [-,-]	2.2 [2.1,2.3]	2.4 [2.3,2.5]	3.0 [2.7,3.4]	2.9 [-,-]	3.0[-,-]
ESMs	0.7 [0.1,1.1]	1 [0.4,1.4]	1.5 [0.7,2]	1.8 [1.1,2.1]	1.9 [1.5,2.2]	2.4 [2,2.8]	2.5 [2.3,3]	2.7 [2.4-3.1]

https://doi.org/10.5194/essd-2026-895
Preprint. Discussion started: 10 November 2026
© Author(s) 2026. CC BY 4.0 License.



Open Access Earth System Science Data Discussions

Table 7: Decadal mean in the five components of the anthropogenic CO_2 budget for different periods, and last year available. All values are in GtC yr^{-1}, and uncertainties are reported as ±1σ. Fossil CO_2 emissions include cement carbonation. The table also shows the budget imbalance (B_{IM}), which provides a measure of the discrepancies among the nearly independent estimates. A positive imbalance means the emissions are overestimated and/or the sinks are too small. All values are rounded to the nearest 0.1 GtC and therefore columns do not necessarily add to zero.

Mean (GtC/yr)

		1960s	1970s	1980s	1990s	2000s	2010s	2016-2025	2025	2026 (Projection)
Total emissions (EFOS + ELUC)	Fossil CO2 emissions (EFOS)*	3±0.2	4.6±0.2	5.4±0.3	6.4±0.3	7.8±0.4	9.5±0.5	10±0.5	10.5±0.5	10.4±0.5
	Land-use change emissions (ELUC)	1.8±0.7	1.7±0.7	1.6±0.7	1.8±0.7	1.7±0.7	1.6±0.7	1.3±0.7	1.2±0.7	1.4±0.7
	Total emissions	4.9±0.7	6.3±0.7	7.1±0.8	8.2±0.8	9.5±0.8	11.2±0.8	11.3±0.9	11.7±0.9	11.8±0.9
Partitioning	Growth rate in atmos CO2 (GATM)	1.7±0.07	2.8±0.07	3.4±0.02	3.1±0.02	4±0.02	5.1±0.02	5.4±0.02	4.4±0.2	4.6±0.8
	Ocean sink (SOCEAN)	1.3±0.5	1.6±0.6	2±0.6	2.3±0.6	2.4±0.6	2.9±0.6	3.0±0.6	3.2±0.7	3.1±0.7
	Terrestrial sink (SLAND)	1±0.3	1.7±0.5	1.5±0.5	2±0.4	2.3±0.4	2.6±0.6	2.5±0.7	3.6±0.9	4.1±1.4
Budget	BIM= EFOS +ELU	0.8	0.3	0.2	0.8	0.7	0.7	0.4	0.5	

https://doi.org/10.5194/essd-2026-895
Preprint. Discussion started: 10 November 2026
© Author(s) 2026. CC BY 4.0 License.



		1960s	1970s	1980s	1990s	2000s	2010s	2016-2025	2025	2026 (Projection)
Imbalance	C-(GATM+SOCEAN+SLAND)									

*Fossil emissions excluding the cement carbonation sink amount to 3.1±0.2 GtC/yr, 4.7±0.2 GtC/yr, 5.5±0.3 GtC/yr, 6.4±0.3 GtC/yr, 7.9±0.4 GtC/yr, 9.7±0.5 GtC/yr, and 10.1±0.5 GtC/yr for the decades 1960s to 2016-2025 respectively and to 10.6±0.5 GtC/yr for 2025, and 10.6±0.2 GtC/yr for 2026.

4320
4321

https://doi.org/10.5194/essd-2026-895
Preprint. Discussion started: 10 November 2026
© Author(s) 2026. CC BY 4.0 License.



Table 8. Cumulative CO_2 for different time periods in gigatonnes of carbon (GtC). Fossil CO_2 emissions include cement carbonation. The budget imbalance (B_{IM}) provides a measure of the discrepancies among the nearly independent estimates. All values are rounded to the nearest 5 GtC and therefore columns do not necessarily add to zero. Uncertainties are reported as follows: E_{FOS} is 5% of cumulative emissions; E_{LUC} pre-1959 is 1σ spread from the DGVMs, E_{LUC} post-1959 is 0.7*number of years (where 0.7 GtC yr^{-1} is the uncertainty on the annual E_{LUC} flux estimate); G_{ATM} uncertainty is held constant at 5 GtC for all time periods; S_{OCEAN} uncertainty is calculated as the sum of annual uncertainties, assuming errors are fully correlated through time. Annual uncertainties combine the ensemble spread of GOBMs and fCO_2-products, their mean differences, and systematic uncertainties (see Supplement S3.5); prior to 1959, a relative uncertainty of 30% was applied (see Supplement S.3.1). S_{LAND} is the 1σ spread from the DGVMs estimates.

Mean (GtC yr^{-1})

		1750-2025	1850-2021	1850-2025	1959-2025	1850-2026
Emissions	Fossil CO2 emissions (EFOS)	510±25	470±25	510±25	430±20	520±25
	Land-use change emissions (ELUC)	275±55	240±50	245±50	110±45	245±50
	Total emissions	785±60	710±55	755±55	545±50	765±55
Partitioning	Growth rate in atmos CO2 (GATM)	315±5	275±5	295±5	235±5	300±5
	Ocean sink (SOCEAN)	210±60	185±50	200±55	145±40	200±55
	Terrestrial sink (SLAND)	210±45	180±40	190±40	125±30	195±40
Budget imbalance	BIM=EFOS +ELUC-(GATM+SOCEAN+SLAND)	50	70	70	40	70

https://doi.org/10.5194/essd-2026-895
Preprint. Discussion started: 10 November 2026
© Author(s) 2026. CC BY 4.0 License.



Open Access Earth System Science Data Discussions

4338

https://doi.org/10.5194/essd-2026-895
Preprint. Discussion started: 10 November 2026
© Author(s) 2026. CC BY 4.0 License.



Table 9. Average annual growth rate in fossil CO_2 emissions over the most recent decade (2016-2025) and the previous decade (2006-2015). The data for the World include the cement carbonation sink. IAS are emissions from international aviation and shipping. The rest of the world is defined as World minus China, USA, India, EU27, and IAS.

	World	China	USA	India	EU27	OECD	Non-OECD	IAS	Rest of the World
2006-2015	1.9 %	5.6 %	-1.4 %	6.3 %	-2.3 %	-1.0 %	4.1 %	1.7 %	1.6 %
2016-2025	0.9 %	2.7 %	-0.8 %	3.5 %	-2.9 %	-1.4 %	2.1 %	-0.6 %	0.4 %

https://doi.org/10.5194/essd-2026-895
Preprint. Discussion started: 10 November 2026
© Author(s) 2026. CC BY 4.0 License.



Open Access Earth System Science Data Discussions

4345 **Table 10.** Major known sources of uncertainties in each component of the Global Carbon Budget, defined as
4346 input data or processes that have a demonstrated effect of at least ±0.3 GtC yr^{-1}.

Source of uncertainty	Time scale (years)	Location	Evidence
Fossil CO2 emissions (EFOS; Section 2.1)			
energy statistics	annual to decadal	global, but mainly China & major developing countries	(Korsbakken et al., 2016, Guan et al., 2012)
carbon content of coal	annual to decadal	global, but mainly China & major developing countries	(Liu et al., 2015)
system boundary	annual to decadal	all countries	(Andrew, 2020a)
Net land-use change flux (ELUC; section 2.2)			
land-cover and land-use change statistics	continuous	global; in particular tropics	(Houghton et al., 2012, Gasser et al., 2020, Ganzenmüller et al., 2022, Yu et al. 2022)
sub-grid-scale transitions	annual to decadal	global	(Wilkenskjeld et al., 2014, Bastos et al., 2021)
vegetation biomass	annual to decadal	global; in particular tropics	(Houghton et al., 2012, Bastos et al., 2021)
forest degradation (fire, selective logging)	annual to decadal	tropics; Amazon	(Aragão et al., 2018, Qin et al., 2021, Lapola et al., 2023)
wood and crop harvest	annual to decadal	global; SE Asia	(Arneth et al., 2017, Erb et al., 2018)
peat burning	multi-decadal trend	global	(van der Werf et al., 2010, 2017, 2025)

https://doi.org/10.5194/essd-2026-895
Preprint. Discussion started: 10 November 2026
© Author(s) 2026. CC BY 4.0 License.



Atmospheric growth rate (GATM; section 2.4) no demonstrated uncertainties larger than ±0.3 GtC yr-1 . The uncertainties in annual GATM have been estimated as ±0.2 GtC yr-1, although the conversion of the growth rate into a global annual flux assuming instantaneous mixing throughout the atmosphere introduces additional errors (see Section 2.4.2).			
Ocean sink (SOCEAN; section 2.5)			
sparsity in surface fCO2 observations	mean, decadal variability and trend	global, in particular southern hemisphere	(Gloege et al., 2021, Denvil-Sommer et al., 2021, Hauck et al., 2023a; Dong et al., 2024b, Roobaert et al 2026)
riverine carbon outgassing and its anthropogenic perturbation	annual to decadal	global, in particular partitioning between Tropics and South	(Aumont et al., 2001, Lacroix et al., 2020, Crisp et al., 2022)
Discrepancy between interior ocean anthropogenic carbon storage from models and observation-based estimates	annual to decadal	global	(Friedlingstein et al., 2022a, this study, DeVries et al., 2023, Müller et al., 2023)
near-surface temperature and salinity gradients	mean on all time-scales	global	(Watson et al., 2020, Dong et al., 2022, Bellenger et al., 2023, Dong et al., 2024a, Ford et al 2024)
Land sink (SLAND; section 2.6)			
strength of CO2 fertilisation	multi-decadal trend	global	(Wenzel et al., 2016; Walker et al., 2021; Norby et al., 2025))
response to variability in temperature and rainfall	annual to decadal	global; in particular tropics	(Cox et al., 2013; Jung et al., 2017; Humphrey et al., 2018; 2021)
nutrient limitation and supply	annual to multi-decadal	global	(Zaehle et al., 2014)
carbon allocation and tissue turnover rates	annual to decadal	global	(De Kauwe et al., 2014; O'Sullivan et al., 2022)

https://doi.org/10.5194/essd-2026-895
Preprint. Discussion started: 10 November 2026
© Author(s) 2026. CC BY 4.0 License.

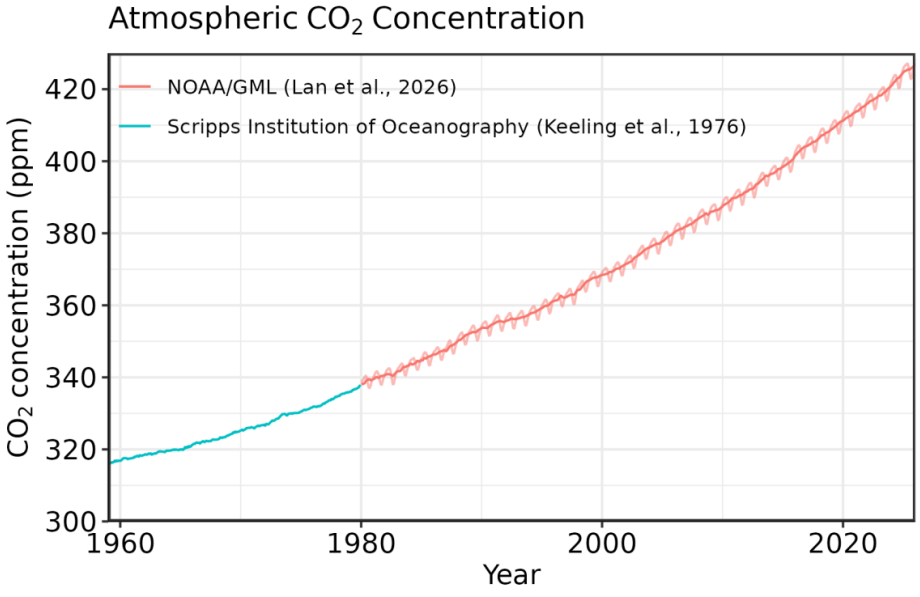


tree mortality	annual	global in particular tropics	(Hubau et al., 2020; Brienen et al., 2020)
response to diffuse radiation	annual	global	(Mercado et al., 2009; O'Sullivan et al., 2021)

4347

4348

4349 **Figures**



4350

https://doi.org/10.5194/essd-2026-895
Preprint. Discussion started: 10 November 2026
© Author(s) 2026. CC BY 4.0 License.



Open Access Earth System Science Data Discussions

4351 **Figure 1.** Surface average atmospheric CO_2 concentration (ppm). Since 1980, monthly data are from
4352 NOAA/GML (Lan et al., 2026) and are based on an average of direct atmospheric CO_2 measurements from
4353 multiple stations in the marine boundary layer (Masarie and Tans, 1995). The 1958-1979 monthly data are from
4354 the Scripps Institution of Oceanography, based on an average of direct atmospheric CO_2 measurements from the
4355 Mauna Loa and South Pole stations (Keeling et al., 1976). To account for the difference of mean CO_2 and
4356 seasonality between the NOAA/GML and the Scripps station networks used here, the Scripps surface average
4357 (from two stations) was de-seasonalised and adjusted to match the NOAA/GML surface average (from multiple
4358 stations) by adding the mean difference of 0.667 ppm, calculated here from overlapping data during 1980-2012.

4359

https://doi.org/10.5194/essd-2026-895
Preprint. Discussion started: 10 November 2026
© Author(s) 2026. CC BY 4.0 License.



Open Access Earth System Science Data Discussions

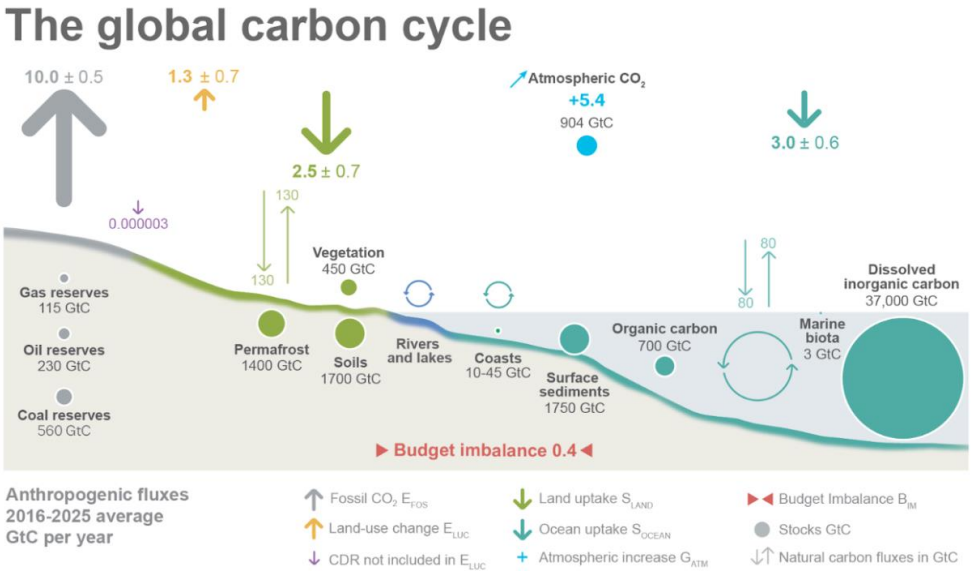


Figure 2. Schematic representation of the overall perturbation of the global carbon cycle caused by anthropogenic activities, averaged globally for the decade 2016-2025. See legends for the corresponding arrows. Fluxes estimates and their 1 standard deviation uncertainty are as reported in Table 7. The CDR estimate is for the year 2025. The uncertainty in the atmospheric CO_2 growth rate is very small (±0.02 GtC yr^{-1}) and is neglected for the figure. The anthropogenic perturbation occurs on top of an active carbon cycle, with fluxes and stocks represented in the background and taken from Canadell et al. (2021) for all numbers, except for the carbon stocks in coasts which is from a literature review of coastal marine sediments (Price and Warren, 2016). Fluxes are in GtC yr^{-1} and reservoirs in GtC. This figure was produced by Nigel Hawtin.

https://doi.org/10.5194/essd-2026-895
Preprint. Discussion started: 10 November 2026
© Author(s) 2026. CC BY 4.0 License.

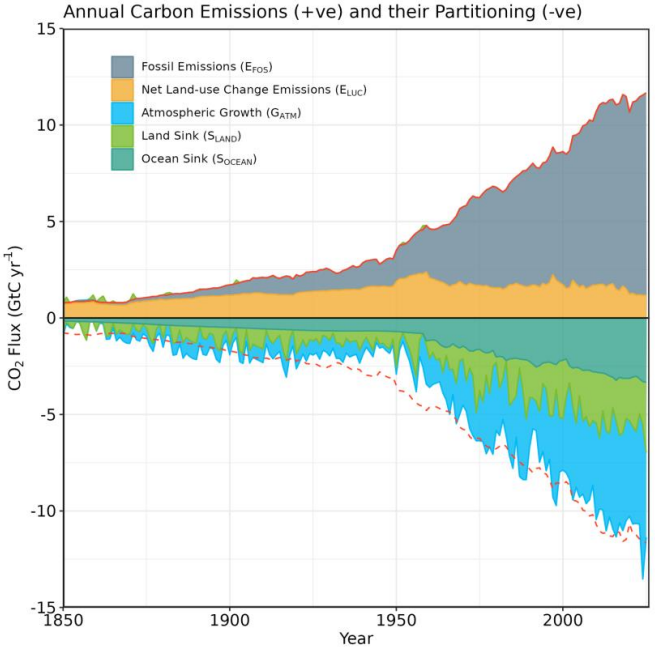
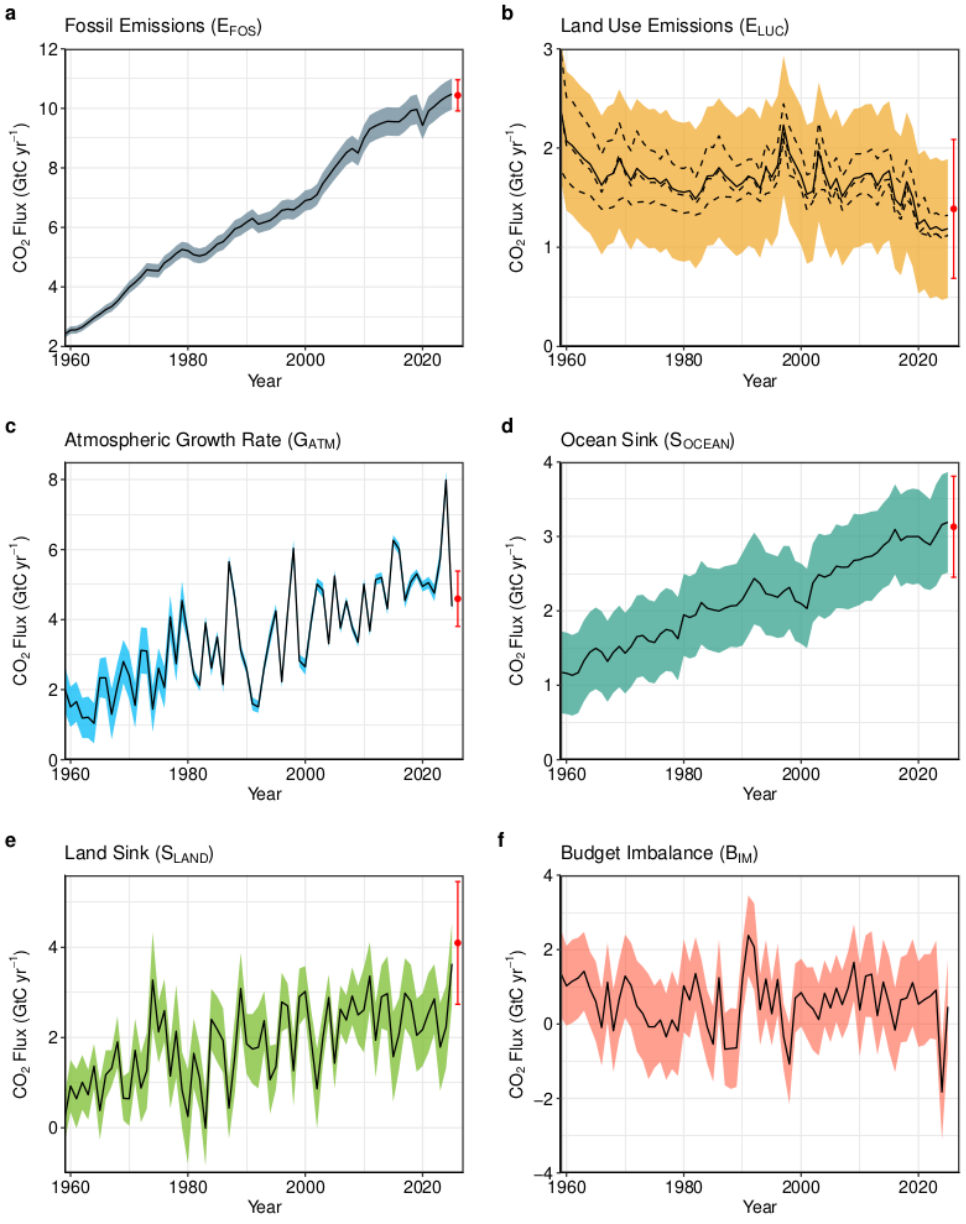


Figure 3. Combined components of the global carbon budget as a function of time, for fossil CO_2 emissions (E_{FOS}, including a small sink from cement carbonation; grey) and emissions from land-use change (E_{LUC}; brown), as well as their partitioning among the atmosphere (G_{ATM}; cyan), ocean (S_{OCEAN}; blue), and land (S_{LAND}; green). The figure shows annual estimates of each flux (in GtC yr^{-1}) since the year 1850. The partitioning is based on nearly independent estimates from observations (for G_{ATM}) and from process model ensembles constrained by data (for S_{OCEAN} and S_{LAND}) and does not exactly add up to the sum of the emissions, resulting in a budget imbalance (B_{IM}) which is represented by the difference between the bottom red line (mirroring total emissions) and the sum of carbon fluxes in the ocean, land, and atmosphere reservoirs. The E_{FOS} estimate is based on a mosaic of different datasets and has an uncertainty of ±5% (±1σ). The E_{LUC} estimate is from three bookkeeping models (Table 4) with uncertainty of ±0.7 GtC yr^{-1}. The G_{ATM} estimates prior to 1959 are from Joos and Spahni (2008) with uncertainties equivalent to about ±0.1-0.15 GtC yr^{-1} and from Lan et al. (2026) since 1959 with uncertainties of about +-0.07 GtC yr^{-1} during 1959-1979 and ±0.02 GtC yr^{-1} since 1980. The S_{OCEAN} estimate prior to 1959 is the average from Khatiwala et al. (2013) and DeVries (2014) with uncertainty of about ±30%. After 1959, it is the average of an ensemble of models (GOBMs) and an ensemble of *f*CO_2-products (with adjustments and corrections, Table 4) with uncertainties of about ±0.6 GtC yr^{-1} (see Supplement S.3.5). The S_{LAND} estimate is the average of an ensemble of models (DGVMs) (Table 4) with uncertainties of about ±1 GtC yr^{-1}. See the text for more details of each component and their uncertainties.

https://doi.org/10.5194/essd-2026-895
Preprint. Discussion started: 10 November 2026
© Author(s) 2026. CC BY 4.0 License.



4388

https://doi.org/10.5194/essd-2026-895
Preprint. Discussion started: 10 November 2026
© Author(s) 2026. CC BY 4.0 License.



Open Access Earth System Science Data Discussions

4389 **Figure 4.** Components of the global carbon budget and their uncertainties as a function of time, presented
4390 individually for (a) fossil CO_2, including cement carbonation emissions (E_{FOS}), (b) emissions from land-use
4391 change (E_{LUC}), (c) growth rate in atmospheric CO_2 concentration (G_{ATM}), (d) the ocean CO_2 sink (S_{OCEAN}), (e)
4392 the land CO_2 sink (S_{LAND}), (f) the budget imbalance (B_{IM}) that is not accounted for by the other terms. Individual
4393 estimates from the three bookkeeping models are shown as dashed lines for E_{LUC} in panel (b). Positive values of
4394 S_{LAND} and S_{OCEAN} represent a flux from the atmosphere to land or the ocean. All data are in GtC yr^{-1} with the
4395 uncertainty bounds representing ±1 standard deviation in shaded colour. Data sources are as in Figure 3. The red
4396 dots indicate our projections for the year 2026 and the red error bars the uncertainty in the 2026 projections (see
4397 methods).

4398

4399

4400

4401

4402

4403

4404

4405

4406

https://doi.org/10.5194/essd-2026-895
Preprint. Discussion started: 10 November 2026
© Author(s) 2026. CC BY 4.0 License.

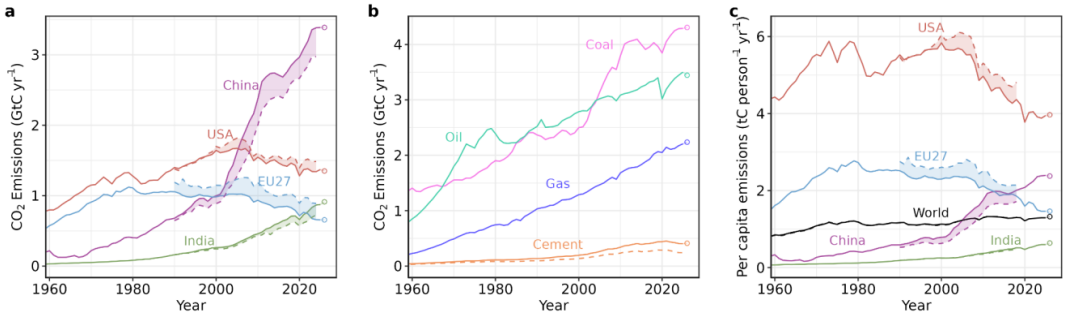


Figure 5. Fossil CO_2 emissions for (a) territorial (solid lines) and consumption (dashed lines) emissions for the top three country emitters (USA, China, India) and for the European Union (EU27), (b) global emissions by fuel type, including coal, oil, gas, and cement, and cement minus cement carbonation (dashed), and (c) per-capita emissions the world and for the large emitters as in panel (a). Territorial emissions are from Andrew & Peters (2026), while consumption-based emissions are updated from Peters et al. (2011). See Section 2.1 and Supplement S.1 for details of the calculations and data sources.

https://doi.org/10.5194/essd-2026-895
Preprint. Discussion started: 10 November 2026
© Author(s) 2026. CC BY 4.0 License.

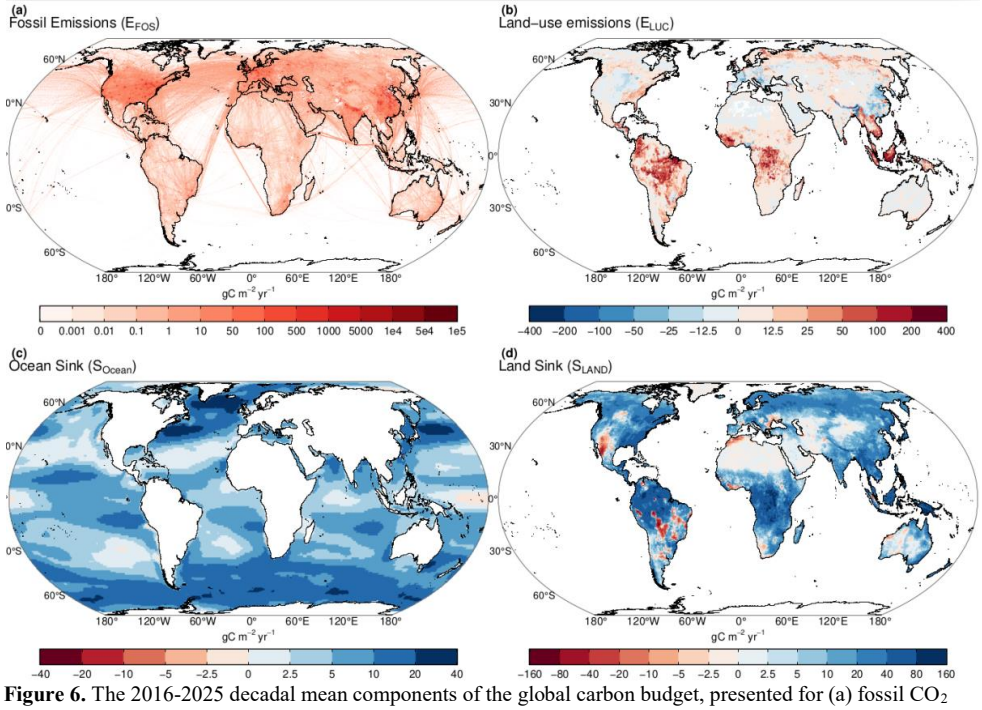


Figure 6. The 2016-2025 decadal mean components of the global carbon budget, presented for (a) fossil CO_2 emissions (E_{FOS}), (b) land-use change emissions (E_{LUC}), (c) the ocean CO_2 sink (S_{OCEAN}), and (d) the land CO_2 sink (S_{LAND}). Positive values for E_{FOS} and E_{LUC} represent a flux to the atmosphere, whereas positive values of S_{OCEAN} and S_{LAND} represent a flux from the atmosphere to the ocean or the land (carbon sink). In all panels, red colours represent a source (flux from the land/ocean to the atmosphere), blue colours represent a sink (flux from the atmosphere into the land/ocean). All units are in gC m^{-2} yr^{-1}. Note the different scales in each panel. E_{FOS} data shown is from GCP-GridFEDv2026.0 and does not include cement carbonation. The E_{LUC} map shows the average E_{LUC} from the three bookkeeping models plus emissions from peat drainage and peat fires. BLUE and LUCE provide spatially explicit estimates at 0.25° resolution. Gridded E_{LUC} estimates for OSCAR are derived by spatially distributing their national data based on the spatial patterns of BLUE gross fluxes in each country (see Schwingshackl et al., 2022). S_{OCEAN} is the anthropogenically perturbed atmosphere-ocean flux calculated from the GOBMs simulation A minus simulation B. S_{LAND} data shown is the average of the DGVM simulations S3-S4+S0+δL, where δL is estimated from the bookkeeping models.

https://doi.org/10.5194/essd-2026-895
Preprint. Discussion started: 10 November 2026
© Author(s) 2026. CC BY 4.0 License.



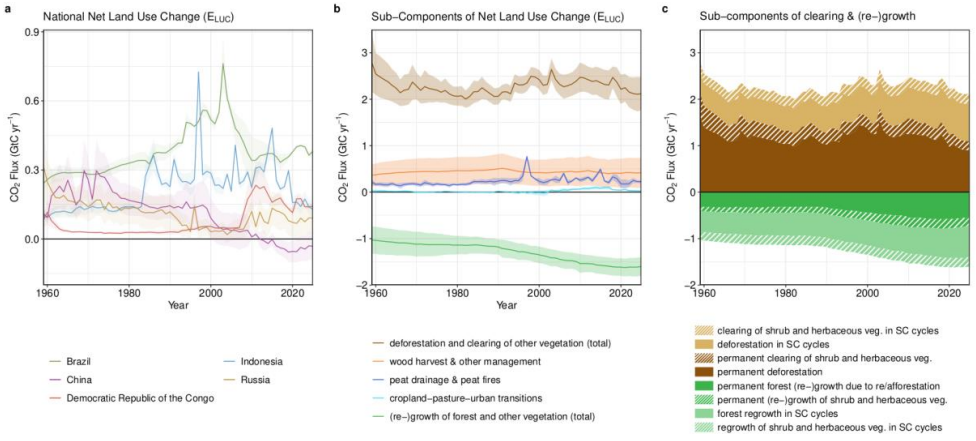


Figure 7. Net CO_2 exchanges between the atmosphere and the terrestrial biosphere related to land-use change. (a) Net CO_2 emissions from land-use change from the five countries with largest cumulative emissions since 1959. Values shown are the average of the three bookkeeping models, with shaded regions as ±1σ uncertainty. (b) Sub-components of E_{LUC}: (i) emissions from deforestation and clearing of other vegetation (total; that is including permanent deforestation and clearing and deforestation and clearing in shifting cultivation cycles), (ii) emissions from peat drainage & peat fires, (iii) removals from (re-)growth of forest and other vegetation (total; that is including permanent (re-)growth and regrowth in shifting cultivation cycles), (iv) net fluxes from wood harvest and other forest management (comprising slash and product decay following wood harvest, regrowth after wood harvest, and fire suppression), and (v) emissions and removals from transitions between cropland, pasture, and urban areas. The sum of the five components is net E_{LUC} shown in Figure 4b. (c) Sub-components of 'deforestation and clearing of other vegetation (total)' and of '(re-)growth of forest and other vegetation (total)', where SC denotes shifting cultivation.

https://doi.org/10.5194/essd-2026-895
Preprint. Discussion started: 10 November 2026
© Author(s) 2026. CC BY 4.0 License.

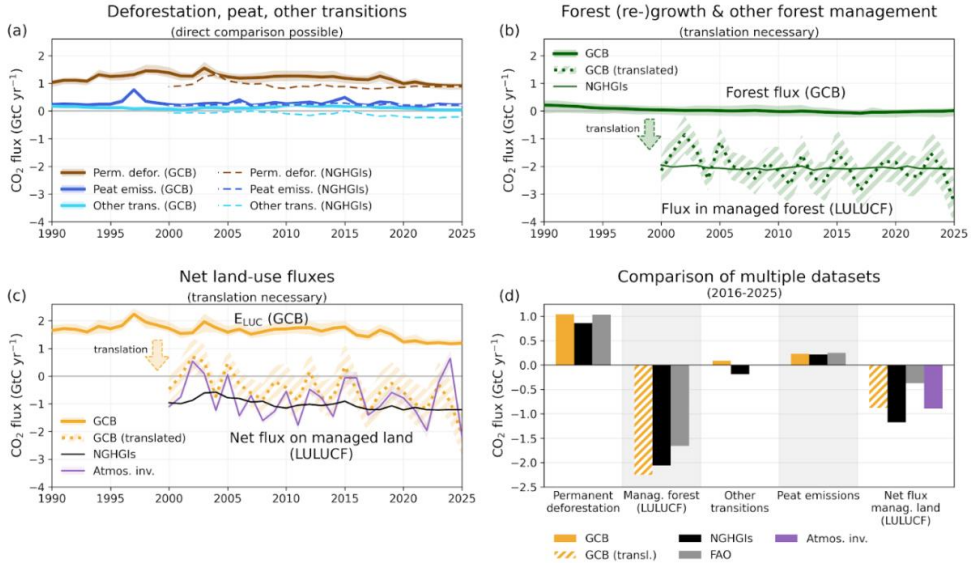
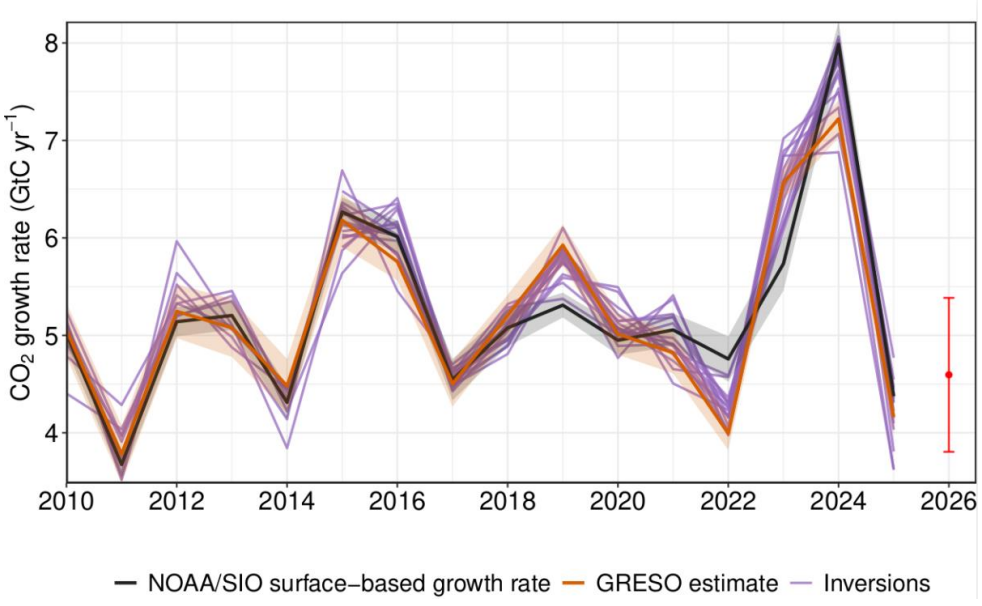


Figure 8. Comparison of GCB land-use CO_2 flux estimates (following the GCB definition of E_{LUC}) with national greenhouse gas inventories (NGHGIs; following the NGHGI definition of land-use, land-use change, and forestry, LULUCF, thus including all CO_2 fluxes on managed land) and atmospheric inversion systems (CO_2 fluxes on managed land) in panels (a) - (c) and additionally with FAO estimates in panel (d). To compare GCB results with NGHGIs, a translation is necessary for some subcomponents. (a) 'Permanent deforestation', 'peat drainage & peat fires', and 'other transitions', which can be directly compared. (b) 'Forest (re-)growth & other forest management', for which a translation is necessary. This subcomponent includes removals from permanent forest (re-)growth, emissions and removals from wood harvest & other forest management, and emissions and removals in shifting cultivation cycles. (c) Net land-use CO_2 fluxes, for which a translation is necessary. The translation of GCB estimates to NGHGI estimates in (b) and (c) is done by adding the natural land sink in managed forests estimated by DGVMs (see Supplement S.2.4) to the GCB estimates (see also Table S11). Lines show the means of the GCB datasets (three bookkeeping models or three peat drainage datasets plus peat fires, respectively) and of 16 atmospheric inversion estimates, respectively. Shaded areas denote the full range across GCB estimates, the standard deviation for atmospheric inversions, and, for translated estimates, the combined standard deviation (estimated by uncertainty propagation) from bookkeeping model estimates of land-use change fluxes and DGVM estimates of the natural land sink in managed forests. The GCB definition of E_{LUC} and the NGHGI definition of LULUCF fluxes are equally valid, each in its own context. (d) GCB, NGHGI, FAO, and atmospheric inversion estimates averaged over 2016–2025 (see also Table S11). FAO forest flux estimates include fluxes in both managed and unmanaged forests. The FAO estimate for net flux on managed land (LULUCF) does not include other land-use transitions. NGHGI data are from the LULUCF data hub V4.1.0 (Melo et al. 2026) and FAO data are from Tubiello et al. (2026) and FAOSTAT (FAO, 2026c).

https://doi.org/10.5194/essd-2026-895
Preprint. Discussion started: 10 November 2026
© Author(s) 2026. CC BY 4.0 License.



Open Access Earth System Science Data Discussions



4469

4470 **Figure 9:** Annual atmospheric CO_2 growth rates based on observations from the surface network (by NOAA
4471 (National Oceanic and Atmospheric Administration) and SIO (Scripps Institution of Oceanography)), as well as
4472 using the Growth Rate from Satellite Observations (GRESO) approach using OCO-2 (from 2015 onwards) and
4473 GOSAT based XCO_2 observations (from 2010 onwards) with uncertainties. To obtain G_{ATM}, the observation-
4474 based growth rates in units of ppm yr^{-1} are converted to units of GtC yr^{-1} by multiplying by a conversion factor
4475 (CF) of 2.124 GtC per ppm, assuming the observations to represent the annual mean mass change of CO_2
4476 throughout the atmosphere. The purple lines are the atmospheric growth rates (in GtC yr^{-1}) calculated as the sum
4477 of the fluxes derived by the atmospheric inversions. The G_{ATM} projection for 2026 is shown in red.

https://doi.org/10.5194/essd-2026-895
Preprint. Discussion started: 10 November 2026
© Author(s) 2026. CC BY 4.0 License.

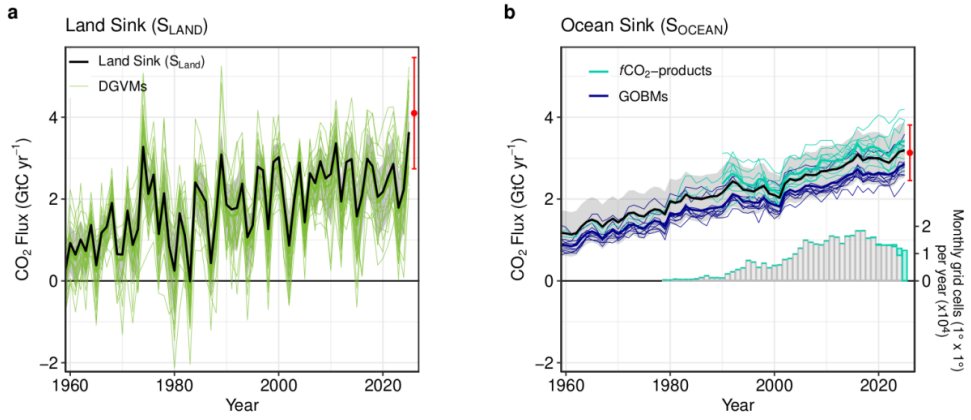


Figure 10. (a) The land CO_2 sink (S_{LAND}) estimated by individual DGVMs (thin green lines). The DGVM multi-model mean is shown as the thick green line. The S_{LAND} budget estimate (black with ±1σ uncertainty), is the DGVM multi-model mean adjusted for the δL bias. For years 2015-2025, S_{LAND} is also adjusted for LOAC. The S_{LAND} projection for 2026 is shown in red. (b) Comparison of the anthropogenic atmosphere-ocean CO_2 flux showing the budget values of S_{OCEAN} (black; with the uncertainty in grey shading), individual ocean models (royal blue), and the ocean fCO_2-products (cyan). Corrections were applied to S_{OCEAN} (black) for the warm layer/cool skin effect for fCO_2-products. Individual model lines as well as fCO_2-product ensemble means (thick cyan line) do not include this correction, with the exception of 3 fCO_2-products (UoEX-UEPFFNU, AOML-ET and JMA-MLR) that include temperature corrections as part of their air-sea CO_2 flux calculation (see section 2.5). Two fCO_2-products (Jena-MLS, LDEO-HPD) extend back to 1959. All fCO_2-products were adjusted for the pre-industrial ocean source of CO_2 from river input to the ocean, by subtracting a source of 0.65 GtC yr^{-1} to make them comparable to S_{OCEAN} (see Section 2.5). The bar-plot in the lower right illustrates the number of monthly gridded values in the SOCAT v2026 dataset (Bakker et al., 2026a). Grey bars indicate the number of grid cells in SOCAT v2025, and coloured bars indicate the newly added grid cells in v2026.

https://doi.org/10.5194/essd-2026-895
Preprint. Discussion started: 10 November 2026
© Author(s) 2026. CC BY 4.0 License.

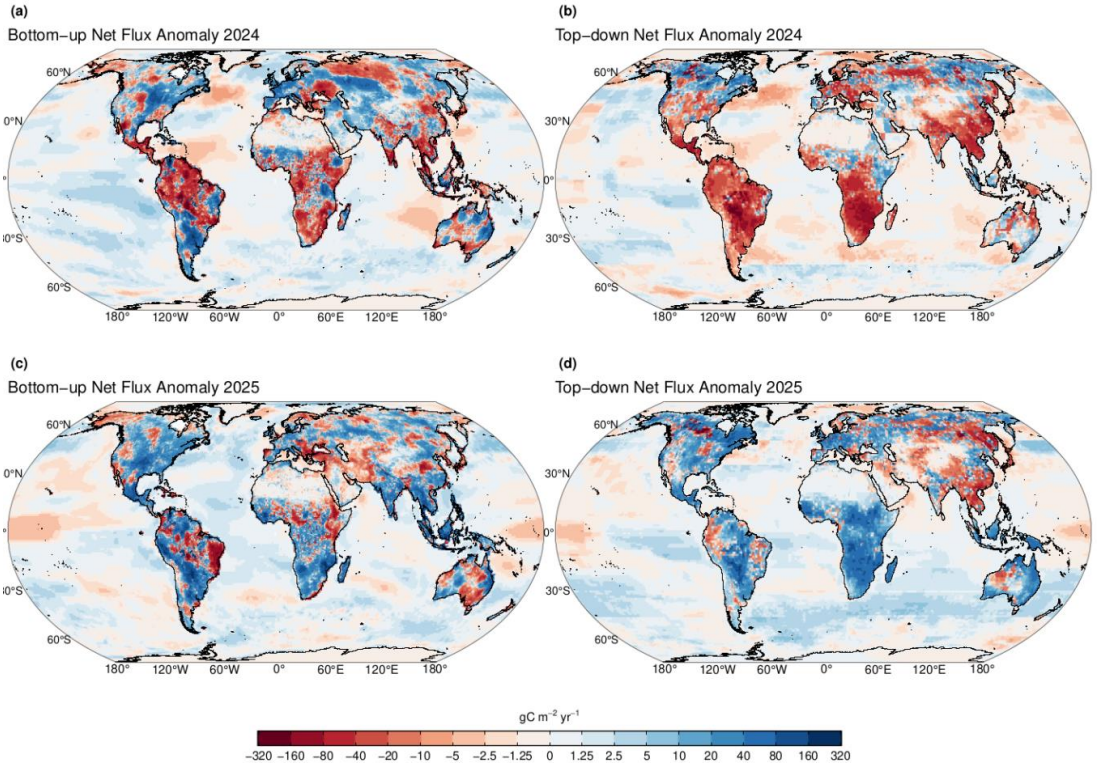


Figure 11. Anomalies in net land and ocean fluxes for 2024 and 2025 relative to the 2016-2025 decadal mean. Maps show the a) 2024 bottom-up (DGVMs S_{LAND} and BKMs E_{LUC} for land; GOBMs and fCO_2 products for ocean), b) 2024 top-down (atmospheric inversions), c) 2025 bottom-up, and d) 2025 top-down fluxes. Units are gC m^{-2} yr^{-1}.

https://doi.org/10.5194/essd-2026-895
Preprint. Discussion started: 10 November 2026
© Author(s) 2026. CC BY 4.0 License.

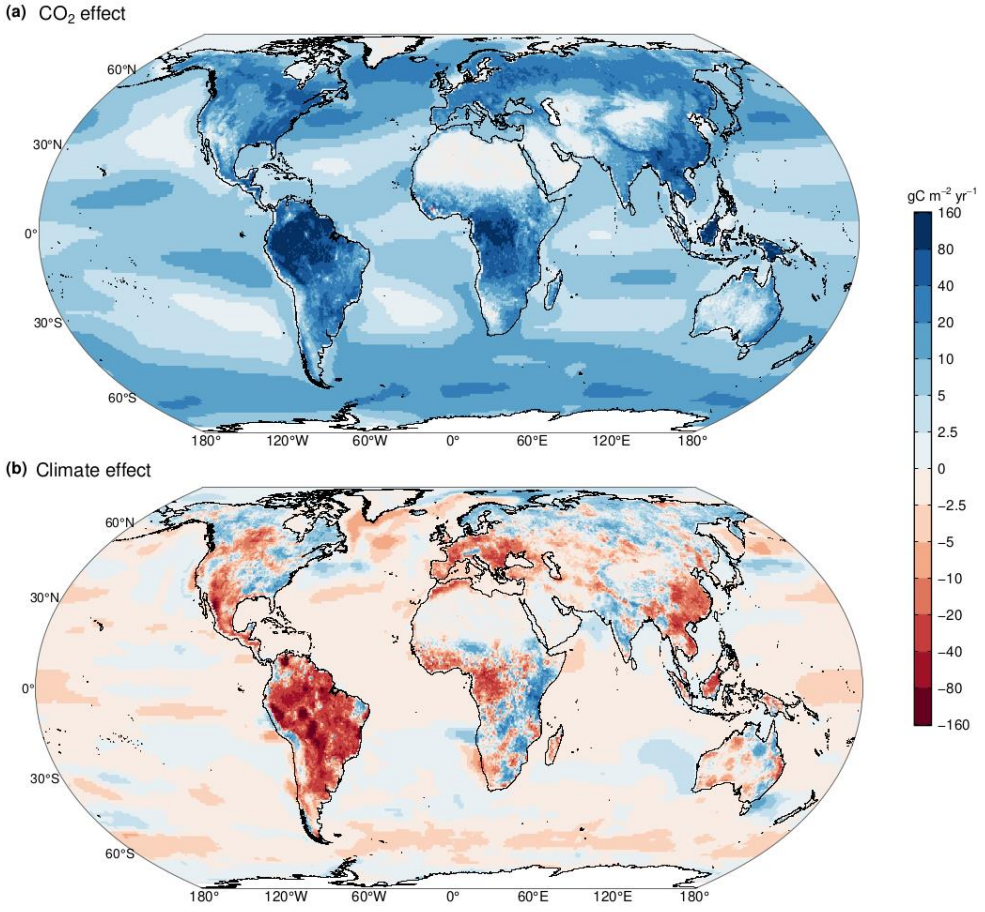
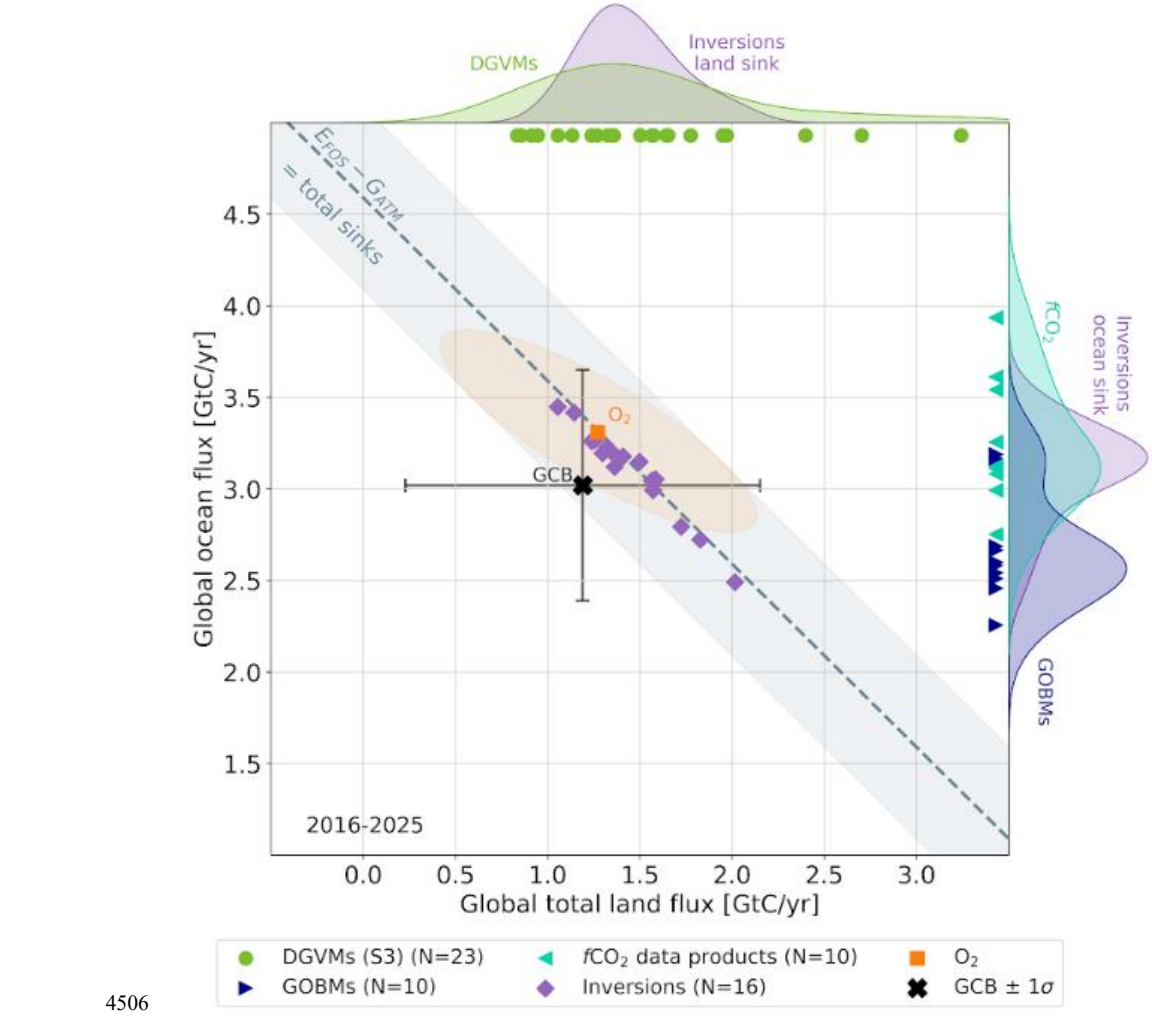


Figure 12. Attribution of the anthropogenically-perturbed ocean (S_{OCEAN}) and land (S_{LAND}) CO_2 sinks to (a) increasing atmospheric CO_2 concentrations and (b) changes in climate, averaged over the 2016-2025 decade. All data shown is from the processed-based GOBMs, DGVMs, and BKMs. The DGVM CO_2 flux was adjusted for dL from the bookkeeping models. See Supplement S.3.2 and S.4.1 for attribution methodology. Units are in gC m^{-2} yr^{-1} (note the non-linear colour scale). Positive values (blue) are CO_2 sinks, negative values (red) are CO_2 sources.

https://doi.org/10.5194/essd-2026-895
Preprint. Discussion started: 10 November 2026
© Author(s) 2026. CC BY 4.0 License.



4506

4507

https://doi.org/10.5194/essd-2026-895
Preprint. Discussion started: 10 November 2026
© Author(s) 2026. CC BY 4.0 License.



Open Access Earth System Science Data Discussions

Figure 13. The 2016-2025 decadal mean global S_{OCEAN} and net atmosphere-land fluxes derived from the ocean models and fCO_2 products (y-axis, right and left pointing blue triangles respectively), and from the DGVMs (x-axis, green symbols), and the same fluxes estimated from the atmospheric inversions (purple symbols). The shaded distributions show the densities of the ensembles of individual estimates. The black central cross ('GCB') is the mean (±1σ) of S_{OCEAN} and ($S_{LAND} - E_{LUC}$) as assessed in this budget. The grey diagonal line represents the constraint on the global land + ocean net flux, i.e. global fossil fuel emissions minus the atmospheric growth rate from this budget ($E_{FOS} - G_{ATM}$). The orange square represents the same global S_{OCEAN} and atmosphere-land fluxes as estimated from the atmospheric O_2 constraint (the ellipse drawn around the central atmospheric O_2 estimate is a contour representing the 1σ uncertainty of the land and ocean fluxes as a joint probability distribution). Positive values are CO_2 sinks. Note that the inverse estimates have been scaled for a minor difference between E_{FOS} and GridFEDv2026.0 (Jones et al., 2026). The 'GCB' central mean estimate includes the S_{LAND} ,E_{LUC}, and S_{OCEAN} global estimates from Table 7. The inversions and fCO_2 products include the river adjustment (see Section 2). No further adjustments or corrections were applied to the individual bottom-up estimates.

https://doi.org/10.5194/essd-2026-895
Preprint. Discussion started: 10 November 2026
© Author(s) 2026. CC BY 4.0 License.

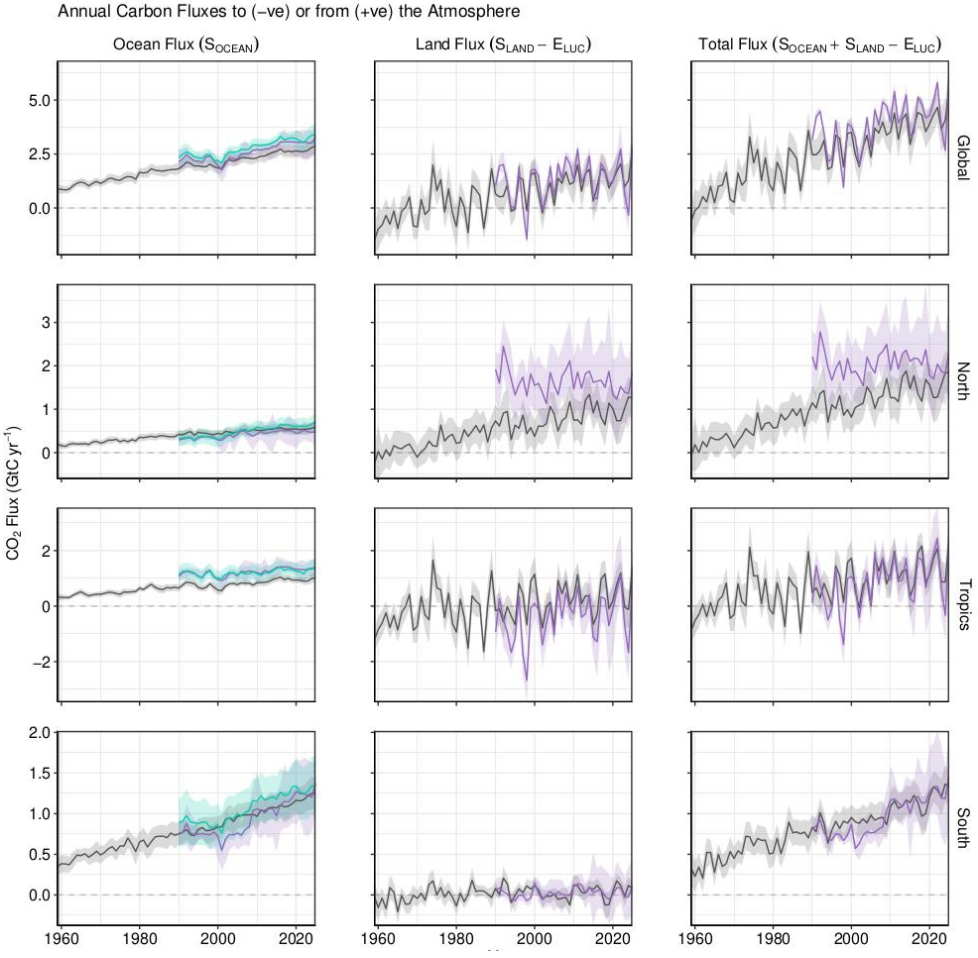


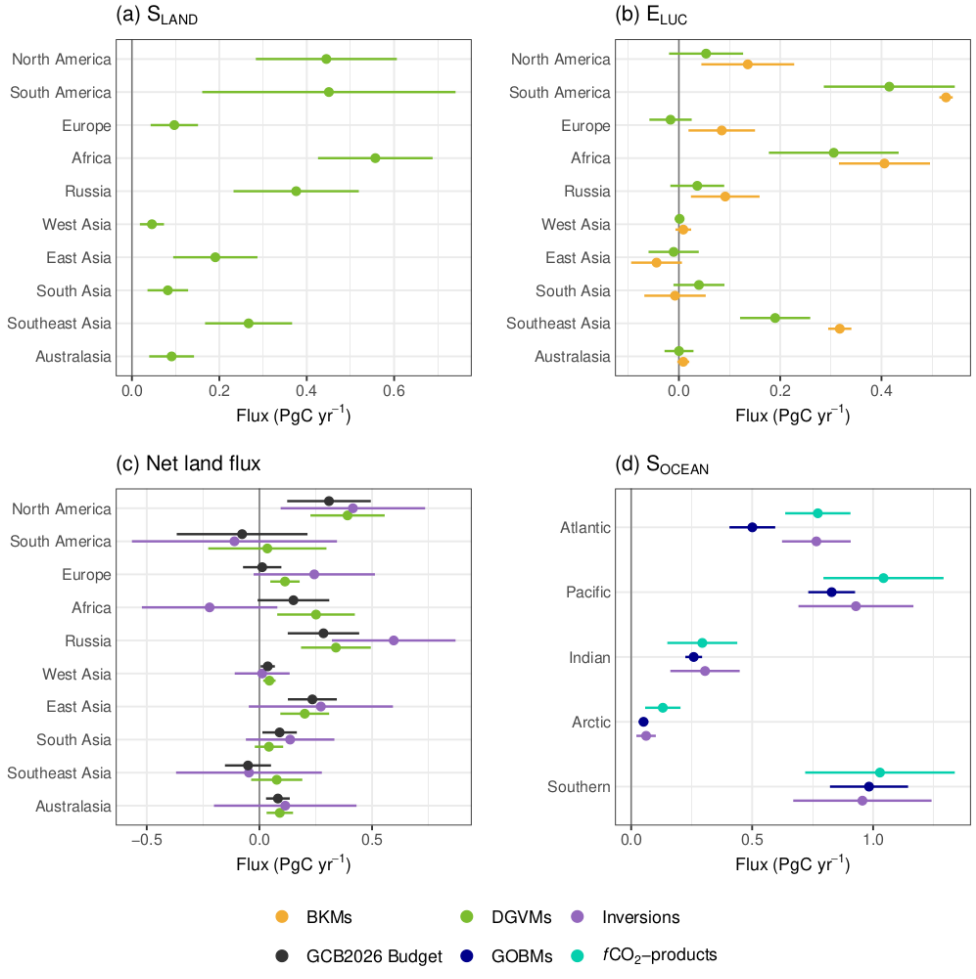
Figure 14. Anthropogenic CO_2 fluxes between the atmosphere and the Earth's surface separated between land and oceans, globally and in three latitude bands. The ocean flux is S_{OCEAN} and the land flux is the net atmosphere-land fluxes from the DGVMs. The latitude bands are (top row) global, (2nd row) north (>30°N), (3rd row) tropics (30°S-30°N), and (bottom row) south (<30°S), and over ocean (left column), land (middle column), and total (right column). Estimates are shown for: process-based models (DGVMs for land, GOBMs for oceans, simulation A minus B); inversion systems (land and ocean); and fCO_2-products (ocean only). Inversions and fCO_2-products are the contemporary fluxes minus the preindustrial natural steady-state and riverine fluxes (see Table S14). Positive values are CO_2 sinks. Mean estimates from the combination of the process models for the land and oceans are shown (black line) with ±1σ of the model ensemble (grey shading). For the total uncertainty in the process-based estimate of the total sink, uncertainties are summed in quadrature. Mean estimates from the atmospheric inversions are shown (purple lines) with their full spread (purple shading). Mean estimates from the

https://doi.org/10.5194/essd-2026-895
Preprint. Discussion started: 10 November 2026
© Author(s) 2026. CC BY 4.0 License.



Open Access Earth System Science Data Discussions

4534 fCO_2-products are shown for the ocean domain (light blue lines) with uncertainty as the combination in
4535 quadrature of ±1σ of the model ensemble and the ±1σ of the GOBM preindustrial mean flux (Table S14). (light
4536 blue shading).



4537

https://doi.org/10.5194/essd-2026-895
Preprint. Discussion started: 10 November 2026
© Author(s) 2026. CC BY 4.0 License.



Open Access Earth System Science Data Discussions

4538 **Figure 15.** Decadal mean (a-c) land and (d) ocean fluxes for RECCAP-2 regions over 2016-2025. For land
4539 fluxes, S_{LAND} is estimated by the DGVMs (green bars), with the δL adjustment included. Uncertainty is the
4540 combination (in quadrature) of ±1σ spread among DGVMs for the sum of simulations S3-S4+S0 and the ±1σ
4541 spread among bookkeeping models (BKM) δL estimates. A positive S_{LAND} is a net transfer of carbon from the
4542 atmosphere to the land. E_{LUC} fluxes are shown for both DGVMs (green) and BKMs (orange). The BKM
4543 uncertainty is defined as the ±1σ spread among BKMs. The DGVM uncertainty combines (in quadrature) the
4544 ±1σ spread among DGVMs for the sum of simulations S0-S4 and the ±1σ spread among BKM δL estimates.
4545 Note, a positive E_{LUC} flux indicates a loss of carbon from the land. The net land flux is shown for DGVMs
4546 (green), atmospheric inversions (purple), and the GCB2026 budget (black; DGVM S_{LAND} - BKM E_{LUC}). The
4547 ocean sink (S_{OCEAN}) is estimated by GOBMs (royal blue), *f*CO_2-products (cyan), and atmospheric inversions
4548 (purple). *f*CO_2-products and atmospheric inversions have been adjusted for pre-industrial steady-state and river
4549 fluxes but the *f*CO_2-products were not corrected for the cool skin effect at regional scale. Uncertainty is
4550 estimated as the ±1σ spread for GOBMs. For *f*CO_2-products and atmospheric inversions uncertainty is
4551 calculated as the combination in quadrature of ±1σ of the model ensemble and the ±1σ of the GOBM
4552 preindustrial mean flux. Positive values are CO_2 sinks. Region definitions can be found at:
4553 https://www.globalcarbonproject.org/reccap/